Novel fibre-optic-based interferometric sensors exploiting coherent and low-coherence signal processing techniques

by

Awad Samir Gerges

A thesis submitted for the Degree of

Doctor of Philosophy

University of Kent at Canterbury

Physics Laboratory

March 1990

Acknowledgements

I would like to express my greatest gratitude to Prof. D. A. Jackson, Professor of Applied Optics, University of Kent at Canterbury, England, for his encouragement, guidance and helpful advice during the theoretical and experimental phases of my work. I would particularly like to thank him for his valuable support during the writing-up stage of this thesis .

Grateful thanks are due to all the staff of the Fibre Optic group, University of Kent, particularly Dr. T. P. Newson, Dr. F. Farahi and Dr. J. D. C. Jones for their kind help and co-operation during my experimental work.

My deep thanks to Mr. R. Povey, for his help in designing the electronic circuits, thanks also to Miss D. Bowyer, Mr. K.M.Stevens, Mr.B.Kenward, and all the members of the electrical and mechanical workshops for their valuable help. I am also grateful to Miss D.Finn for preparing the photographic plates included in this thesis.

I would like to thank my parents for their encouragement from an early age. My heartfelt gratitude to my wife, for her encouragement and support, and to my children, Mary, Nermean and Miena who have been waiting patiently for their Dad to finish his Ph.D.

I am also much indebted to Military Technical College in Egypt, the Egyptian Government and its representative in London " Defence Attachè Office " for their support to undertake this study. This support is gratefully acknowledged.

Abstract

The work presented in this thesis is concerned with the introduction of several novel fibre-optic-based interferometric sensors. The main objectives have been to design practical sensors which are remote, passive, insensitive to environmental perturbations and capable of re-initialisation when it is switched on.

A sensor for temperature or strain measurement is demonstrated using a short coherence length light source. A novel signal processing technique, based on either tracking the point of maximum visibility (zero path imbalance) or the first quadrature point, has been introduced. The advantages of both techniques are that the value of the measurand can be recovered when the sensor is 'powered up' and the accuracy of the sensor is nearly independent of drift in the source wavelength. The potential of using multi-mode laser diodes, as alternatives to the low coherence-length sources such as LED's or SLD's commonly used in 'white light' fibre-optic interferometric sensors has been studied. It is shown that the main advantage gained in using such sources is improved resolution due to the significant increase in the launched optical power. The use of such sources however is subject to certain restrictions.

A novel form of sensor in which the sensing element is a miniature hemispherical air cavity Fabry Perot interferometer has been introduced. The properties of the cavity are theoretically studied and then verified experimentally. This new cavity design has been exploited for two different types of thermometers.

A novel accelerometer, in which the sensing element is a weighted diaphragm, has also been introduced. The displacement of the diaphragm produced by acceleration is measured using a similar miniature hemispherical air-spaced Fabry-Perot interferometer, of which one mirror is mounted on the diaphragm. The design of the accelerometer has been developed to have minimal sensitivity to environmental and source frequency drift by exploiting the very high common mode rejection ratio achieved using two miniature hemispherical cavities, constructed either side of the diaphragm. Two laser diodes, with distinct wavelengths, are used to illuminate the system in such

a way as to increase its unambiguous dynamic range. The system outputs are processed differentially such that the detrimental effects caused by the optical sources frequency jitter as well as environmental perturbations are strongly minimised.

Table of Contents

List of the abbreviations used in the thesis

AS ..... Analogue switch

att. ..... Signal attenuator

BS ..... Beam splitter

DA ..... Differential amplifier

DAC ..... Digital to analogue converter

DC ..... Fibre-optic directional coupler

FOIS ..... Fibre-optic interferometric sensors

HGBM ..... High gain bandwidth mode

LD ..... Laser diode

LED ..... Light emitting diode

LGBM ..... Low gain bandwidth mode

LP filter ..... Low pass filter

M ..... Mirror

MLD ..... Multi-mode laser diode

MV ..... Multi-vibrator

PD ..... Photodiode

PZT ..... Piezo-electric transducer

SG ..... Signal generator

SLD ..... Super luminescent diode

TS ..... Translation stage

T.T.L ..... Synchronous T.T.L. pulses

CHAPTER (1)

Introduction to fibre optic interferometric sensors

(1.1) Introduction

Optical fibre based sensors have been the subject of a large research effort in recent years [1-4]. Sensors of this type offer many advantages over conventional sensing techniques, including high sensitivity for a wide range of physical measurands (such as temperature, pressure, magnetic field, vibration, etc). Optical fibre sensors are constructed from dielectric materials, so that they can be used in high voltage, electric or magnetic fields, high temperature, corrosive or other stressing environments. They are also versatile, such that fibre sensors can be configured in arbitrary shapes.

In the past few years many fibre optic sensor have been developed, these devices may be categorised by transduction mechanisms into two main types : amplitude (intensity) sensors and phase (interferometric coherent) sensors. In the former type the physical perturbation interacts with the fibre, or some device attached to the fibre, to directly modulate the intensity of the light in the fibre. The advantages of intensity modulated sensors are their simplicity of construction and compatibility with multi-mode fibre technology [5]. Examples of such sensors include simple microbend-loss pads [6], optical reflection sensors [7], as well as more complex sensors such as vortex shedding flow-meters [8]. Interferometric fibre optic sensors have the major additional advantage that the measurement is related to an intrinsic property of the light such as its velocity, wavelength or frequency - in marked contrast to the intensity modulated sensing devices.

Interferometric sensors are generally more complex than intensity sensors, however they offer both large dynamic range coupled with extremely high resolution and can be operated remotely as a single sensor or in a multiplexed network [9,10].

In this chapter we consider the general design and signal processing of fibre optic interferometric sensors. This discussion brings out the difficulty of routinely measuring slowly varying measurands such as temperature, pressure, acceleration, etc. Finally we introduce the outline of this thesis, which covers the development of novel forms of fibre optic based interferometric sensors designed for quasi-static measurands, such as temperature and acceleration. Established techniques for signal processing are introduced and methods to extend the unambiguous measurement range.

(1.2) Fibre optic interferometric sensors :

The basis of an interferometric optic-sensor is the measurement of a physical parameter through the phase modulation which it produces in an optical beam via a sensing element. Measurements of this type require that the relative alignment of the bulk-optic components, constituting the interferometer, are maintained with high precision. In a monomode fibre the coherence properties of the propagation beam are maintained, hence it is possible to produce an interferometer from single mode optical fibre, this permits flexible inter-connections within the sensing system and eliminates the problems associated with the geometrical instability (misalignment) of conventional interferometers.

The basic concept of a fibre-optic interferometric sensor is shown in figure (1-1). Light from a suitable source, typically a gas laser or solid state laser, is coupled into an input fibre which transfers the beam to the sensing interferometer where it is optically encoded by the measurand. Subsequently the optical power from the interferometer is transferred via another optical fibre (the same optical fibre in the case of reflective configurations) to a suitable optical detector, typically a photodiode, for signal processing.

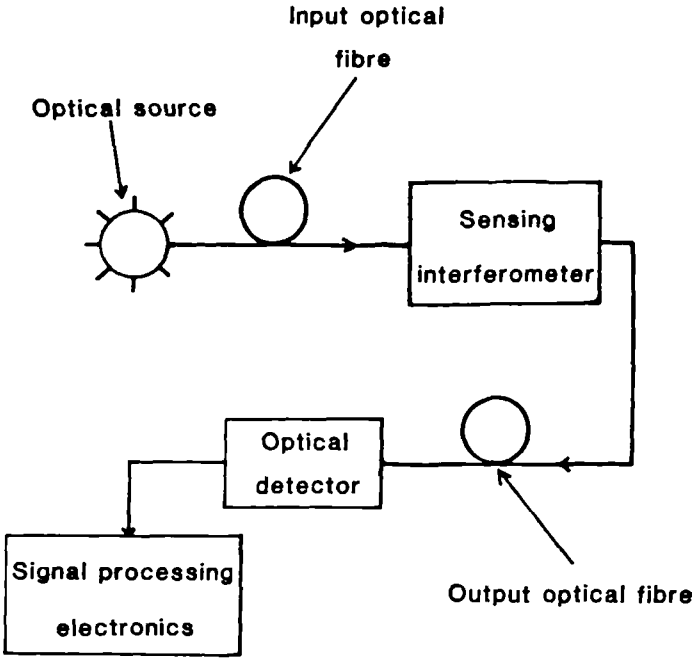

Figure (1-1) : Schematic diagram of basic FOIS.

Fibre optic interferometric sensors can conveniently classified into two main categories :

(a) Intrinsic :

in which the optical beam always remains within the fibre, and is guided to the measurement point where the measurand locally modifies the optical properties of the fibre waveguide. Intrinsic sensors may subdivided into direct and indirect sensors. In the former type the measurand modulates the optical path-length directly by changing the optical properties of the fibre, as examples temperature changes affect both the length of the fibre as well as its index of refraction [11]. In the case of indirect intrinsic sensors the measurand modulates the optical path-length via an auxiliary sensing element. The optical fibre is bonded to some form of conventional sensing element or coated with a material to locally modify the physical properties of the fibre, for example

magnetic field, electric field and chemicals (gases) can be detected using an optical fibre coated with a film of another material, which is sensitive to the measurand under investigation [12-14]. Single mode fibre interferometers may be categorised into the following groups. (i) Two beam interferometers, such as Michelson and Mach-Zehnder configurations. (ii) Multiple beam interferometers, such as Fabry-Perot interferometer and the ring resonator. (iii) Reciprocal path Sagnac interferometer, and (iv) polarimetric interferometers [15].

It is generally found that although the fibre-optic interferometer can be made sensitive to many different measurands, the fibre is particularly sensitive to temperature and pressure. It is therefore common practice to attempt to eliminate these unwanted signals by either thermally isolating the sensor or exposing the two arms forming the interferometer to exactly the same temperature and pressure perturbations.

(b) Extrinsic :

the optical fibre is used to convey optical power to some form of classical interferometric measurement system, i.e the optical beam is not guided in the measurement volume. In many sensor applications advantage may be gained by using this form of fibre optic-based system, for example the system's high susceptibility to temperature and pressure perturbation can be reduced, hence it is possible to design sensing systems for applications outside the controlled environment of the laboratory. Monomode fibre is used in many of these systems to maintain the coherence properties of the emergent beam (spatial and temporal coherence properties). Extrinsic sensors have been developed for holography [16], laser Doppler velocimetry [17], temperature [18], vibration and acceleration measurements [19,20].

(1.3) Signal processing techniques for interferometric sensors :

The basic function of signal processing is to translate the optical phase information, induced in the sensing interferometer, to an electrical signal for analysis by conventional electronic techniques. Numerous signal processing techniques are reviewed by many authors [3,4,9,10], where the advantages and the limitations of each are discussed, thus it is necessary to select the most

appropriate technique for the sensor application concerned. Many parameters determine the technique to be used such as; the frequency response of the measurand, the aimed resolution of the sensor and its range of operation. Also it is often important to study the working environment of the sensor to know if it is permissible to use electrically active elements within the sensing interferometer or not.

In this section the transfer function of an interferometric sensor is discussed, together with appropriate techniques for signal processing. For simplicity we will consider only the case of a two-beam interferometric sensor, but many of the techniques described may be applied directly to multiple beam interferometric configurations, such as the ring resonator and the Fabry-Perot etalon.

(1.3.1) Transfer function :

Any two beam optical interferometer produces an intensity output which is dependent on the phase difference between the two beams at the recombination point. The interferometer output intensity, I, may be described by :

$$I = I_{mean}\left[1 + V\,Cos(\Delta\phi)\right] \tag{1.1}$$

where I_{mean} is the mean output power, V is the visibility constant which depends on the relative intensities and polarisation states of the two interfering beams as well as on the coherence properties of the optical source [15], as will be discussed in chapter (2). $\Delta\phi$ is the optical phase retardance, given by :

$$\Delta\phi = \frac{2\pi\nu_o}{C}\Delta L \tag{1.2}$$

where ν_o is the mean optical frequency of the light source, C is the free space velocity of light and ΔL is the optical path-length imbalance of the interferometer. Equation (1.2) shows the direct proportionality of the optical phase retardance, $\Delta\phi$, on the optical path-length imbalance of the interferometer, ΔL, where the constant of proportionality is dependent on the value of the mean optical frequency of the source. Gas lasers emit light with accurately known mean optical

frequency enabling the optical phase measurements to be made with the greatest precision. However solid state laser diodes are preferred in most types of intrinsic fibre optic interferometric systems. This is because a laser diode is much cheaper, smaller in size, robust and compatible with monomode optical fibre, in addition its power consumption is low and its emission frequency can be readily modulated.

This periodic form of the output signal limits the unambiguous range of $\Delta\phi$ to be 2π optical radians, moreover the sensitivity of the sensor, defined as $dI/d(\Delta\phi)$ will fade to zero for values of $\Delta\phi$ equal to $q\pi$, where q is an integer. The positions of maximum sensitivity occur when $\Delta\phi = (2q-1)\pi/2$, named 'quadrature points'.

The main aim of signal processing techniques is to obtain an output signal free from fading and to maintain the resolution of the system as high as possible. This may be achieved by controlling either the path-length imbalance of the interferometer, ΔL, or the mean optical frequency of the source, ν_o. Techniques for recovery of the signal phase information are classified into two main categories, namely homodyne and heterodyne techniques, as discussed below.

(1.3.2) Homodyne techniques :

Homodyne techniques are defined as those in which the signal and reference optical beams, of the interferometer, are coherently mixed without any frequency shifting of either beam. In this case the information, about the measurand, is detected in its original frequency.

According to the frequency response of the measurand, the phase retardance, $\Delta\phi$ may change very slowly, for example when measuring temperature or pressure, or at high frequency, for example when measuring vibrations or acoustic signals. Generally, the phase retardance may be expressed in the form :

$$\Delta\phi(t) = [\phi_o(t) + \phi_{sd}(t)] + \phi_{sa}\, Sin(\omega t) \qquad (1.3)$$

where ϕ_{sd}, ϕ_{sa} are the low frequency and the harmonic (ω is its angular frequency) signal phase

amplitudes respectively and ϕ_o is the phase retardance induced in the interferometer due to the low frequency environmental changes. The output signal is detected using a photo-detector, where its output current, $I_d \alpha I$, may be represented in the form :

$$I_d = I_{d(mean)} \left[1+V\ Cos(\phi_o+\phi_{sd}+\phi_{sa}Sin(\omega t))\right] \tag{1.4}$$

which may be expanded in terms of Bessels harmonics in the form :

$$I_d = I_{d(mean)} \left\{ 1 + V\ Cos(\phi_o+\phi_{sd}) \left[J_o(\phi_{sa}) + 2 \sum_{m=1}^{\infty} J_{2m}(\phi_{sa})\ Cos(2m\omega t)\right] \right.$$

$$\left. - V\ Sin(\phi_o+\phi_{sd}) \left[2 \sum_{m=1}^{\infty} J_{2m-1}(\phi_{sa})\ Sin(2m-1)\omega t\right] \right\} \tag{1.5}$$

where J_m is the Bessel function of the order m. The spectrum of I_d is a spectrum of a phase modulated carrier with the carrier frequency equal to zero. Under normal operating conditions, ϕ_o will fluctuate randomly in time, due to environmental perturbation, causing the amplitude of the Bessel harmonics to fluctuate in a similar manner. Several of the homodyne techniques available, enable the signal phase information to be recovered including the random phase drifts, are described below.

(a) Closed loop tracking techniques :

Closed loop tracking is one of the most effective techniques to recover the signal modulating the relative phase in the interferometer. It is easy to implement, extremely linear and introduces very little excess noise in the sensor.

In this technique, the interferometer is maintained at a quadrature point by either physically controlling the length of the reference arm of the interferometer [21], which is termed 'active homodyne', or by varying the mean optical frequency of the source, illuminating the system [22], which is termed 'active wavelength tracking homodyne'. This is usually achieved by closing the system measuring loop using a feedback servo [23].

The block diagram of the feedback servo, used in references [21-23], is shown in figure (1-2). The photo-diode output current is converted to a voltage, V_d, through a current/voltage converter and then fed to one of the inputs of the servo. If the sensing interferometer has a second (antiphase) output, as in the case of the Mach-Zehnder interferometer, then this output may be fed into the second input of the servo. The first stage of the servo is a differential amplifier which gives zero output voltage when the interferometer is locked at quadrature (when $V_{d1} = V_{d2} = V_{d(mean)}$). If the interferometer has one output only then a reference voltage equal to the mean output voltage of the photodetector, $V_{d(mean)}$, is required as an alternative for the second input to the servo. The error voltage of the differential amplifier is fed to an integrator, then amplified and fed back to the interferometer to maintain it locked at quadrature. If the tracking range of the system is exceeded a rapidly responding circuit resets the integrator, and hence the servo output, to zero. The servo then starts a new tracking cycle with the interferometer locked to an arbitrary quadrature point. The main disadvantage of this type of servo is that each time the system is reset all the information about the phase excursion is lost and the system needs re-initialisation, if the measurand is slowly varying such as temperature.

If the servo had an infinite gain-bandwidth product, (i.e able to compensate for any phase retardance irrespective of its frequency) then the photodetector output voltage, V_d, would remain constant, and the signal of interest would recovered from the servo's feedback voltage.

Practically, the gain-bandwidth of the servo system is limited, hence according to the signal frequency it may be recovered in two modes of operation. If the signal frequency is less than the corner frequency of the feedback servo, it is recovered, as a high gain-bandwidth mode output, from the servo's error voltage. In this mode of operation, a quasi-static signal can be tracked continuously over many periods of the interferometer transfer function. The tracking range of the whole system is limited by the allowable tracking range of the active device controlling the optical path-length of the sensing arm. In the second case, when controlling the system by changing the mean optical frequency of the source, the tracking range is limited by the maximum allowable change in the source optical frequency, $\Delta \nu_{max}$, as well as the optical path-length imbalance of the

sensing interferometer, $\Delta\phi_{max} = \frac{2\pi}{C} \Delta \nu_{max} \Delta L$, this problem will be discussed in more detail in chapter (6).

If the frequency of the signal is higher than the corner frequency of the the feedback servo ($\phi_{sd} = 0$), the servo is used to correct the low frequency drifts in the interferometer, maintaining it locked at quadrature, i.e maintaining $Cos(\phi_o) = 0$ and $Sin(\phi_o) = 1$. If the signal amplitude, ϕ_{sa}, is small then $J_1(\phi_{sa}) \simeq \phi_{sa}/2$. Substituting in equation (1.5), the photodetector output takes the form :

$$I_d = I_{d(mean)} \left[1 - V \phi_{sa} Sin(\omega t)\right] \tag{1.6}$$

where the A.C output of the photodetector represents the modulating signal, this mode of operation is called 'the low gain-bandwidth mode'. Figure (1-3) illustrates the principle of this technique of signal processing as applied to an all fibre Mach-Zehnder interferometer.

Using this signal processing technique, the sensor phase resolution may be estimated as following; differentiating equation (1.1) we get :

$$\delta(I_d) = -I_{d(mean)} V \, \delta(\Delta\phi) \, Sin(\Delta\phi) \tag{1.7}$$

where $(I_{d(mean)} \, V)$ represents the photodetector A.C. output, which may be called 'the interference fringe amplitude'. If the photo-detector current (I_d) is superimposed with a noise of mean amplitude δI_d , then $\delta(\Delta\phi)$ will give the corresponding uncertainity of determining $(\Delta\phi)$ which represents the phase resolution of the interferometric system. If the quadrature condition, $Sin(\Delta\phi) = 1$, is satisfied then :

$$\delta(\Delta\phi) = \frac{\delta I_d}{|I_{d(mean)} \, V|} \tag{1.8}$$

which shows that the phase resolution of an interferometric sensor, maintained at quadrature, may be estimated as the reciprocal of the ratio of the A.C. amplitude of the interference signal to the power spectrum of the noise floor of the photodetector output.

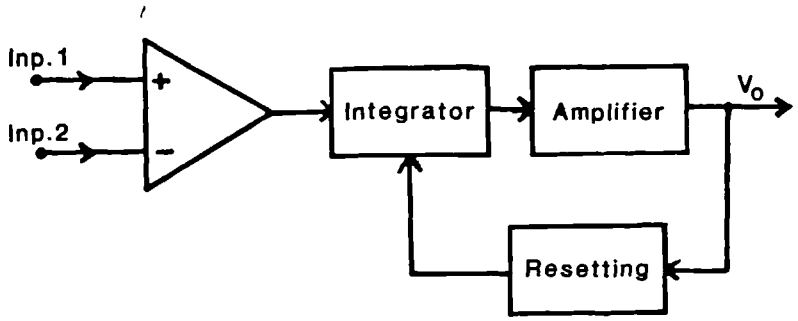

Figure (1-2) : Block diagram of the electronic feedback servo.

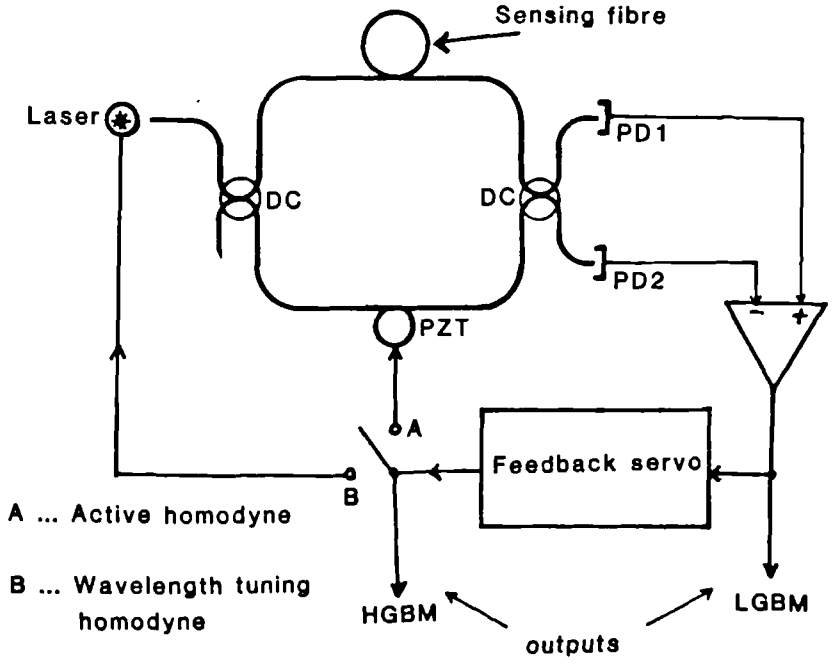

Figure (1-3) : The basic principle of closed-loop homodyne techniques.

(b) Open loop homodyne techniques :

The most straightforward open loop homodyne signal processing technique is based upon ratioing the amplitudes of either the odd or the even harmonics of a homodyne interferometric output. If the signal of interest is sinusoidal, the amplitudes of the harmonics are proportional to the Bessel function of the signal amplitude, hence it is possible to determine the amplitude of the input signal. This technique, in principle, permits unlimited operating range, as discussed in more detail in chapter (5).

An alternative open loop homodyne technique requires the interferometer to be configured such that two outputs, separated by a constant phase (ideally of $\pi/2$ are obtained). These outputs, may be called 'two quadrature outputs', represent the sine and cosine of the interferometric phase and thus can be combined together to provide the signal information without signal fading.

Several techniques have been developed to produce two quadrature outputs from the sensing interferometer. In the first technique, the outputs of a 3x3 or 4x4 coupler have been used in conjunction with further electronic processing to produce the necessary phase-shifted outputs [24,25]. A second technique was introduced by Dandridge et el, where a piezo-electric cylinder employed in the sensing interferometer, was sinusoidally modulated. The output of the interferometer was electronically conditioned to produce the sine and cosine outputs [26]. Alternatively, an unbalanced interferometer may be illuminated by two slightly different optical frequencies, the interferometric phases recovered at each frequency will differ according to equation (1.2). If the frequency difference is arranged such that the corresponding phase difference produced is $(2q-1)\pi/2$, where q is an integer, then two quadrature outputs are obtained. These two outputs may be obtained by using one laser diode, with its injection current (and hence its mean optical frequency) modulated using square pulses [27]. In polarimetric interferometers, a quarter wave plate may be used to shift the phase of the light in one arm of the interferometer by $\pi/2$ before mixing the two beams. The two quadrature outputs can be separated at the output using a polarisation selective beam splitter with its axis aligned parallel to one of the interferometer axes [28].

There are several techniques available for demodulating the two quadrature outputs. One simple way to produce a useful output, provided ϕ_{sa} is small, is to high-pass filter the two quadrature outputs, then by squaring and adding both signals an output proportional to the induced phase modulation is obtained [4]. A more suitable technique for higher level signals is the 'differentiating and cross-multiply' approach, introduced in reference [26], which requires slightly more complex demodulating electronics. An alternative approach, called 'quadrature recombination' was introduced by Kersey et el [29], where a heterodyne type carrier is generated by mixing the interferometer outputs with quadrature components of a local oscillator. Each of these techniques has its advantages and disadvantages, hence the relative merits must be considered for a specific application. Generally the stability and linearity of these techniques of signal processing is worse than those associated with active homodyne tracking techniques [30].

(1.3.3) Heterodyne techniques :

In systems utilising heterodyne signal processing techniques, one beam, of the interferometer, is shifted in optical frequency, with respect to the other, producing a beat frequency at the interferometer output. The signal information is then up-shifted by that frequency to become the phase modulation on the electronic carrier produced at the output photodetector. Demodulation of the heterodyne output may be performed simply using conventional electronic FM detectors such as, phase looked loops or electronic phase trackers [31]. The phase resolution of a heterodyne type interferometric sensor is limited by the signal to noise ratio of the generated electronic carrier and that of the final demodulator. Heterodyne signal recovery methods are very attractive as; (i) the phase detection sensitivity is constant over the whole period of the transfer function of the interferometer, i.e. the recovered signal does not fade, (ii) the phase tracking range is effectively infinite, (iii) the dynamic range of the modulating signal can be very large and (iv) the direction of the fringe motion can be determined. These features can be used very effectively when the interferometric sensor is used for quasi-static measurands. The main types of heterodyne techniques of signal processing are discussed below.

(a) True heterodyne :

A heterodyne signal is conventionally achieved using an acousto-optic modulator, such as a Bragg cell incorporated in one arm of the sensing interferometer [32,33]. The output of the interferometer takes the form :

$$I_d = I_{d(mean)}\, V\, Cos\left[\omega_o t + \Delta\, \phi(t)\right] \tag{1.9}$$

where ω_o is the 'offset' frequency introduced by the Bragg cell [4]. This signal represents a carrier of frequency ω_o which is phase modulated by the interferometer optical phase introduced in equation (1.3). Unfortunately, the conventional Bragg cell is bulky, lossy, electrically active and not readily integrated into a fibre optic interferometer. However, for high frequency signal recovery in conventional hybrid fibre-optic systems the Bragg cell remains the optimum approach for producing the carrier [34].

(b) Pseudo and synthetic heterodyne :

Different techniques have been developed to produce a heterodyne-type carrier output for all fibre interferometric sensors. In these techniques the phase of the interferometer is appropriately modulated. With certain techniques the carrier is not directly generated at the output of the interferometer, and can only be produced by electronic conditioning of the output.

Pseudo-heterodyne is one of the most simplest techniques for carrier production, as the sensor output requires the minimum of subsequent electronic processing. Equation (1.2) shows that the optical phase induced in an interferometer, of path-length imbalance ΔL, is a linear function of both the laser frequency and ΔL. Hence if either, of these parameters, is modulated with a serrodyne waveform of frequency ω_o of appropriate amplitude the interferometer phase will be driven over an integer number of complete interference fringes ($= 2q\pi$ optical radians, q = 1, 2, 3, ...). The heterodyne-type carrier is obtained by band-pass filtering the output of the interferometer at $q\omega_o$. The phase of the interferometer is swept using either a frequency modulated laser diode [35] or a piezo-electric fibre stretcher [36] deployed in one arm of the interferometer. The

former method can be particularly useful for multiplexing several sensors with different path-length imbalances, where the amplitude of modulation is adjusted such that integral numbers of fringes are generated at the outputs of the interferometers [37].

An alternative pseudo-heterodyne technique has been reported, where the carrier is produced by sinusoidally modulating the interferometer's phase and conditioning the output signal. Various electronic techniques have been developed to synthesise a heterodyne-type carrier from the output of the interferometer including gating using synchronous square pulses [38, 39]. The advantages and limitations of this technique of carrier production are discussed in more detail in chapter (6). Another technique has been introduced by Cole et el, where two harmonics signals are filtered from the output, of the interferometer, at frequencies of ω_o and $2\omega_o$ (ω_o is the modulating frequency) then multiplied by a local signal of frequencies $2\omega_o$ and ω_o respectively. Each of the two outputs is filtered at $3\omega_o$, hence they are combined differentially to produce the carrier [40]. This technique of carrier production is known as 'synthetic heterodyne'.

(1.4) Problems associated with quasi-static measurands :

The advantages of fibre optic interferometric sensors have been discussed in the above sections, however there are some problems which are encountered with this type of sensor, especially when they are used to sense slowly varying measurands, such as pressure and temperature. Here we discuss the common problems encountered when a fibre optic interferometric sensor is used to sense such measurands.

(a) Ambiguity and initialisation :

Throughout the previous discussion on signal processing it was clear that the unambiguous range of an interferometric sensor, illuminated by a monochromatic source is limited to one interference fringe, corresponding to an optical path-length change of one wavelength or 2π optical radians. A range of signal processing techniques have been developed to overcome this limitation, such as fringe counting and homodyne tracking techniques, however if the system is inter-

rupted (for example switched off and on) the absolute value of the measurand cannot be ascertained without some form of re-initialisation. It is therefore important to use techniques which extend the unambiguous measurement range or allow the system to be uniquely initialised.

(b) Optical and electronic noise :

It is clear, from the previous discussions, that the phase resolution of any signal recovery technique is set by the noise in the output of the system. Noise arises in the output of an interferometer due to (i) shot and thermal noise in the photodetector, (ii) the 1/f intensity noise associated with most of the solid state lasers, this tends to reduce the ultimate accuracy of the system at low frequency, (iii) the phase noise arising in an unbalanced interferometer due to the short term frequency jitter of the laser diodes [41] and (iv) electronic noise produced when the signal is processed [42]. These different noise sources tend to reduce the ultimate resolution of the sensor, and hence its dynamic range, particularly at low frequency. Different techniques have been introduced to minimise the noise at interferometric systems, as that used by Newson et al [43].

(c) The long term frequency stability of the source :

In interferometers with arms of different optical path-length, the long term frequency (wavelength) stability of the laser source is one of the most important factors as the source wavelength is the basic unit of measurement of the sensor. From equation (1.2) we can see that any uncertainty $\delta\nu_o$, in the value of the emission frequency of the laser diode, results in an error in the optical phase ($\Delta\,\phi$) of :

$$\delta(\Delta\,\phi) = \frac{2\pi\,\Delta L}{C}\,\delta\nu_o \qquad (1.10)$$

It can be seen that the frequency stability requirement of the laser diode, $\delta\nu_o$, is determined, both by the accuracy desired of the sensor and the optical path-length imbalance of the sensing interferometer. In section (1.3.1) it was shown that solid state laser diodes are more compatible with intrinsic fibre-optic interferometric sensors, but the main disadvantage of the laser diode is that its

emission frequency is a function of several environmental parameters. Different techniques have been reported to stabilise the emission frequencies of laser diodes over a long term periods [44-46].

(d) Low frequency environmental effects :

Although an optical sensor may designed to sense a specific measurand, it is often perturbed by many other physical environments, such as temperature, pressure, acoustic interference, etc. From equation (1.5) we can see that these environmental effects produce signals, ϕ_o, which when detected are indistinguishable from the effects of the desired measurand, ϕ_{sd}, especially if both effects have the same frequency response. This indicates how critical the design of the sensing interferometer is as it must be made sensitive only to the measurand of interest [47], as shown in chapter (6).

(1.5) Enhanced-range techniques of signal processing :

In section (1.3) it was shown that the periodic nature of the interferometric transfer function limits the unambiguous range of the basic interferometric sensor. In this section we review the various techniques by which this unambiguous range (and hence the sensor dynamic range) can be extended.

(a) Dual wavelength techniques :

One of the oldest techniques to increase the unambiguous range of an interferometer is to illuminate it with two different wavelengths. This technique has recently been used to enhance the measurement range of different types of fibre-optic interferometric sensors [48-50].

Consider an interferometer of path-length imbalance ΔL, illuminated by two mono-chromatic sources of different wavelengths λ_1 and λ_2, the interferometer will now produce two separate outputs, related to each wavelength. Different techniques have been used to separate these outputs such as, synchronous switching [48] or via a dispersive optical element [50]. If we

neglect the chromatic dispersion of the interferometer, the optical phases induced in the interferometer are :

$$\Delta\phi_1 = \frac{2\pi}{\lambda_1}\Delta L \tag{1.11}$$

and

$$\Delta\phi_2 = \frac{2\pi}{\lambda_2}\Delta L \tag{1.12}$$

Hence the differential phase between the two outputs (the effective phase difference) is :

$$\begin{aligned}\Delta\phi_{eff} &= \Delta\phi_1 - \Delta\phi_2 \\ &= \frac{2\pi}{\lambda_{eff}}\Delta L\end{aligned} \tag{1.13}$$

where the effective wavelength $\lambda_{eff} = \lambda_1\lambda_2/(\lambda_2-\lambda_1)$, which is greater than either of the wavelengths of the individual sources λ_1 and λ_2. The unambiguous measurement range, of the dual wavelength interferometer, is then extended to one effective wavelength (corresponding to an effective optical phase change of 2π radians).

From the definition of λ_{eff} it is clear that as $\lambda_2-\lambda_1$ decreases, the effective wavelength, and hence the unambiguous range of the system increases, however there are practical considerations which restrict the minimum value of $\lambda_2-\lambda_1$ which can be used. This is because the error induced in λ_{eff} by wavelength drift, of either source, becomes significant if ΔL is finite restricting the maximum permissible value of λ_{eff}, this is discussed further in chapter (6).

(b) Dual interferometry :

An alternative technique for enhancing the unambiguous range of a fibre-optic interferometric sensor has been demonstrated by Leilabady et el [51]. In this technique two independent outputs are obtained from two interferometers implemented along the fast and the slow axes of the same length of a highly birefringent fibre. The optical path-length imbalances of the two interferometers are $\Delta L_f = n_f L$ and $\Delta L_s = n_s L$, where L is the geometrical path-length imbalance of the fibre forming the interferometer, n_f and n_s are the indices of refraction of the fibre core

along its fast and slow axes respectively. The differential phase between the two interferometers is proportional to $(n_f - n_s)L$, hence the unambiguous range is extended by the ratio $n_i/\Delta n$, where i = f or s and $\Delta n \simeq n_f - n_s$. Recently, this technique was used to simultaneously recover variations in temperature and strain [52].

(c) White light interferometry :

A more general technique to enhance the measurement range is based once again on a classical technique often called 'white light interferometry', where the system is illuminated either by a large number of monochromatic sources, as example a multi-mode laser, or a broad-band source. The transfer function of an interferometer illuminated by one of these sources has unique features which can be utilised when sensor re-initialisation is necessary, moreover the unambiguous measurement range, in principle, is unlimited. This technique is studied in detail in chapters (2) and (3). Recently both white light and dual wavelength interferometry have been used in a system illuminated with two broad-band sources of different mean wavelengths. The sensor is initialised as a 'white light' interferometer and then used as a dual-wavelength interferometer to determine the absolute path-length imbalance of the sensor [53].

(d) Frequency modulated continuous wave interferometry (FMCW) :

This technique of signal processing offers the widest measurement range. Here an unbalanced interferometer is illuminated by a frequency modulated laser diode, where the optical path path-length imbalance of the interferometer is measured from the harmonic contents of the output signal. Both serrodyne and sinusoidal frequency modulation have been used in different systems, generally much poorer resolution is obtained with FMCW compared with conventional interferometric techniques [54,55]. FMCW can be used simultaneously with another technique of signal processing, such that it is used only to identify the order of the interference fringe while the optical phase can be measured with higher resolution using the other technique, as introduced by Taylor et el [56].

(1.6) Introduction to the presented work :

The principle objective of the research undertaken for this thesis was the realisation of fibre optic based sensors for the measurement of quasi-static measurands. The system was required to be able of re-initialisation when switched on, be insensitive to environmental perturbations, have an extended measurement range and long term stability. Three different measurands are studied in this work; temperature, displacement and acceleration, although the same concepts apply equally well to many other quasi-static measurands.

In chapter (2), the theoretical bases of white light interferometry is studied using a single interferometer and a system constructed of a remote interferometer coherently tuned with a receiving interferometer. In this chapter the properties of the partially coherent optical sources used in fibre-optic sensing applications are reviewed and then the potential of CW multi-mode laser diodes as an alternative to the low coherence-length sources, previously used in such interferometric systems is studied. In chapter (3) we describe the practical implementation of two similar methods which exploit the technique of white light interferometry. In the first method a novel feedback servo is designed which allows the position of zero path-length imbalance, of the interferometer, to be located and maintained, and thus provides a unique operating point for the system. Hence the problems associated with the initialisation of interferometric sensors (i.e., determining the order of the interference) was overcome. In the second method, the feedback servo was developed to lock the interferometer to the quadrature point nearest to the position of zero path-length imbalance; that is, a phase difference of $\pi/2$ radians, this methods also provides a unique operating point for the system, moreover the sensor may be used to measure quasi-static measurands as well as high frequency measurands. In the second part of chapter (3) a multi-mode laser diode is used as an alternative to the low coherence-length sources to increase the resolution of sensing systems.

In chapter (4) we introduce a novel form of sensor, based on fibre optic technology, in which the sensing element is a miniature hemispherical air cavity Fabry Perot interferometer, addressed via a monomode optical fibre. The interferometer's transfer function is studied using

the Gaussian beam optics and then verified experimentally. In the experiments described, the sensor was used for the measurement of temperature, although it can be designed to sense different measurands such as, displacement, refractive index or pressure. To sense a quasi-static measurand, such as temperature, the interferometer is illuminated by a source of low coherence length, and a second receiving interferometer was used to balance the optical paths in the system, so that interference may be observed. Two different designs of temperature probes, based on the hemispherical cavity, were introduced. In the first design the probe was tested at temperatures below $100^{o}C$ while the second probe was designed to measure very high temperatures, above the softening temperature of the optical fibre. The hemispherical cavity can also be designed to serve as an A.C. sensor, such as a microphone or a contact vibration sensor.

In chapter (5) we describe a novel design of fibre-optic accelerometer based upon the hemispherical Fabry-Perot interferometer, introduced in chapter (4), in this design the sensing head is electrically passive and can be interrogated remotely. The sensing element is a weighted circular diaphragm. The displacement of the centre of the diaphragm produced by acceleration is studied theoretically and verified experimentally with the device used as a contact vibration sensor. In chapter (6) the low frequency performance of the accelerometer is studied. A modified optical design of the accelerometer is introduced such that the detrimental effects caused by optical sources frequency jitter as well as environmental perturbations are strongly reduced, moreover it is designed to have minimal cross-coupling. Two laser diodes, with distinct wavelengths, are used to illuminate the system in such a way as to increase its dynamic range and hence to re-initialise the accelerometer within this range.

The purpose of the concluding chapter (7) is to provide some overall comments, where necessary, and to suggest the directions for the future work.

References

[1] T.G.Giallorenzi, J.A.Bucaro, A.Dandridge, G.H.Sigel, JR., J.H.Cole, S.C.Rashleigh and R.G.Priest, " Optical fibre sensor technology " IEEE J. of Quantum Electronics, Vol.QE-18, No.4, April 1982, P.626.

[2] B.Culshaw, " Optical Fibre transducers ", The radio and electronic engineer, Vol.52, No.6, June 1982, P.283.

[3] D.A.Jackson " Monomode optical fibre interferometers for precision measurements ", J.Phys.E: Sci. Instrum. Vol.18, 1985, P.981.

[4] D.A.Jackson and J.D.C.Jones, " Fibre Optic Sensors ", Optica Acta, Vol. 33, No.12, 1986, P.1469.

[5] B.E.Jones, "optical fibre sensors and systems for industry " j. of physics E:Scientific Instruments, Vol.18, 1985, P.770.

[6] K.McKay, M.Mitchelmore and A.Van Blyenburgh, " Remote sensing on the battlefield with fibre optic cable ", The seventh European Fibre Optic Communication and Local Area Network conference, Amesterdam, June 1989, Conference proceeding P. 381.

[7] M.Corke, " Fibre optic sensors: Present and future ", Optical Engineering Reports, September 1987, P.4A,5A.

[8] J.H.Lyle and C.W.Pitt, " Vortex shedding fluid flowmeter using optical fibre sensor " Electronics Letters, Vol.17, 1981, P.244.

[9] D.A.Jackson, " Overview of fibre optic interferometric sensors ", Current Advances on Sensors, The Adam Hilger Series On Sensors, IOP publishing limited, 1987.

[10] A.D Kersey, A.Dandridge and T.B.Teveten, " Recent advances in

demodulation/multiplexing techniques for interferometric fibre sensors ", SPIE, Vol.734 Fibre Optics'87: Fifth international conference on fibre optics and opto-electronics, 1987, P.261.

[11] G.B.Hocker, " Fibre-optic sensing of pressure and temperature ", Applied Optics, Vol.18, No.9, May 1979, P.1445.

[12] N.Hartman, D.Vahely, R.Kidd and M.Browning, " Fabrication and testing of a Nickel-coated single mode fibre magnetometer ", Electronics Letters, Vol.18, No.5 March 1982, P.224.

[13] K.P.Koo, G.H. Sigel and JR. " An electric field sensor utilising a piezoelectric Polyvinylidene Fluoride (PVF_2) film in a single-mode fibre interferometer ", IEEE J. of quantum electronics, Vol. QE-18, No.4, April 1982, P.670.

[14] F.Farahi, P.A.Leilabady, J.D.C.Jones and D.A.Jackson, " Interferometric fibre-optic hydrogen sensor ", J.Physics E: Scientific Instruments, Vol. 20, 1987, P.432.

[15] " Workshop on single mode optical fibre sensor technology ", Course notes, University Of Kent and Sira Ltd. U.K., 1985, P.71-96.

[16] J.D.C.Jones, M.Cork, A.D.Kersey and D.A. Jackson, " Single-mode fibre optic holography ", J. Physics E: Scientific Instruments, Vol.17, 1984, P. 271.

[17] D.A.Jackson, J.D.C.Jones and R.K.Y.chan, " A high-power fibre optic laser doppler velocimeter " J.Physics E: Scientific Instruments, Vol.17, 1984, P.977.

[18] A.S.Gerges, T.P.Newson, F.Farahi, J.D.C.Jones and D.A.Jackson " A Hemispherical Air Cavity Fibre Fabry-Perot Sensor " Optics Communication Vol.68, No.3, Oct.1988, P.157.

[19] A.C.Lewin, A.D.Kersey and D.A.Jackson, " Non-contact surface vibration analysis using a monomode fibre optic interferometer incorporating an open air path " J.Physics E: Scientific Instruments, Vol.18, 1985, P.604.

[20] A.S.Gerges, T.P.Newson, J.D.C.Jones and D.A.Jackson, " High sensitivity fibre-optic accelerometer " Optics Letters, vol.14, No.4, Feb. 1989, P.251.

[21] D.A.Jackson, R.Priest, A.Dandridge and A.B.Teveten, " Elimination of drift in a single mode optical fibre ", Applied Optics, Vol.19, 1980, P.2926.

[22] A.Dandridge and A.B.Teveten, " Phase compensation in interferometric fibre optic sensors ", Optics Letters, Vol.7, 1982, P.279.

[23] K.Fritsch and G.Adamovsky ," Simple circuit for feedback stabilisation of a single-mode optical fibre interferometer ", Rev.Sci.Instrum. Vol.52 ,No.7, Jul.1981, P.996.

[24] K.P.Koo, A.B.Teveten and A.Dandridge, " Passive stabilisation scheme for fibre interferometers using 3x3 fibre directional couplers " Applied Physics Letters, Vol.41, No.7, Oct.1982, P.616.

[25] Th.Niemeier and R.Ulrich, " Quadrature outputs from fibre interferometer with 4x4 coupler ", Optics Letters, Vol.11, No.10, Oct.1986, P.677.

[26] A.Dandridge, A.B.Teveten and T.G.Giallorenzi, " Homodyne demodulation scheme for fibre optic sensors using phase generated carrier ", IEEE J. Quantum Electronics, Vol. QE-18, October 1982, P.1647.

[27] A.D.Kersey, D.A.Jackson and M.Corke, "Demodulation scheme for fibre interferometric sensors employing laser frequency switching ", Electronics Letters, Vol.19, Feb. 1983, P.102.

[28] D.A.Jackson, A.D.Kersey and A.C.Lewin, " Fibre gyroscope with passive quadrature detection ", Electronic Letters, Vol.20, No.10, May 1984, P.399.

[29] A.D.Kersey, M.Corke, J.D.C.Jones and D.A.Jackson, " Signal recovery techniques for unbalanced fibre interferometric sensors illuminated by laser diodes " IEE Conference on Optical Fibre Sensors, London, 1983, P.43.

[30] " Workshop on single mode optical fibre sensor technology ", Course notes, University Of Kent and Sira Ltd. U.K., 1985, P.153.

[31] P.Horowitz and W.Hill ," The art of electronics ", Cambridge University Press, 1986, P.628.

[32] F.J.Eberhardt and F.A.Andrews, " Laser heterodyne system for measurement and analysis of vibration " , J. Acoust. Soc. Am., Vol.48, 1970, P.603.

[33] D.E.N.Daves and S.Kingsley, " Method of phase-modulating signals in optical fibres : application to optical-telemetry systems ", Electronics Letters, Vol.10, 1974, P.21.

[34] M.A.Nokes, B.C.Hill and A.E.Barelli, " Fibre optic heterodyne interferometer for vibration measurements in biological systems ", Rev. Sci. Instruments, Vol. 49, June 1978, P.722.

[35] D.A.Jackson, A.D.Kersey, M.Corke and J.D.C.Jones, " Pseudo-heterodyne detection scheme for optical interferometers ", Electronics Letters, Vol.18, 1982, P.1081.

[36] P.Akhavan Leilabady, J.D.C.Jones and D.A.Jackson, " Monomode fibre optic strain gauge with simultaneous phase and polarisation state detection ", Optics Letters, Vol.10, November 1985, P.576.

[37] I.Sakai, G.Parry and R.C.Youngquist, " Multiplexing fibre optic sensor by frequency modulation : cross term consideration ", Optics Letters, Vol.11, 1986, P.183.

[38] B.Y.Kim and H.J.Shaw, " Phase-reading, all-fibre-optic gyroscope ", Optics Letters, Vol.9, No.8, August 1984, P.378.

[39] A.C.Lewin, A.D.Kersey and D.A.Jackson," Two wide-dynamic-range signal-recovery schemes for the fibre-optic gyroscope ", IEE Proceedings, Vol.132. Pt.J., No.5, October 1985, P.271.

[40] J.H.Cole, B.A.Danver and J.A.Bucaro, " Synthetic-heterodyne interferometric demodulation

" , IEEE J. Quantum Electronics, Vol. QE-18, April 1982, P.694.

[41] A.Dandridge and A.B.Tveten, " Phase noise of single-mode diode lasers in interferometer systems ", Applied Physics Letters, Vol.39, No.7, October 1981, P.530.

[42] D.A.Jackson ," Introduction to fibre optic interferometers and their application as sensors ", Report prepared for the Optical Sensors Collaborative Association (OSCA), March 1988, P.20.

[43] T.P.Newson, F.Farahi, J/.D.C.Jones and D.A.Jackson," Reduction of semiconductor laser diode phase and amplitude noise in interferometric fibre optic sensors ", The seventh conference on Fibre Optics and Opto-electronics, London, 1989, SpIE Conf. Proceedings, Vol.1120, Paper 16.

[44] B.Dahmani, L.Hollberg and R.Drullinger, " Frequency stabilisation of semiconductor lasers by resonant optical feedback ", Optics Letters, Vol.12, No.11, Nov.1987, P.876.

[45] D.J.Webb, J.D.C.Jones and D.A.Jackson, " Laser diode frequency stabilisation techniques for interferometric sensors ", Proceeding of Fibre Optics'88 : Sixth International conference on fibre optic and optoelectronics, London, April 1988, SPIE, Vol.949, Paper No. 27.

[46] Z.Bingkun, Z.Hanyi, W.Yuanxiang, Z.Jianying, L.Jian and P.Zhenwu, " 24 h frequency stabilisation of an slm external-cavity semiconductor laser " Electronics Letters, Vol 23, No. 5, Feb 1987, P.194.

[47] A.S.Gerges, T.P.Newson and D.A.Jackson, " Practical fibre-optic-based submicro-g accelerometer free from source and environmental perturbations " Optics Letters, Vol. 14, No.20, October 1989, P.1155.

[48] A.D.Kersey, A.Dandridge, and W.K.Burns, " Two-wavelength fibre gyroscope with wide dynamic range " Electronics Letters, Vol.22, 1986, P.935.

[49] D.J.Webb, J.D.C.Jones and D.A.Jackson, " Extended range interferometry using a coherence

tuned synthesised dual wavelength technique with multimode fibres ", Electronics Letters, Vol.24, No.18, Sep 1988, P.1173.

[50] A.S.Gerges, T.P.Newson and D.A.Jachson, " Extrinsic dual-wavelength fibre-optic based accelerometer with common mode compensation ", OFS-6 '89- Paris, Springer Proceedings in physics, Vol.44, September 1989, P.207.

[51] P.A.Leilabady, J.D.C.Jones, M.Corke and D.A.Jackson, " A Dual interferometer implemented in parallel on a single birefringent monomode optical fibre ", J. Physics E: Sci.Instrum. Vol.19, 1986, P.143.

[52] F.Farahi, D.J.Webb, J.D.C.Jones and D.A.Jackson, " Simultaneous measurement of temperature and strain : Cross sensitivity considerations ", J. of Lightwave Technology, Vol. 8, No. 2, February 1990, P. 138.

[53] A.D.Kersey and A.Dandridge, " Dual-wavelength approach to interferometric sensing ", SPIE, Vol.798 Fibre optic sensors 2, 1987, P.176.

[54] P.Giles, D.Uttam, B.Culshaw and D.E.N.Daves, " Coherent optical-fibre sensors with modulated laser source ", Electronics Letters, Vol.19, No.1, January 1983, P.14.

[55] D.J.Webb, R.M.Taylor, J.D.C.Jones and D.A.Jackson, " Interferometric optical path difference measurement using sinusoidal frequency modulation of a diode laser ", Optics Communications, Vol.66, No.5,6, May 1988, P.245.

[56] R.M.Taylor, D.J.Webb, J.D.C.Jones and D.A.Jackson, " Extended-range fibre polarimetric strain sensor ", Optics Letters, Vol.12, No.9, September 1987, P.744.

CHAPTER (2)

Interferometry using low coherence–length sources

(2.1) Introduction

We have already seen that interferometric sensors offer the most accuracy in optical metrology [1,2]. A basic problem which must be addressed in all systems of this kind is how to transduce optical information from the interferometer to an electrical signal in an accurate and reproducible manner over a reasonably large measurement range.

We have also seen that two fundamental difficulties arise in all interferometric sensors. Firstly, the unambiguous measurement range of the system is limited by the periodic nature of the interferometric transfer function to a change in the optical phase of (2π) radians, or one interferometric fringe. Secondly, the basic unit of measurement is the source wavelength, which cannot be regarded as constant- especially for diode lasers.

We have discussed the possibility of extending the unambiguous dynamic range using phase tracking techniques, to follow changes in optical path length over many wavelengths, but this method is only useful provided that the tracking process is never interrupted-for example, by power failure. Under these circumstances, the instrument would have to be re-initialised. Another useful approach is to derive two outputs from the interferometer of different periods, so that the phase difference between the two outputs has a longer period than that of either of the outputs separately. This technique is analogous to the familiar mechanical vernier. Two approaches have been discussed for producing the two outputs. One uses a single source with a birefringent fibre

interferometer [3]. Two outputs are derived, one corresponding to each of polarisation eigen-modes of the fibre used. Because the two modes have different refractive indices, the periods of the interferometric transfer functions for each mode differ slightly. The second approach uses a non-birefringent interferometer, but employs two sources simultaneously, with distinct wavelengths [4]. An output is derived from the interferometer for both of the sources.

None of the techniques described above address the problem of wavelength drift of the source used. The error introduced by this effect may become very severe in unbalanced interferometers where path length differences of a great many wavelengths exist. It would be possible to correct this difficulty by either stabilising or measuring the source wavelength using an auxiliary optical system [5]. However, we have sought a different approach which does not rely on an accurate determination of the source wavelength. The technique makes use of an interferometer illuminated by a short coherence-length source, and the visibility of the output interference signal is measured. The visibility function is not periodic, and has its maximum at a position independent of the source wavelength (in a non dispersive medium), the two basic problems discussed above are hence circumvented.

In this chapter we are going to study the theoretical basis of white light interferometry and the different low coherence-length sources used in fibre-optic sensing applications. Finally we will study the potential of CW multi-mode laser diodes as an alternative to these sources, previously used in such interferometric systems.

(2.2) Interference of partially coherent light :

In the previous chapter the use of an interferometer illuminated by a monochromatic light was considered. The phase difference among the component beams of the interferometer was considered constant during the time of measurement, this is called perfectly coherent light. Light from a real optical source is never strictly coherent, because any source consists of very many radiation atoms and hence it has a finite dimensions. Moreover even the sharpest radiated line will

have a finite spectral width. For these reasons any optical source may be classified by its coherence properties, where the degree of coherence varies from very high for sources, such as gas laser, to very low for broad band sources such as white light lamps. Generally the amplitude and the phase of the radiated field, from a real source of light, will vary with time in a random fashion, such that it is more meaningful, to define the irradiance I, as a statistical time average.

The transfer function of an interferometer illuminated by a partially coherent light is described as a function of the mean optical frequency of the light and of a corresponding auto-correlation function, which describes the coherence properties of source. Considering the case of interference of two stationary fields E_1 and E_2 , the irradiance I is defined as:

$$I = \langle (E_1 + E_2).(E_1^* + E_2^*) \rangle \tag{2.1}$$

$$= \langle |E_1|^2 + |E_2|^2 + 2\mathrm{Re}[E_1 . E_2^*] \rangle$$

where Re [ ] means the real part of the enclosed complex quantity and < > means time averaged, i.e

$$\langle f \rangle = \lim_{T \to \infty} \frac{1}{T} \int_0^T f(t)dt \tag{2.2}$$

A stationary field has the property that its time average is independent of the choice of the origin of time [6-8] . If the optical fields are considered to have the same state of polarisation, so that their vectorial nature can be ignored, then equation (2.1) can be written in the form:

$$I = I_1 + I_2 + 2\mathrm{Re} \langle E_1 E_2^* \rangle$$

where $I_1 = \langle |E_1|^2 \rangle$, $I_2 = \langle |E_2|^2 \rangle$ and $2\mathrm{Re} \langle E_1 E_2^* \rangle$ is called the interference term.

If the two fields E_1 and E_2 originate from the same source and differ because of a difference in their optical paths, the interference term can be expressed as $2\mathrm{Re} \langle E(t)E^*(t+\tau) \rangle$, where τ is the retardation time of one beam in the interferometer with respect to the second.

The function $\Gamma_{11}(\tau) = \langle E(t)\, E^*(t+\tau) \rangle$ is known as the self coherence function of the field

and the normalised auto-correlation function $\gamma_{11}(\tau)$, which is called the degree of partial coherence is defined as:

$$\gamma_{11}(\tau) = \frac{\Gamma_{11}(\tau)}{\sqrt{I_1 I_2}} \tag{2.3}$$

$\gamma_{11}(\tau)$ is a complex function which may be represented in the form of a magnitude and a phase, i.e. $\gamma_{11}(\tau) = |\gamma_{11}(\tau)|\, e^{i\Delta\phi(\tau)}$. In terms of $|\gamma_{11}(\tau)|$ we have the following types of coherence:

$|\gamma_{11}(\tau)| = 1$ Complete coherence

$0 < |\gamma_{11}(\tau)| < 1$ Partial coherence

$|\gamma_{11}(\tau)| = 0$ Complete incoherence

From the definition of $\gamma_{11}(\tau)$, it has the following properties :

$$|\gamma_{11}(0)| = 1$$

$$|\gamma_{11}(\tau)| \leq 1 \text{ for } all\ \tau$$

In a two beam interferometer with path-length difference ΔL , the interference pattern may be observed if the absolute value of $\gamma_{11}(\tau)$ has a value other than zero, where $\tau = \Delta L/C$ and C is the free-space speed of light. The irradiance is then expressed as follows:

$$I = I_1 + I_2 + 2\sqrt{I_1 I_2}\ \mathrm{Re}[\gamma_{11}(\tau)]$$

$$= (I_1 + I_2)\left[1 + \frac{2\sqrt{I_1 I_2}}{I_1 + I_2}\ |\gamma_{11}(\tau)|\ \mathrm{Re}[e^{i\Delta\phi(\tau)}]\right]$$

$$= (I_1 + I_2)\left[1 + \frac{2\sqrt{I_1 I_2}}{I_1 + I_2}\ |\gamma_{11}(\tau)|\ Cos\ \Delta\phi(\tau)\right] \tag{2.4}$$

where $\Delta\phi(\tau) = 2\pi n \nu\tau = \frac{2\pi\nu n}{C}\Delta L$,

n is the index of refraction of the optical medium of the interferometer (fibre core) and ν is the light frequency. As $Cos\Delta\phi(\tau)$ varies from 1 to -1, the intensity will vary between the limits, I_{max}

and I_{min} respectively. The interference visibility is defined as the ratio :

$$V = \frac{I_{max} - I_{min}}{I_{max} + I_{min}} \tag{2.5}$$

$$= V_o \, |\gamma_{11}(\tau)|$$

where V_o is called the visibility constant. It gives the maximum value of the fringe visibility, which occurs when the interferometer is balanced, ie when $\Delta L = 0$, and $\gamma_{11}(0)=1$, hence :

$$V_o = 2 \frac{\sqrt{I_1 I_2}}{I_1 + I_2} \tag{2.6}$$

The function $|\gamma_{11}(\tau)|$ is governed by the coherence properties of the source, while the visibility constant V_o is dependent on the quality of the interferometer. In particular case, if $I_1 = I_2$ then $V_o = 1$ and equation (2.4) may be written in the more familiar form :

$$I = I_{mean} \, (1 \pm V Cos \, \Delta\phi(\tau)) \tag{2.7}$$

where $I_{mean} = (I_1 + I_2)$. The positive and negative signs correspond to the two complementary outputs, which are available at the output of some interferometric configuration, such as Mach-Zehnder and Michelson interferometers.

For the signal processing schemes, we have used, it was more convenient to work in terms of the interference fringe amplitude, A, rather than the fringe visibility, where :

$$A = I_{max} - I_{min} \tag{2.8}$$

$$= A_o \, |\gamma_{11}(\tau)|$$

It may be noted that the maximum fringe amplitude ($A_o = 4\sqrt{I_1 I_2}$) results also when the two arms of the interferometer are exactly balanced ($\Delta L = 0$).

From equations (2.5 and 2.8) it is clear that the interference fringe visibility as well as the fringe amplitude are directly proportional to the absolute value of the auto-correlation function of the optical source. In practice the fringe amplitude (visibility) may be changed due to several

factors, not just the auto-correlation function of the source. As an example any perturbation leading to a change in the relative polarisation state of the two interfering fields E_1 and E_2, would result in a change of the fringe amplitude (visibility).

Whatever happens to the interferometric system as a whole, the maximum value of the fringe amplitude (visibility) always results when the interferometer is exactly balanced, ie when $\Delta L = 0$. The physical meaning of balancing the interferometer is to have equal group delays in its arms. This implies a fixed position of $\Delta L = 0$, if the interferometer arms are of non-dispersive medium. If not, this position will change, specially if the arms of the interferometer are very long, as a function of the mean wavelength of the light illuminating the system. A second-order dispersion effect may change the pattern of interference fringes, specially if a very broad light source is used [9].

(2.3) The auto-correlation function of quasi-monochromatic sources :

The electric field radiated from a real optical source can be represented by an infinite number of monochromatic fields, it can be described mathematically as :

$$E(t) = \int_0^\infty E_o(\nu)\, Cos[\, 2\pi\nu t + \phi(\nu)\,]\, d\nu \qquad (2.9)$$

where $E_o(\nu)d\nu$ is the amplitude of the field in a band of frequencies from ν to $\nu+d\nu$ and $\phi(\nu)$ is the corresponding phase constant.

For quasi-monochromatic light, the spectral distribution function is peaked about $\nu = \nu_o$, and tends to zero rapidly as ν departs much from the vicinity of the mean frequency ν_o , the optical field may then be written in the form :

$$E(t) = E_o(t)\, Cos[\, 2\pi\nu_o t + \phi(t)\,] \qquad (2.10)$$

where $E_o(t)$ and $\phi(t)$ are slowly varying functions compared with $Cos(2\pi\nu_o t)$. Real quasi-monochromatic light fields have randomly varying amplitudes $E_o(t)$ and phases $\phi(t)$, such that it must be described statistically. The corresponding output irradiance of an interferometer, with

path-length imbalance of ΔL , considering $V_o = 1$, may be represented as :

$$I = I_{mean} \left[1 + |\gamma_{11}(\Delta L)| \, Cos \left(\frac{2\pi\nu_o}{C} \Delta L \right) \right] \tag{2.11}$$

where I_{mean} is the average intensity of the interferometer output. Equation (2.11) represents the output of an interferometer illuminated with the mean frequency of the source, ν_o , and with an auto-correlation function, $\gamma_{11}(\Delta L)$, which must be calculated based on the statistical properties of the light source.

The ststistical properties of the light is governed by the radiation broadening mechanisms of the source, which can be classified into homogeneous and inhomogeneous broadening. If all of the radiated atoms have the same transition centre frequency and the same resonance lineshape then the broadening is termed homogeneous; such as natural life-time and collision broadening mechanisms, the corresponding spectral profile is described by a Lorentzian spectral distribution function. On the other hand, in some situations each atom has a slightly different resonance frequency for the same transition. The corresponding lineshape is then the average of the individual ones and the mechanism is termed inhomogeneous, where the corresponding spectral profile is described by a Gaussian distribution function. Doppler broadening, local variations of the source temperature, pressure, applied magnetic field and source crystal imperfections lead to inhomogeneous broadening [10].

The Weiner-Khintchine theorem states that the normalised auto-correlation function $\gamma_{11}(\tau)$ is given by the inverse Fourier transform of the normalised power spectral density function, $P(\nu) \alpha | E_o(\nu) |^2$, as follows :

$$\gamma_{11}(\tau) = \int_0^\infty P(\nu) \exp[-2\pi i \nu\tau] \, d\nu \tag{2.12}$$

where $\int_0^\infty P(\nu) \, d\nu = 1$. It is more usual to express the spectral density function of light sources as $P(\nu - \nu_o)$, where ν_o is the mean optical frequency of the source. The inverse Fourier transform of $P(\nu - \nu_o)$ is given by $\gamma_{11}(\tau) \exp(2\pi i \nu_o \tau)$, [11].

For homogeneous broadening mechanisms, the source spectral density $P(\nu)$ is represented by the normalised Lorentzian distribution function as :

$$P(\nu) = \frac{2\,\overline{\Delta\nu}}{\overline{\Delta\nu}^2 + 4\pi^2(\nu - \nu_o)^2} \tag{2.13}$$

where $\frac{1}{2\pi}\,\overline{\Delta\nu}$ is the mean half power width of the spectral function of the source. The corresponding auto-correlation function may be represented by :

$$\gamma_{11}(\Delta L) = e^{-[\frac{|\Delta L|}{L_c} + i\frac{2\pi\nu_o}{C}\Delta L]}$$

and its modulus is:

$$|\gamma_{11}(\Delta L)| = e^{-|\Delta L|/L_c} \tag{2.14}$$

where L_c is the 1/e coherence length of the source, $L_c = \frac{C}{\overline{\Delta\nu}}$.

For inhomogeneous broadening mechanisms, the spectral density is represented by a normalised Gaussian distribution function in the form :

$$P(\nu) = \frac{1}{\Delta\nu}\, e^{[-\pi(\frac{\nu - \nu_o}{\Delta\nu})^2]} \tag{2.15}$$

where $\frac{1}{\sqrt{\pi}}\,\Delta\nu$ represents the 1/e power width of the Gaussian spectral function [12,13]. The auto-correlation function may be written as :

$$\gamma_{11}(\Delta L) = e^{-[\frac{\pi}{2}(\Delta L/L_c)^2 + i\frac{2\pi\nu_o}{C}\Delta L]}$$

and

$$|\gamma_{11}(\Delta L)| = e^{-\frac{\pi}{2}(\Delta L/L_c)^2} \tag{2.16}$$

where $L_c = \frac{C}{\sqrt{2}\,\Delta\nu}$.

In both cases, it is clear that; as the spectral width of the light, illuminating the system, increases the visibility function will fall off more rapidly. Figure (2-1) illustrates the normalised

auto-correlation function versus the path-length imbalance of the interferometer, normalised with respect to the coherence length of the light, as calculated using equations (2.14, 2.16). Both the visibility function and the fringe amplitude are maximum when the path-length imbalance is zero and decrease towards zero when the path-length imbalance exceeds the coherence length of light.

Figure (2-2) shows a simulation of the output of an interferometer illuminated by a source of coherence-length of 15 μm with Lorentzian line profile. The interference fringe occurring from $\Delta L = \lambda_o/2$ to $\Delta L = +\lambda_o/2$, where λ_o is the mean optical wavelength of the source ($\lambda_o = C/\nu_o$), may be called the central fringe of interference. In a non-dispersive system, it has the maximum amplitude within the whole interference pattern of the system irrespective of the line profile of the optical source, or the interferometric system. This feature is central to the signal processing scheme introduced in chapter (3) where an electronic servo is used to locate the central interference fringe and then to lock the interferometer either to position of zero path-length imbalance, i.e. at the position of maximum interference visibility, or at $\Delta L = \lambda_o/4$, the point in the transfer function we have called 'the first quadrature point with negative slope'. From the above discussions, it is clear that a source with a short coherence length is preferred for such techniques as the corresponding auto-correlation function will be sharper and hence the position of the central interference fringe may be located more accurately.

(2.4) Partially coherent sources for interferometric fibre-optic sensors :

The properties of the sources required for fibre optic interferometric sensors depend critically on the application and the method of signal processing. Conventional interferometric techniques require that the coherence length of the source is very long, therefore single mode laser sources are used.

For applications based on 'white light' interferometry, it is often advantageous to use a source with as short a coherence length as possible. Typical coherence lengths of various optical sources are shown in figure (2-3), where their coherence-length are seen to range from a few microns (Tungestun filament sources) to several Kilo-meters for He-Ne single mode gas lasers.

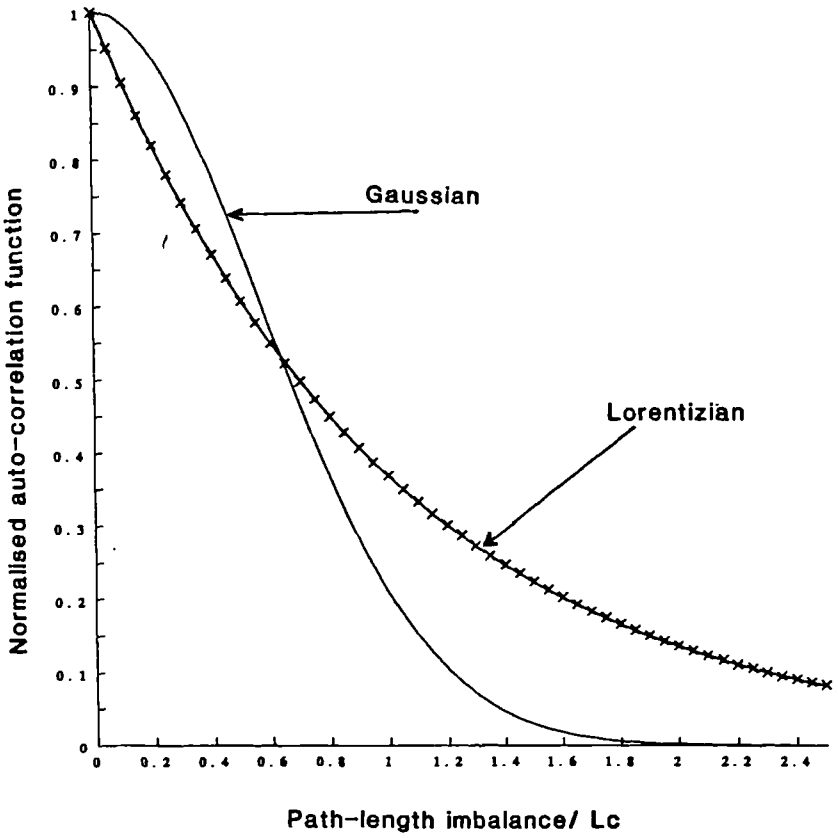

Figure (2-1) : The normalised auto-correlation function versus the path-length imbalance of the interferometer, normalised w.r.t. the coherence length.

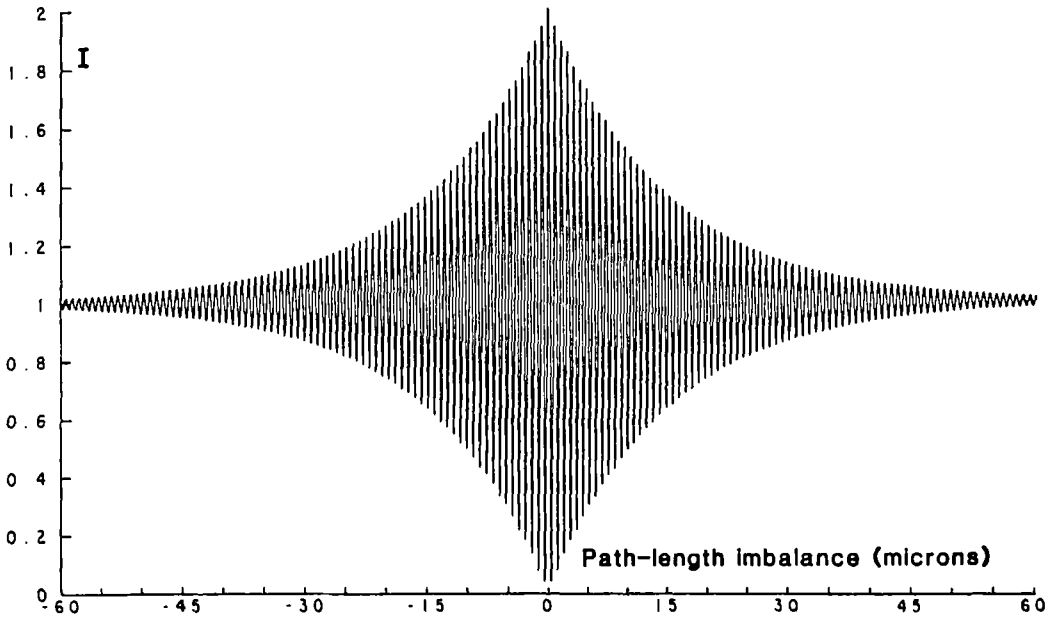

Figure (2-2) : Computer simulation of the output of an interferometer illuminated by a broad-band Lorentizian source as a function of the optical path difference.

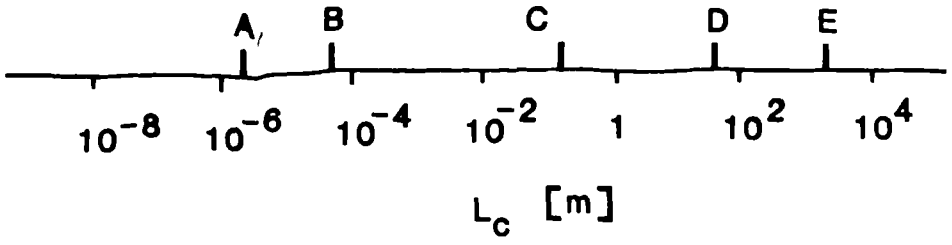

Figure (2-3) : Typical coherence lengths of various optical sources.

A : Tungestun lambs, B : LED, C : red cadmium line,

D : monomode laser diode, E : HeNe single-mode laser.

The main, common, requirement for an optical source, apart from its coherence properties, is its ability to couple a useful amount of power into the fibre, such that the signal to noise ratio at the output of the system, and hence its phase resolution, is large. The relatively small diameter of the optical fibre core requires the use of sources with very high spatial coherence for efficient coupling of radiation into the fibre.

Tungestun filament sources emit useful power with a very short coherence length. The principle disadvantage of such sources is the very low launching efficiency in coupling its output beam into a fibre, this is mainly because of their extended emitting area and great beam divergence. Despite these problems this type of source has been used to illuminate interferometric fibre optic sensing systems, utilising multi-mode fibre links (core diameter $\approx 100\mu m$). A coherence length of about $2\mu m$ has been reported for this type of source [14,15].

The most commonly used low coherence-length sources are the light emitting solid state diodes (LED's). These sources are available at a variety of wavelengths. Structures have been optimised to enable efficient coupling of their output power into multi-mode optical fibre. Their coherence length is suitable for white light interferometric sensing techniques ($\approx 30\mu$ m or less).

One advantage of white light interferometry is that multi-mode fibre may be used hence even with LED sources the power coupled into the sensor system is sufficient to produce reasonable signals at the output [16-19]. In general multi-mode fibres are not the best fibre to be used within interferometric systems as many factors limit its applicability. Light emerging from a multi-mode fibre may be regarded as emerging from an extended source, such that fringes of equal inclination are produced at the output. To obtain a reasonable interference visibility, the path length-imbalance of the interferometer must be limited . The fibre links must also be protected against thermal and mechanical instabilities, to avoid power re-distribution among the different propagation modes, inside the multi-mode fibre links, thus causing signal degradation due to relative modal delays [20]. A major requirement with multi-mode fibre linked interferometers is that no spatial filtering of the light should occur.

The use of single mode optical fibre is extremely important for interferometric systems. It acts as a low-pass spatial filter which renders the output field to be spatially coherent and hence increases the usable range of the optical path-length imbalance of the sensors. Monomode optical fibres can be used to link two interferometers (or more), to form a part of the interferometric system itself or to form the system completely. Recent work has been done to maximise the coupling efficiency of surface-emitting LED's to single mode fibres. Power coupling efficiency of -35 dB to -28 db was reported to a 4.5 μm and 5 μm core diameter monomode fibre respectively [21,22].

A novel solid state optical source known as a super luminescent diode (SLD), commonly used in fibre optic gyroscopes, has also been used in white light interferometry by Al-Chalabi et el, where a single mode optical fibre was used to link the source optical power to a system of bulk-optic Mach-Zehnder interferometers [23]. SLD is essentially a laser diode in which one of the output facets has an anti-reflection coating to prevent the build up of stimulated emission [24]. The spot size and the numerical aperture of these sources are still very well matched to typical monomode fibre. At the present time, due to limited demand, their price is much higher than that of laser diode sources.

The coherence properties of semiconductor lasers both below and above threshold have been the subject of research for a number of years. Below threshold, the output spectral envelope is very broad and resembles an LED. When it is driven through the 'lasing' threshold, the stimulated gain causes the injected carriers to recombine. The charge density thus saturates, and the spectral envelope narrows-eventually to permit the oscillation of only a single longitudinal mode [25,26]. In order for a semiconductor laser to show single longitudinal mode operation, its structure must produce very uniform distribution of charge carriers and photons. Homogeneous broadening mechanisms are usually predominant in single mode semiconductor lasers driven below and in the vicinity of threshold [25-27]. The dimensions of the 'laser shape' are such that it is possible to focus the output power of these laser diodes to a very small diffraction limited spot, so that the beam may be efficiently coupled into monomode optical fibre [28].

The coherence length of a range of GaAlAs laser diodes was measured by Dandridge as a function of the injection current [29]. He showed that these laser diodes can be used as low coherence-length sources if biased below threshold. Coherence lengths of less than hundred microns was reported for laser diodes biased just below threshold where the spontaneous emission is predominant. Around the threshold region the spontaneous emission spectrum will resolve into a discrete multi-mode spectrum with a very complicated coherence properties [30]. The use of multi-mode lasers as the source for white light interferometry is discussed in section (2.5).

Solid-state laser diodes, biased below threshold, have been used by many authors to illuminate interferometric systems constructed from monomode fibre [31-33]. The advantages of using these sources are :(i) the coherence-length can be tuned by changing the diode injection current, (ii) when operated as a conventional laser it greatly facilitate the alignment of the optical system due to its greatly increased optical output, (iii) they are relatively inexpensive and (iv) a hybrid operation is also possible, where the system could be initialised with the laser diode biased below threshold, and then switching the laser on, above threshold, to permit much higher resolution.

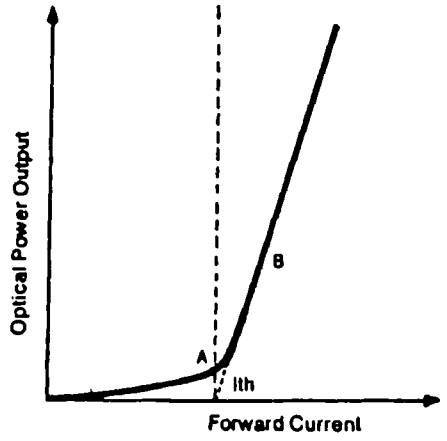

Figure (2-4) : Output characteristic of a typical laser diode.

A : below threshold, B : above threshold.

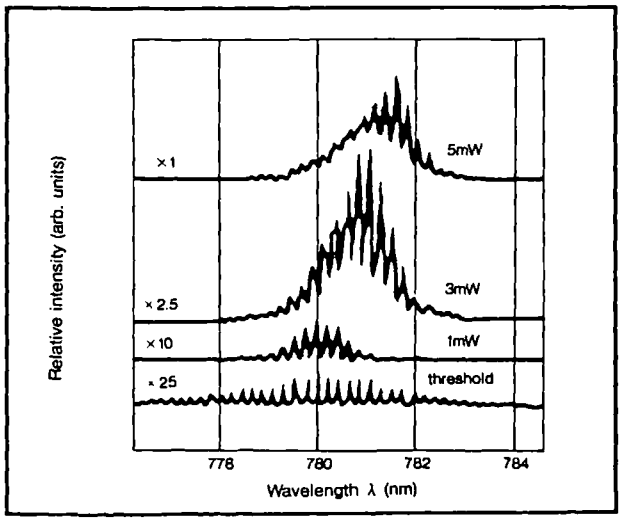

Figure (2-5) : Typical spectra of a multi-mode laser diode, under CW operation.

The penalty for operating a laser diode below threshold is that the amount of light emitted will be relatively low, by comparison to the potential of the device when lasing in the normal way as shown by a typical laser characteristic in figure (2-4).

Multi-mode laser diodes, such as those used in compact disc players, have coherence properties which could be very useful for interferometric sensors. The lasers are available and cheap and offer a small emitting area, therefore it is possible to couple suitable level of optical power into monomode fibres. The coherence properties of these sources are more complex than LED's and as shown later, this leads to certain restrictions in the operation of tandem interferometers for sensor applications.

(2.5) Multi-mode laser interferometry :

The emission spectrum of a multi-mode laser may be considered as a continuous, wide-band, spontaneous emission spectrum characteristic of a Gaussian random noise process superimposed with multi-longitudinal modes of oscillation. Figure (2-5) shows a typical emission spectra, under CW operation, for a Mitsubishi laser diode, ML4406. The peak wavelength is dependent on the operating temperature and the injection current of the laser [34]. The oscillation line-width ranges from several hundred MHz to a few GHz, with homogeneously broadened line shape. The envelope of the oscillation mode intensities is normally approximated to a Lorentzian function, centred at the peak wavelength of the laser diode [35-37].

For an interferometric system, illuminated with a multi-mode laser, interference fringes are only observed for discrete values of the interferometer path-length imbalance. This may be explained by considering the linear combination of the output intensity corresponding to each mode superimposed on the output intensity corresponding to spontaneous emission [13].

The output irradiance of a two beam interferometer, with optical path-length imbalance of ΔL , illuminated with a multi-mode laser diode may be represented as :

$$I = I_s[1 + K_s \, Cos \, \Delta\phi_o(\Delta L)] + \sum_{j=-m/2}^{+m/2} I_j[1 + K_j \, Cos \, \Delta\phi_j(\Delta L)] \qquad (2.17)$$

where m is even and (m + 1) is the total number of modes of oscillation, including the central one. I_j,K_j and $\Delta\phi_j(\Delta L)$ are the intensity, visibility function and optical phase corresponding to the j^{th} mode respectively. $\Delta\phi_j(\Delta L) = \frac{2\pi\nu_j}{C}\Delta L$, where ν_j is the frequency of the j^{th} mode. I_s,K_s are the intensity and the visibility function corresponding to the spontaneous emission respectively, while $\Delta\phi_o(\Delta L)$ is the optical phase corresponding to its mean (peak) frequency , ν_o. The visibility function of each mode (or of the spontaneous emission) is given by the inverse Fourier transformation of the corresponding power spectral function of the mode. In equation (2.17), the peak frequency of spontaneous emission was considered to match that of the central mode of oscillation.

The irradiance I contains an average DC level, I_{mean}, plus an oscillatory term I_{osc}, where :

$$I_{mean} = I_s + \sum_{j=-m/2}^{m/2} I_j \tag{2.18}$$

$$I_{osc} = I_s K_s \, Cos\, \Delta\phi_o(\Delta L) + \sum_{j=-m/2}^{m/2} I_j K_j Cos\Delta\phi_j(\Delta L) \tag{2.19}$$

The output irradiance of the interferometer may be represented in the familiar form of equation (2.11) as if the system is illuminated with the mean frequency of the source ν_o. The corresponding absolute value of auto-correlation function can be calculated as:

$$|\gamma_{11}(\Delta L)| = \frac{I_{osc}}{I_{mean}\, Cos\, \Delta\phi_o(\Delta L)}$$

$$= \frac{1}{I_{mean} Cos\Delta\phi_o(\Delta L)} \left[I_s K_s \, Cos\, \Delta\phi_o(\Delta L) \right.$$

$$\left. + \sum_{j=-m/2}^{m/2} K_j I_j \, Cos\, \Delta\phi_j(\Delta L) \right] \tag{2.20}$$

Neglecting the effects of dispersion in the medium of the laser cavity, its group index of refraction n_g may be considered as a constant, independent of the emitted wavelength.

Correspondingly each successive mode is separated by an equal frequency ΔF, given by :

$$\Delta F = \frac{C}{2l_{cav}} \tag{2.21}$$

where l_{cav} is the optical length of the laser cavity, $l_{cav} = n_g\, l$ and l is the length of the laser cavity [38]

For simplicity we assume the modes of oscillation are symmetrically distributed about the mean frequency ν_o . It is also reasonable to assume that all the modes have the same spectral width, thus neglecting the chromatic dispersion of the interferometer medium (within the band-width of the source) we get :

$$a)\ K_{-m/2} = \cdots = K_o = \cdots = K_{m/2} = K$$

$$b)\ I_{-j} = I_j$$

$$c)\ \nu_j = \nu_o + j\,\Delta F$$

Knowing that $Cos(A-B) = CosA\ CosB + SinA\ SinB$, the absolute value of the source auto-correlation function may be simplified as :

$$|\gamma_{11}(\Delta L)| = \frac{1}{I_{mean}} \left[(I_o K + I_s K_s) + 2K \left[\sum_{j=1}^{m/2} I_j\, Cos\left(\frac{2\pi\,\Delta L}{C}\, j\,\Delta F\right)\right]\right] \tag{2.22}$$

Equation (2.22) proves the linearity of the Fourier transformation, i.e if the normalised spectral distribution function, of the source, is a superposition of individual distribution functions the corresponding auto-correlation function will be a similar superposition of the auto-correlation functions of each individual distribution [11].

The visibility function K is a Lorentzian auto-correlation function, $K = \exp[-|\Delta L|/L_{cm}]$, where L_{cm} is the coherence length corresponding to the modal spectral line-width. Reisinger et el [39] proved that the apparent value of L_{cm} as determined by measuring the source auto-correlation function, interferometrically, is much less than the corresponding value if it is determined by measuring the modal spectral width. They explained this phenomenon as a direct result of the

source second-order dispersion ($dn_g / d\lambda \neq 0$), leading to unequal modal frequency separation [37,38]. Spontaneous emission is a wide-band Gaussian radiation profile, hence the visibility function K_s may takes the form : $K_s = \exp[-\pi/2\,(\Delta L / L_{cs})^2]$, where L_{cs} is the coherence length corresponding to spontaneous emission line-width. Generally the spontaneous emission line width is much greater than that of the oscillating modes, hence $L_{cs} \ll L_{cm}$.

Figures (2-6 a,b) illustrate a computer simulation of the spectrum of a typical multi-mode laser diode together with the corresponding absolute value of its auto-correlation functions, as calculated using equation (2.22), versus the optical path-length imbalance of the interferometer, ΔL . The spectral profile of the source was generated from the superposition of a Gaussian profile representing the spontaneous emission, with peak wavelength of 800 nm and 1/e spectral width of about $8.7x10^{11}$ Hz, and a set of symmetrical oscillating modes. The modal line-width was taken as 7 GHz with an intermodal separation of 150 GHZ. The variation in the intensity of the modes was obtained by multiplying the modal pattern with a Lorentzian function, centred at the peak frequency and with half-power width of $\pm$ 300 GHz , figure (2-6 a), and $\pm$600 GHz, figure (2-6 b).

It can be shown, from equation (2.22) and as illustrated in figure (2-6) that for $\Delta L = 0$, the visibility functions K and K_s equal unity, hence $|\gamma_{11}(0)| = 1$. As ΔL increases the relative phases of the modes change continuously, as they oscillate at different frequencies, thus the amplitude of the total interference signal and hence $|\gamma_{11}(\Delta L)|$ decreases dramatically. If ΔL continues to increase the value of $|\gamma_{11}(\Delta L)|$ will start to increase again giving rise to a large amplitude interference packet as the phase difference between each adjacent modes approaches 2π, ie at $(2\pi\,\Delta L\,\Delta F)/C = 2\pi$ which corresponds to $\Delta L = 2\,l_{cav}$. The amplitude of this peak will be less than unity because of the modal line width, second order dispersion effects leading to unequal frequency spacing between adjacent pairs of modes, non-uniform line width of the various longitudinal modes and the effect of spontaneous emission [38]. Similar sets of interference packets will be observed at $\Delta L = 2pl_{cav}$, where p is an integer and may be associated with the order of the interference packet ($p = 0, \pm 1, \pm 2$, ...). As p increases the amplitude of the interference packets

will monotonically decrease following the Lorentzian visibility function $K(\Delta L)$ and vanish as $\Delta L \gg L_{cm}$. When the value of ΔL is set such that $2pl_{cav} \neq \Delta L \neq 2(p+1)l_{cav}$ i.e. between these sharp peaks the effective degree of coherence is very small and signal processing similar to that used in ' white light ' interferometry may be adopted. Detailed analysis of $|\gamma_{11}(\Delta L)|$ shows that there remain residual coherent signals in these regions, which acts as an additional source of noise. Comparing figures (2-6 a) and (2-6 b) we can conclude that as the number of oscillating modes increases, the level of this residual signal, and hence the system noise, is less.

The interference packet width (W) is defined as the optical path-length imbalance required to reduce the interference visibility by a factor of e^{-1} . It can be estimated by knowing the number of modes (m + 1) and the power distribution among them. It is clear, from the figures, that ; $W \propto 1/m$, which means that as the number of modes increases, the fringe pattern width will decrease .

Figure (2-7) shows the calculated irradiance of an interferometer illuminated by a multi-mode laser diode this plot was obtained by substituting the absolute value of the multi-mode laser auto-correlation function, calculated using equation (2.22), in equation (2.11). Figure (2-7) illustrates also the reduction of the coherent signal, generated between the sharp packets of interference, when the operating point is set between the second and third order of interference packets rather than the zero and the first order.

It is clear, from the above discussions, that by using a multi-mode laser, with specific properties, it is possible to replace the low power low coherence-length sources normally used in 'white light' fibre-optic interferometric systems. The main advantage being that as more optical power may be coupled into the system, the overall resolution may be improved. In addition one has the major benefit associated with the use of 'white light' technique that is possible to identify the order of interference, and hence to re-initialise the system.

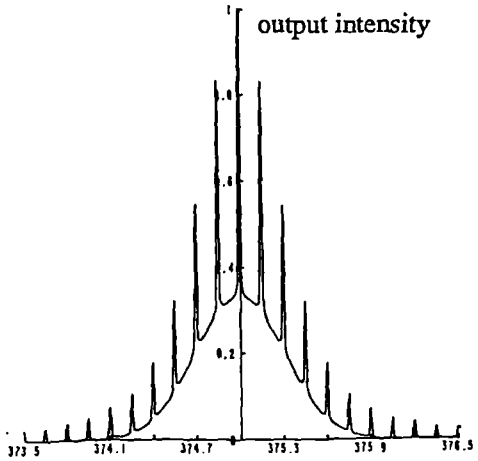

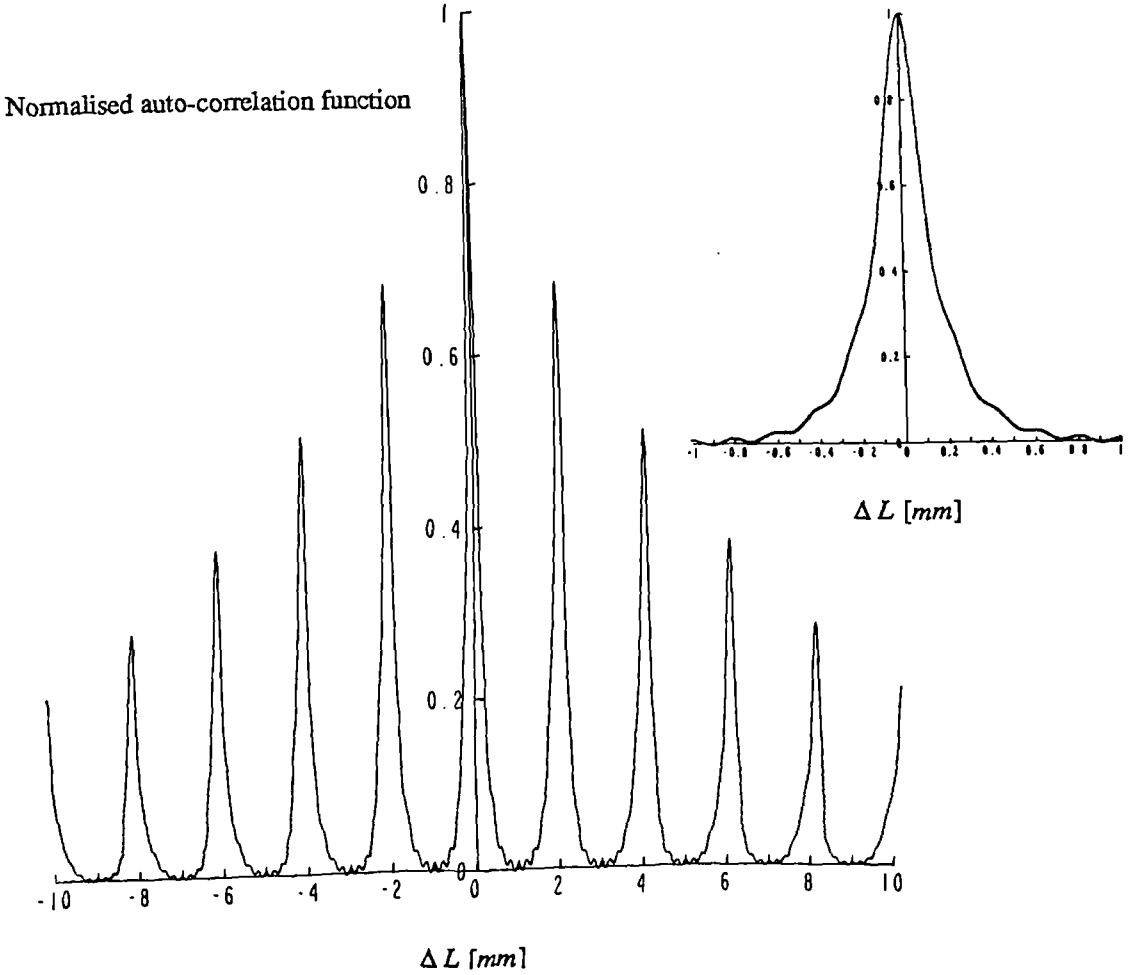

Figure (2-6 a) : Computer simulation of the characteristics of a typical multi-mode LD.

Upper : Spectrum, Lower : Auto-correlation function.

The modal pattern half-power width = ± 300 *GHz*.

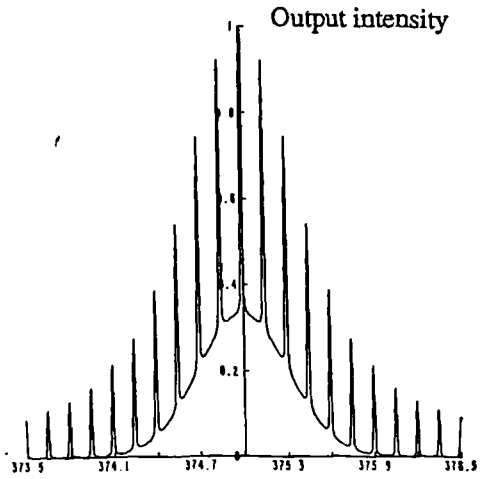

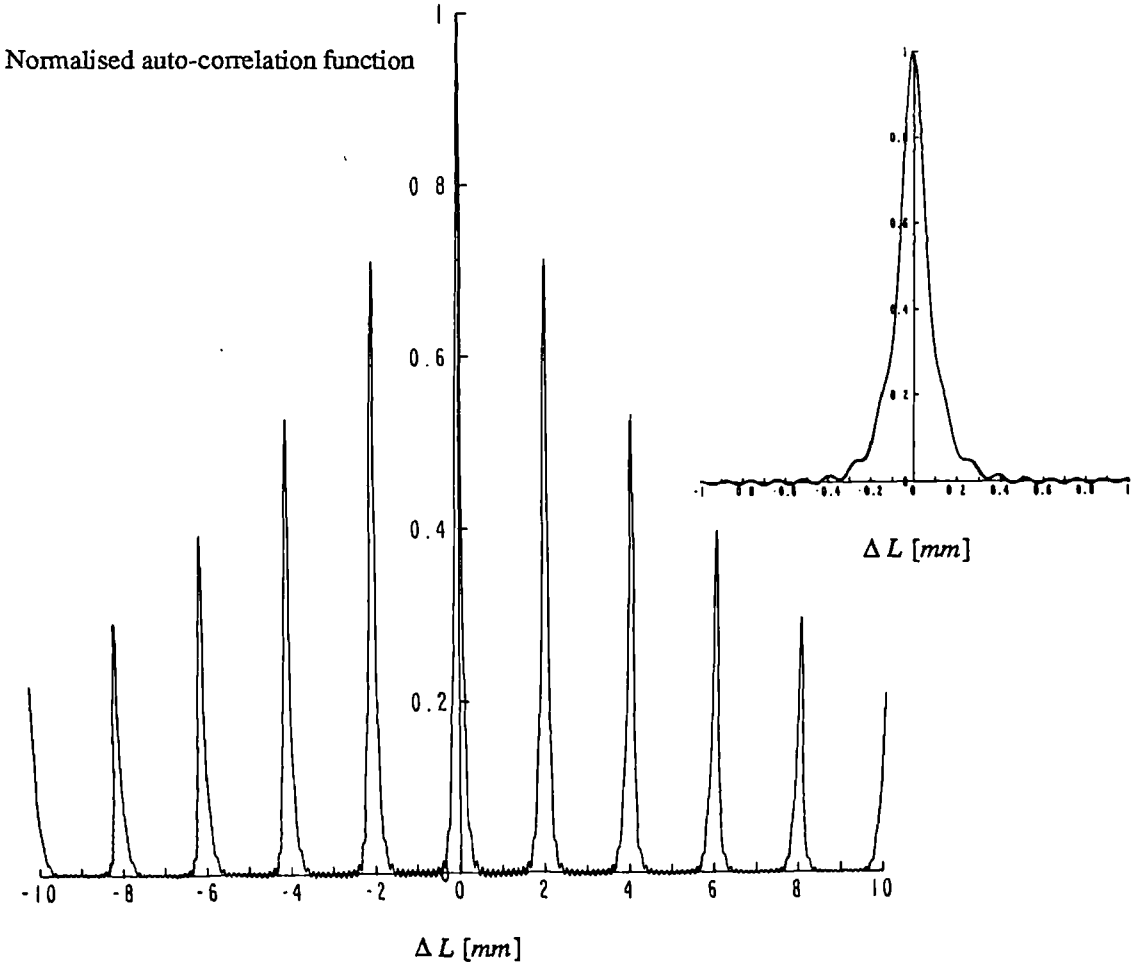

Figure (2-6 b) : Computer simulation of the characteristics of a typical multi-mode LD.

Upper : Spectrum, Lower : Auto-correlation function.

The modal pattern half-power width = ± 600 *GHz*.

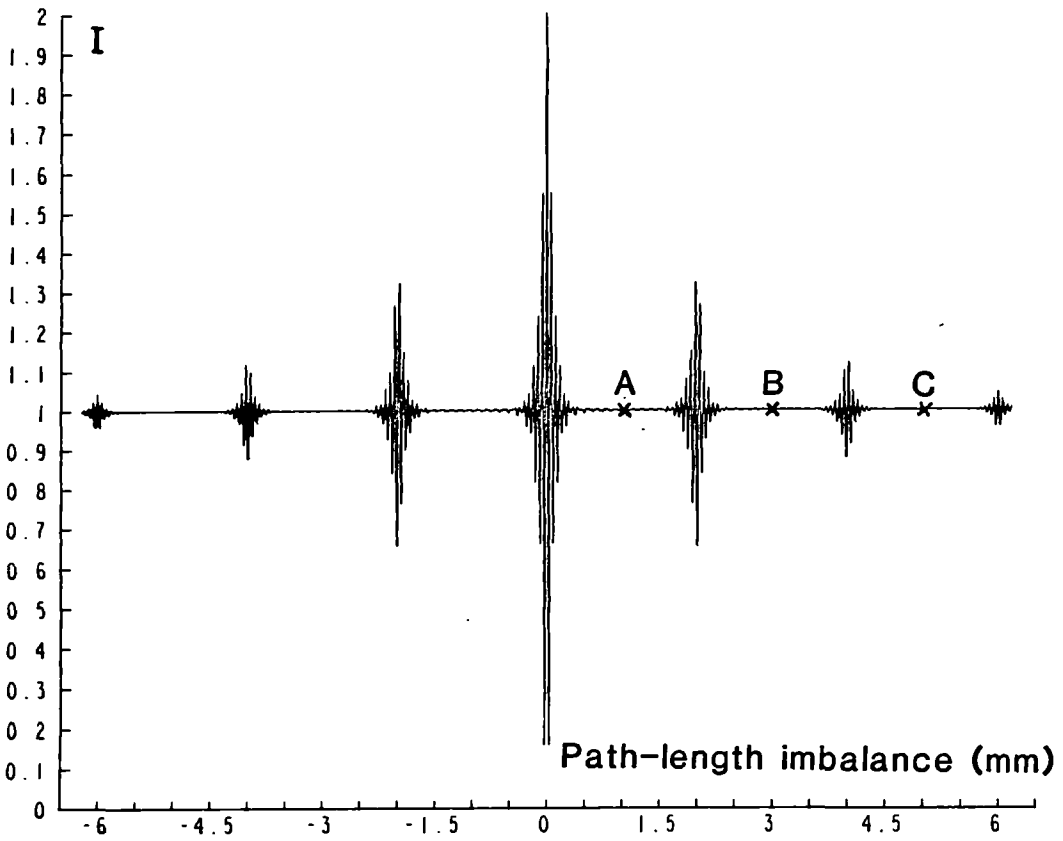

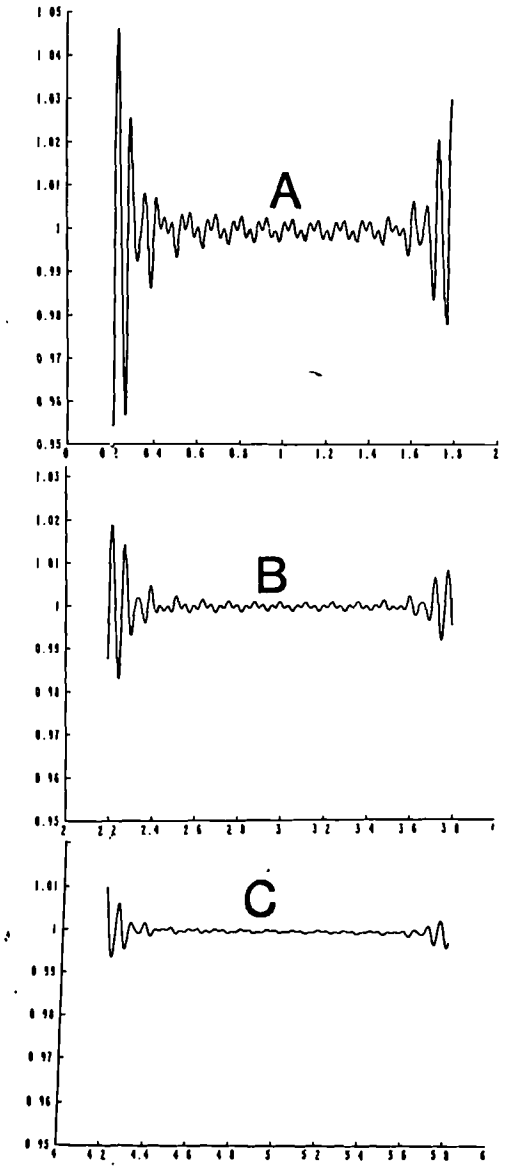

Figure (2-7) : Computer simulation of the output of an interferometer, illuminated by a multi-mode laser diode. The residual coherent signals generated at *Delta* $L = A, B, C$ are illustrated.

(2.6) Two interferometers in tandem :

In an interferometric system, consisting of two interferometers in tandem, the output light from the first interferometer (in sensor applications it is usually termed as 'the sensing interferometer') is used to illuminate a second (receiving) interferometer, with an optical path-length imbalance closely matched to the first.

(2.6.1) Broad band source illumination :

If a system, of two tandem interferometers, is illuminated with a broad-band source, with a coherence length much shorter than the optical path-length imbalance of the first interferometer, no interference signal will be observed at the output of the first interferometer. If the optical path-length imbalance of the second interferometer is adjusted to match that of the first interferometer, within the coherence length of the light source, an interference signal will be observed at the output of the whole system. The phase and visibility of which are functions of the difference between the optical path-length imbalance in the two interferometers.

If the interferometers are coupled via a fibre optic link, the resulting optical configuration forms the basis of a practical remote interferometric sensor system. The sensing interferometer is placed inside the measurand field and the receiving interferometer is situated in a controlled environment, far from the field.

Figure (2-8) shows a simple example of the remote interferometric sensing system. The sensing interferometer is a fibre-optic Michelson interferometer, while the receiving interferometer is a bulk-optic one. The irradiance (I) at the output of the whole system may be calculated as :

$$I = \int_0^\infty H_s(\nu)\, H_r(\nu)\, P(\nu)\, d\nu \qquad (2.23)$$

where $H_s(\nu)$ and $H_r(\nu)$ are the spectral transfer functions of the sensing and receiving interferometers respectively. $P(\nu)$ is the source normalised power spectral density function; such that $\int_0^\infty P(\nu)\, d\nu = 1$. Let us assume that the power splitting ratio of either the coupler or the bulk-optic

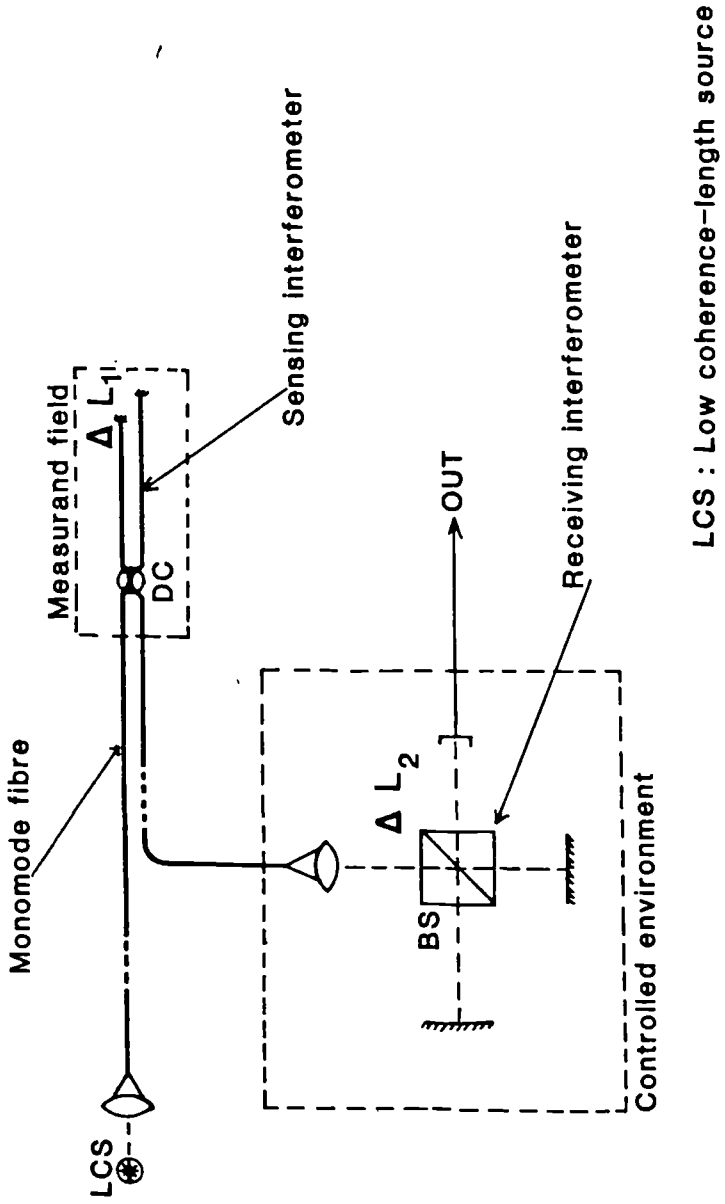

Figure (2-8) : A fibre optic sensing interferometer in tandem with a bulk-optic receiving interferometer.

beam splitter to be 1/2 and neglecting all the optical losses in the system, the transfer functions of the Michelson interferometers are :

$$H_s(\nu) = \frac{1}{2} + \frac{1}{2} Cos(\frac{2\pi\nu}{C} \Delta L_1) \tag{2.24}$$

$$H_r(\nu) = \frac{1}{2} + \frac{1}{2} Cos(\frac{2\pi\nu}{C} \Delta L_2) \tag{2.25}$$

where ΔL_1 and ΔL_2 are the optical path-length imbalances of the sensing and receiving interferometers respectively. Substituting in equation (2.23), the irradiance I will be :

$$I = \frac{1}{4} \int_0^\infty \left[1 + Cos(\frac{2\pi\nu}{C} \Delta L_1) + Cos(\frac{2\pi\nu}{C} \Delta L_2) \right.$$

$$\left. + \frac{1}{2} Cos[\frac{2\pi\nu}{C} (\Delta L_1 - \Delta L_2)] + \frac{1}{2} Cos[\frac{2\pi\nu}{C} (\Delta L_1 + \Delta L_2)] \right] P(\nu)\, d\nu \tag{2.26}$$

The illuminating source is a quasi-monochromatic one, with a mean light frequency of ν_o and hence it is more appropriate to express its spectral density function as $p(\mu)$, where $\mu = (\nu - \nu_o)$ and $\int_{-\infty}^{\infty} p(\mu)\, d\mu = 1$. Knowing that $Cos(x) = \mathrm{Re}[e^{-ix}]$ then :

$$\int_0^\infty Cos(\frac{2\pi\nu}{C} \Delta L)\, p(\nu)\, d\nu = \mathrm{Re} \left[\int_{-\infty}^{\infty} e^{-i(\frac{2\pi\mu}{C} \Delta L + \frac{2\pi\nu_o}{C} \Delta L)} p(\mu)\, d\mu \right] \tag{2.27}$$

According to Weiner-Khintchine theorem, the right side of equation (2.27) equals $|\gamma_{11}(\Delta L)|\, Cos(\frac{2\pi\nu_o}{C} \Delta L)$, and hence the irradiance I will take the form :

$$I = I_{mean} \left[1 + |\gamma_{11}(\Delta L_1)|\, Cos(\frac{2\pi\nu_o}{C} \Delta L_1) + |\gamma_{11}(\Delta L_2)| Cos(\frac{2\pi\nu_o}{C} \Delta L_2) \right.$$

$$+ \frac{1}{2} |\gamma_{11}(\Delta L_1 + \Delta L_2)|\, Cos[\frac{2\pi\nu_o}{C} (\Delta L_1 + \Delta L_2)]$$

$$\left. + \frac{1}{2} |\gamma_{11}(\Delta L_1 - \Delta L_2)|\, Cos[\frac{2\pi\nu_o}{C} (\Delta L_1 - \Delta L_2)] \right] \tag{2.28}$$

where I_{mean} is the average intensity at the system output, $I_{mean} = \frac{1}{4}$ of the input power to the system which is unity if the spectral density is a normalised function. The necessary condition for a remote sensing system is that the path-length imbalance of the sensing interferometer, ΔL_1 , must be chosen such that the absolute value of $\gamma_{11}(\Delta L_1)$,and hence the second term in equation (2.28) equals zero.

Figure (2-9 a,b) shows the predicted output of the receiving interferometer as a function of the path-length imbalance, ΔL_2 . Figure (2-9 a) shows the output of the system when it is illuminated by a low coherence-length source, with coherence length L_c with $|\gamma_{11}(\Delta L)| = \exp(-\Delta L/L_c)$. When ΔL_2 is less than L_c , the interference effects observed are a result of interference occurring solely within the receiving interferometer. When this condition is satisfied, the system irradiance may be expressed as :

$$I_{\Delta L_2 \ll L_c} = I_{mean}\left[1+ |\gamma_{11}(\Delta L_2)| Cos(\frac{2\pi\nu_o}{C}\Delta L_2)\right] \qquad (2.29)$$

which is equivalent to a single interferometer, with path-length imbalance of ΔL_2 , illuminated by a low coherence length source as described in equation (2.11). This indicates that, within this range, the output of the system is independent of the sensing interferometer. The maximum visibility of this set of fringes is unity, which occurs at $\Delta L_2 = 0$.

Far from the central pattern of interference fringes, interference can occur in two regions when $(\Delta L_1 \pm \Delta L_2)$ is less than L_c . The output of the system may be expressed by :

$$I_{(\Delta L_1 \pm \Delta L_2) \ll L_c} = I_{mean}\left[1+\frac{1}{2}|\gamma_{11}(\Delta L_1 \pm \Delta L_2)| Cos[\frac{2\pi\nu_o}{C}(\Delta L_1 \pm \Delta L_2)]\right] \qquad (2.30)$$

which is equivalent to the output of a single interferometer, having an optical path-length imbalance of $\Delta L_1 \pm \Delta L_2$. This means that any optical path change in either of the two interferometers will produce a change in the fringe visibility as well as the phase of the final output signal. The profile of these interference patterns, corresponding to this condition, is the same as that of the

central one, except that the visibility is reduced by a factor of 2 . The maximum visibility is 0.5, which occurs at $\Delta L_2 = \pm \Delta L_1$.

(2.6.2) Multi-mode laser illumination :

If the system is illuminated by a multi-mode laser, its output will be more complicated because of the additional modulation caused by the discrete source frequencies, as shown in the computer generated visibility function sown in figure (2-9 b). Each interference pattern in figure (2-9 a) is replaced with a complete set of interference packets as discussed in section (2.5). The maximum visibility of the central set of interference packets remains unity at $\Delta L_2 = 0$ and 0.5 for the two side sets at $\Delta L_2 = \pm \Delta L_1$. The form of the visibility function in figure (2-9 b) was calculated by substituting the auto-correlation function for a multi-mode laser given in equation (2.22) for the value $\exp(-\Delta L / L_c)$ used in the simulation of figure (2-9 a).

To satisfy the necessary condition $|\gamma_{11}(\Delta L_1)| = 0$, the path-length imbalance of the sensing interferometer, and hence that of the matching receiving interferometer, may be chosen to be :

(a) Much greater than the coherence length L_{cm} to insure that no interference will occur due to either one interferometer alone or the combined interferometer of path-length imbalance of $(\Delta L_1 + \Delta L_2)$. The only interference signal will be generated by the combined, balanced, interferometer, of path-length imbalance $(\Delta L_1 - \Delta L_2)$.In this case, the working range of the system is very large, as it is limited only by the tracking range of the receiving interferometer.

(b) In the range between two successive packets of interference, i.e. $<L_{cm}$ provided the following condition is satisfied :

$$(p\, l_{cav} + 3W) < \Delta L_1 < [(p+1) l_{cav} - 3W] \qquad (2.30)$$

where W is the interference packet width. This condition ensures that the coherence signals generated in the sensing interferometer (or the matching receiving interferometer) are minimised. It also ensures that the path-length imbalance of the combined interferometer of $\Delta L_1 + \Delta L_2 \neq 2p\, l_{cav}$.

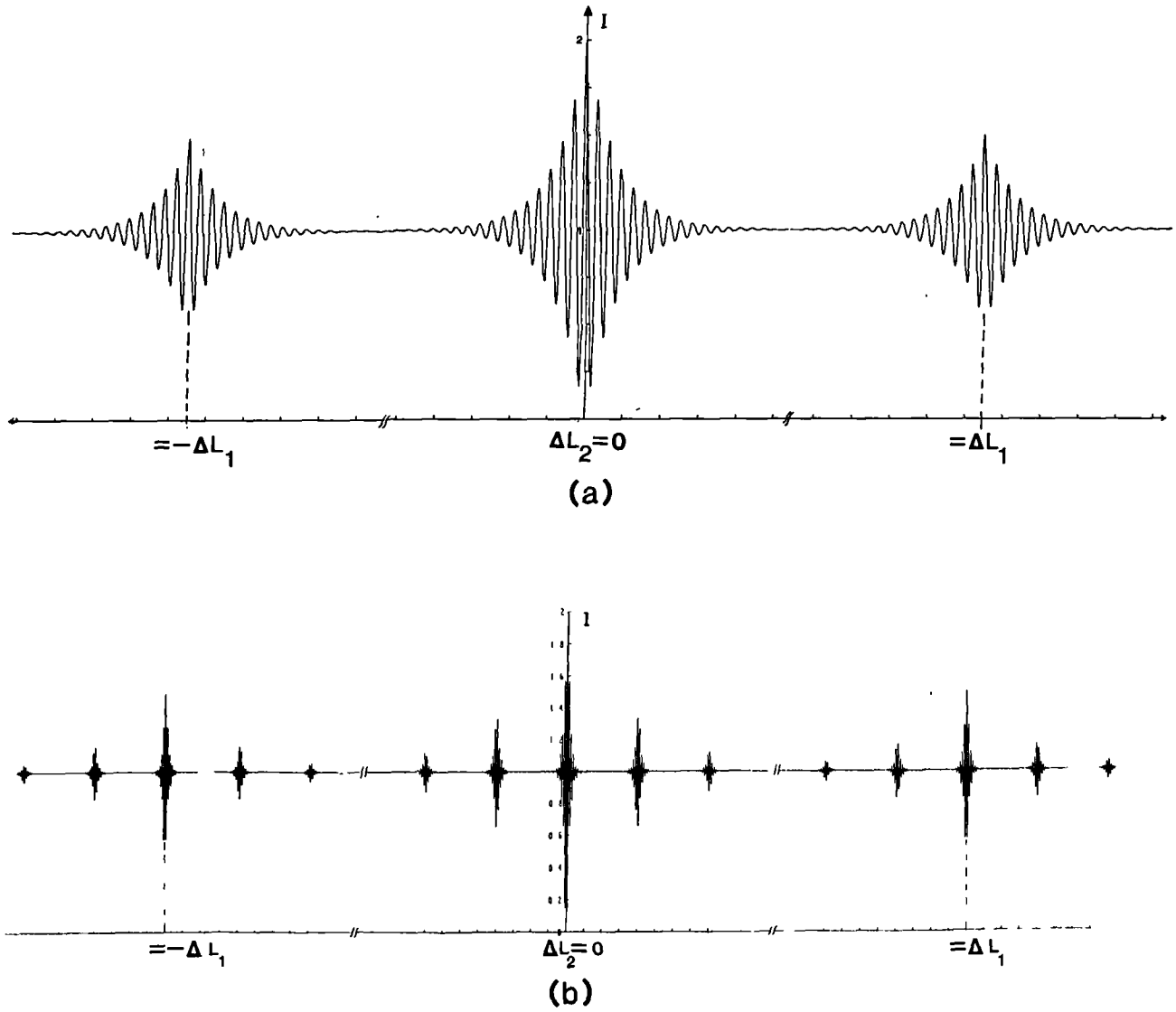

Figure (2-9) : Output from the receiving interferometer as a function of its optical path-length imbalance.

(a) : Broad-band source illumination, (b) : Multi-mode laser diode illumination.

The working range of the system is limited by the properties of the multi-mode laser as indicated by equation (2.30).

If the path-length imbalance of the sensing interferometer, ΔL_1 , is adjusted such that p=0 i.e its operating point is between the zero and the first order of the interference packets, the optical path-length imbalance of the sensing interferometer, can be as short as 200 microns. Due to the limited number of oscillating modes, a very weak interference signal is produced within the receiving interferometer alone. This signal is independent of the sensing interferometer, hence it contributes noise to the final output of the system and limits the system resolution. As p increases, the level of this interference signal decreases monotonically improving the system resolution. Thus if ΔL_1 is adjusted such that the operating point, of the sensing interferometer, lies between the first and the second order of the interference packets, the system resolution will be better than that obtained if the operating point is adjusted to lie between the zero and the first order packets and so on.

From the above discussions it is clear that as ΔL_1 increases, the system resolution will continuously improve until the order of magnitude of the weak interference signal becomes comparable to the other sources of noise i.e. shot, intensity, electronic noises when the system's resolution will remain constant. In general the effects of the source frequency jitter will be negligible as the path imbalance of the tandem interferometers remains small,[31], and the output corresponding to the individual interferometers are very weak.

(2.7) Coherent multiplexing of interferometric sensors :

If a number of fibre-optic interferometric sensors are arranged so that their outputs are returned back to the user via a common optical bus, then some method of distinguishing the returns from different sensors must be used, so that the individual signal can be recovered. This practical technique is known as multiplexing of optical sensors. Four basic methods have been reported, they are time division, wavelength, frequency and coherent multiplexing [39-42]. The

principle of coherence multiplexing is to construct a network of sensing interferometers, with different optical path-length imbalances. The optical path-length imbalance of each interferometer must be significantly greater than the coherence length of the optical source used to illuminate the system. Furthermore, the difference between the path-length imbalances of the sensors must be greater than the source coherence length also to minimise the cross-talk between them. The phase information of the sensors is recovered by balancing the path-difference of each sensing interferometer using a separate receiving interferometer for each sensor to allow parallel signal demultiplexing, as discussed in the previous case of two tandem interferometers. A number of multiplexing configurations have been demonstrated by Brooks et el [42]. In applications where the measurand varies slowly in time it is feasible to use a single receiving interferometer with large tracking range such that it can be sequentially tuned to each sensor in the network [43]. There is a very little data on the low frequency phase resolution obtained in coherence multiplexed systems, however the tracking technique introduced in chapter (3) shows that a tracking resolution of about 1.6 mrad with auto-initialisation is possible for a single sensing interferometer [44]. This system could possibly be developed for a sensor network for slowly varying measurands.

(2.8) Conclusion :

A theoretical study of white light interferometry and its applications in fibre-optic sensing techniques has been reviewed. The advantage of using white light techniques is the ability to initialise the system, an increase in the unambiguous range and the independence from drifts in the source wavelength. The basis of this technique is to measure the changes of the interference visibility (fringe amplitude) together with the phase changes at the output interference signal of the system, illuminated by a low coherence-length source. Multi-mode laser diode can be used as an alternative to conventional low coherence-length source normally used in 'white light' interferometry and provided certain operating conditions, where a much better resolution may be achieved.

References

[1] D.A.Jackson, " Monomode optical fibre interferometers for precision measurement ", J.Physics E: Scientific Instruments, Vol. 18, 1985, P.981.

[2] D.A.Jackson and J.D.C.Jones," Fibre Optic Sensors ",Optica Acta, Vol. 33, No.12, 1986, P.1469.

[3] P.A. Leilabady, J.D.C.Jones and D.A.Jackson, " Monomode fibre optic strain gauge with simultaneous phase and polarisation state detection ", Optics Letters, Vol. 10, November 1985, P.576.

[4] A.D.Kersey, A.Dandridge and W.K.Burns," Two wavelength fibre gyroscope with wide dynamic range ", Electronics Letters,22 No.18, August 1986, P.935.

[5] D.J.Webb, J.D.C.Jones and D.A.Jackson, " Laser diode frequency stabilisation techniques for interferometric sensors ", Proceeding of fibre optics'88 Conference, SPIE, London, April 1988, Vol.949 paper 27.

[6] M.Born and E.Wolf, " principles of optics " , Pergamon Press, Chapter 10, 1980.

[7] W.H.Steel, " Interferometry " , Cambridge University Press, Chapters 6,7, 1983.

[8] G.R.Fowles, " Introduction to modern optics " , Holt, Rinehart and Winston, Inc. Chapter 3, 1968.

[9] L.Thevenaz, J.Pellaux and J.Von Der Weid, " All-fibre interferometer for chromatic dispersion measurements ", J.Of Lightwave Technology, Vol. 6, No. 1, January 1988, P. 1.

[10] J.Wilson and j.F.B.Hawkes, " Optoelectronics: An introduction " Prentice-Hall International Inc., 1983, P. 193.

[11] P.M.Chirlian, " Signals, Systems and the Computer " , Intext Press, Inc. 1973. P.42 - 114.

[12] H.Zajac, " Optics " Addison-Wesley Publishing Comp.Inc., Chapter 12, 1974.

[13] M.V.Klein and T.E.Furtak, " Optics ", J.Wiley & Sons,Inc., Chapter 8, 1986.

[14] Th. Bosselmann and R.Ulrich. " High accuracy position-sensing with fibre-coupled white-light interferometers ", Proceeding of the second international conference on OFS, VDE-VERLAG, Stuttgart, September 1984, P.361.

[15] K.Takada, K.Chida, J.Noda and S.Nakajima, " Trench depth measurement system for VLSI dram's capacitor cells using optical fibre and Michelson interferometer ", J.Of Lightwave Technology, Vol.LT-5, No.7, July 1987, P.881.

[16] G.Beheim," Fibre-optic thermometer using semiconductor-etalon sensor ", Electronics Letters, Vol.22, No.5, February.1986, P.238.

[17] C.Mariller and M.Lequime ," Fibre-optic white-light birefringent temperature sensor ", SPIE, Vol.789 Fibre Optic Sensors II, 1987, P.121.

[18] G.Beheim, " Fibre-linked interferometric pressure sensor ", Rev.Sci. Instruments, Vol.58, No.9, September 1987, P.1655.

[19] D.J.Webb, J.D.C.Jones and D.A.Jackson ," Extended-range interferometry using a coherence-tuned synthesised dual-wavelength technique with fibre links ", Electronics Letters, Vol.24, No.18, September 1988, P.1173.

[20] D.J.Webb, " An investigation of optical interferometric techniques for the sensing of slowly varying measurands ", Phd. thesis, University Of Kent, U.K., 1988, P.83-94.

[21] K.Chen and D.Kerps, " Coupling efficiency of surface-emitting LED's to single-mode fibres", J. of Lightwave Technology, Vol. LT-5, No. 11, November 1987, P. 1600.

[22] D.N.Christodoulides, L.A.Reith and M.A.Saifi, " Theory Of LED coupling to single-mode

fibres ", J. of Lightwave Technology, Vol.LT-5, No. 11, November 1987, P.1623.

[23] S.A.Al-Chalabi, B.Culshaw and D.E.N.Davies, " Partially coherent sources in interferometric sensors", Proceeding of the first international conference on Optical Fibre Sensors, IEE conference publication No.221, London, April 1983, P.132.

[24] D.A.Jackson ," Introduction to fibre optic interferometers and their application as sensors ", Report prepared for the Optical Sensors Collaborative Association (OSCA), March 1988, P.74.

[25] W.V.Smith and P.P.Sorokin," The Laser ", New York: McGraw Hill, Chapter 3, 1966.

[26] S.Iida, K.Takata and Y.Unno, " Spectral behaviour and line width of (Ga Al) As- Ga As double-heterodyne lasers at room temperature with strip geometry configuration " IEEE J. of Quantum Electronics, Vol. QE-9, No. 2, Feb. 1973, P.361.

[27] B.Zee," Broadening mechanisms in semiconductor (Ga As) lasers: Limitations to single mode power emission ", IEEE J. of Quantum Electronics, Vol.QE-14, October 1987, P.727.

[28] " Workshop on single mode optical fibre sensor technology ", Course notes, University Of Kent and Sira Ltd., U.K., 1985, P.62.

[29] A.Dandridge, " Measurement of the spectral characteristics of CW diode lasers ", Applied Optics, Vol. 20, No. 14, July 1981, P.2336.

[30] A.D.Kersey, A.Dandridge, A.B.Teveten, T.G.Giallorenzi, " Single-mode fibre Fourier transform spectrometer ", Electronics Letters, Vol.21, No.11, May 1985, P.463.

[31] A.Dandridge, " Zero path-length difference in fibre-optic interferometers ", J. of Lightwave Technology, Vol.LT-1, No.3, September 1983, P.514.

[32] A.S.Gerges, F.Farahi, T.P.Newson, J.D.C.Jones and D.A.Jackson ," Fibre optic interferometric sensor using a low coherence source: dynamic range enhancement ", International

Journal of Opto-Electronics, Vol.3, No.4, 1988, P.311.

[33] T.P.Newson, F.Farahi, J.D.C.Jones and D.A.Jackson, " Combined interferometric and polarimetric fibre-optic temperature sensor with a short coherence length source ", Optics communications, Vol.68, No.3, October 1988, P.161.

[34] Mitsubishi opto-electronic components for optical-fibre communication systems and optical semiconductor devices, Mitsubishi Electric Corp. 1988.

[35] P.Brosson, J.E.Pipper and N.B.Patel ," Variation of spontaneous emission with current in GaAs Homo-structure and Double-Heterostructure injection lasers ", IEEE J.Of Quantum Electronics, Vol.QE-9, No.2, February 1973, P.273.

[36] L.W.Gasperson, " Threshold characteristics of multi-mode laser oscillators " J. Of Applied Physics, Vol.46, No.12, December 1975, P.5194.

[37] A.R.Reisinger, C.D.David, JR.,K.L.Lawley and A.Yariv, " Coherence of a room temperature CW GaAs/GaAlAs injection laser ", IEEE J. of Quantum Electronics, Vol. QE-15, No. 12, December 1979, P. 1382.

[38] C.A.Brackett ," Second-order dispersion in oscillating GaAs junction lasers ", IEEE J.Of Quantum Electronics, Vol.QE-8, No.2, February 1972, P.66.

[39] A.R Nelson, D.H.McMahon, and R.L.Gravel " Passive multiplexing system for fibre-optic sensors ", Applied Optics, Vol.19 , No.17, September 1980, P.2917.

[40] H.Ishio, J.Minowa and K.Nosun ," Review and status of wavelength division multiplexing technology and its application ", J. Of Lightwave Technology, Vol LT-2, No.4, 1984, P.448.

[41] I.Sakai, R.C.Youngquist and G.Parry, " Multiplexing of optical fibre sensors using a frequency-modulated source and gated output ", J. Lightwave Technology, Vol. LT-5, No.7, July 1987, P. 932

[42] J.L.Brooks, R.H.Wentworth, R.C. Youngquist, M.Tur,B.Y.Kim,and H.J.Shaw," Coherence multiplexing of fibre optic interferometric sensors " , J. of Lightwave Technology, LT-3, October 1985, P.1062.

[43] F.Farahi, T.P.Newson, J.D.C.Jones and D.A.Jackson, " Coherent multiplexing of remote Fibre optic Fabry Perot system ", Optics Communications, Vol.65, No.5, March 1988, P.319.

[44] A.S.Gerges, F.Farahi, T.P.Newson, J.D.C.Jones and D.A.Jackson ," A hemispherical air cavity fibre Fabry-Perot Sensor ", Optics Communications, Vol. 68, No.3, October 1988, P.157.

CHAPTER (3)

Coherent tuned fibre–optic sensing systems, with extended range and self initialisation

(3.1) Introduction

We have seen that interferometric fibre optic sensors have, in general, limited unambiguous operating range, hence they have had limited applicability for measurement of low frequency measurands, such as temperature, strain and displacement, due to the problem of initialising the system, i.e. should the interferometer be switched off, all information about the measured phase will be lost and the new initial condition must be determined when the system is turned on again [1,2]. As discussed in chapter (2), these problems are avoided in 'white light' interferometry, where a broad band light source and a nearly balanced interferometer is used.

In this chapter, we describe the practical implementation of two similar methods which exploit the technique of 'white light' interferometry. In the first method, a Mach-Zehnder interferometer is locked to the maximum of the visibility function, which corresponds to a zero path-length (phase) difference in the interferometer. In the second method, the interferometer is locked to the quadrature point nearest to the position of maximum visibility; that is, a phase difference of $\pi/2$ rads. In both methods, a monomode laser diode, biased below threshold was used as a low coherence-length source.

For both methods, the resolution is limited by the noise level present in the photodiode outputs. However, the resolution using the second method is markedly superior. This is because in

the first method, one is locking to a turning point of a function (the variation of visibility with path length) where the sensitivity is obviously small. The second method is essentially hybrid, in that the servo first locates the position of maximum visibility, and then locates the nearest quadrature point- thus effectively making a phase measurement. However, the slope of intensity versus path difference is a maximum at quadrature, so that the available resolution is greater. In practice, we obtained a phase resolution of $5\ mrad/\sqrt{Hz}$ when locking to maximum visibility [3], and $0.26\ mrad/\sqrt{Hz}$ when locking to the first quadrature point. The second method possesses the resolution of a true interferometer, but retains the wide measurement range associated with the visibility function [4].

In the second part of the chapter we use a multi-mode laser diode as an alternative to the low coherence-length sources. As discussed in chapter (2), the advantage of using these lasers is to increase the signal to noise ratio, and hence the resolution of sensing systems. A system of two tandem Michelson interferometers, linked by a monomode fibre is used as a remote displacement sensor, where a phase resolution of about 5 μ rad / $\sqrt{Hz}$ is obtained [5].

(3.2) Zero path-length tracking in FOIS; system initialisation :

(3.2.1) The signal processing technique :

In principle, a measurement of the absolute value of the interference visibility (or the fringe amplitude) could be used to determine the order of the fringe being observed at the output of an interferometer illuminated by a broad band source and hence the system could be initialised if it is switched off and on again. In practice that is not the case, because many factors affect the value of the visibility constant V_o and hence the absolute value of the visibility will not be a function of the path-length imbalance only. If the visibility function is measured at a path-length imbalance of ΔL relative to that corresponding to an imbalance of $\Delta L'$, the dependence on the visibility constant is cancelled and the ratio of the visibilities at the two positions is a function of their path-length imbalances only ($\Delta L - \Delta L'$). Moreover the value of $V(0)$ / $V(\Delta L)$ is greater than

unity for all the values of $\Delta L \neq 0$. This means that whatever happens to the system, the maximum visibility (fringe amplitude) always occurs when the optical path-length difference of the interferometer is zero. This fact led to the idea of a simple scheme of signal processing, where a measurand, with frequencies within the tracking band-width, acts on one arm of the interferometer, the other, reference, arm is automatically adjusted to maintain the system at the point of maximum interference amplitude (visibility), which is a fixed position in a non-dispersive system. The measurand is then determined from the signal fed back to the reference arm. The accuracy of such a system is determined both by the accuracy with which the point of zero path-length imbalance can be determined and how well characterised is the relationship between the feedback signal and the length of the reference arm.

(3.2.2) The experimental system :

The experimental arrangement, illustrated in figure (3-1), was used to demonstrate the principle of tracking either the position of maximum interference visibility or the position of the first quadrature point. It consisted of a Mach-Zehnder interferometer using both fibre and bulk optic components. All-fibre-optic variants optimised for specific measurands are equally possible. A laser diode Hitachi HL 7801E biased below threshold was used as a low coherence source, illuminating the optical system with a mean operating wavelength of 790.3 nm. Equal lengths of monomode optical fibre were used in making the signal and reference arms of the interferometer, both were contained in a thermally insulated chamber to minimise environmental effects. A 10 cm length of the signal arm was contained inside a furnace. Two piezo-electric fibre stretchers were deployed in the two arms of the interferometer. The two anti-phase outputs of the interferometer were detected and differentially amplified to reduce the intensity noise. The collimator of the signal arm was mounted on a translation stage with a micro-meter to adjust the interferometer to have a nearly zero optical path difference [6].

To measure the source auto-correlation function, a sinusoidal signal was applied to one of the piezo-electric fibre stretchers, and adjusted to scan one complete interference fringe. The

interference fringe amplitude (the AC output of the photodiodes) was measured as a function of the path length imbalance ΔL , induced by the translation stage in steps of 5 μm , about the position of maximum interference amplitude, (where $\Delta L = 0$). The measured values were normalised relative to their maximum value, results are shown in figure (3-2). The e^{-1} reduction in the values of the fringe amplitude determined the source coherence length to be approximately of $50\mu m$. The normalised values of the interference fringe amplitude (visibility) represents the absolute values of the auto-correlation function, which is an even function of ΔL, such that the negative side of the function is symmetrical about the vertical axis.

Using the least square fitting technique, the source normalised auto-correlation function can be described, near $\Delta L = 0$, with the quadratic function :

$$|\gamma_{11}(\Delta L)| = a+b(\Delta L/L_c)+c(\Delta L/L_c)^2 \qquad (3.1)$$

where a = 1.0 , b = - 0.84579705 and c = 0.19758684, ΔL is measured in μm and $L_c = 50\mu m$. This function is plotted also in the same figure.

(3.2.3) Maximum visibility location method:

Using the micro-translation stage, the optical path-length of the reference arm of the Mach-Zehnder interferometer is adjusted to be slightly shorter than that of the sensing arm. Then the electronic servo was used to apply a feedback voltage to the piezo-electric fibre stretcher deployed in the reference arm (PZT-1) to increase the optical path-length of this arm and hence to locate the position of the zero path-length imbalance of the interferometer as follows :

A saw-tooth (ramp) voltage with a frequency of 1 kHz was applied to the piezo-electric fibre stretcher in the sensing arm (PZT-2). The amplitude of the applied voltage was sufficient to drive the interferometer over one fringe per cycle. The differential outputs from the photodiodes were then band pass filtered at 1 kHz, giving a sinusoidal output with an amplitude proportional to the fringe amplitude, A. This signal serves as the input to the servo system. The servo acts by applying a digitally controlled voltage to PZT-1, in order to control the path-length imbalance.

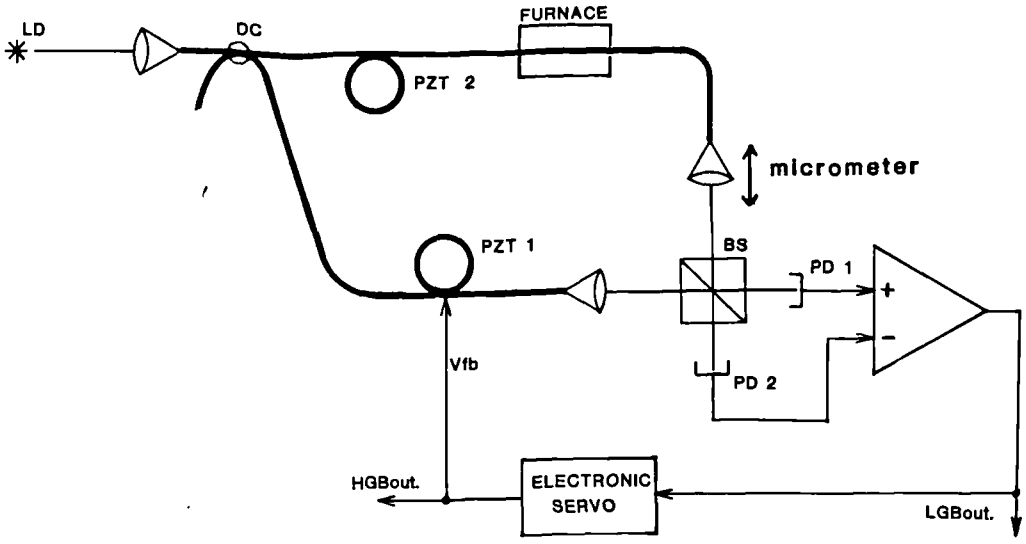

Figure (3-1) : The optical arrangement used to demonstrate the tracking systems.

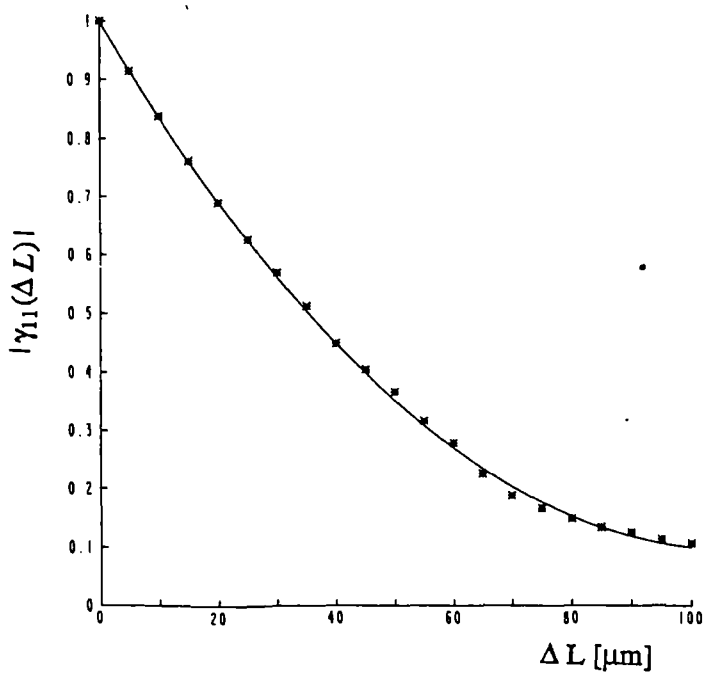

Figure (3-2) : The normalised auto-correlation function of the light emitted from the laser diode, Hitachi HL 7801E (biased below threshold), as a function of the interferometer path-length imbalance. $I = 38.5\ mA$, $I_{th} = 42mA$; * * * : measured points, solid curve : least square fitting.

The servo operates in two stages. Firstly, the voltage is incremented unidirectionally in steps corresponding to path changes of about $\lambda/4$, so causing the fringe amplitude to increase. When the amplitude has just passed through its maximum this coarse phase is inhibited and the second phase is initiated, the voltage applied to the PZT at the termination of phase-1 is maintained. The second stage operates bidirectionally applying additional voltage steps equivalent to $\lambda/240$, until the amplitude is maximised. The second stage of the servo continues to operate in order to maintain the path imbalance to zero, and so compensate phase changes produced by an applied measurand. A schematic diagram of the electronic feedback servo is shown in figure (3-3 a). Figure (3-3 b) shows the form of the servo output and the corresponding path-length imbalance at each value of the servo output, the circuit diagram of the feedback servo is discussed in appendix (A).

The value of the measurand is therefore found from the voltage applied by the servo to the fibre stretcher, PZT-1. Moreover, this quantity is also available, in digital form, at the outputs of the digital counters used to control the feedback voltage, given that the relative size of the voltage steps is known accurately.

The accuracy with which the position of zero path-length imbalance can be determined is set by the noise floor at the input of the electronic servo used to maximise the observed fringe amplitude as well as the source auto-correlation function. If the level of this noise is (n), within the band-width of the servo, then the minimum detectable change of the optical path-length ΔL_{min}, about the zero position, is estimated as follows :

From equation (2.8) the amplitude of the AC signal at the output of the photodetectors (S) may be written as :

$$S = \varepsilon_1 A$$

$$= \varepsilon_1 A_o |\gamma_{11}(\Delta L)| \qquad (3.2)$$

where ε_1 is the conversion factor for optical power to electrical voltage for the photodetector and the differential amplifier used. At $\Delta L = 0$, the signal amplitude is $S_o = \varepsilon_1 A_o$, corresponding to

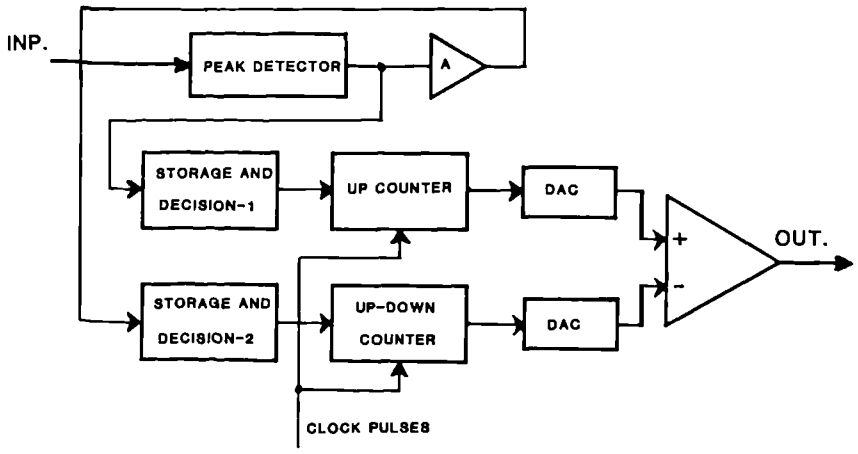

Figure (3-3 a) : Block diagram of the first (maximum visibility tracking) digital servo.

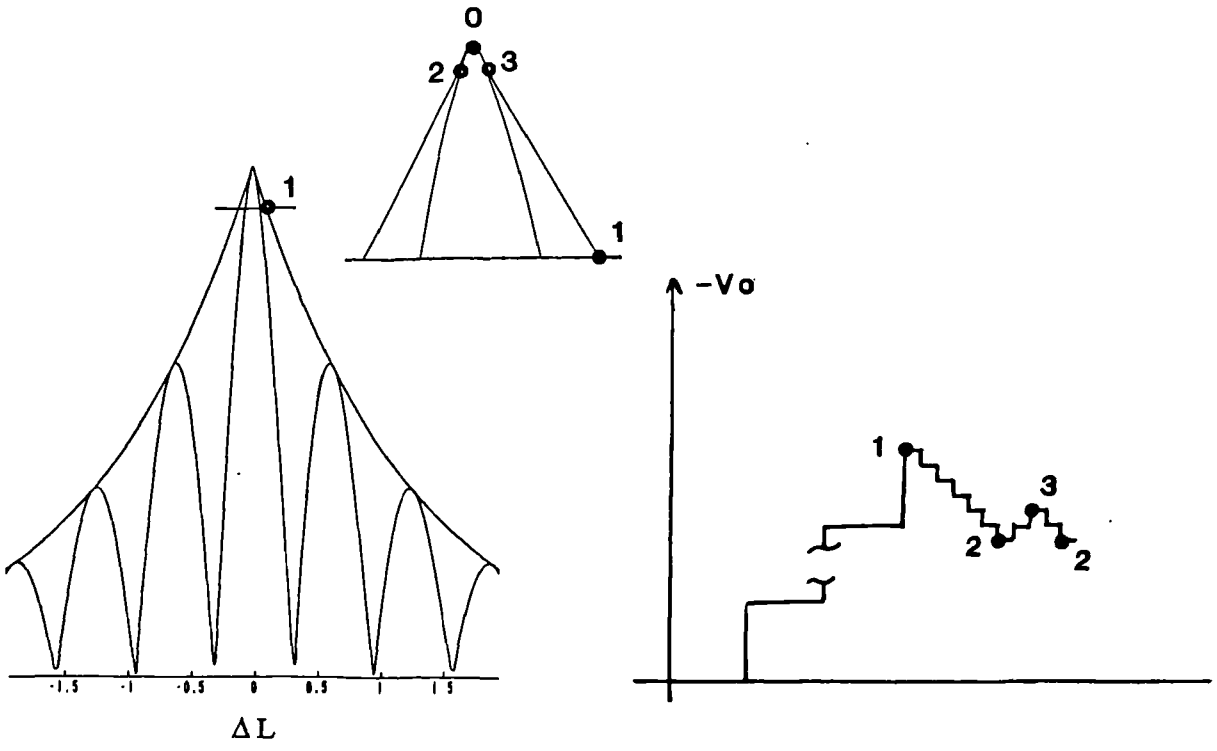

Figure (3-3 b) : The form of the servo feedback digital signal. The first stage of the servo locates the point (1) and then the second stage continuously tracks the point (0).

the central interference fringe. The minimum change (reduction) in the photodetector outputs to be detected by the servo equals the level of the noise floor (n) and hence the minimum detectable path-length change may be calculated as :

$$S(\Delta L_{\min}) = S_o - n$$

$$= S_o \, |\gamma_{11}(\Delta L_{\min})| \tag{3.3}$$

and hence

$$|\gamma_{11}(\Delta L_{\min})| = 1 - \frac{n}{S_o} \tag{3.4}$$

where $\frac{n}{S_o}$ is the inverse of the signal to noise ratio at the output of the differential amplifier, where the interferometer is balanced.

(3.2.4) Testing the system as a low frequency sensor :

The system was used to demonstrate the interferometer as a displacement and strain sensor. For displacement measurements the position of the collimator of the sensing arm was moved with respect to the beam splitter in steps of 5 μm . The feedback voltage to the PZT-1, balancing the interferometer, was recorded by re-triggering the servo each time, the results are shown in figure (3-4). The ability of the servo for continuous tracking, of low frequency measurands, was then demonstrated by using the interferometer as a strain sensor. A strain was induced in the sensing arm by applying a slow varying voltage to PZT-2, this was successfully tracked by the servo as shown in figure (3-5). The effectiveness of the tracking system is shown in figure (3-6) where the upper trace shows the AC signal (interference amplitude) before the servo is applied and the lower trace shows the level of the signal after the servo has maximised the interference amplitude (near zero path-length imbalance).

The practical resolution of the method, of locking to maximum visibility, may be estimated as follows : The band-width of the filter used after differential amplification of the photodiode outputs was 25 Hz (mean frequency of 1 KHz and quality factor of 40). Within this band-width,

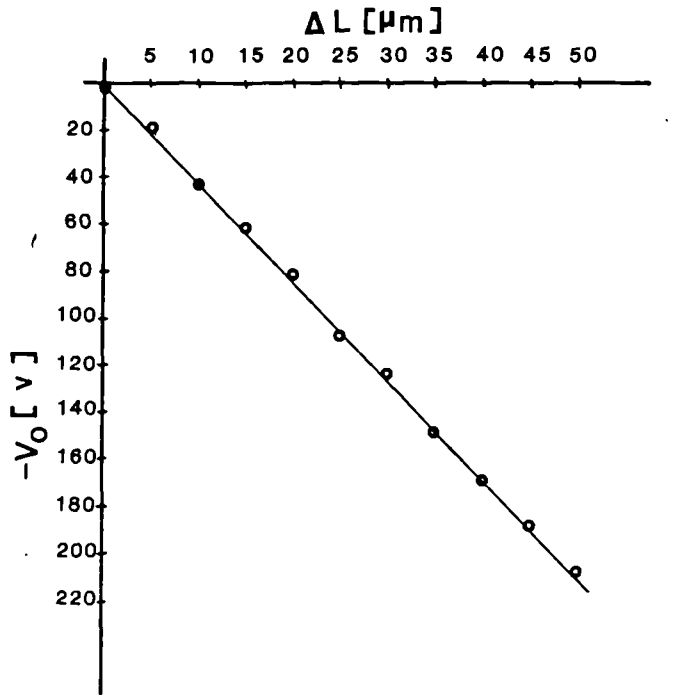

Figure (3-4) : Output voltage of the first servo against displacement.

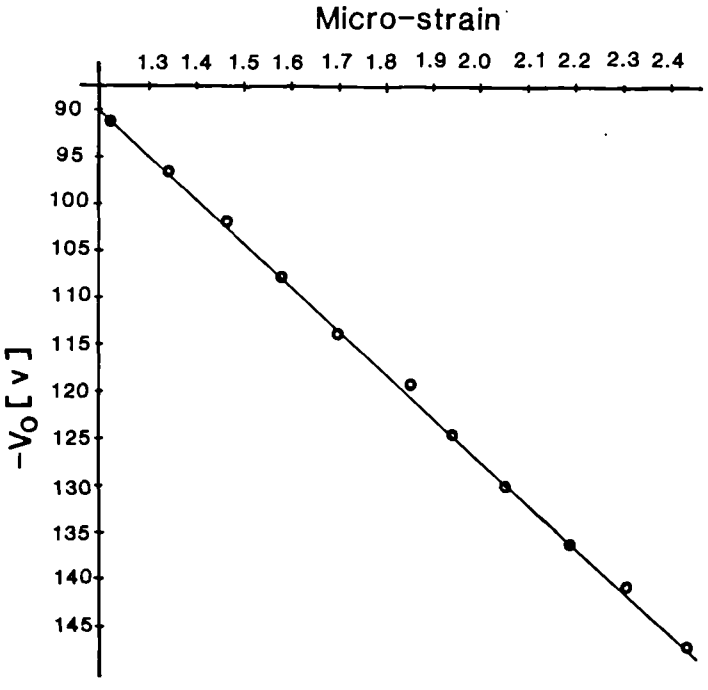

Figure (3-5) : Output voltage of the first servo against strain.

the measured signal to noise ratio was 85.6 dB. This value may be converted to a phase resolution by using equation (3.4), which yields a phase resolution of 24.3 mrads. This value in turn, limits the minimum useful path-length increment in the high accuracy stage of the servo, which was therefore chosen of about 25 mrads.

(3.3) The first quadrature tracking technique :

(3.3.1) The signal processing scheme :

One of the most effective techniques to recover the input signal, modulating the relative phase (ϕ_d) in a two-beam interferometric sensors, is the active homodyne technique, introduced by Jackson et el [7].

In this technique a fibre stretcher is incorporated into the reference arm of the interferometer. It forms part of a servo feedback loop to maintain the interferometer locked to one of its points of maximum sensitivity, corresponding to $\phi_d = (2q - 1)\,\pi/2$, where q is an integer. At these points, known as quadrature points, the two anti-phase outputs of a Mach-Zehnder interferometers are equal and hence their differential output is zero [8].

As discussed in chapter (1), a practical servo system will have a finite gain band-width product thus two forms of outputs are available from this system depending on whether the measurand frequencies are higher or lower than the band-width of the servo electronics. When the frequencies are lower the output of the system is taken from the feedback loop (high gain band-width mode output). The variations in ϕ_d caused by the measurand are cancelled by controlling the reference arm. When the measurand frequencies are much higher than the band-width of the servo system, the variations in ϕ_d are no longer compensated for by the servo system and the output is measured at the photodetector differential output as an error signal (low gain band-width mode output). The servo system merely acts to maintain the mean phase of the interferometer at a quadrature point, compensating only for slow drifts in the phase caused by environmental changes. The system may be considered linear for small amplitude high frequency measurands,

such that $\phi_d \ll 1$, [1].

The tracking range of the system is limited by the maximum (allowable) range of the compensating element (the fibre stretcher and the elastic properties of the fibre, in case of fibre interferometer). Because of this limited tracking range, the system needs frequent resetting, a simple servo, as that discussed in section (1.3.2), will in general lock to any quadrature point rather than the specified 'first quadrature point' on resetting. Such a sensor therefore has an unambiguous range constrained by the tracking limits. In addition each time the system is switched on it needs initialisation because the order of the quadrature point (the integer q) may take any value [9].

In our system we developed an active homodyne signal processing technique to lock the interferometer to the quadrature point nearest to the position of maximum visibility with negative slope; that is, where the phase difference between the signal and the reference arms is exactly $\pi/2$ radians. This happens when q = 1, hence it may be called the first quadrature point. Each time this system is switched on, or reset, it locks to the same quadrature point, the system then has the capability of self-initialisation. This technique possesses the high resolution of phase measurement, but retains the extended range associated with active homodyne technique of signal processing and the self initialisation of white light techniques.

(3.3.2) First quadrature location method :

This method represents a development of the previous one. The same optical configuration, shown in figure (3-1) was used to demonstrate the idea of first quadrature location and phase tracking, to maintain the system at the 'q = 1' quadrature point. In these experiments the ramp signal was disconnected and the feedback servo replaced with the version designed for first quadrature location. It employs a modified form of the two stage digital servo described previously, followed by a third analogue stage. The operation is as follows: after reset, the first stage rapidly decrements the path-length difference, of the interferometer, in steps slightly less than $\lambda/4$ generating a series of interference fringes of increasing amplitude. The envelope of this signal is monitored and used to locate the point of maximum interference amplitude as discussed before

(section 3.2.3). At this point, just beyond the maximum amplitude the up counter (in the first stage) is inhibited maintaining the interferometer at this near maximum point, then the second stage controls the optical path-length difference of the system. The operation of the second stage however is different to that described previously. This time it operates unidirectionally in steps of $\lambda/240$, and acts not to maximise the visibility, but to equate the photodetector outputs-that is, to locate the first quadrature point. The visibility function is symmetrical; hence, to avoid ambiguity, the quadrature point is always approached from the same direction. The interferometer is then continuously locked to this point using an integrator. In principle the system could be kept at quadrature by operating the second counter in a closed loop Up/Down mode, however the digital noise associated with continuous switching of the counter would give rise to a significantly higher noise level. The output of the integrator is superimposed on the total feedback voltage to ensure that the system is locked at this point. If the tracking range limits of the integrator are approached, then the process is reset automatically, and the first quadrature point is located as before. A schematic diagram of the electronic feedback servo is shown in figure (3-7), where the position of the first quadrature point is illustrated, the complete circuit diagram of the servo is discussed in appendix (B).

In this system a low band-width integrator was used (with a corner frequency of about 120 Hz). It was therefore possible to measure slowly varying measurands, such as temperature, directly from the feedback voltage. Rapidly varying low amplitude measurands were determined directly from the error voltage [7].

In this method, the visibility measurement is used only to locate the central fringe; a second stage of operation then locks to the nearest quadrature point. It is therefore only necessary for the visibility measurement to have an equivalent spectral resolution of $< \lambda/4$. It is evident that the longer the coherence length of the source, the poorer the resolution of the path length measurement. The required resolution of $\lambda/4$ therefore sets an upper limit on the coherence length, $L_{c\,\max}$, of the source which can be used. In fact, from equation (3.4), this limit is given by :

$$\frac{n}{S_o} < 1 - |\gamma_{11}(\lambda/4, L_{c\,\max})| \qquad (3.5)$$

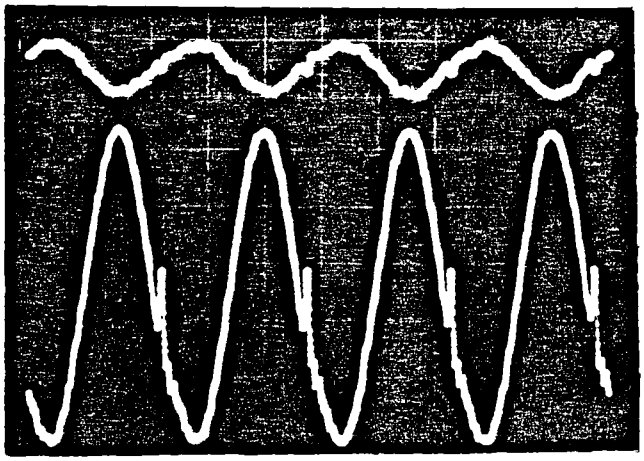

Figure (3-6) : Fringe amplitude before (upper trace) and after (lower trace) switching the first servo on.

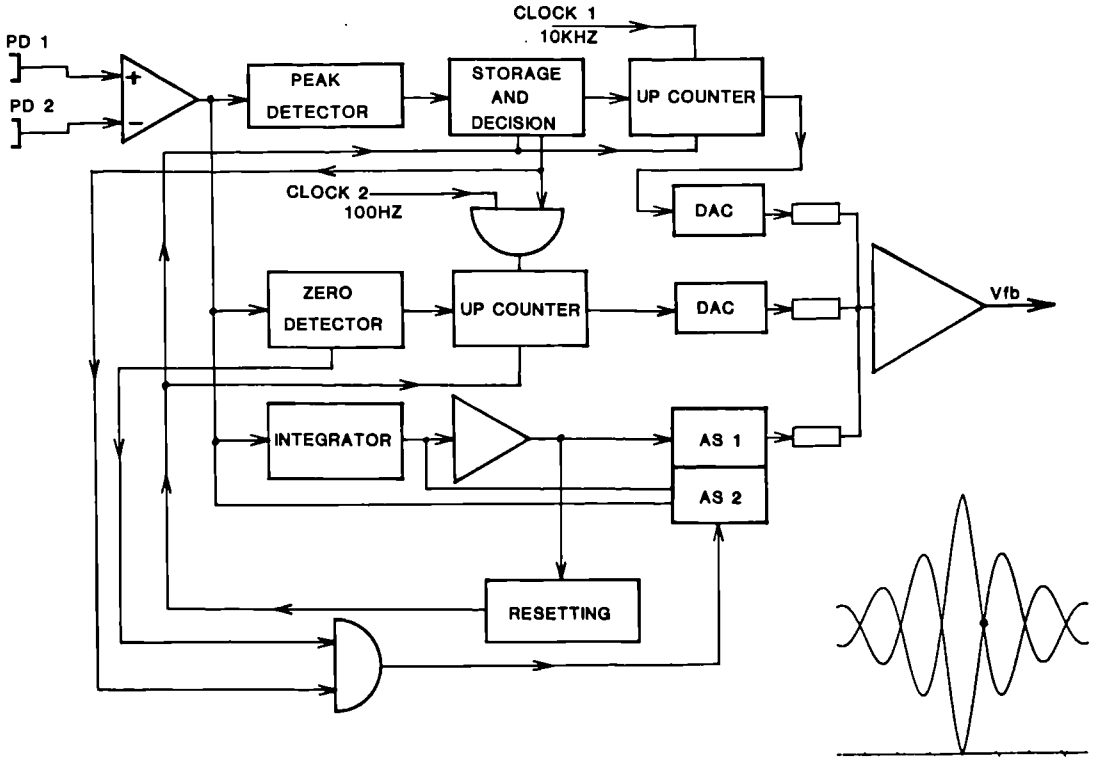

Figure (3-7) : Block diagram of the second (first quadrature tracking) servo.

where $|\gamma_{11}(\lambda/4\ ,\ L_{c\ max})|$ represents the auto-correlation function of the source at path-length imbalance of $\lambda/4$. Once the central fringe has been located, the phase resolution within which the quadrature point may be found is set by the noise floor at the input of the integrator of the servo used to locate the first quadrature point, which may be calculated using equation (1.8), independent of the resolution of the digital stages of the servo. This is true because the value of the measurand is again given by the voltage applied to the PZT-1. However in this case the feedback voltage is a summation of the first and second stages digital outputs and the output of the third analogue stage ($V_{fb} = V_1 + V_2 + V_a$), such that the value of the analogue voltage compensates any error caused by the the first stage due to its lower resolution.

(3.3.3) Testing the system as a DC and AC sensor :

The optical system shown in figure (3-1) with its first quadrature tracking servo, was used to demonstrate the concept of a fibre optic temperature sensor. Part of the fibre forming the sensing arm was heated in a variable temperature furnace, both the temperature of the furnace (measured with a thermocouple) and the feedback voltage to the PZT-1 tracking the point of first quadrature were then recorded. The A.C. resolution of the interferometer was also measured, by comparing the noise level to an A.C. signal generated by sinusoidally straining part of the fibre arms over a known amount (with amplitude corresponds to 0.56 optical radians).

The resolution of the system was estimated, as is usual in an active homodyne system, from the magnitude of the D.C. noise floor in the interferometer output and the voltage corresponding to the fringe amplitude. The r.m.s. noise floor was approximately 15.4 mV at the output of the differential amplifier, while the central fringe amplitude equalled 5.5 V, corresponding to a phase resolution of 2.8 m rad (calculated from equation (1.8)) giving a temperature resolution of 0.33 mK. Representative data are shown in figure (3-8), in which the total feedback voltage applied by the electronic servo is shown against the temperature of the sensing fibre present inside the furnace. The system was deliberately reset, to illustrate the capability of the servo to return back to the same position. Figure (3-9) illustrates the ability of the second system to sense an AC signals

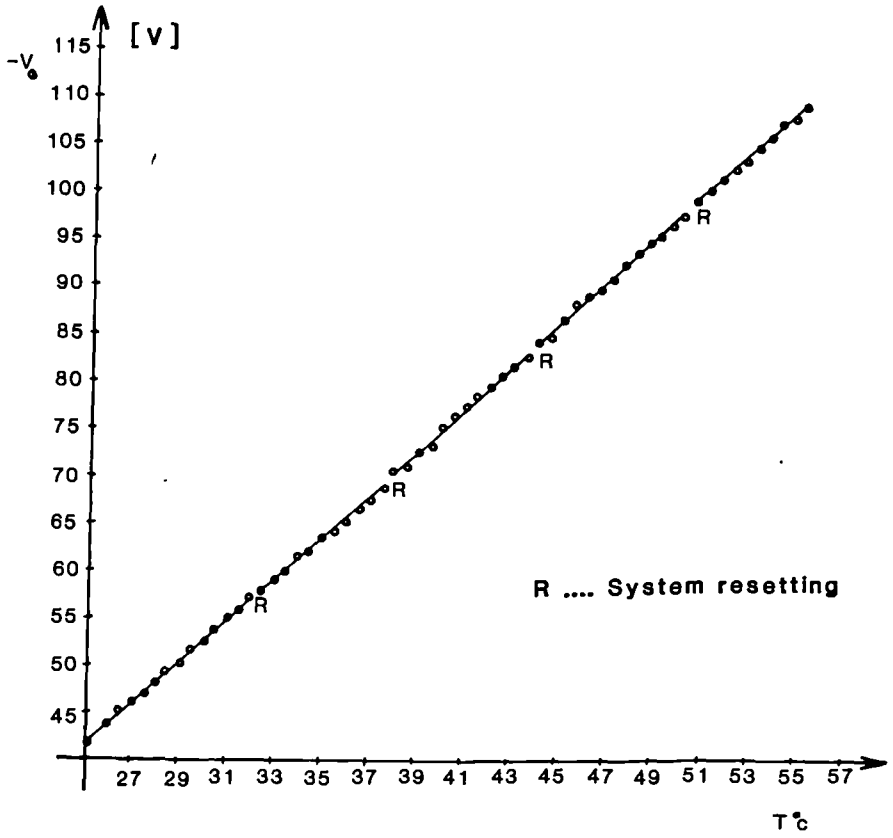

Figure (3-8) : Output voltage of the second servo against temperature.

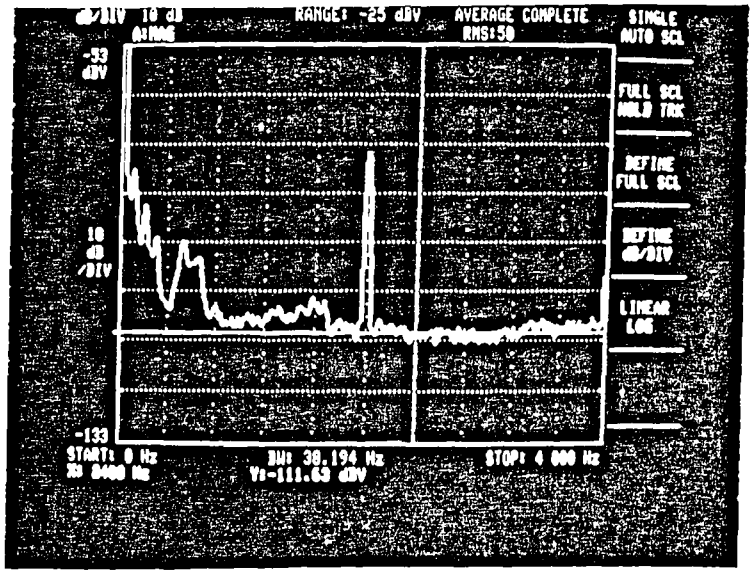

Figure (3-9) : Spectrum of the photodiode output, illustrating an AC signal detected by the interferometer when it was locked at the first quadrature point.

as a low gain band-width mode output where a small amplitude signal(0.56 radians) was applied as an AC strain using the fibre stretcher present in the signal arm.

(3.4) System noise, limitations and possible developments :

It is instructive to consider the fundamental limits of the phase resolution available using the either method, as set by the photodetector shot noise. In our experiments, the mean optical power at the output of each port of the interferometer was about 73.4 nW. The measured visibility of the central fringe (V_o) in these experiments was 0.75. This value is less than unity due to the polarisation mismatch between the recombining beams. Using this value for the visibility, the photo diode current, I_p, with the system locked to the position of zero path-length imbalance, $I_p = I_{mean}(1 + V_o)$, was 64.23 nA. The theoretical photodiode shot-noise current ($\sqrt{2I_p e}$) is 14.34 fA $(HZ)^{-1/2}$, hence the corresponding signal to noise ratio, within the 25 Hz band-width, is 91.68 dB. The dark current level at the output of each photodiode was about -125 dB, thus the noise level due to both effects may be estimated as : $n_t = \sqrt{(n_s)^2 + (n_d)^2}$, where n_s and n_d are the levels of the shot and dark current noise respectively. The theoretical limited signal to noise ratio is 89.61 dB. Using equation (3.1) this may be converted to a phase resolution of about 16 mrad (3.2 $mrad\ (Hz)^{-1/2}$) which may be compared with the experimentally obtained value of 24.3 mrad.

For the second method, in which the interferometer was locked to the first quadrature point, the mean photodiode current was 37 nA. This corresponds to a shot-noise limited phase resolution of 87 μrad for the 120 Hz bandwidth of the analogue servo system used ($\approx 8\mu rad\ (Hz)^{-1/2}$). The rather poorer 2.8 mrad resolution obtained in practice is thought to arise from source and environmental low frequency noise.

As noted in the theory section, there is an upper limit on coherence length of the source that can be used in the technique of locking to the first quadrature point. The coherence length must be sufficiently short that the central fringe can be unambiguously identified by its visibility. The upper limit may be calculated from equation (3.1), and using the noise level observed in our

experiments, this implies $L_c < 3.2$ mm. It is clear that this condition is comfortably exceeded by the source used in practice, for which $L_c \approx 50\ \mu m$.

The accuracy of the techniques we have described here are fundamentally limited by the accuracy of the path length compensating transducer. The piezo-electric fibre stretcher was used for reasons of convenience and availability, but is not the optimum choice, particularly since it is hysteretic. However, transducers having a positional accuracy better than 1 nm (for example) are available as standard commercial products; such as the Digital Piezo Transducer (DPT). It has no hysteresis and a claimed long term stability of less than 1 nm per day [11]. An alternative approach which offers even greater accuracy is to measure the path length change produced by the transducer using an auxiliary interferometer illuminated by a high stability laser, as described by Bosselmann [12].

To summarise, the chief advantage of the technique presented here is that it allows a measurand induced phase modulation in an interferometer to be determined unambiguously over a wide range. Furthermore, the interferometer is always returned to exactly the same phase value whenever it is switched on. This is in contrast to other methods in which the order of interference is generally undetermined. Moreover, because the interferometer is operated with a zero path imbalance, the wavelength of the source is unimportant. There is a slight dependence on wavelength when locking to the first quadrature point, but the effect remains insignificant for physically reasonable wavelength drifts. This is unlike conventional interferometers where usually only the fractional fringe information is determined, and not the fringe number, so that the total phase error is proportional not to the fractional wavelength change $\Delta\lambda/\lambda$, but to the product of the fringe number and $\Delta\lambda/\lambda$ [13].

The signal to noise ratio of this system is lower than that reported for typical interferometric sensors using a lasing source because of the significantly lower power coupled into the fibre from the laser diode, biased below threshold. This problem may be solved as follows :
After locking the system to the first quadrature point, an electronic circuit may be designed to increase the laser diode injection current very gently, passing through the threshold level. The

feedback servo will apply a small DC voltage to the interferometer, to keep it locked to the same quadrature point. This voltage may be considered as a fixed error in the total feedback voltage, representing the measurand. When the tracking range of the servo is about to be exceeded and just before the system resets the electronic circuit is used to decrease the injection current to the first level again, below threshold, to locate the first quadrature point. If this concept could be realised in practice it would be very useful, because the interferometer would be locked at a position of maximum sensitivity with an output signal of much higher signal to noise ratio and very low phase noise, as $\Delta L = \lambda /4$, [14] and very high long term system stability. As an example, if the source frequency changes within $\pm$ 10 Ghz, the corresponding phase will drift with $\pm$ 42 nrads.

We believe that this technique could be applied with advantage in multiplexed interferometric sensor arrays. A receiving interferometer containing a path length modulator would be used to address a number of remote interferometers, such as fibre Fabry-Perots [15]. The sensing interferometers would have path imbalances which differed from each other by much more than the coherence length of the source. The digital to analogue converter in the processing electronics would then apply a path imbalance in the receiving interferometer equal to the nominal imbalance of i^{th} sensing interferometer. The servo would then lock to exactly balance the receiving and sensing interferometers (or lock to the first quadrature point). The signal applied to the path length modulator then represents the phase of the i^{th} sensing interferometer. An advantage of this approach is that the sensing interferometers would be entirely passive.

(3.5) A coherent tuned sensor based upon a multi-mode laser diode :

(3.5.1) Introduction :

In chapter (2), we have shown that by using a multi-mode laser diode, with specific properties it is possible to replace the low power low coherence-length sources normally used in 'white light' systems, where more optical power may be coupled into the fibre, hence improving the system resolution. In this section we verify this concept experimentally by using a 5 mW multi-mode

semiconductor laser diode, Mutsubishi (ML4406) to illuminate a sensing system consisting of two Michelson interferometers linked by a monomode fibre.

(3.5.2) Experimental verification :

Prior to setting up the tandem interferometric system it was established that a launching efficiency of order of 10 % could be achieved with 5μ *m* core, monomode, optical fibre. At laser current of 80 mA the optical spectrum of the light emerging from the fibre was measured using the optical spectrum analyser (MS 9001 B1), which is shown in figure (3-10).

The laser was used to illuminate the optical system, shown in figure (3-11). Its output was collimated and launched into the input port of an optical fibre directional coupler. The sensing interferometer was connected to one of the output ports of the coupler via a few meters of fibre. The output beam was collimated with a lens which also served as an auto-collimator to collect the output signal from the sensing interferometer. This light was then transferred by the input fibre to

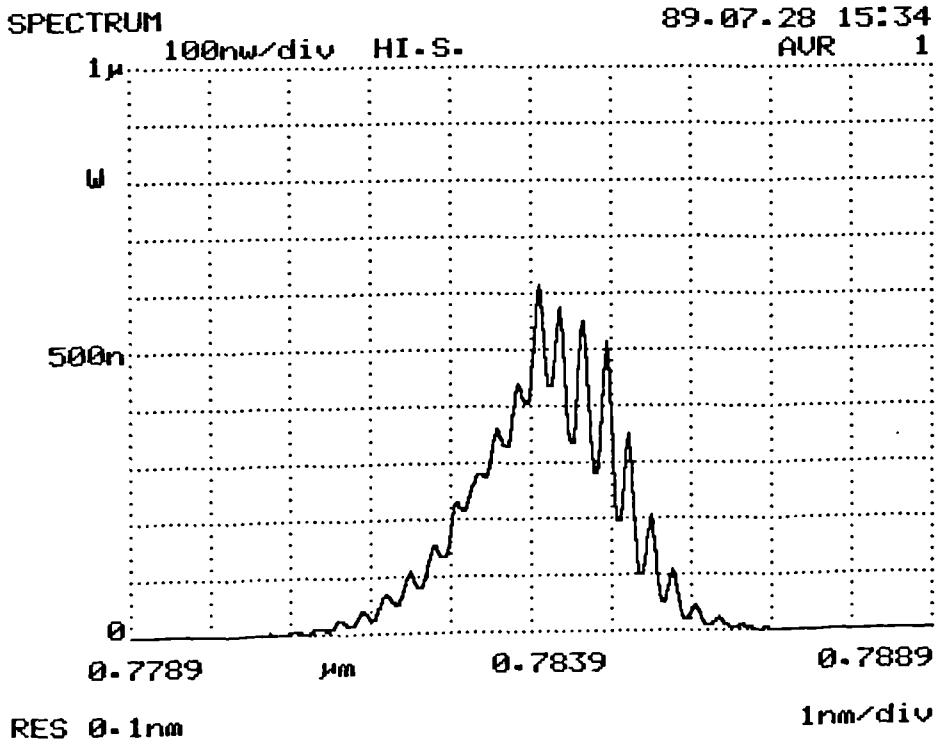

Figure (3-10) : Optical spectrum of the light emetting from the multi-mode laser diode Mitsubishi (ML-4406), as measured under CW-mode operation.

the receiving interferometer via the directional coupler. The mean output power detected at the output of the receiving interferometer was 6 μW. The output fibre from the other output port of the coupler was cleaved at an angle and placed into an index matching gel to avoid reflections.

The sensing interferometer was a bulk-optic Michelson interferometer with one of its mirrors mounted on a micro-translation stage, TS-1, the second mirror was mounted on a piezo-electric transducer, to permit fine control of the interferometer path-length imbalance. The other output of the sensing interferometer was detected by photo-detector (PD-1) , enabling the source auto-correlation function to be determined. The receiving interferometer was a Michelson with similar features. The output of the two tandem interferometers was detected by photo-detector (PD-2) in order to study the performance of the system acting as a simple remote displacement sensor.

To measure the source auto-correlation function, the sensing interferometer was adjusted until it was nearly balanced. A sinusoidal signal was then applied to the PZT-1 and its amplitude set such as to scan one complete interference fringe. The interferometer was finely balanced using the translation stage and the PZT. The interference fringe visibility was measured as a function of the path-length imbalance ΔL_1.

To study the performance of the system with the interferometers in tandem, a sinusoidal signal was applied to the second PZT, in the receiving interferometer. The path-length imbalance of the sensing interferometer was adjusted to be $\simeq 0.5\, l_{cav}$. The path length imbalance of the receiving interferometer (ΔL_2) was then adjusted to match the path-length imbalance of the sensing interferometer (ΔL_1). This was accomplished as follows: the path-length imbalance of the receiving interferometer was adjusted via a translation stage (TS-2) and set such that it corresponded to the point in the transfer function just before the position of maximum visibility. A feedback servo was next used to apply a feedback voltage to PZT-2 locking the tandem system at the first quadrature point nearest to this position of maximum visibility. With the system locked, signal to noise ratio measurements were then made with the system operating in this mode. As the receiving interferometer is potentially a source of noise due to environmental perturbations, it was also

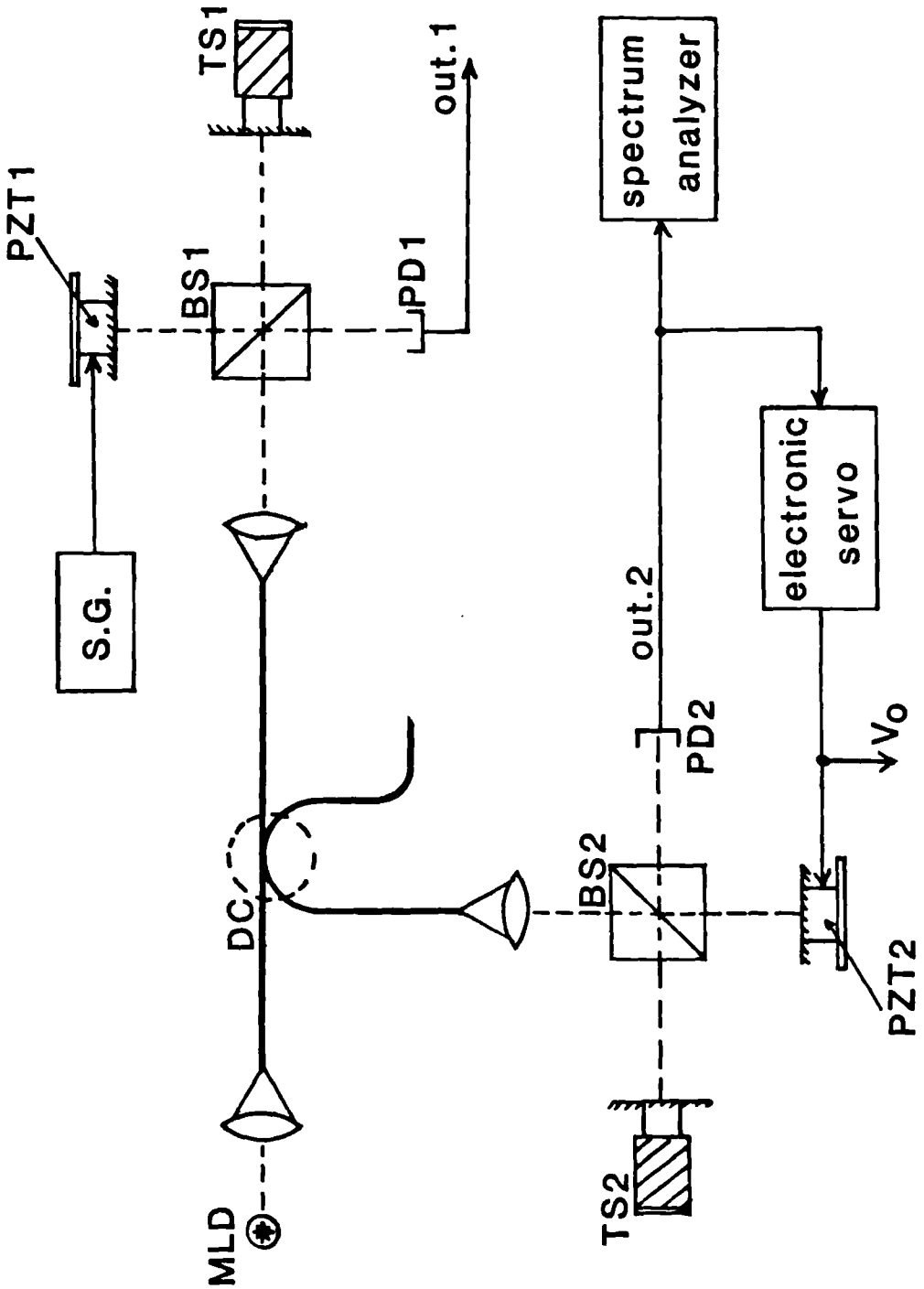

Figure (3-11) : The optical set-up used to characterise the multi-mode laser diode.

necessary to measure this noise in order to make a more accurate accessment of the overall noise of the system.

To measure the amplitude of the interference signal produced only in the receiving interferometer, the servo loop output was disconnected and with the path-length imbalance of the receiving interferometer kept virtually constant, the path-length imbalance of the sensing interferometer was then increased such that it was more than 20 times the laser cavity length (l_{cav}) and set so as not to coincide with one of the $2pl_{cav}$ resonances. During these measurements care was taken to maintain the mean output level of the whole system unchanged. This procedure ensures that no interference signals will be produced due to the sensing interferometer or the two interferometers in tandem. The intensity noise associated with the movement of PZT-2 was also measured simply by blocking off the other mirror of the Michelson receiving interferometer. The performance, of the system, was measured for a range of values of ΔL_1 corresponding to 1.5 l_{cav}, 2.5 l_{cav}, 3.5 l_{cav} etc.

Finally to demonstrate the system acting as a simple remote displacement sensor, the path-length imbalance ΔL_1 was adjusted to one of the 'n' operating points, in this case n = 10 equivalent to $\Delta L_1 \equiv 20.5\, l_{cav} \approx 22.87\ mm$. The receiving interferometer was then adjusted to rebalance the system which was kept locked at the first quadrature point as discussed in section (3.2). A small displacement signal was next applied to the sensing interferometer by applying a slowly increasing voltage to PZT-1. The corresponding feedback voltage applied by the servo in the receiving interferometer, to maintain the system locked at the same quadrature point, was measured as a function of the input displacement.

(3.5.3) Performance :

Figure (3-12 a,b) illustrates the absolute value of the source auto-correlation function (interference visibility) as measured verses the interferometer path-length imbalance. Figure (3-12 a) shows the location of the sets of interference packets and their peak values for a range of path-length imbalances between 0 - 28 mm. As the auto-correlation function is an even function

of ΔL , the complete function may be obtained by reflecting it about the vertical axis. The variation of the fringe visibility, of the central interference packet verses the path-length imbalance (in steps of 10 interference fringes = 7.84 μm), is illustrated in figure (3-12 b), these results resemble that obtained by Grattan et el for the Sharp laser diode ' Sharp LTO-23-MDO' [16]. Using a least square fitting technique, the visibility function of the central packet may be represented as: $V(\Delta L) = a + b(\Delta L) + c(\Delta L)^2$, where a = 0.942241606, b = -4.7652716×10^{-3} and c = -2.45009707×10^{-5}, where ΔL is measured in μm . This function is plotted also in figure (3-12 b).

Figure (3-13 a) shows the variation of the mean noise floor of the two tandem interferometers compared with the residual interference signal, produced in the receiving interferometer alone. It can be seen ,from the figure that the level of the system noise is much higher than the level of the mean noise floor when ΔL_1 is small i.e. about 10.8 dB for $\Delta L_1 = 0.5\, l_{cav}$, and decreases gradually as ΔL_1 increases. For values of $\Delta L_1 > 20\, l_{cav}$ the overall system noise approaches the minimum value associated with the receiving interferometer. These values were measured with a system band-width of 477.5 Hz. The corresponding phase resolution of the system varies in a similar fashion from $\approx 2.19\times10^{-5} rad/\sqrt{Hz}$ for $\Delta L_1 \approx 0.5\, l_{cav}$ to better than $5\mu\, rad/\sqrt{Hz}$ as $\Delta L_1 > 20\, l_{cav}$ as shown in figure (3-13 b). This value is very close to the theoretical limit of 2.8 $\mu\, rad/\sqrt{Hz}$ set by the photo-detector shot noise, the difference may be attributed to the electronic noise in the system.

The output voltage of the feedback servo , applied to PZT-2, is plotted verses the displacement of the mirror of the sensing interferometer in figure (3-14) for a displacement range of 28 microns, the displacement resolution of the system was $\geq 6.24x10^{-13} m$.

From the data shown in figure (3-13 a), it can be seen that the path-length difference between each successive interference packets is 2.231 mm, thus the laser cavity length is about 1.116 mm, and the mode separation is 134.4 GHz. The peak value of the central packet of interference is much larger than the successive interference packets, this indicates that a considerable fraction of the laser output power is emitted spontaneously and that dispersion has some

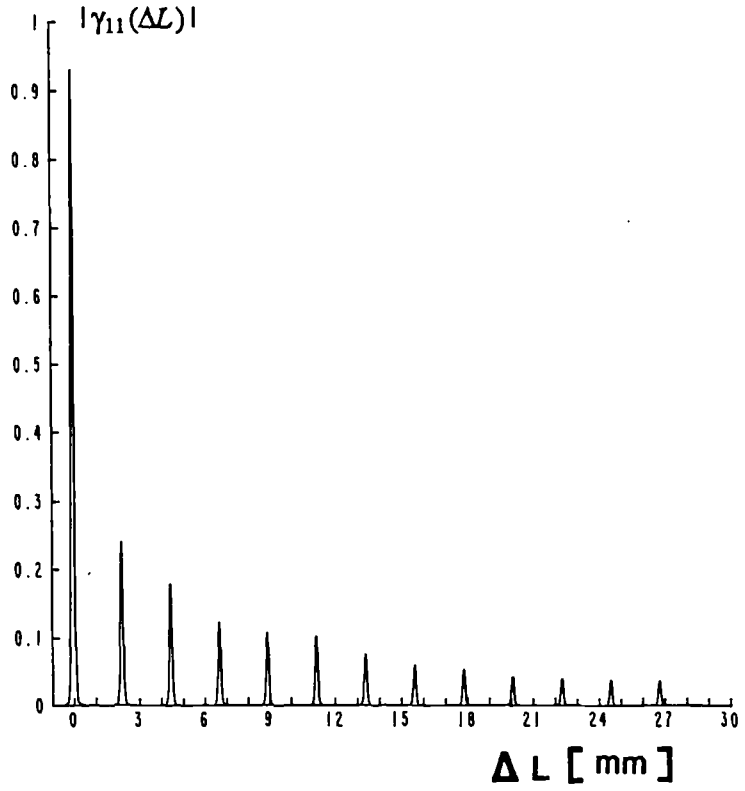

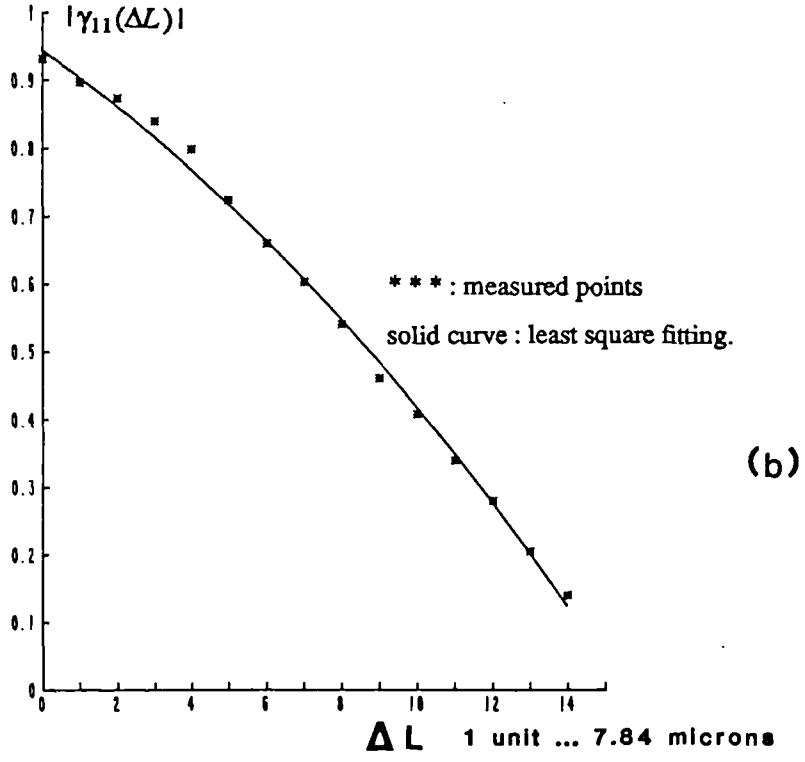

Figure (3-12) : The multi-mode laser diode normalised auto-correlation function;

(a) : location and peak values of the sets of interference packets,

(b) : the visibility variation of the central interference packet;

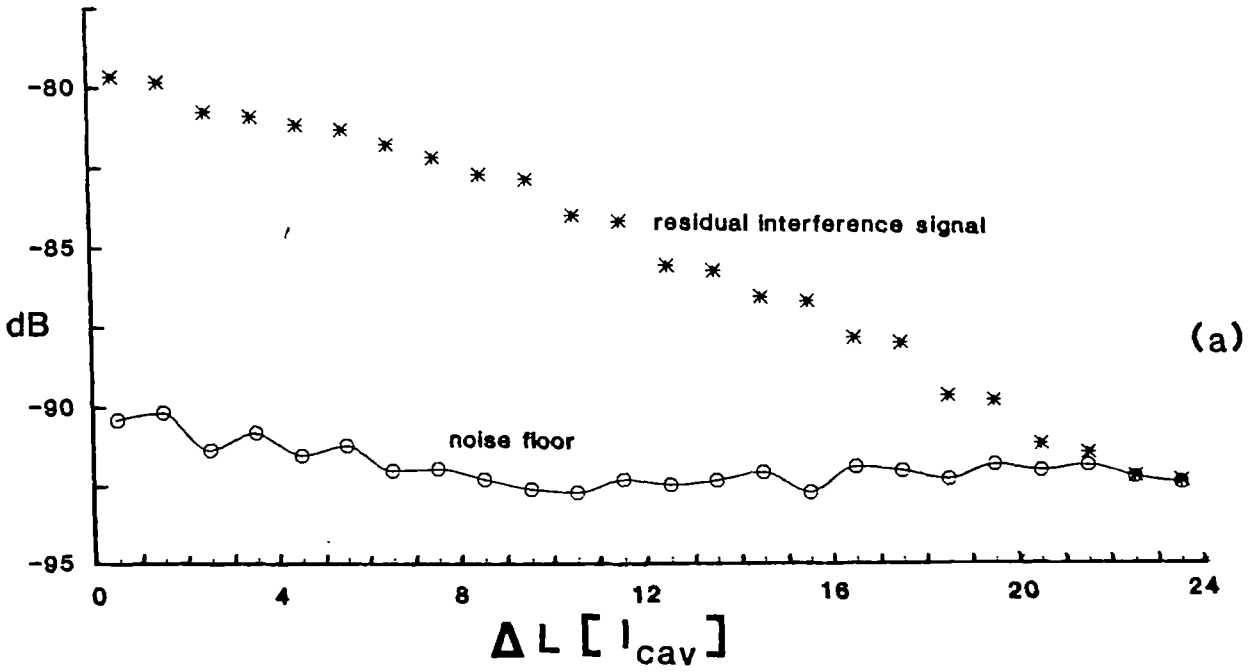

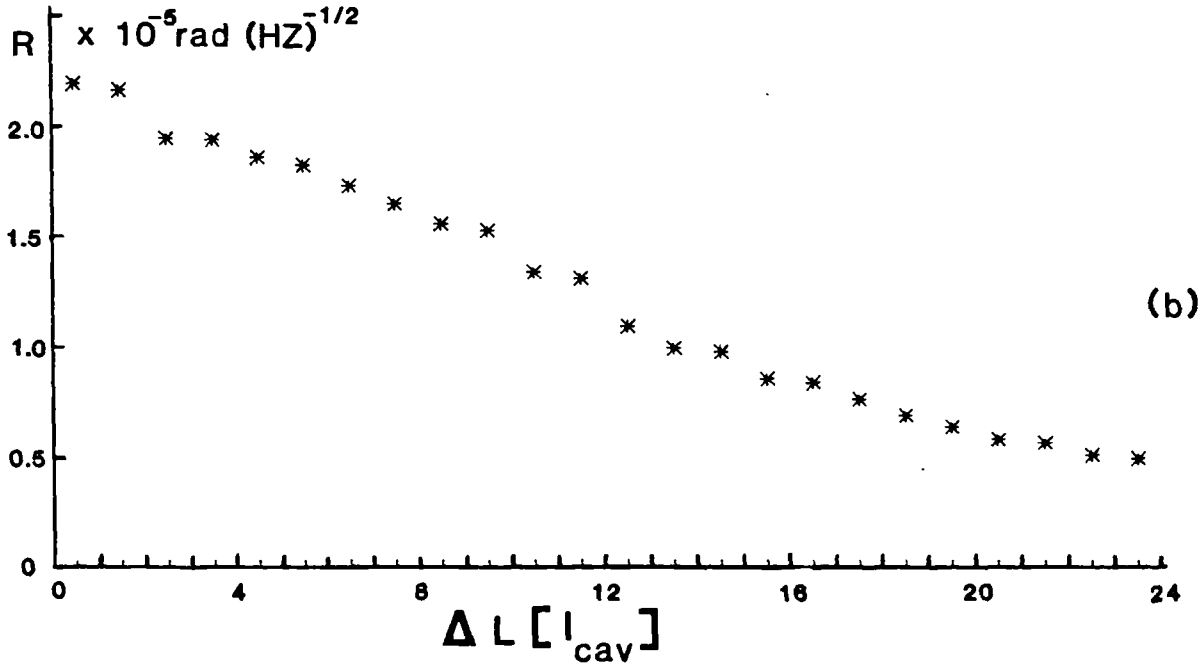

Figure (3-13)

(a) : The variation of the mean noise floor of the two tandem interferometers compared with the residual interference signal due to the receiving interferometer.

(b) : The variation of the system phase resolution.

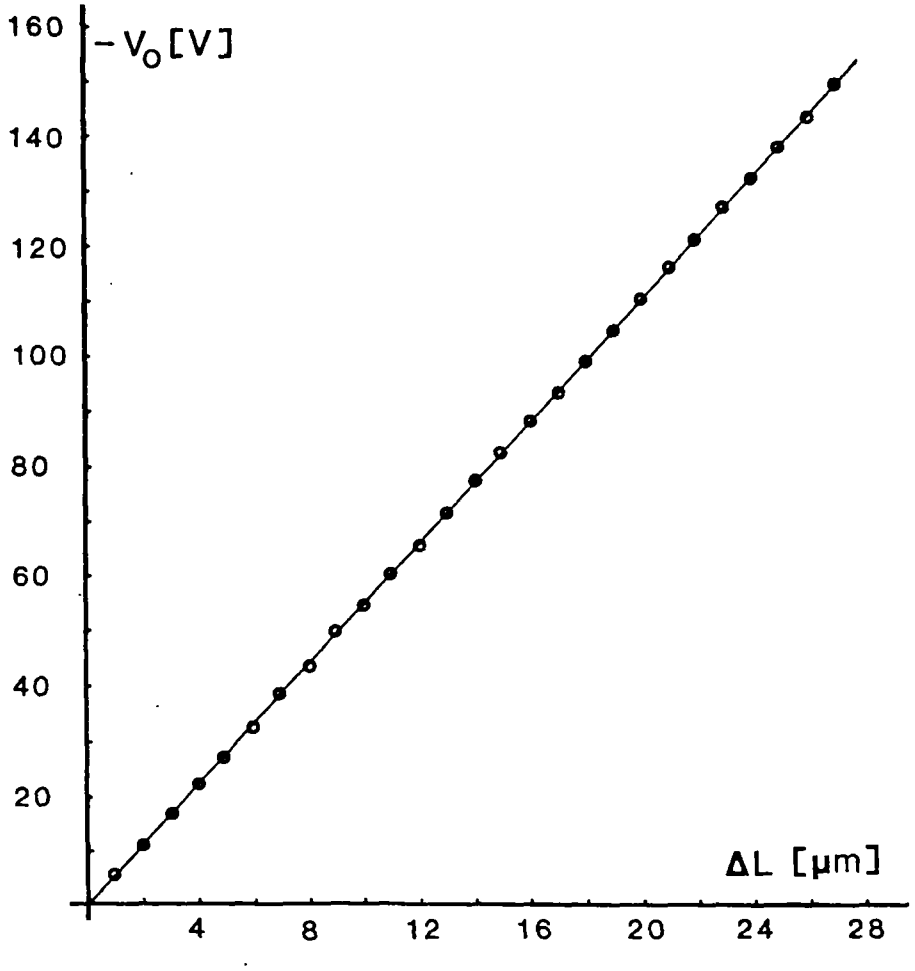

Figure (3-14) : The output voltage of the second feedback servo against the displacement of the mirror of the sensing interferometer.

effect on the observed laser spectrum, this is also clear in the laser spectrum as shown in figure (3.10).

The interference packet width, W, is nearly 85 μm , this effective coherence length is sufficiently short to satisfy the necessary condition to locate the central interference fringe, as discussed in equation (3.5). According to the criterion set by equation (2.30), the permitted working range between two successive packets is nearly 0.6 mm; the corresponding dynamic range is $\approx 9.7x10^8$.

In principle, for $\Delta L_1 \gg L_{cm}$ the system resolution is independent of either the sensor path-length or the source wavelength stability. Practically when the sensor length is increased the matched optical path-length imbalance of the receiving interferometer will also increase. In this case the system long-term stability will depend critically on the stability of the receiving interferometer. Hence it must be contained in a highly stabilised environment and designed carefully using materials with very low expansion coefficients. Moreover the piezo-electric transducer, deployed in the receiving interferometer, must be very stable; such as the Digital Piezo Transducer referenced in section (3.4).

(3.6) Conclusions :

A signal processing technique has been developed for fibre optic interferometric sensors illuminated by low coherence-length sources. In this technique, the system is locked either to the position of max interference visibility or to the first quadrature point. Such a sensor, based on the second technique, therefore has the full resolution of a conventional interferometer, but has the major advantage of an unambiguous operating point. We have demonstrated the first technique for slowly varying measurands and the second technique both for slowly varying and periodic measurands. The use of multi-mode laser diodes as an alternative to the low power low coherence-length sources normally used in 'white light' systems was demonstrated. The main advantage being that as more optical power is coupled into the system, the overall resolution may be improved by a factor of 100 times or more.

References

[1] D.A.Jackson, " Monomode optical fibre interferometers for precision measurement ", J.Physics E:Scientific Instruments, Vol.18, 1985, P.981.

[2] D.A.Jackson and J.D.C.Jones," Fibre Optic Sensors ",Optica Acta,Vol. 33, No.12, 1986, P.1469.

[3] A.S.Gerges, F.Farahi, T.P.Newson, J.D.C.Jones and D.A.Jackson ," An interferometric fibre-optic sensor using a short coherence-length source ", Electronics Letters, Vol. 23, No.21, October 1987, P.1110.

[4] A.S.Gerges, F.Farahi, T.P.Newson, J.D.C.Jones and D.A.Jackson ," Fibre optic interferometric sensor utilising low coherence-length source : resolution enhancement ", Electronics Letters, Vol.24, No. 8, April 1988, P.472.

[5] A.S.Gerges, T.P.Newson and D.A.Jackson ," A coherent tuned fibre-optic sensing system, with self initialisation, based upon a multi-mode laser diode ", Submitted to Applied Optics, October, 1989.

[6] A.Dandridge ," Zero path-length difference in fibre optic interferometers ", J. Of Lightwave Technology, Vol.LT-1, No.3, September 1983, P.514.

[7] D.A.Jackson, R.Priest, A.Dandridge and A.B.Teveten ," Elimination of drift in single mode optical fibre interferometers using a piezo-electrically stretched fibre ", Applied Optics, Vol.19, No.17, September 1980, P.2926.

[8] " Workshop on single mode Optical Fibre Sensor Technology " Course notes, University of Kent and Sira Ltd., U.K, 1985, P.145.

[9] K.Fritsch and G.Adamovsky ," Simple circuit for feedback stabilisation of a single-mode optical fibre interferometer ", Rev. Scientific Instruments, Vol.52 ,No.7, July 1981, P.996.

[10] P.Horowitz and W.Hill ," The art of electronics ", Cambridge University Press, 1986, P.31.

[11] Digital Piezo Transducers, Technical catalogue, Queensgate Instruments Ltd, 1988.

[12] T.Bosselmann ," Multimode-fibre coupled white-light interferometric position sensor ", NATO ASI Series, Vol. E132,eds: ANChester, SMartellucci, AM Vega Scheggi (Martinus Nijh-off, 1987), P.429.

[13] " Workshop on single mode Optical Fibre Sensor Technology " Course notes, University of Kent and Sira Ltd., U.K, 1985, P.182.

[14] A.Dandridge and A.B.Teveten ," Phase noise of single-mode lasers in interferometer systems ", Applied Physics Letters, Vol.39, No.7, October 1981, P.530.

[15] A.D Kersy, D.A.Jackson and M.Corke ," A simple Fabry-Perot Sensor ", Optics Communications, Vol.45, No.2, March 1983, P.71.

[16] K.T.V.Grattan, A.W.Palmer, N.Y.Ning and B.T.Meggitt, " Interferometric sensors-Extension of range using low coherence light from laser diodes ", EFOC/Lan'89 Conference, Amesterdam, Holland, June 1989, Conference Proceeding P. 375.

CHAPTER (4)

A hemispherical air cavity fibre Fabry–Perot sensor: applications to temperature measurement

(4.1) Introduction

The general advantages of fibre optic sensors have been discussed in chapter (1), the introduction of the systems into the general measurement field has been relatively slow because of the inherent difficulties in mass-producing sensing systems of this type.

The most basic form of the monomode fibre optic sensor is the two beam interferometer, which may be of the Mach-Zehnder [1], Michelson [2] or low-finesse fibre Fabry-Perot [3] configuration. In each case, the transduction mechanism is the phase modulation of the fibre guided beam. The disadvantage of the first two configurations, for example when they are used as temperature sensors, is the presence of the extra fibre which serves as the reference arm and which tends to increase the system sensitivity to unwanted environmental perturbations, especially when operated remotely. Significant advantages are offered by employing reflective Fabry-Perot interferometers. They are truly remote in that the signal is not corrupted by any perturbations occurring along the fibre lead section and the measurand can be localised by reducing the length of the Fabry-Perot sensing element to almost a point sensors. Although the fibre Fabry-Perot interferometer has been used successfully as a remote temperature sensor [4], a number of problems limit its applicability. These difficulties arise from the use of an optical fibre sensing element, as the dependence of optical path length on temperature is not well characterised. This is because the

thermal properties of the fibre will therefore vary from batch to batch, so that it is difficult to fabricate many sensors with the same specification, and it is generally necessary to calibrate each one. Also, these thermal properties may change over a period of time, thus necessitating periodic re-calibration. In a fibre sensing element, the change of optical path length with temperature arises chiefly from the temperature dependence of the refractive index.

The concept of a sensing air cavity addressed remotely via an optical fibre link is one of the simplest solutions to have a highly stable sensing element. Many authors introduced this idea in their reflective, intensity modulation, sensing systems to measure temperature or pressure [5,6]. The basic principle of these sensors is based upon the use of an air cavity at the end of a multi-mode fibre link, with a reflecting baffle forming the other end of the cavity; the measurand induced deflection of the reflecting baffle modulates the intensity of the light reflected, and hence re-captured by the fibre. This light is monitored remotely and processed in comparison with a reference light signal from the same optical source, ideally the source should have a low coherence length to avoid additional intensity modulation via interference. There are presently several pressure sensors based on this technology, some of them are fully microprocessor controlled and targeted at the medical applications [7]. It is well known that the sensitivity of these sensors, based on light intensity modulation, is much worse than that reported for interferometric sensing systems [8].

Air spaced Fabry-Perot interferometers have been demonstrated for several measurands, an acoustic sensor based on an air cavity Fabry-Perot interferometer has been described in which the sensor head was constructed at the end of a single-mode optical fibre, where a coated diaphragm formed the far end of the Fabry-Perot sensing interferometer [9]. A different variation of an open-path Fabry-Perot interferometric sensor with a monomode fibre lead, for measuring temperature in a gas flow and steam turbine, has also been reported, here the sensing cavity length was about 2 cm [10]. In these systems it was necessary to use a collimating lens to re-focus the reflected beam, from the far end of the interferometer, into the monomode fibre core. This lens introduces an excess optical path-length inside the sensing interferometer, which may be a source

of erroneous phase changes, superimposed on the true phase of the signal. It may also restrict the working range of the sensor itself, for example the maximum working temperature. Another possibility is to use very short Fabry-perot cavities (shorter than 200 μm), this is not suitable for many applications and signal processing techniques [11].

In this chapter we have developed a novel interferometric sensor, based on fibre optic technology, in which the sensing element is a miniaturised hemispherical air-spaced Fabry-Perot interferometer, addressed via a monomode optical fibre. This sensor does not require any optical components to be installed inside the cavity because the spherical reflector, forming the second mirror of the interferometer, is matched, in curvature, the wave-front of the Gaussian beam ejected from the fibre end ensuring very efficient re-launching of the light back into the fibre. As will be seen, the nature of the interferometer's transfer function enables us to control the value of the interference visibility. This can be used to produce many interferometers with the same specifications. Moreover the radius of curvature of the spherical reflector can be freely chosen, increasing the flexibility in design over range and resolution. The hemispherical Fabry-Perot air cavity enables one to design fibre-optic based sensors for displacement, refractive index or temperature measurements (section (4.5)). The interferometer can be designed to serve as a microphone, a miniature accelerometer or a contact vibration sensor (chapters 5 and 6). As the sensing element is so compact, this arrangement effectively combines the advantages of the fibre optic sensor with the reproducibility of a conventional interferometer.

(4.2) The hemispherical Fabry-Perot interferometer, illuminated by a coherent source :

(4.2.1) Optical arrangement and transfer function :

The optical configuration and details of the hemispherical air cavity Fabry-Perot sensor are shown in figure (4.1-a). A spherical reflecting surface, with radius of curvature (R), was used as the outer mirror of the air cavity Fabry-Perot interferometer, while the inner mirror of the interferometer was formed by the fibre face itself.

The optical properties of the air cavity were analysed theoretically using the familiar

Kogelnik's ABCD ray transfer matrix formalism [12,13] which describes the propagation of Gaussian beams. The transfer matrix of the hemispherical cavity is calculated using its equivalent lens representation, as shown in figure(4.1-b). The spherical mirror is replaced by a lens, with the same focal length (f = R/2), where the lens spacing, from the fibre end, is the same as the mirror spacing (d). The ray paths through the two structures are the same except that the ray pattern is folded in the actual system and unidirectional in the equivalent configuration, such that the fibre end, in the actual system, is replaced by two fibre ends, one serves as a transmitter and the other as a receiver. The transfer matrix, T , is calculated by multiplying the transfer matrices of the optical components forming the equivalent configuration, such that :

$$\mathbf{T} = \mathbf{T}_3\,\mathbf{T}_2\,\mathbf{T}_1 = \begin{bmatrix} A & B \\ C & D \end{bmatrix} \tag{4.1}$$

where

$$\mathbf{T}_{1,3} = \begin{bmatrix} 1 & d \\ 0 & 1 \end{bmatrix} \tag{4.2}$$

and

$$\mathbf{T}_2 = \begin{bmatrix} 1 & 0 \\ -2/R & 1 \end{bmatrix} \tag{4.3}$$

From the foregoing; the elements, of the matrix T , are:

$$A = 1 - \frac{2d}{R} \tag{4.4}$$

$$B = d\left(2 - \frac{2d}{R}\right) \tag{4.5}$$

$$C = -\frac{2}{R} \tag{4.6}$$

$$D = 1 - \frac{2d}{R} \tag{4.7}$$

where d is the length of the air cavity and R is the radius of curvature of the curved reflecting surface. The stability condition for this cavity, for which the ray position stays close to the optical

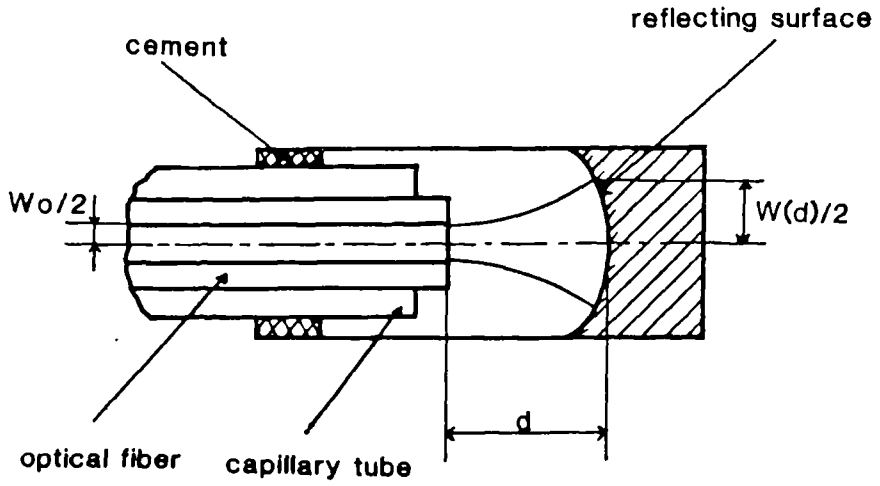

(a)

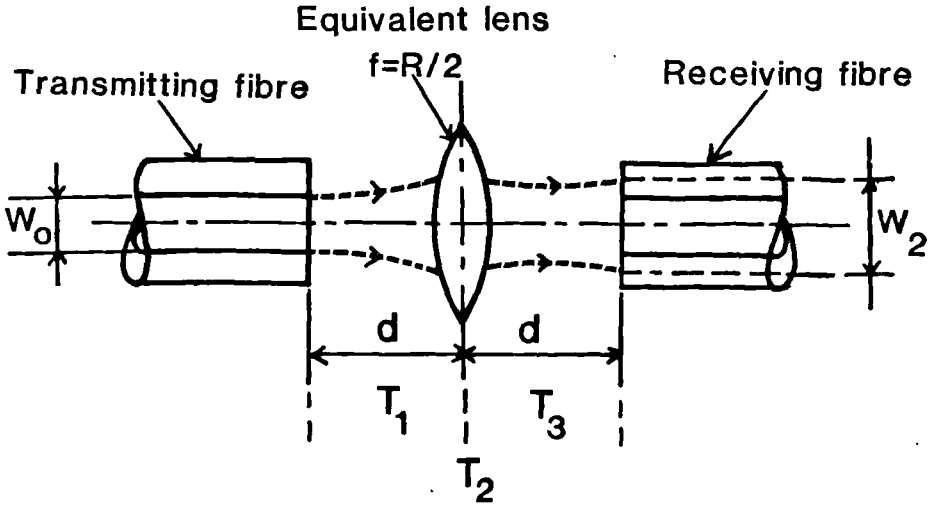

(b)

Figure (4-1) :

(a) : The hemispherical air-cavity Fabry-Perot interferometer.

(b) : The equivalent lens representation.

axis even after many transits between the fibre end and the spherical mirror [13], is that:

$$0 \leq 1 - \frac{d}{R} \leq 1 \tag{4.8}$$

To a good approximation, the beam emerging from the fibre into the cavity has a Gaussian irradiance profile of diameter equal to that of the fibre core, and may hence be described by the factor q_1 [14], where:

$$\frac{1}{q_1} = \frac{1}{R_1} - \frac{i\lambda}{\pi W_1^2} \tag{4.9}$$

R_1 is the radius of curvature of the wave-front of the emerging beam ($R_1=\infty$),W_1 is the beam width, which approximately equals to the core diameter of the fibre W_o , $i = \sqrt{-1}$ and λ is the wavelength of the light.

After transformation by the ABCD matrix, the beam is described by the parameter q_2, where:

$$q_2 = \frac{Aq_1 + B}{Cq_1 + D} \tag{4.10}$$

To a good approximation, the fraction of the optical power recaptured by the fibre is given by:

$$G = \frac{W_o^2}{W_2^2} \tag{4.11}$$

where W_2 is the width of the reflected beam at the fibre face, assuming the reflectivity of the curved surface to be unity ($\frac{1}{q_2} = \frac{1}{R_2} - \frac{i\lambda}{\pi W_2^2}$). From the foregoing, it can be proved that :

$$W_2 = W_o \left[A^2 + \left(\frac{\lambda B}{\pi W_o^2}\right)^2\right]^{\frac{1}{2}} \tag{4.12}$$

and hence :

$$G(d) = \left[1 - \frac{4d}{R} + \frac{4d^2}{R^2} + \frac{4\lambda^2}{\pi^2 W_o^4}\left(\frac{d^4}{R^2} - \frac{2d^3}{R} + d^2\right)\right]^{-1} \tag{4.13}$$

Figure (4.2) illustrates a plot of the function G against the cavity length (d) for different values of the radius of curvature of the outer mirror for the air spaced cavity. It is clear that the intensity reflected back to the fibre decreases rapidly with cavity length when two plane surfaces form the cavity ($R = \infty$). This behaviour is markedly different from the case when the Fabry-Perot is in the form of a monomode fibre, where the optical power is guided inside the fibre and hence the reflected intensity is independent of mirror separation. For planoconcave cavities two peaks in reflectance are observed. The first peak corresponds to d = 0 and the second corresponds to matching the radius of curvature of the emerging wave-front of the Gaussian beam with that of the mirror; this occurs when the cavity length nearly equals the radius of curvature of the mirror.

If r_1 and r_2 are the intensity reflection coefficients of the fibre end and the curved surface respectively, then the intensities reflected from these two surfaces (I_1, I_2) are:

$$I_1 = r_1 I_i \tag{4.14}$$

$$I_2 = r_2(1 - r_1)^2\, G(d) I_i \tag{4.15}$$

where I_i is the intensity of the incident light.

If the source of light illuminating the cavity is coherent, i.e. the source coherence length is much longer than the cavity length, interference will occur between light reflected from the fibre face and that reflected from the curved surface. As the reflectivities, of both the fibre end and the mirror, are low (for example, $r_1 \leq 0.04$), higher order reflections may be neglected. The sensing element may be regarded as a two beam interferometer with the familiar transfer function:

$$I_D = I_i\, [r_1 + r_2(1 - r_1)^2\, G(d)] \times [1 \pm V\, Cos\, \Delta\, \Phi(\tau)] \tag{4.16}$$

where I_D is the detected intensity from the interferometer, V is the visibility constant and

$$\Delta\, \Phi(\tau) = \frac{4\pi d n}{\lambda} \tag{4.17}$$

where n is the refractive index of the medium filling the cavity ($n \approx 1$ for air). The visibility (V) is a function of the reflectivities (r_1 and r_2) and the cavity length (d). Neglecting polarisation

effects, the visibility may be calculated using equation (2.6) as :

$$V(d) = \frac{2\sqrt{r_1 r_2 (1-r_1)^2\, G(d)}}{r_1 + r_2 (1-r_1)^2\, G(d)} \tag{4.18}$$

The variation of the calculated visibility, V(d), with the cavity length is shown in figure (4.3). The radius of curvature is taken to be 5 mm. The visibility is plotted for r_2 = 0.0434, 0.1, and 0.8 with r_1 = 0.04 . The figure shows that for r_2 = 0.0434, the value of $r_2(1-r_1)^2 = r_1$ and then I_1 equals I_2 where G = 1. Hence the visibility is maximum (equals unity) near the confocal position, where d = R, within a range of about $\pm 50\ \mu m$. Because G(d) is nearly an even function in the neighbourhood of d = R, then as | d-R | increases, G(d) decreases. As G(d) decreases, I_2 will be smaller than I_1 and hence the visibility will decrease. The situation is different for $r_2 \gg r_1$, because at G(d) = 1, the intensity I_1 is much less than I_2 and hence the visibility is less than unity. As | d-R | increases, G(d) decreases and hence the value of I_2 . At two positions d_1 and d_2, far from d = R, the value of $r_2(1-r_1)^2\, G(d_{1,2}) = r_1$ and then the visibility becomes unity. The position of maximum visibility with shorter d is preferred as an operating point for the interferometer because the condition of the cavity stability, equation (4.5), is satisfied. The interference visibility will remain nearly unity within a range of the same order as the first case and then it decreases with further increase of | d - R |. Practically the value of the maximum visibility is less than unity due to the slight difference of the polarisation states of the two interfered beam as a result of their reflection from two different surfaces.

(4.2.2) Fabrication of the sensing element :

A number of Fabry-Perot sensing elements were constructed, in which two different techniques were successfully used to form the outer mirror. In the first technique, the mirror was formed by solidifying molten solder on the end of a capillary tube. In the second, the curved reflector was formed by pressing a steel sphere(ball bearing) into an aluminium surface. A relatively low reflectivity mirror is enough for this configuration as it is necessary to match the reflectivity of the fibre end so that the visibility of the interferometer is maximised.

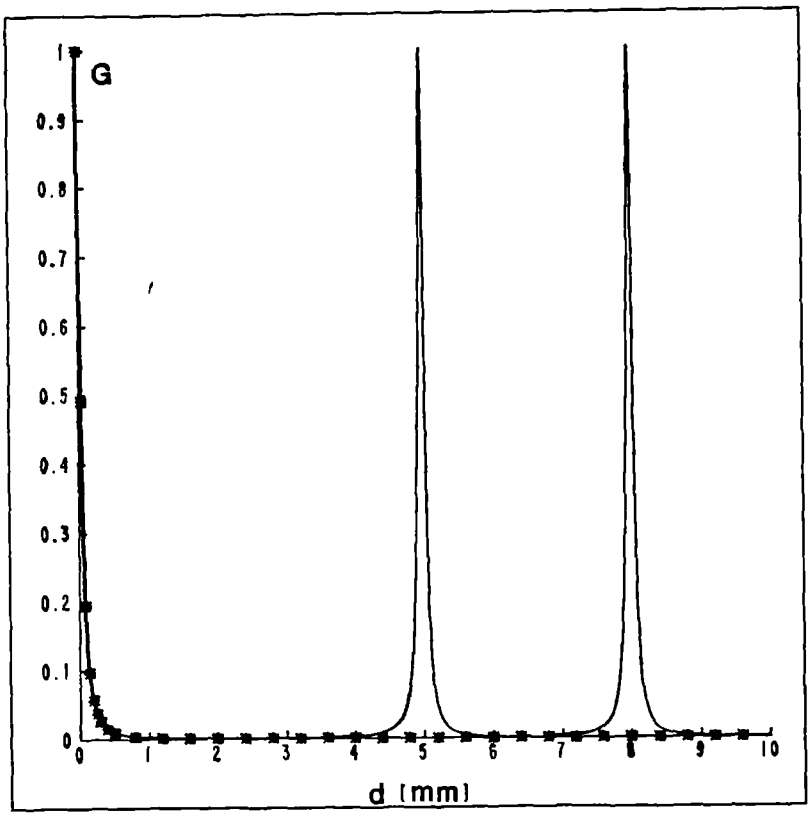

Figure (4-2) : The function (G) against the cavity length (d)

* * * : $R = \infty$, solid curves : $R = 5$, 8 *mm* respectively.

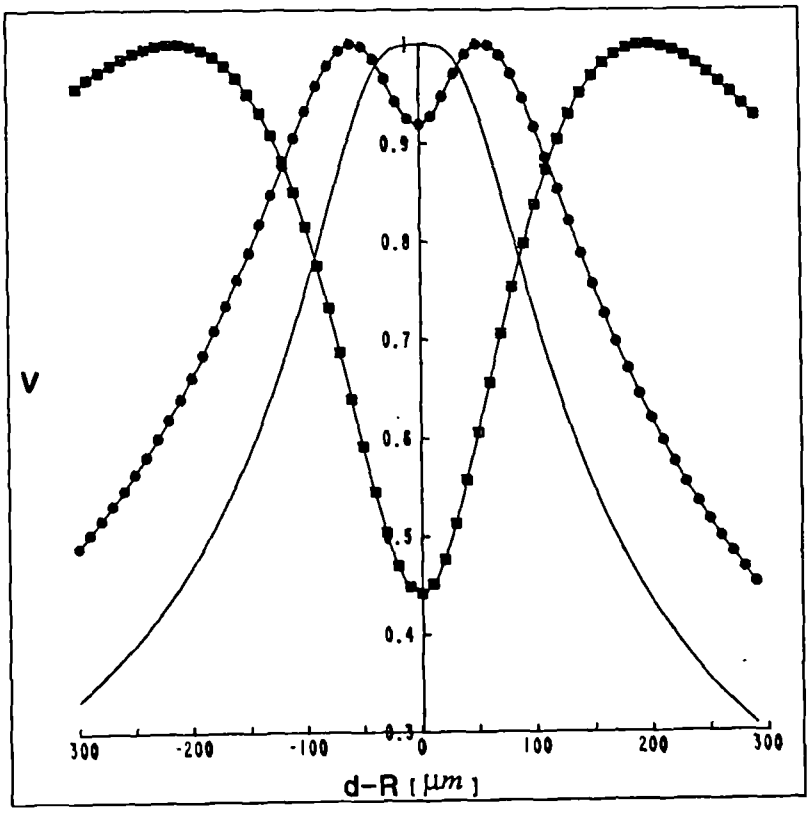

Figure (4-3) : The variation of the visibility against the cavity length.

solid : $r_2 = 0.0434$, circles : $r_2 = 0.1$ and squares : $r_2 = 0.8$.

In the first technique, a capillary tube, whose internal diameter provided a sliding fit for the jacketed fibre (approximated 0.25 mm outer diameter), was dipped into a container of molten solder and withdrawn. During solidification a reasonable reflecting surface was obtained by increasing the pressure inside the tube. In principle, the curvature of this surface can be accurately controlled by varying the pressure inside the tube during solidification. Radii of curvature of approximately 5 mm were produced by this approach. The fibre was then inserted to the point at which maximum interference visibility is obtained, and cemented into position.

In the second technique, a steel ball was pressed into a clean aluminium plate, thus producing a concave spherical mirror of low reflectivity. The radius of curvature of the mirror can be reproduced simply hence enabling the production of a large number of optical sensors with near identical performance; also, as it is very easy to produce mirrors of different radii the sensing length can be set for a specific measurand. The reflectivity can be controlled if necessary by polishing or coating. A scanning electron microscope, Cambridge-STEROSCAN 600, was used to study the surface of one spherical mirror, produced using the second technique. A magnified image of the surface is shown in figure (4-4), where the magnification factor is 500. In the photo a linear scale corresponds to 40 μm is shown also. The diameter of the optical Gaussian beam at the surface of the mirror is calculated using the familiar equation :

$$W(d) = W_o \left[1 + \left(\frac{\lambda d}{\pi W_o^2}\right)^2\right]^{\frac{1}{2}} \qquad (4.19)$$

As an example if the cavity length is about 5 mm, the corresponding beam diameter is 255 μm . Figure (4-4) shows that the mirror surface is relatively smooth and consequently it will refocus a reasonable fraction of the light back into the fibre, as is found experimentally.

To fabricate a sensing element, a curved mirror is fixed at the end of a glass tube with an internal diameter chosen to provide a sliding fit with another glass capillary tube which held the fibre fixed along its axis. When the position of maximum visibility is adjusted, as discussed in section (4.5.1), the two tubes are cemented together forming the sensing element.

(4.2.3) The interferometer and experimental characterisation :

The optical configuration used to characterise the sensing element is shown in figure (4-5). A laser diode (Hitachi 7801E), was used to illuminate the system with a mean operating wavelength of 790.3 nm, and its output was launched into a fibre directional coupler. The air cavity Fabry-Perot interferometer was constructed at the end of one of the output arms of the coupler with the other arm cleaved at an angle and placed into an index matching gel to avoid reflection. For test purposes the low reflectivity mirror was mounted on a piezo-electric transducer in front of the capillary tube containing the fibre fixed at its axis. The optical axis of the mirror was adjusted to coincide with the axis of the capillary tube. The capillary tube was mounted on a translation stage to roughly adjust the cavity length (d). The fine control of this length was obtained by applying a DC voltage to the PZT, which gave a maximum displacement of 100 μ m. A sinusoidal signal was also applied to the same PZT and adjusted to scan one complete interference fringe. The output interference signal, of the interferometer, was then detected where, both, the fringe visibility and the mean output intensity were measured with different values of cavity length. Knowing that the reflectivity of the fibre end is about 0.04, the intensity reflected from the far end of the interferometer (the spherical mirror) and recaptured by the fibre was calculated for different values of the cavity length. The experiment was repeated with mirrors having radii of curvature of 3.17, 4.76 and 6.35 mm respectively. The variation of the measured intensity recaptured by the fibre (I_2) and the interference visibility, normalised, with the cavity length are shown in figure (4.6) a,b respectively. These results shows a good agreement with that expected using the simple theoretical model introduced in section (4.2.1). The reflectivities of the three spherical mirrors were 0.13, 0.1 and 0.07 respectively where the maximum visibility in the three cases was about 0.94 .

(4.2.4) The remote configuration :

In some applications the environment is such that the sensing element must be remote from the optical fibre; for example for sensing very high temperature above the softening point of the fibre.

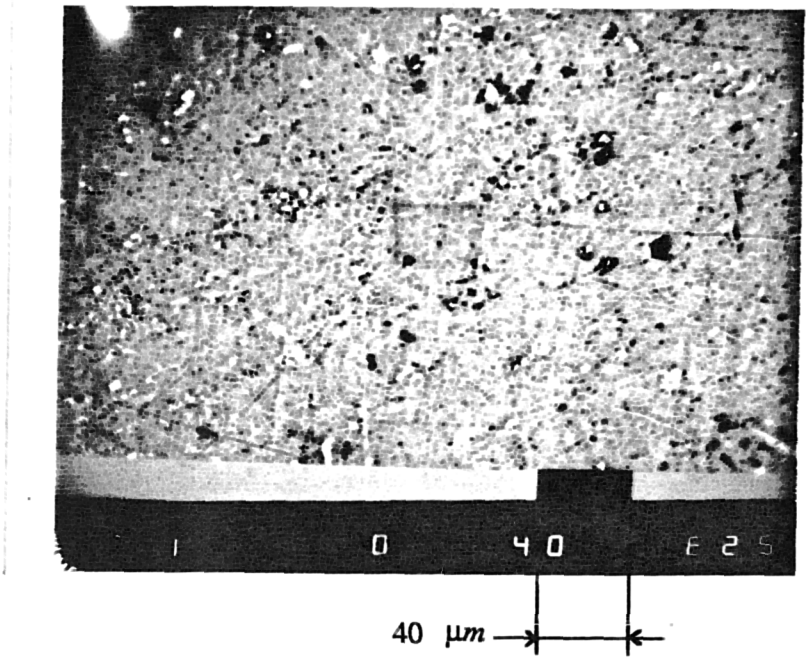

Figure (4-4) : A magnified image of the surface of the spherical mirror.

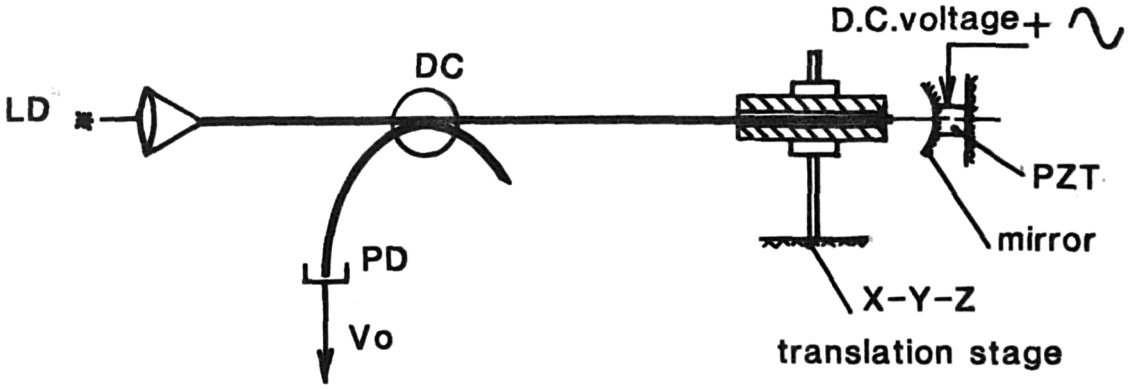

Figure (4-5) : The optical configuration used to characterise the hemispherical cavity.

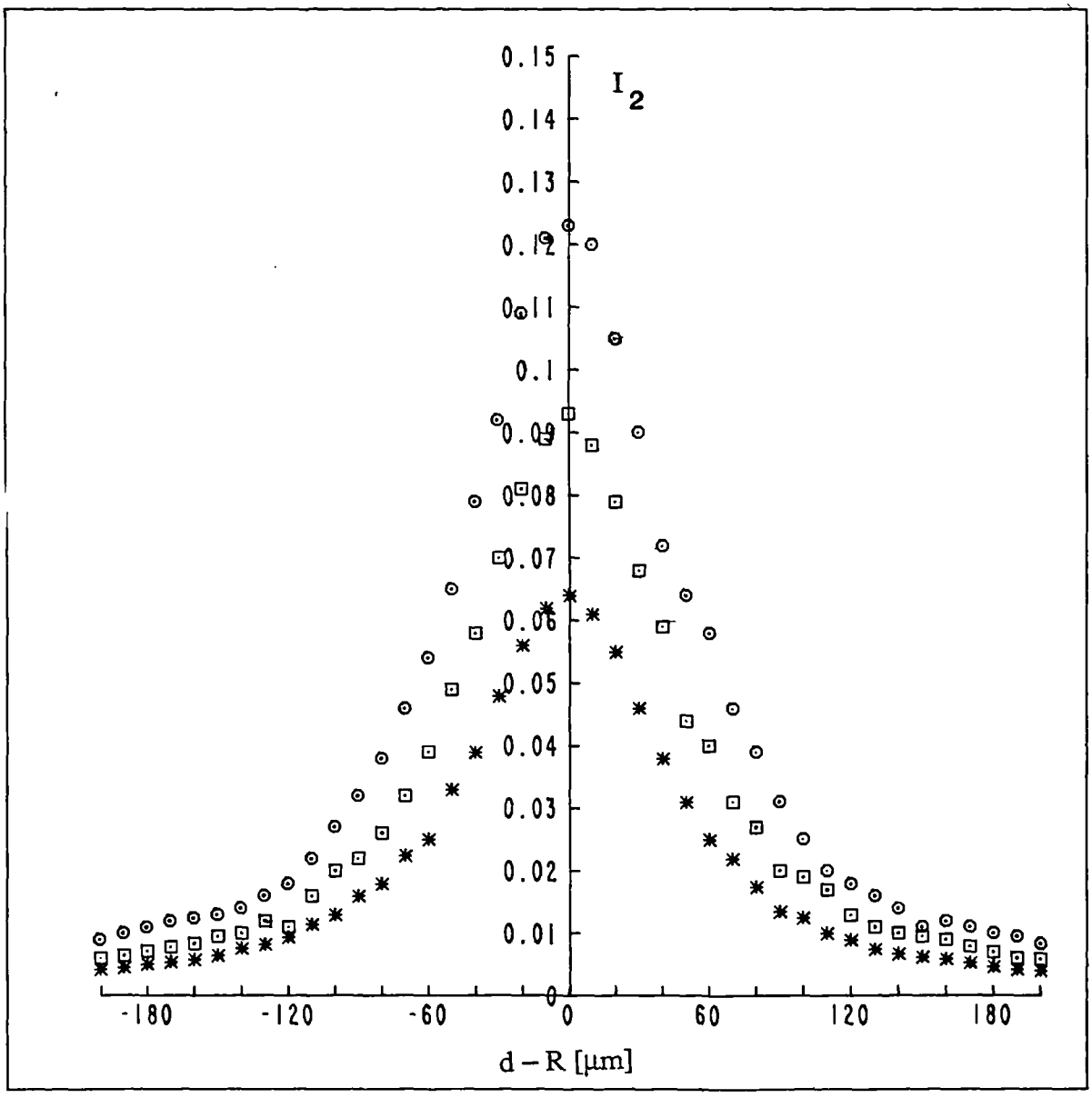

Figure (4-6 a) : The variation of the measured fraction of the optical power recaptured by the fibre with the cavity length.

circles : R = 3.7 mm, squares : R = 4.76 mm and * * * : R = 6.35 mm.

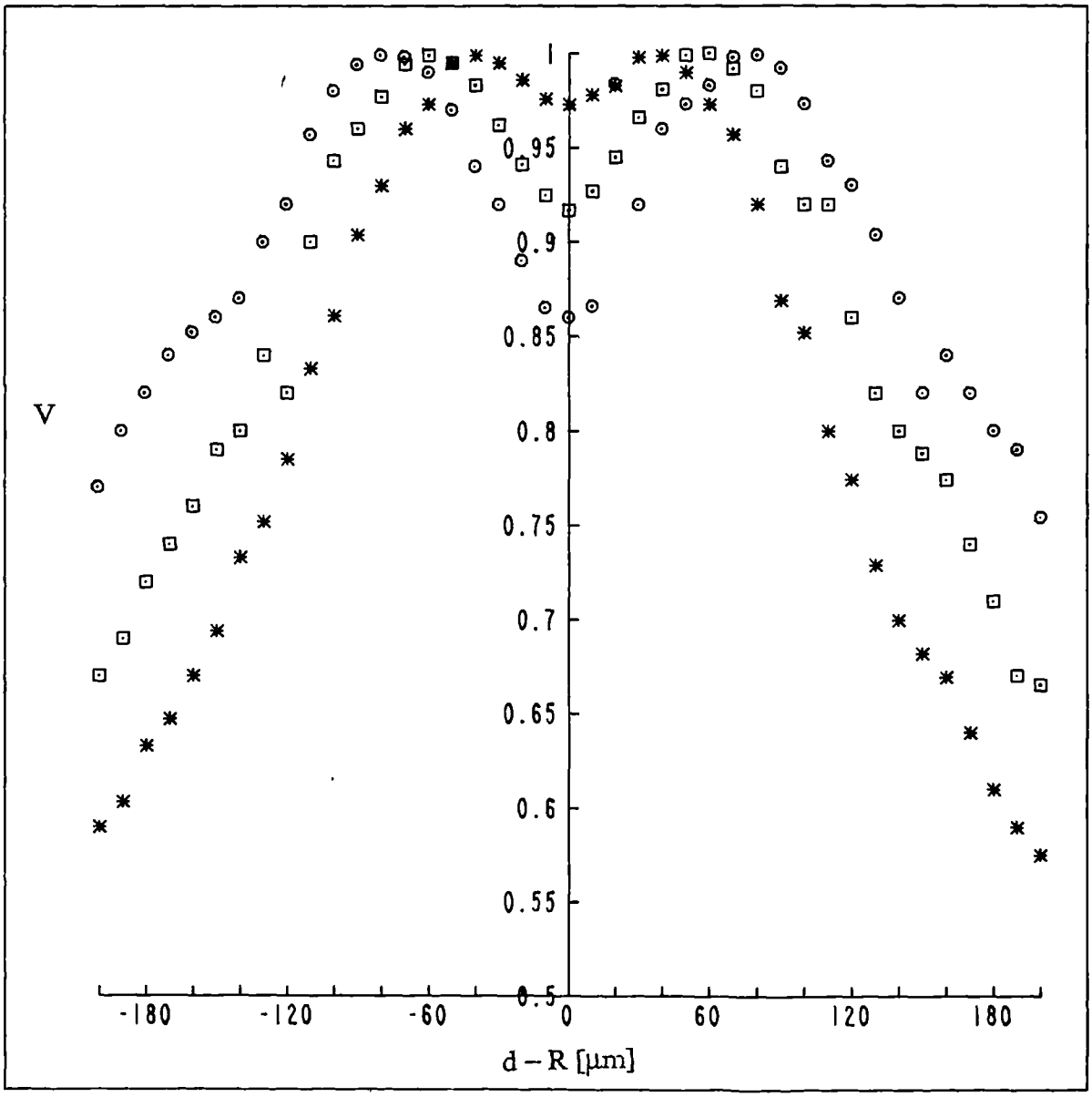

Figure (4-6 b) : The variation of the measured fringe visibility with the cavity length.

circles : R = 3.7 mm, squares : R = 4.76 mm and * * * : R = 6.35 mm.

According to design, of the remote sensing element, the incident optical beam may be either collimated (plane Fabry-Perot sensing element) or focused (hemispherical Fabry-Perot) at the front (plane) surface of the sensing element. In the first case, when the incident beam is collimated, the optical configuration is critically dependent on the angular tilting of the sensing element, if it is tilted such that it is not oriented perpendicularly to the incident beam, the collimating lens will focus the returning light back shifted from the fibre core reducing the signal re-captured by the fibre. For the second case, when the beam is focused, the only angular restriction is due to the change in the beam diameter reaching the collecting aperture of the fibre core. Lewin studied the angular dependence of the recovered signal in both cases and proved that the focused system is nearly 10 times more stable than the collimated system [15]. This makes the hemispherical Fabry-Perot configuration more advantageous as a remote sensing element.

An optical configuration, used to demonstrate the remote hemispherical Fabry-Perot interferometer, is as shown in figure (4.7), where the output Gaussian beam was focused (had a beam waist) at the surface of a half mirror, about 25 cm far from the fibre end, which was used as the inner mirror of the Fabry-Perot sensor. A concave mirror, radius of curvature of 20 mm, was used as the outer mirror of the interferometer. The spherical mirror was mounted on a translation stage with a PZT, to enable control of the cavity length, as in the previous case. The reflectivities of the mirrors were much higher than the reflectivity of the fibre end, hence the detected output signal was due to interference inside the hemispherical cavity, where an interference visibility of 0.93 was obtained when the cavity length was adjusted at the position of maximum visibility. Figure (4.8) shows the output interference signal at the system output. This configuration may be used in a system of two tandem interferometers illuminated by a low coherence-length source, where the receiving interferometer is adjusted to match the optical path-length imbalance of the sensing cavity.

(4.3) The interferometer, illuminated by a low coherence-length source :

In chapter (2), the concept of interferometers illuminated by a low coherence-length source was studied, where the transfer function of two Michelson interferometers in tandem was

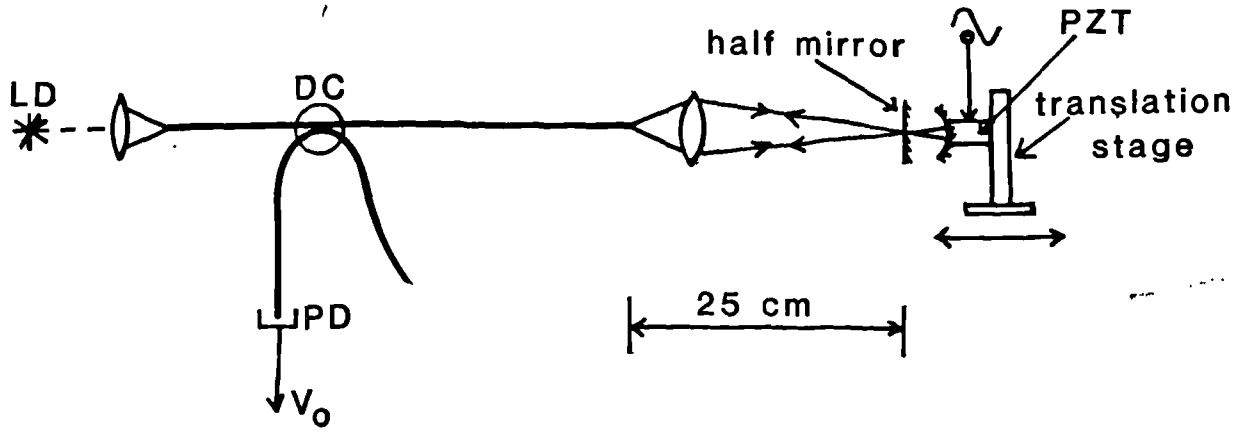

Figure (4-7) : The optical configuration used to demonstrate the remote configuration.

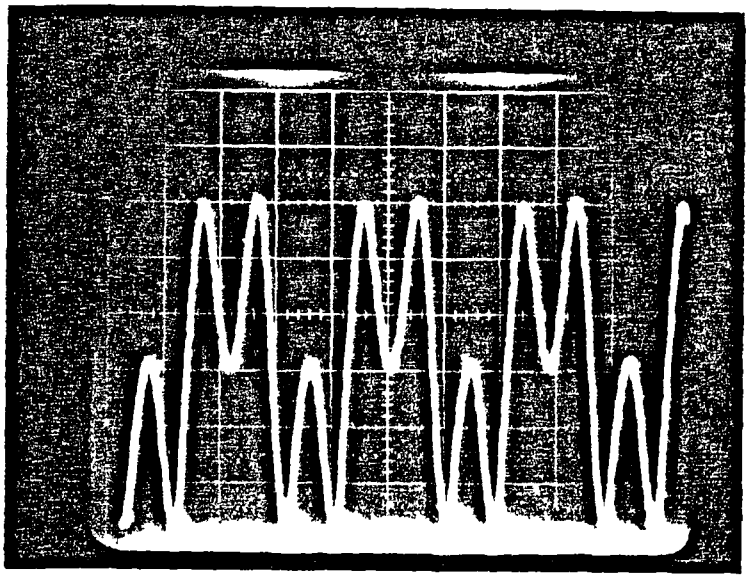

Figure (4-8) : The output interference signal at the output of the remote hemispherical interferometer.

discussed. We now discuss the case when a hemispherical Fabry-Perot interferometer forms the sensing interferometer.

(4.3.1) Transfer function of the interferometer in a tandem configuration.

When a hemispherical Fabry-Perot interferometer is illuminated using a low coherence source, such that the coherence length (L_c) is much less than the path-length imbalance of the interferometer (2d), then interference effects would not normally be observed. However, as discussed in chapter (2), interference fringes are produced when the sensing interferometer is interrogated by a receiving interferometer in tandem to balance the optical paths within the coherence length of the light. For simplicity we shall assume that there are no polarisation changes, and that spatial coherence effects may be neglected.

If the cavity imbalance (2d) is much greater than the coherence length of the light then applying the same technique used in section (2.6), where the spectral transfer function of the sensing interferometer H_s takes the form of equation (4.16), the detected intensity from the two interferometers in tandem may be represented as:

$$I = I_{mean}\Big(1 + V_2 Cos(\frac{2\pi\nu}{C}\,\Delta L_2) + V_3 Cos\,[\frac{2\pi\nu}{C}(\Delta L_1 + \Delta L_2)] + V_4 Cos\,[\frac{2\pi\nu}{C}(\Delta L_1 - \Delta L_2)]\Big) \qquad (4.20)$$

where ΔL_1 and ΔL_2 are the path-length imbalance of the cavity and the receiving interferometer respectively ($\Delta L_1 = 2d$) and V_2, V_3 and V_4 are interference visibilities. If the cavity length is adjusted to match the condition of maximum intensity recaptured by the fibre and the receiving interferometer to exactly balance the sensing interferometer, then; $d = R = \dfrac{\Delta L_2}{2}$.

As the illuminating source has a low coherence length, then the auto-correlation function representing the coherence properties of the light must be considered in calculating the visibility functions, V_2, V_3 and V_4. Neglecting the visibility constant due to different reflectivities of the

receiving interferometer, then :

$$V_2 = \int_0^\infty P(\nu)\, Cos\, [\frac{2\pi\nu}{C}\, (\Delta L_2)]\, d\nu$$

$$= |\gamma_{11}(\Delta L_2)| \qquad (4.21)$$

where P(ν) represents the normalised spectral distribution function of the light illuminating the system and hence $\gamma_{11}(\Delta L)$ is the auto-correlation function of the source. It is clear that the visibility function (V_2), which represents the central peak of the transfer function of the system, is only dependent on the coherence properties of the light source.

The visibility functions, representing the two side peaks of the system transfer function, V_3 and V_4, are directly proportional to the source auto-correlation function only if the sensing interferometer is nearly kept unperturbed (ΔL_1 = constant). Generally these functions are not only dependent on the properties of the light source but also on the properties of the hemispherical Fabry-Perot interferometer. It can be proved that:

$$V_3 = \int_0^\infty V(\Delta L_1)\, P(\nu)\, Cos\, [\frac{2\pi\nu}{C}\, (\Delta L_1 + \Delta L_2)]\, d\nu \qquad (4.22)$$

and

$$V_4 = \int_0^\infty V(\Delta L_1)\, P(\nu)\, Cos\, [\frac{2\pi\nu}{C} (\Delta L_1 - \Delta L_2)]\, d\nu \qquad (4.23)$$

where

$$V(\Delta L_1) = \frac{\sqrt{r_1 r_2 (1-r_1)^2 G(\Delta L_1)}}{r_1 + r_2 (1-r_1)^2 G(\Delta L_1)}$$

At d = R, the function $V(\Delta L_1)$, where $\Delta L_1 = 2d$, is independent of the wavelength, λ. But at $d \neq R$, it shows a weak wavelength dependence via $G(\Delta L)$ as in equation (4.13), this dependence increases when |d-R| increases; however, for quasi-monochromatic sources, with coherence lengths of the order of 100 μ m, or less, the value of $V(\Delta L)$ may be approximated as a constant value calculated at the mean frequency of the light (ν_o). Using this approximation equations

(4.22) and(4.23) can be simplified to the following forms:

$$V_3 = |\gamma_{11}(\Delta L_1 + \Delta L_2)|\, V_o(\Delta L_1) \tag{4.24}$$

and

$$V_4 = |\gamma_{11}(\Delta L_1 - \Delta L_2)|\, V_o(\Delta L_1) \tag{4.25}$$

where $V_o(\Delta L)$ is the value of $V(\Delta L)$ calculated at $\nu = \nu_o$. Equations (4.24) and (4.25) show that the dependence of the visibility on path-length imbalance is a function not only of the coherence properties of the source, but also of the properties of the sensing hemispherical cavity.

(4.3.2) Visibility function control :

By appropriate design of the sensing interferometer it is possible to shape the dependence of the visibility on the path-length imbalance of a hemispherical Fabry-Perot interferometer, which may be required in some signal processing techniques. For example, it may be possible to determine the order of the interference fringe being observed at the output of a system consisting of a hemispherical Fabry-Perot interferometer, as a sensing interferometer, and a receiving Michelson interferometer by measuring the change of the interference visibility. Under these circumstances, a sharp visibility function is advantageous in order to improve the system ability to identify the order of the interference fringe. Phase measurement of the interference signal is also needed in such a system to permit a true interferometric resolution of the sensing system.

To achieve a sharp varying visibility function, let us consider the case of a sensing interferometer, designed such that the condition $r_1 = r_2\,(1 - r_1)^2$ is satisfied hence the condition for maximum visibility is obtained at d = R, where G(d) = 1. Let us consider also that the system is preadjusted such that $\Delta L_1 = \Delta L_2 = 2R$. When the measurand starts to affect the sensing cavity changing ΔL_1, if the receiving interferometer is kept unperturbed then the coherent matching condition is not maintained any more and the visibility function will decrease. But because of the cavity properties, described by the factor $V(\Delta L_1)$ which decreases as ΔL_1 changes from R, then the visibility function may be made to decrease more rapidly than the auto-correlation function of the source.

Within a limited range, such that the corresponding changes of $\Delta L_1 \approx \pm 50\,\mu m$, about the position of maximum visibility, the function $V(\Delta L_1)$ may be approximated to unity, as shown in figure (4-3), and then the visibility of the output signal may be considered as a source only dependent function, as the case of ordinary two-beam interferometers.

(4.4) Transfer function of a misaligned hemispherical cavity :

In this section we study the effects on the cavity transfer function when the axis of symmetry of the spherical mirror is not coincident with that of the fibre. This study is based largely on the method introduced by Yura and Hanson [16] and used by McKinley et el [17]. For the hemispherical cavity misalignment results from either shifting or tilting the axis of the mirror, of which the most important practical application is the mirror tilting about its vertex.

If we assume that the mirror has a tilt error described by a zero-mean jitter of $\delta\theta$ then, according to reference [16], the spot diameter of the reflected Gaussian beam W_2' is :

$$(W_2')^2 = W_o^2 \left[A^2 + \frac{\lambda^2 B^2}{\pi^2 W_o^4} \right] + 2(B')^2 \sigma_\theta^2 \qquad (4.26)$$

where σ_θ is the one-sigma jitter variance of the mirror and B' is the B element of the matrix $\mathbf{T'} = \mathbf{T_3}\,\mathbf{T_2}$. From the equations (4.2) and (4.3), $B' = d$, hence the fraction of the optical power recaptured by the fibre, when the mirror is tilted, may be represented as :

$$G' = \left(\frac{W_o^2}{W_2'^2}\right)$$

$$= \frac{1}{[G(d)]^{-1} + \frac{2d^2}{W_o^2}\sigma_\theta^2} \qquad (4.27)$$

Equation (4.27) shows that if the mirror is not tilted ($\sigma_\theta = 0$), the value of the function $G' = G(d)$, as defined in equation (4.13). It shows also that at d = R, G(d) = 1 and hence G' falls sharply as σ_θ increases. This dependence is similar to the case of an optical cavity, of the same length, with the optical beam collimated and a plane mirror forming its far end. The length of the

hemispherical cavity is usually adjusted to give maximum interference visibility, which happens at $d \neq R$ and hence G(d) is much less than unity. Substituting in equation (4.27), the variations of G', as a function of σ_θ, will be much slower than the first case. As an example, if the reflectivities $r_1 = 0.04$ and $r_2 = 0.8$, maximum visibility is obtained at the position where G(d) = 0.054. Figure (4.9) shows the variations of G' as a function of the tilting, σ_θ, for G(d) = 1 (plane mirrors Fabry-Perot interferometer) and 0.054 (hemispherical Fabry-Perot interferometer), the cavity length, d, was considered as 5 mm in both cases. As shown in figure (4-9), the half power tilting angle is 0.04^o and 0.18^o respectively, which shows higher tilting stability of the hemispherical cavity compared with a plane mirrors Fabry-Perot interferometer of the same path-length imbalance.

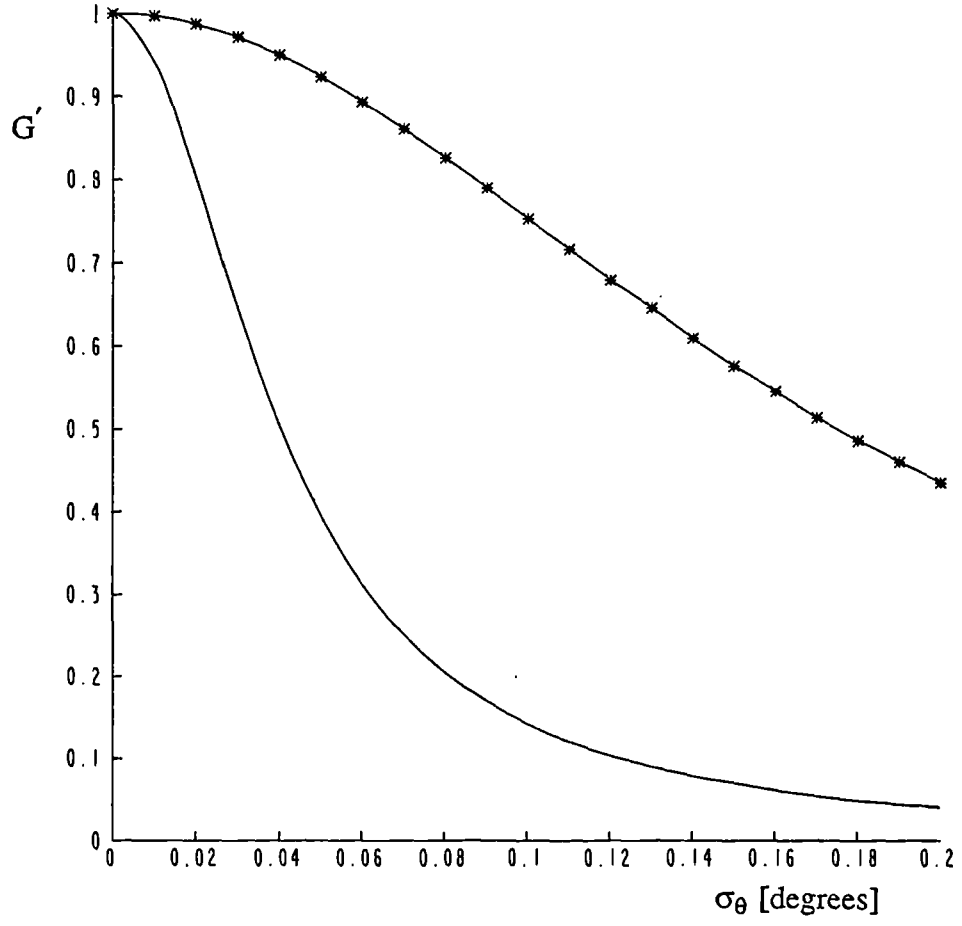

Figure (4-9) : The tilting sensitivity of G' against the angular jitter of the mirror.

Solid : plane-mirrors Fabry Perot cavity and * * * : hemispherical cavity, of the same optical imbalance.

(4.5) Temperature probes based upon the hemispherical cavity :

Considerable research has been performed to develop fibre-optic thermometers [18-20]. Various designs have been introduced for use in harsh environments. The Fabry-Perot configuration is chosen in many designs because the sensing region is remotely located and hence the output of the sensor is not corrupted by any perturbations in the input fibre. In this section we introduce two different designs of temperature probes based on the hemispherical Fabry-Perot configurations. We believe that these designs may form the basis of practical fibre optic-based thermometers.

(4.5.1) Temperature probe 'I' :

Here the probe is designed to measure temperature below the maximum working temperature of the optical fibre, hence the end face of the input fibre can be used to form one of the mirrors of the Fabry-Perot cavity, as discussed in section (4.2.1). The optical set-up of the system is shown in figure (4-10 a), where the hemispherical Fabry-Perot air cavity acts as the sensing interferometer and the conventional Michelson interferometer was used for the receiving interferometer. In principal, any interferometer type can be used as a receiver.

(a) Construction of the system :

A spherical mirror, with radius of curvature of 12.7 mm was fixed at the end of a glass tube with an internal diameter chosen to provide a sliding fit with another glass capillary tube which held the fibre fixed along its axis, as shown in figure (4-10 a), a single mode laser diode, Hitachi HL 7801E, was initially biased above threshold to illuminate the system with a highly coherent light. The mirror was mounted on translation stage, TS-1, with a piezo-electric transducer, PZT-1. A sinusoidal signal was applied to PZT-1 and then the cavity length ΔL_1 was adjusted, roughly using the translation stage and finely by applying a D.C. voltage to PZT-1 (added to the modulation signal) to give maximum interference visibility. At this position, the two tubes were cemented together forming the sensing element, then the translation stage and PZT-1 were

disconnected. The laser diode injection current was then decreased below threshold (such that it behaved as a low coherence-length source) thus no interference signal was observed at the output of the interferometer. The receiving interferometer was assembled and adjusted to be similar to the path-length imbalance of the hemispherical cavity, see chapter (3). A sinusoidal signal was then applied to PZT-2 and its amplitude was adjusted to scan the receiving interferometer through one interference fringe. This interference signal was maximised by closely matching the optical path-length difference of the receiving interferometer. Hence the interferometers acted as a remote, passive sensor. The output interference signal of the system had a very good visibility, of about 0.48 (the maximum visibility of two tandem interferometers is 0.5).

(b) Testing probe 'I' as a thermometer :

In order to test the probe as a temperature sensor the sensing element was contained within a variable temperature furnace as shown in figure (4-10 b). The temperature of the furnace was also measured using a calibrated thermocouple. The transduction mechanism of the probe being the thermal expansion of the glass tube. An electronic feedback servo was used to lock the system to the quadrature point nearest to maximum visibility through PZT-2, as discussed in chapter (3). Continuous tracking of the change in the optical phase produced by the sensing element was compensated, by the servo, keeping the system locked at this quadrature point. The servo feedback voltage was measured as a function of the temperature of the sensing element, the corresponding results are shown in figure (4-11).

The temperature sensitivity of the sensing element was measured to have a mean value of 2.155 rad/K, which corresponds to a linear expansivity of 1.08 x $10^{-5}K^{-1}$ for the glass tube, this is consistent with typical known values.

The maximum measurement range is limited by the tracking range of PZT-2, which was about 100 μ m, corresponding to a temperature range of ≈ 389K. The resolution of the system is mainly dependent on the noise level of the photodiode output and on the temperature sensitivity of the sensing element. In our system the bandwidth of the tracking servo was 120 Hz and the

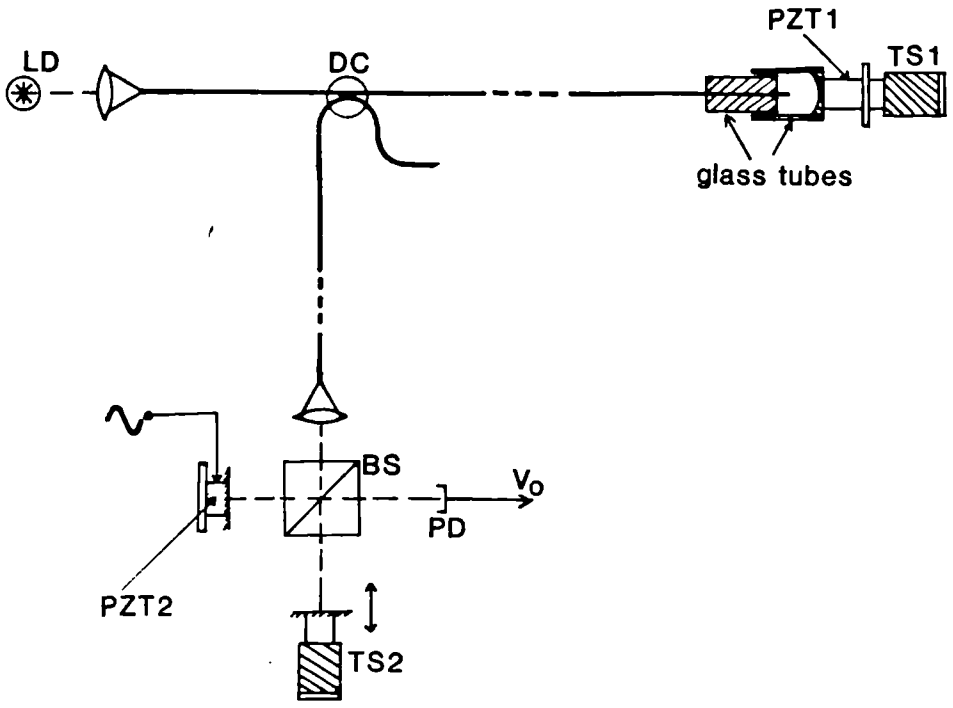

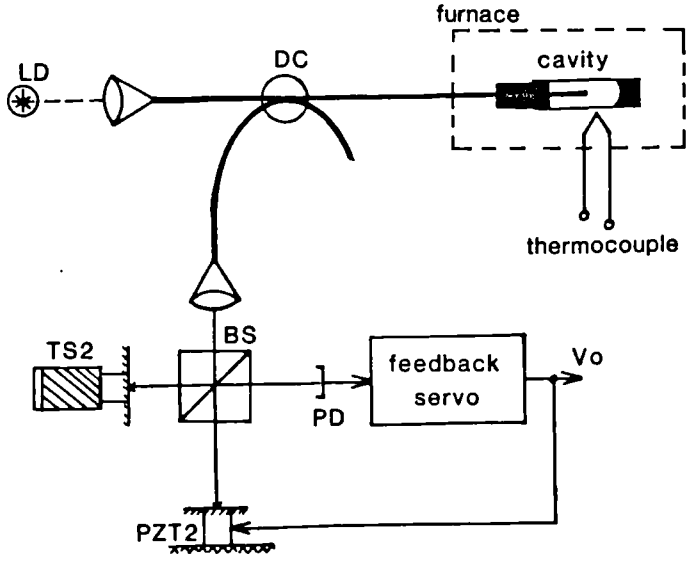

Figure (4-10) : The optical set-up used to demonstrate temperature probe 'I'.

(a) : For constructing the system and (b) : for testing the probe.

Note : The laser diode was biased below threshold.

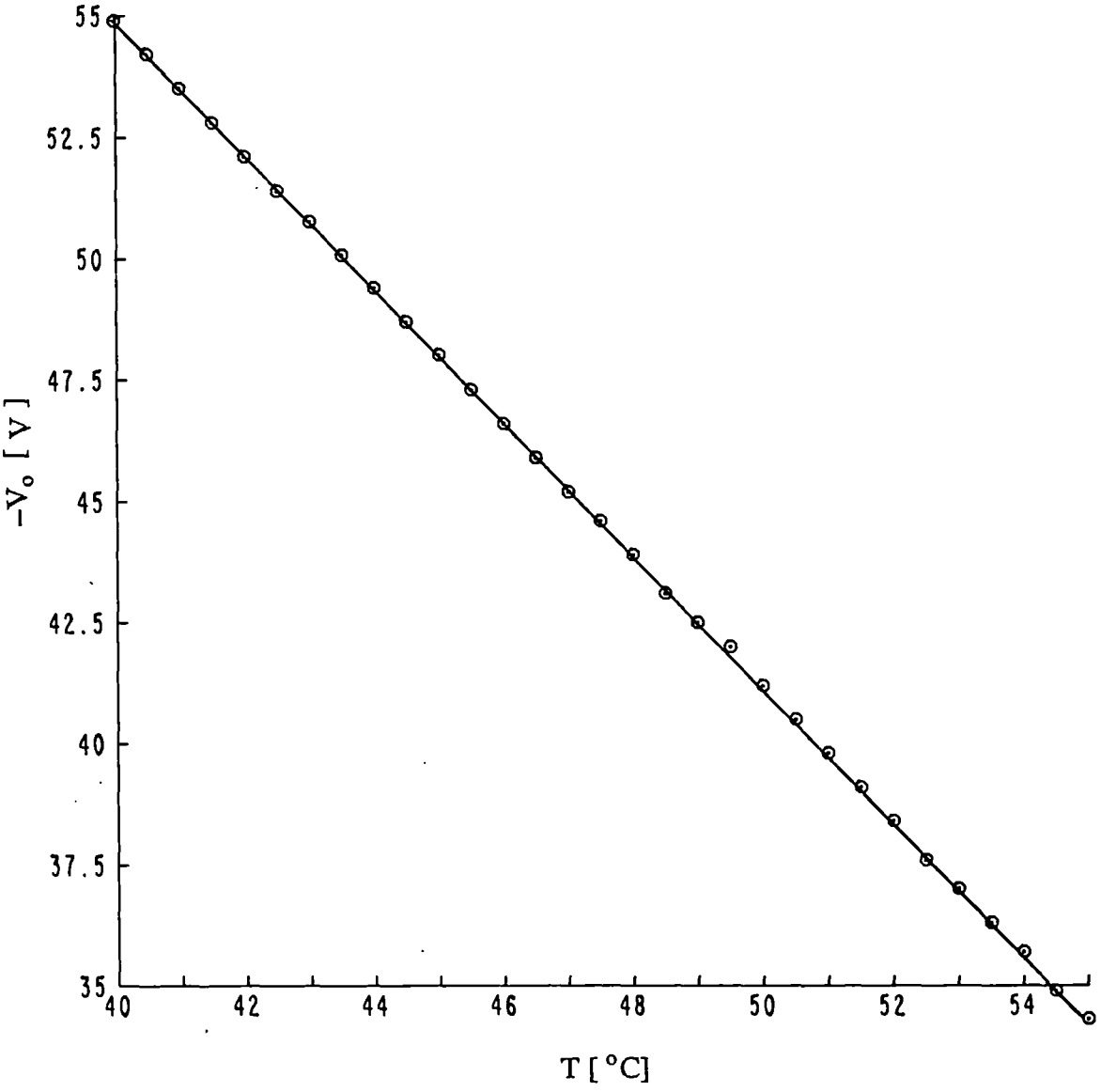

Figure (4-11) : The tracking voltage applied by the servo against the temperature of probe 'I'.

signal to noise ratio was about 56 dB, corresponding to an optical-phase resolution of 1.6 m rad, and hence to a temperature resolution of 0.74 mK. The practical dynamic range of the system is thus about 5 x 10^5, which compares favourably with that obtained using fibre interferometers illuminated by sources of longer coherence length [11]. The accuracy of the measurement was determined from the manufacturer's data for the calibrated thermocouple, and was in the order of 0.1 K.

(4.5.2) Temperature probe 'II' :

In this second design, the probe was designed to measure temperatures above the softening temperature of the fibre, hence the sensing element had to be located remotely from the input/output fibre. For this design it is preferable to use a solid etalon as the remote sensing element. This type of sensing element does not suffer from relative misalignment of its mirrors and provided it can be attached to a tube which is rigid at high temperature (such as ceramic) a stable high temperature sensor can be realised. Fabricating the probe in the form of an etalon also gives a wider choice for the optical materials which can be used, hence it is possible to optimise the design of the sensing element for range, resolution and size. In section (4.2.4) we have seen that it is more advantageous to focus the incident optical beam at the front surface of the sensing element rather than to have the beam collimated. In principle, when the beam is focused, a thin plane parallel etalon may be used as a sensing element, but in order to obtain an adequate resolution, without requiring extremely high optical-phase resolution, the sensing element needs to be relatively thick ~ 0.3 - 1 cm, making the hemispherical cavity the optimum configuration for the sensing element.

(a) construction of probe 'II' :

The construction of the sensing probe is shown in figure (4-12), where the sensing element is an optical hemisphere constructed from an optical material with a high melting temperature, quartz in this case although sapphire would give a higher maximum temperature. The length of

the sensing element, d, was selected such as to match the curved surface of the wavefront of the Gaussian beam, emerging from the fibre and focused at the flat surface of the etalon, with the surface of the hemisphere (as discussed in section (4.2)). This occurs when d = R/n, where n is the index of refraction of the material forming the sensing element.

The basic transduction mechanism of the sensor is the temperature dependence of the optical path length of the sensing element, which is governed by the physical expansion of the element and its change in refractive index. If the temperature of the sensing element changes by δT, the corresponding change in the interferometric phase, $\delta(\Delta\,\phi)$, may be represented by :

$$\delta(\Delta\,\phi) = \frac{4\pi\, d}{\lambda}\,[n\alpha + \frac{\partial n}{\partial T}]\,\delta(T) \qquad (4.28)$$

where α is the linear expansion coefficient and $\partial n/\partial T$ is the temperature coefficient of the refractive index of the material forming the sensing element.

The sensing element was fixed at the end of a quartz tube by trapping it with a cap made from two quartz tubes which fitted over the sensor supporting tube as indicated in figure (4-12). The input fibre was adjusted axially with respect to the sensing hemisphere until the optical beam was focused at the centre of the flat surface of the sensing hemisphere.

(b) Testing probe 'II' :

The optical configuration shown in figure (4-13) was used to test a sensing probe, where a multi-mode laser diode Mitsubishi (ML-4406) was used to illuminate the system. The length of the sensing element was 4.02 mm with an index of refraction of 1.4535, which gives an optical path-length imbalance of 2 n d = 11.67 mm. This optical path-length imbalance was chosen specifically to match the properties of the multi-mode laser diode (studied in section (3.5)) which has a cavity length of, $l_{cav} = 1.116mm$. The optical path-length of the sensing element corresponded to $\simeq 10.5\, l_{cav}$, thus no interference signal will be obtained at the output of the sensing Fabry-Perot interferometer. Hence a receiving interferometer is required, to recover the thermally induced changes in the optical path difference of the sensor, as discussed in section (2.6.2).

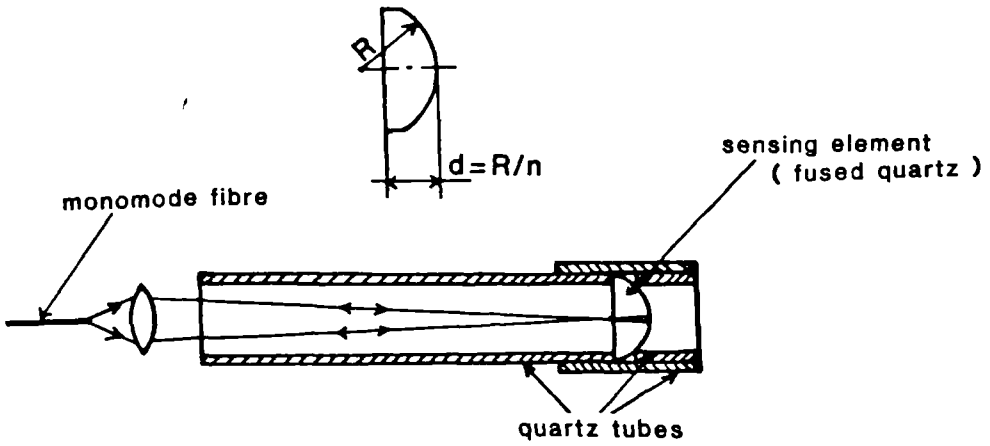

Figure (4-12) : The construction of the high temperature probe (probe 'II').

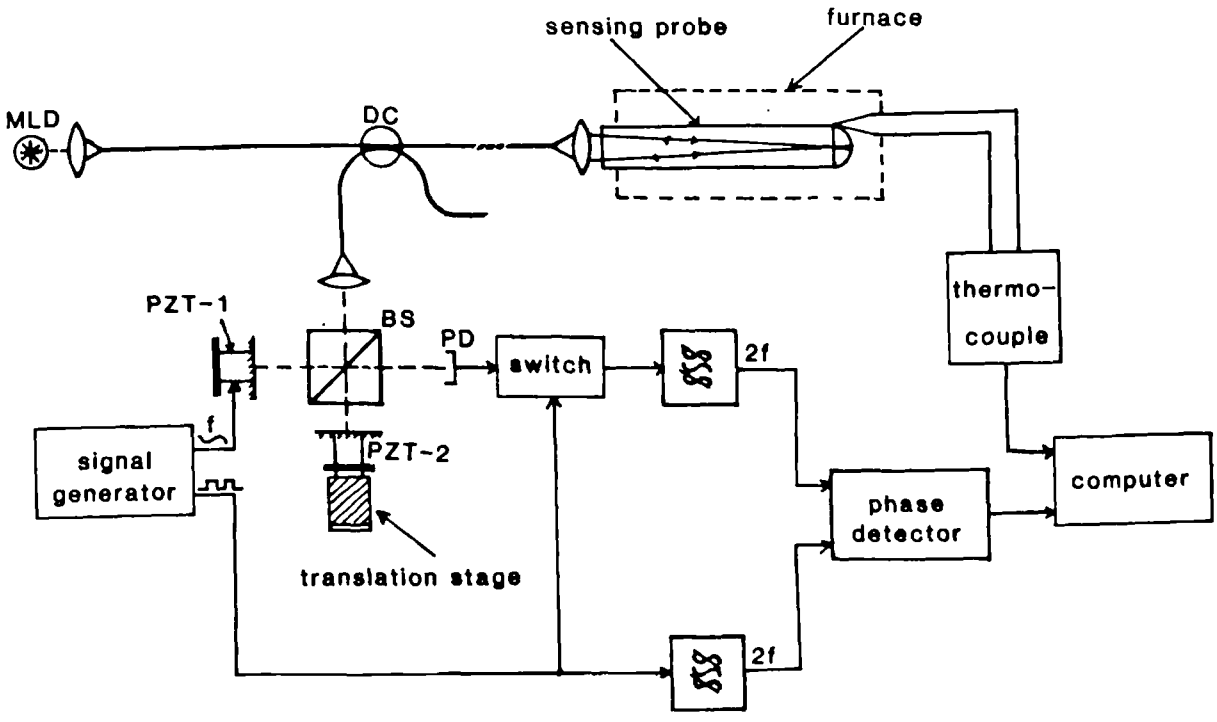

Figure (4-13) : The optical set-up used to test probe 'II'.

In our system a receiving Michelson interferometer was used. The sensing probe was tested using a cylindrical furnace, its temperature was monitored using a high temperature thermocouple. The experiments were performed by first setting the temperature of the furnace to $\simeq 1000^{o}C$ and then adjusting the optical path-length imbalance of the receiving interferometer to give the maximum interference visibility at the output of the two interferometers. A sinusoidal signal was applied to PZT-1, in the receiving interferometer, with its amplitude adjusted to scan an optical phase of 2.82 radians. The detected output signal was electronically gated and filtered to produce an electronic carrier modulated by the optical phase (see section (6.2)). During the cooling period of the furnace, the phase change of the carrier was measured relative to a reference carrier and these values were stored in a computer as a function of the temperature of the furnace over a temperature range of about $250^{o}C$. The cooling rate of the furnace was about $12^{o}C$/min. This method of signal recovery is an open loop technique where the receiving interferometer is kept unperturbed during measurement. Although this technique is electronically simpler than closed loop tracking techniques, the measurement range is limited by the reduction in visibility of the overall interference signal as the path-length imbalance of the tandem interferometer ($\Delta L_1 - \Delta L_2$) increases, within the specified limits as defined in section (2.6.2).

Figure (4-14) a,b shows the output interference signals and the corresponding signal to noise ratio at the electronic carrier (at the output of the filter) at the beginning and at the end of the measurement temperature range respectively. At the beginning of the range, i.e when $\Delta L_1 = \Delta L_2$, the effective interference visibility was about 0.19, which is much less than expected (O.5 for two interferometers in tandem). This was because of the D.C. optical power reflected from the face of the input fibre to the sensor, If this power is excluded a calculated visibility of 0.42 is obtained, which is satisfactory for this type of remote sensor.

The temperature dependence of the optical phase change, induced in the system, is shown in figure (4-15). The mean phase sensitivity, of the sensor, was 0.7264 radians/degree (standard deviation of 0.024), which is consistent with known values for fused quartz [21]. The sensor shows a good linearity over this measurement range, which indicates that values for temperature

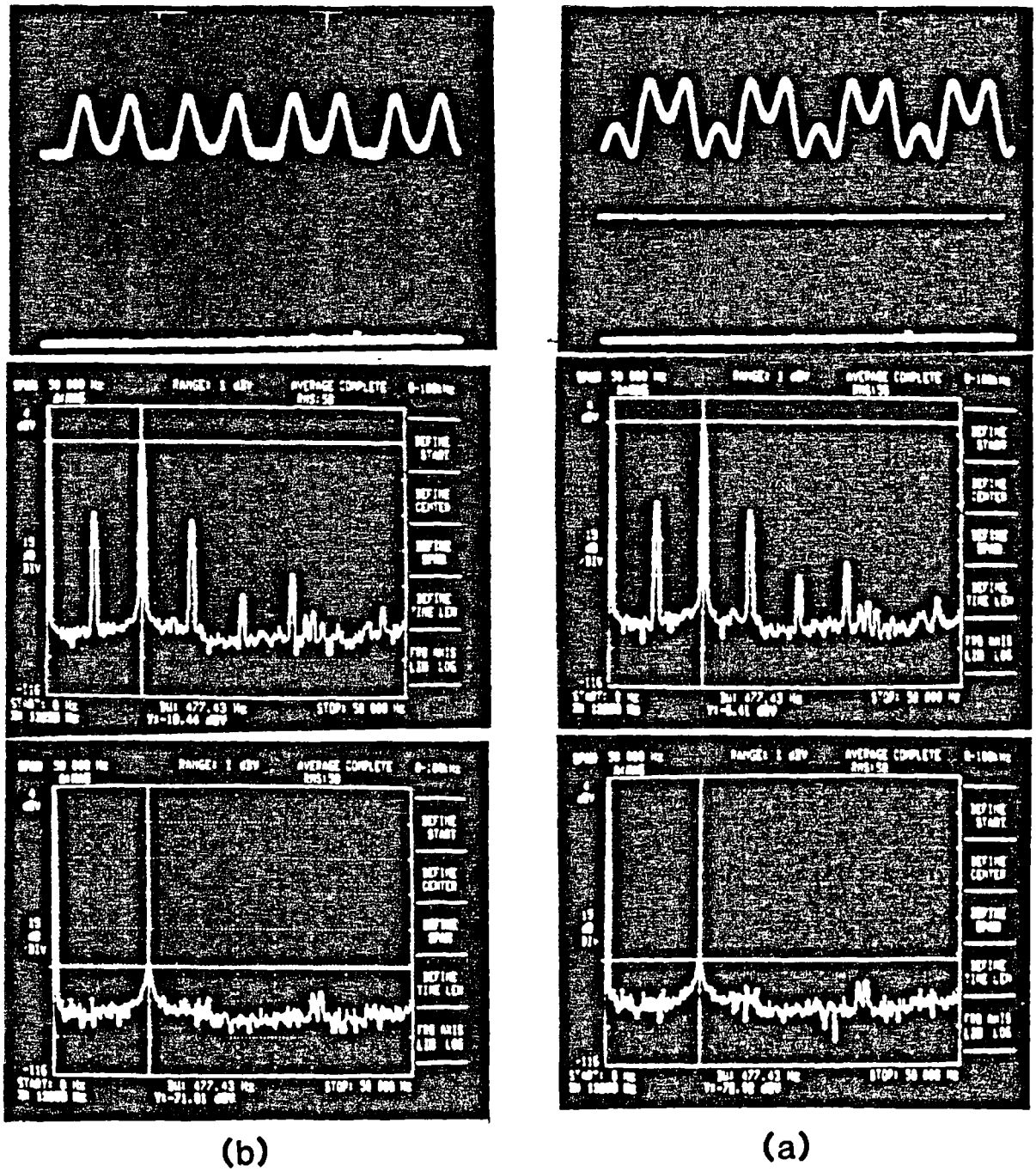

Figure (4-14) : The output interference signal, the signal spectrum and the spectrum of the noise floor at the beginning (figure a) and the end (figure b) of the continuous measurement range.

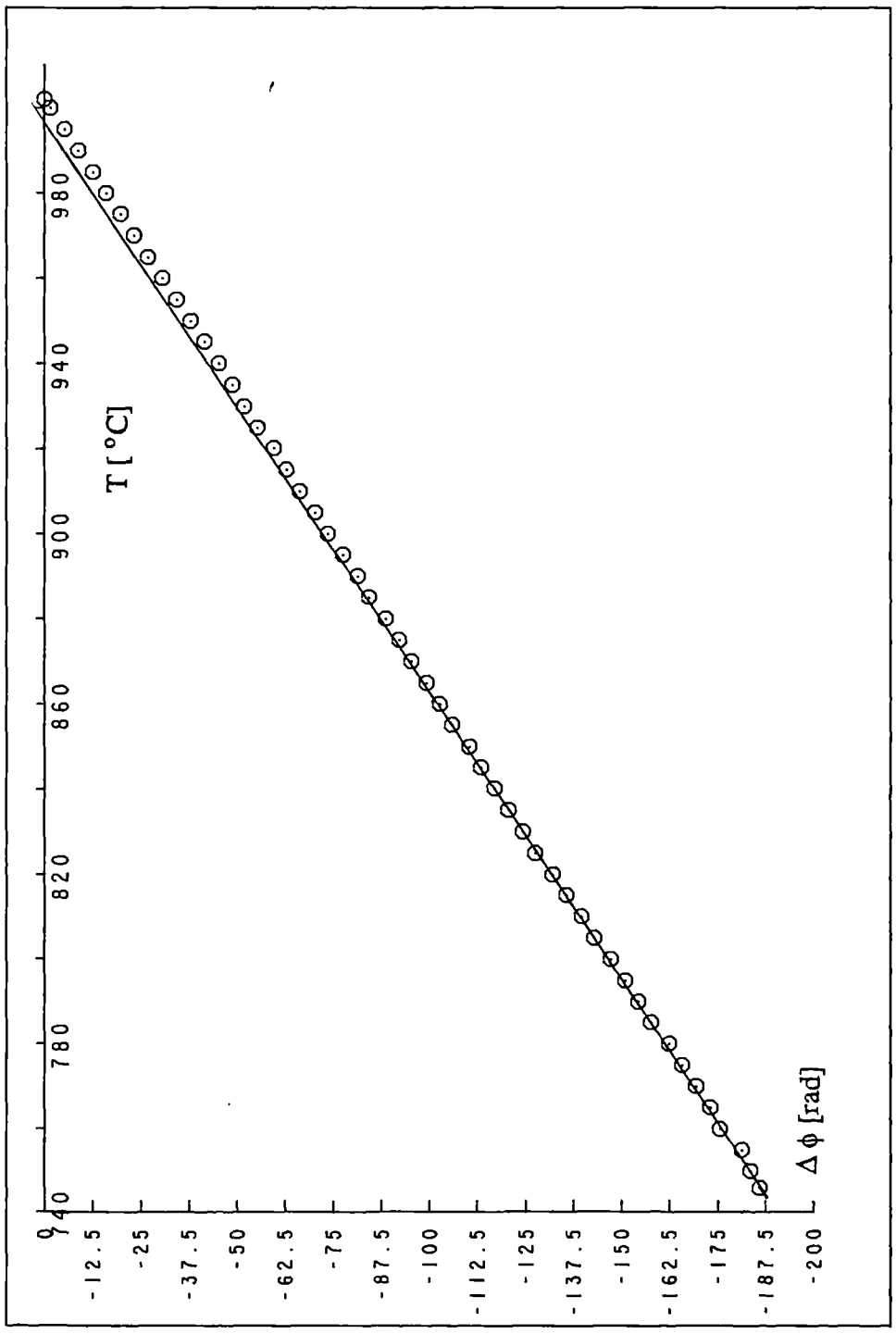

Figure (4-15) : The optical phase change induced in probe 'II' against its temperature.

coefficient of the refractive index as well as for the linear expansion coefficient do not differ significantly within this temperature range. Experimentally no changes in the optical properties of the sensing element were discovered after heating and cooling it over the temperature range 20^o–$1020^o C$.

At the beginning of the measurement range, the signal to noise ratio of the output electronic carrier was 66.5 dB within a measurement bandwidth of 477.4 Hz. The optical path length of the sensing interferometer was about 10.5 l_{cav}, hence according to the results shown in figure (3.16 a) an excess noise of about 8.7 dB is produced as a result of the small coherent signal produced solely within the receiving interferometer. This level must be added to the noise floor of the system, as discussed in section (3.5). Hence the ratio of the useful signal to the total noise is reduced by 8.7 dB to be 57.8 dB, this corresponds to a phase resolution of $5.9\times10^{-5}\ rad/\sqrt{Hz}$. Considering the situation at the end of the measurement range, the signal to noise ratio of the carrier was 61 dB, as shown in figure (4-14 b), hence the corresponding phase resolution is $1.1\times10^{-4} rad/\sqrt{Hz}$.

The basic concept for the high temperature probe was that it should be constructed as a single unit. Unfortunately, due to lack of work shop time it was not possible to realise such a unit and the probe was made in two parts as indicated in figure (4-12). The axes of the collimator and probe were adjusted such as they coincided before data was taken. Over a range of $\approx 250^o C$ the relative alignment of their optic-axes varied slowly such that data could only be taken continuously over this temperature range. A fully engineered version of this sensor would not suffer from this problem and should be capable of operating over the full design range. Nevertheless the system produced reproducible data up to temperature in excess of $1000^o C$.

(4.6) Conclusions :

In this chapter we have introduced a novel form of sensor, based on fibre-optic technology, its optical properties have been analysed theoretically. Simple techniques were used to form the sensing element and then its properties were investigated experimentally. The optical properties,

of the hemispherical cavity, particularly when operated remotely, show a higher geometrical stability than that of a plan mirror Fabry-Perot interferometer of the same path-length imbalance.

The sensing element can be designed as an active sensor for AC measurands, where the total phase excursion is not required. It can be used also as a passive sensor, with remote interrogation, where it is well suited for both A.C. and slowly varying localised measurands.

Two different designs of remotely interrogated temperature probes, based upon the hemispherical Fabry-Perot configuration were demonstrated and experimentally implemented. These temperature probes show high-stability and repeatable performance within a dynamic ranges of the order of 5×10^5. Although we have demonstrated the specific example of temperature measurement, other applications are equally possible, since the technique effectively measures the optical path length between the mirrors of the sensing interferometer. Therefore, measurements of displacement may readily be made. Furthermore, many physical variables - such as pressure, flow-rate or vibration may be transduced straightforwardly to a displacement as shown in chapters (5,6).

References

[1] G.B.Hocker ," Fibre-optic sensing of pressure and temperature ", Applied Optics, Vol.18, No.9, May 1979, P.1445.

[2] M.Corke, A.D.Kersey and D.A.Jackson, " Temperature sensing with single-mode optical fibre ", J.Physics E: Scientific Instruments, Vol. 17, 1984,P.988.

[3] A.D.Kersey, D.A.Jackson, and M.Corke, " A simple Fabry-Perot sensor ", Optics Communications, Vol.45, No.2, March 1983, P.71.

[4] F.Farahi, T.P.Newson, P.Akhavan Leilabady, J.D.C.Jones and D.A.Jackson, " A multiplexed remote fibre optic Fabry-Perot sensing system ", International Journal of Optoelectronics, Vol.3, No.1, 1988, P.79.

[5] R.T.Murry, E.R.Cox, D.E.Smith and P.G.Wright ," Fibre optic sensors for automobiles ", Journal of Optical Sensors, Vol.1, No.4, 1986, P.317.

[6] E.W.Saaski, J.C.Hartl, G.L.Mitchell, R.A.Wolthuis and M.A.Afromowitz ," Multi-mode fibre optic pressure sensor with extended range ", SPIE, Vol.838, Fibre Optic and Laser Sensors V, 1987, p.46.

[7] M.Corke ," Fibre optic sensors: Present and future ", Optical Engineering Reports, September 1987, P.4A,5A

[8] D.A.Jackson and J.D.C.Jones, " Fibre optic sensors ", Optica Acta, Vol.33, No.12, 1986, P.1469.

[9] M.Matsumoto, K.Fujimura, K.Hattori and H.Naono, " Fibre-optic acoustic sensor based on Fabry-Perot interferometer ", Proceeding of OFS'86 conference, Tokyo, 1986, P.43.

[10] P.Ferdinand, Ch.Liu and A.Kleitz, " Fibre optic sensor for temperature measurement in gas flow and steam turbine ", SPIE, Vol.1798, Fibre optic sensors II, The Hague, 1987, P.142.

[11] D.A.Jackson " Monomode optical fibre interferometers for precision measurements ", J.Physics E: Scientific Instruments, Vol.18, 1985, P.981.

[12] J.T.Verdeyen " Laser Electronics " Prentice-Hall, Inc., 1981, Chapters 3-5.

[13] H.Kogelnik and T.Li,"Laser beam and resonators ", Applied Optics, Vol.5, No.10, October 1966, P.1550.

[14] S.Ramo, J.R.Whinnery and T.V.Duzer, " Fields and waves in communication electronics ", J.Wiley and Sons, Inc., 1984, P.769.

[15] A.C.Lewin, " An investigation of optical fibre interferometric vibration and rotation measurement techniques ", Phd.thesis, University Of Kent, U.K., December 1987, P.113.

[16] H.T.Yura and S.G.Hanson, " Optical beam wave propagation through complex optical systems ", J.Opt. Soc. Am., Vol.4, No.10, October 1987, P. 1931.

[17] W.G.McKinley, H.T.Yura and S.G.Hanson, " Optical system defect propagation in ABCD systems ", Optics Letters, Vol.13, No.5, May 1988, P.333.

[18] R.R.Dils, " High-temperature optical fibre thermometer ", J.Applied Physics, Vol. 54, No.3, March 1983, P.1198.

[19] G.Beheim, " Fibre-optic thermometer using semiconductor-etalon sensor ", Electronics Letters, Vol. 22, No. 5, February 1986, P.38.

[20] C.E.Lee, R.A.Atkins and H.F.Taylor, " Performance of a fibre-optic temperature sensor form - 200 to 1050^{o}C ", Optics Letters, Vol. 13, No.11, November 1988, P.1038.

[21] " Transparent and opaque fused silica " Technical literature Q-A 1/112.1, Heraeus Quarzschmelze Gmbh, Hanau, West Germany, 1988.

CHAPTER (5)

High–sensitivity fibre–optic accelerometer

(5.1) Introduction :

(5.1.1) Acceleration measurement :

Acceleration measurement is extremely important in a great number of industrial and scientific processes, where it is required to determine the acceleration of an object in space relative to a framework. If the object of interest has significant physical size, it must be treated as an extended object which has six degrees of freedom. It can translate in one or more of three directions and rotate about each of the three axes. Thus to monitor the free motion of an object it may be necessary to use up to six sensors, one for each degree of freedom, contact accelerometers and gyroscopes are often used for such measurements.

In practice some degrees of freedom may be nominally constrained eliminating the need for some of the six sensors. Practical installation should always contain a test that evaluates the degree of actual constraint because the sensor will often produce some level of output for the directions of accelerations they are not primarily measuring.

In practical systems, both the frequency and amplitude of acceleration span a very wide range, for example the frequency range can be from near static to megahertz whilst the acceleration level may extend from 10^{-5} to $10^{6} ms^{-2}$. Obviously, it is not possible to cover this range with a general-purpose accelerometer and each application requires careful specification of the required performance in order to realise optimum design.

(5.1.2) Practical problems of acceleration measurement :

Unless an accelerometer is correctly designed it will exhibit many undesirable features such as cross sensitivity to orthogonal acceleration components and other measurands - particularly temperature. In the following section we consider the factors which can affect the performance of a practical accelerometer, these factors are :

a- Cross-Coupling

The cross-coupling factor (transverse response) is measured by accelerating the sensor in a direction perpendicular to the direction of normal use.

b- Coupling compliance

The compliance of the bond made between the sensor and the surface it is mounted on must be adequately stiff. If not, the surface and the sensor form a system that can vibrate in unpredictable ways. As a guide the accelerometer - surface bond should have a resonance frequency well above the working frequency range of the sensor.

c- Cables and pre-amplifiers

Certain types of sensor, notably the piezo-electric types, are sensitive to spurious variation in capacitance and charge. Sources of such charges are the tribo-electric effect of vibrating cables, varying relative humidity that alters electric field leakage and pre-amplifier input condition variations.

d- Influence errors

Ideally the sensor should operate in a perfect environment. In practice possible perturbation sources include temperature changes, electromagnetic interference, nuclear radiation and other environmental inputs which may induce erroneous signal.

e- Subject loading by the sensor

Accelerometers usually contain a mass. As this mass is made smaller, the sensitivity usually

falls, also if the sensor is heavy then it may affect the system being analysed.

(5.2) Conventional accelerometers :

The majority of accelerometers are based on a mass-spring sensing element, and are classed as 'seismic sensors'. For a seismic sensor the displacement of the mass relative to the sensor case is proportional to the acceleration of the sensor, there are at least two measuring techniques to determine this displacement. Firstly 'open-loop', where the un-modified response of the mass relative to the case of the accelerometer is measured. Secondly 'closed loop', where the output signal is proportional to a force generated in the sensor to maintain the mass fixed (relative to the case).

Several methods have been used to monitor the mass response to acceleration. They including electrical-resistance sliding potentiometers, variable inductance, variable capacitance, strain gauges (metallic and semiconductor), piezo-electric and magnetostrictive elements.

The common disadvantage of these approaches is that the sensing element is active, i.e. electronic components are required at the sensing head, the performance of these components may be adversely affected by the working environments of the accelerometer.

Accelerometers based on piezo-electric effect :

Piezo-electric accelerometers are the most commonly used type. The sensing element of a piezo-electric accelerometer is a piezo-electric crystal loaded with a mass (M). Force applied to the piezo-electric substance induces an electric charge that is proportional to the force **F**. Consideration of the law, $\mathbf{F} = M\,\mathbf{a}$, shows that this induced charge is proportional to the magnitude of the applied acceleration (a). Typical piezo-electric materials such as barium titanate with controlled level of impurities, lead zirconate, lead niobate etc are now been used. The sensitivity of these materials is temperature-dependent following a complex non linear law, moreover their working temperature is limited by the Curie's temperature point, of the material, which is typically $\approx 120^{o}C - 600^{o}C$.

To measure the electric charges induced in a piezo-electric sensor an electronic pre-amplifiers that converts charge magnitude to an equivalent voltage is required inside the sensing head. This also limits the working range of the sensor. The system performance, however relies not only on the sensor properties but upon the cables and the pre-amplifiers used with the sensing head. Practically this type of accelerometer cannot provide true DC response [1,2].

In practice piezo-electric accelerometers offer working frequency ranges from 0.1 Hz to 50 KHz and resolution ranging from 2×10^{-5} to 0.5 ms^{-2} with appropriate sensor masses (without cables) of 470 and 3 grammes respectively. The mean dynamic range of these type of accelerometers is about 5×10^{6} with a maximum working temperature of 120^{o} to $400^{o}C$ [2].

Piezo-resistive silicon accelerometers have been reported [3-5], where a silicon spring (called the piezo-resistor) with a silicon mass, attached to it form the sensing head. Acceleration causes the mass to move with respect to the frame, creating stress in the piezo-resistor, which changes its resistance and may be measured using a balanced Wheatstone bridge. This type of accelerometer has a very small size, a moderate working temperature range and a frequency range starts from true D.C.

(5.3) Fibre-optic accelerometers :

Several interferometric fibre-optic accelerometers have been demonstrated, where a single-mode optical fibre forms the sensing element. The first system has been introduced by Teveten et el [6], where the sensing element, based upon a mass spring configuration, was formed by suspending the mass between the two fibre arms of an all fibre Mach-Zehnder interferometer. The accelerometer showed a sensitivity of $\approx 1\ rad/g$, a working frequency range of 40-200 Hz and a dynamic range of 10^{3}. Difficulties were experienced with the system high cross-sensitivity.

An alternative configuration for the mass-spring arrangement has been described in which the fibre was tension wound around a compliant cylinder [7]. This configuration was better as a contact vibration sensor due to its very high sensitivity ($\approx 5 \times 10^{3}\ rad/g$), with a dynamic range of $\approx 10^{4}$. The sensitivity set by this system has a complex resonance behaviour and high cross

coupling Moreover, the sensing head is relatively heavy (≈ 660 grammes) and its size is restricted by the induced birefringence generated by winding the fibre into a tight coil, however its high sensitivity makes it very attractive for some applications, such as seismometers [8].

A third fibre optic configuration for use at DC and very low frequencies (< 1 Hz) acceleration measurement was demonstrated by Bucholtz et el [9]. The acceleration transduction mechanism was based on the non linear displacement-to-strain conversion technique, in which axial strain developed in the fibre depends quadratically on the acceleration induced displacement provided by a linear transducer. By dithering the transducer, the measurement frequency was up-converted from DC to the dither frequency to avoid the low-frequency noises. Fibre strain was measured using an all-fibre Mach-Zehnder interferometer maintained at quadrature. The sensitivity of the system was 2 rad / g at acceleration frequency of 0.014 Hz.

Although these fibre-optic accelerometers are passive and offer high resolution, their performance is critically dependent on the opto-mechanical properties of the fibre, and as these properties depend on temperature and strain, erroneous signals can be produced due to environmental perturbations.

Recently a new design of fibre optic linked accelerometer has been introduced by Jones [10]. It was based on a thermally compensated damped mass spring assembly. The optical sensing technique was based on the coupling of light from the moving fibre (attached to the mass) to a static receiver fibre via a prismatic reflector and a dual transmission filter. The system has a linear range and noise limited resolution of 100 μm and 1 $nm/\sqrt{Hz}$ respectively. The mass of the sensing head was 100 grammes and it was designed to cover a frequency range of 0.1 - 10 Hz and operating temperature of $-30^{o}C$ to $+60^{o}C$.

(5.4) The hemispherical Fabry-Perot fibre accelerometer :

In this chapter we introduce a novel design of fibre-optic accelerometer based upon the hemispherical Fabry-Perot interferometer introduced in chapter (4), in this design the sensing head is electrically passive and can be interrogated remotely. The sensing element is a weighted

circular diaphragm, where the displacement of the centre of the diaphragm, produced by acceleration, is measured by the hemispherical air spaced interferometer which is addressed via a monomode fibre [11].

The use of this type of interferometer, to monitor the response of the diaphragm, offers several advantages. (i) The sensing head needs no conventional optical components, hence it is easy to construct, align and mass produce. (ii) The hemispherical air spaced interferometer has greatly reduced sensitivity to out of plane diaphragm movement, compared with the planer Fabry-Perot interferometers. In an accelerometer this movement may be produced by exciting non-symmetrical vibration modes of the diaphragm. (iii) The system shows only a small cross-sensitivity to the other orthogonal components, hence a tri-axis configuration is possible. (iv) The acceleration sensitivity and the working frequency range can be tuned by changing the diaphragm dimensions or its material to match a specified applications. (v) The accelerometer can operate over a very wide temperature range. In principle this range could be from 70 K to above 1000 K, a similar working range cannot be achieved by any form of conventional accelerometer. (vi) The diaphragm and the mirror could be made of non-magnetic materials such that operation in electromagnetic fields is possible.

To summarise, this device shares the advantages common to many all-fibre interferometric sensors, in that it is compact and sensitive, however as its operation is independent of the fibre properties it offers similar mechanical stability and reproducibility as found in a conventional device.

(5.4.1) Construction of the accelerometer :

The construction of the sensing element is as shown in figure (5.1) . It has the form of a hemispherical Fabry-Perot interferometer. The interferometer is illuminated via a monomode optical fibre, where the end of the fibre forms the inner mirror of the interferometer, as discussed in chapter (4) . A spherical metal mirror with radius of curvature (R) attached to the sensing element was used as the outer mirror . The axis of the fibre is adjusted to match the optical

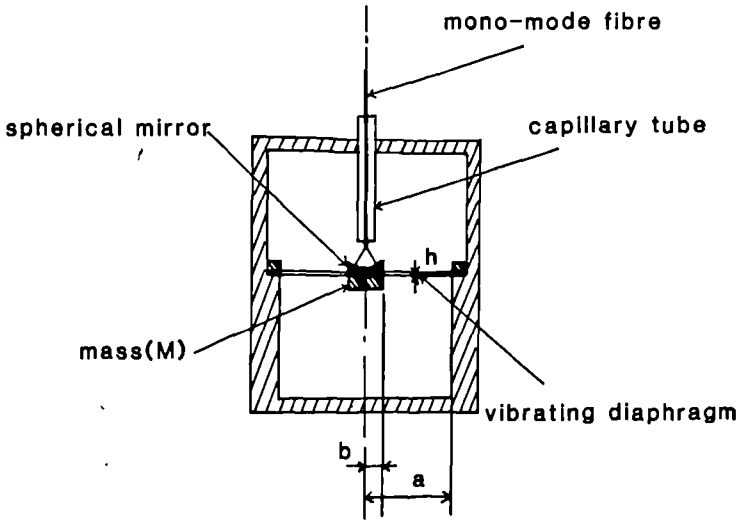

Figure (5-1) : The construction of the hemispherical Fabry-Perot fibre accelerometer.

axis of the curved mirror and the air cavity length is adjusted to give maximum visibility of the interference fringes.

The sensing element is a loaded elastic diaphragm with a passive area at the centre in the form of rigid disc. The purpose of the rigid centre was: (1) to generate higher stresses in the diaphragm at lower deflection levels, thus improving the diaphragm overall performance and increasing the value of its fundamental resonance frequency, (2) to facilitate the mirror/mass attachment, where the spherical mirror is attached centrally to the rigid centre of the diaphragm.

(5.4.2) Theory and transduction mechanism :

As the load acting on the circular diaphragm is symmetrically distributed about the axis perpendicular to the plate through its centre, the deflection surface to which the middle plane of the plate is bent will also be symmetrical. For symmetrical deflection, all points equally distant from the centre of the plate the deflection will be the same, and the maximum deflection is at the centre. In the limiting case of small deflection, the diaphragm is an elastic device. The static

deflection of the centre of the diaphragm (Y_o) is linearly proportional to the magnitude of the applied force (F) acting perpendicular to the plane of the diaphragm at its centre. The deflection of the centre of the diaphragm may be written as :

$$Y_o = A_s \frac{F\,a^2}{16\,\pi\,D} \tag{5.1}$$

D is called the flexural rigidity of the diaphragm, and A_s is a numerical coefficient which depends on the solidity ratio [12,13]. The solidity ratio of the diaphragm is defined as the ratio of the rigid centre and diaphragm radii (b/a),

$$D = \frac{E\,h^3}{12\,(1-\nu^2)} \tag{5.2}$$

$$A_s = 4\left[\frac{c^2-1}{4c^2} - \frac{\ln^2 c}{c^2-1}\right] \tag{5.3}$$

where h is the thickness of the diaphragm, E its modulus of elasticity in tension and compression , ν its Poisson's ratio and c is the reciprocal of its solidity ratio (c=a/b). If the mass of the diaphragm material is much less than that of the solid central disk, the sensing element can be approximated as an equivalent mass spring system. The mass (M) corresponds to the diaphragm load assembly and the spring constant (K) is determined from equation (5.1) as:

$$K = \frac{F}{Y_o}$$

$$= \frac{16\pi D}{A_s a^2} \tag{5.4}$$

The angular frequency of the fundamental mode of the sensing element is calculated by the well known formula $\omega_o = \sqrt{\frac{K}{M}}$.

If (r) is the magnitude of the linear acceleration acting perpendicular to the plane of the diaphragm, then using Newton's second law (F = M r) and equation (5.4) we can get :

$$Y_o = \frac{M\,r}{K} = \frac{r}{\omega_o^2} \tag{5.5}$$

Within this range of small deflection ($Y_o \leq 0.3h$) the diaphragm is a linear transducer and hence the displacement (Y_o) is proportional to the magnitude of the linear acceleration of the device along its axis of symmetry, as discussed below.

If the accelerometer is vibrated harmonically along its axis of symmetry with an amplitude of d_{max} and an angular frequency of $\Omega < \omega_o/3$ and if the damping factor of the sensing diaphragm is negligible, a harmonic acceleration of the same frequency and an amplitude of $r_{max} = d_{max}\,\Omega^2$ will affect the centre of the diaphragm [14]. Correspondingly, a harmonic force of an amplitude $F_{max} = M\,r_{max}$ will make the rigid centre oscillate in a forced vibration regime (or mode) with the same frequency and a steady state amplitude of Y_{max}, which is a function of the diaphragm parameters and Ω. The static displacement of the centre of the diaphragm, $Y_o = \frac{F_{max}}{K} = \frac{r_{max}}{\omega_o^2}$ is the smallest value of Y_{max} within the frequency range below the fundamental resonance frequency, of the diaphragm, and hence it is reasonable to consider its value when the sensor sensitivity is estimated [15].

In our experiment a steel diaphragm with radius 9.5 mm and thickness of 0.051 mm was used while the radius of the rigid centre (b) was ≈ 4 mm. The system was tested using two different loadings of the diaphragm, giving total mass (M) of the diaphragm load assembly of 0.91 and 0.59 grammes respectively. According to equation (5.4), the theoretical value of the fundamental frequency of the diaphragm f_o is 471.6 and 585.7 Hz respectively.

The optical phase change $\Delta\phi$ induced in the hemispherical interferometer (I_1) by a displacement Y_o is :

$$|\Delta\phi| = \frac{4\pi}{\lambda} Y_o$$

$$= \frac{r}{\lambda\pi f_o^2} \qquad (5.6)$$

where λ is the wavelength of the light illuminating the system. The accelerometer sensitivity (S) is defined as:

$$S = \frac{|\Delta\phi|}{r} = \frac{1}{\lambda\pi f_o^2} \qquad (5.7)$$

The static resolution r_{min} of the accelerometer is limited by the phase resolution of the interferometer $\Delta\phi_{min}$ and is a function of the fundamental frequency such that :

$$r_{min} = \lambda\pi f_o^2 \Delta\phi_{min} \tag{5.8}$$

Considering the maximum permitted static deflection of the centre of the diaphragm, $Y_{o\,max} \leq h/3$, a maximum value of the acceleration measured by the accelerometer may be estimated as $r_{max} = \lambda\pi f_o^2 \Delta\phi_{max}$, where :

$$\Delta\phi_{max} = \frac{4}{3} x \frac{\pi h}{\lambda} \tag{5.9}$$

and hence the dynamic range of the accelerometer is simply defined as the ratio $\Delta\phi_{max} / \Delta\phi_{min}$.

The accelerometer can be used as a contact vibration sensor measuring vibration with frequencies below, at or above the fundamental resonance frequency of the sensing diaphragm. Practically, the working frequency range of the system , permitting constant resolution, is limited at the higher side by $f_{max} \approx \frac{f_o}{3}$. The minimum working frequency of the system is constrained by the signal processing scheme and the noise level at the system output, which increases rapidly at very low frequencies [13], however it is possible to operate the system as a D.C. accelerometer.

Equation (5.7) shows that as the fundamental resonance frequency of the diaphragm increases, and hence the working frequency range, the sensitivity of the accelerometer is reduced, such that an optimised design is required to match a specified application.

The output intensity of the sensing interferometer, I_1, may be represented in the familiar form :

$$I = I_{mean} \left[1 + V\, Cos(\phi_o + \Delta\phi \sin\Omega t)\right] \tag{5.10}$$

where I_{mean} is the mean output of the interferometer, ϕ_o is the static phase induced in the interferometer and V is the interference visibility constant. The frequency spectrum of the output may be obtained by expanding equation (5.10) in terms of Bessels coefficients where :

$$Cos(\chi\, Sin\psi) = J_o(\chi) + 2 \sum_{m=1}^{\infty} J_{2m}(\chi)\, Cos(2m\,\psi)$$

and

$$Sin(\chi\, Sin\psi) = 2 \sum_{m=1}^{\infty} J_{2m-1}(\chi)\, Sin[(2m-1)\,\psi]$$

and then equation (5.10) takes the form :

$$I = I_{mean}\left\{1 + V\, Cos\phi_o\, [J_o(\Delta\,\phi) + 2\sum_{m=1}^{\infty} J_{2m}(\Delta\,\phi)\, Cos(2m\Omega t)]\right.$$

$$\left. - V\, Sin\phi_o [\, 2 \sum_{m=1}^{\infty} J_{2m-1}(\Delta\,\phi)\, Sin(2m-1)\Omega t]\right\} \qquad (5.11)$$

where the phase modulation amplitude of the interferometer is contained within the Bessel coefficients $J_1, J_2, J_3, J_4,$, etc.

Equation (5.11) shows that the amplitudes of the frequency harmonics of the output are dependent on both the optical phase change, $\Delta\,\phi$, as well as the interferometric static phase represented by $Sin\phi_o$ and $Cos\phi_o$. As ϕ_o varies randomly with the environmental perturbations, the signal will fade for certain values of ϕ_o, as discussed in chapter (1). Several methods, by which this signal fading problem can be avoided, are reported [16].

(5.4.3) Experimental characterisation, as a vibration sensor :

The optical arrangement used to interrogate the movement of the diaphragm and hence to characterise its performance, as a contact vibration sensor, is shown in figure (5-2). A laser-diode, Mitsubishi (ML4102), was used to illuminate the system with a mean wavelength of 787 nm. The fibre-optic system was constructed using low loss (< 0.8 db) 50-50 ±5% fibre optic directional couplers (Sifam S82C50). The accelerometer (I_1) was constructed with a spherical mirror with radius of curvature of ≈ 3.85 mm. The second interferometer, I_2, of similar configuration, was used to calibrate the accelerometer. The laser-diode could be locked by a feedback servo to compensate for very low frequency phase shifts caused by temperature changes and to maintain the accelerometer (interferometer I_1) at quadrature.

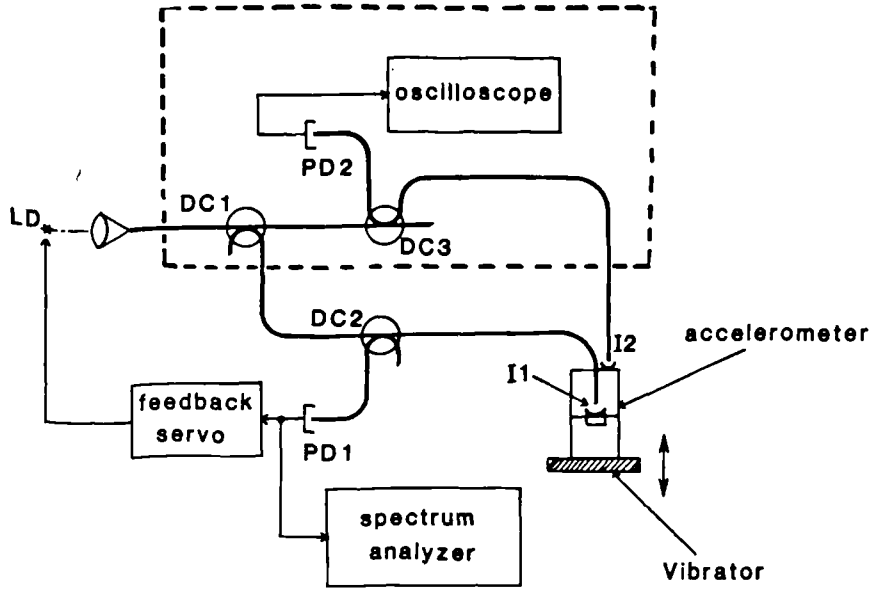

Figure (5-2) : The optical arrangement used to characterise the accelerometer.

Note : The optical elements inside the dashed box are used to calibrate the sensor only, in normal use they are not required.

The accelerometer was fixed on the top of a mechanical vibrator with its axis parallel to the direction of vibration. The vibrator was driven sinusoidally in the frequency range 40 - 250 Hz. The amplitude displacement of the vibrator (d_{max}) was set such that the phase change induced in I_2 corresponded to 2π optical radians (ie, $d_{max}= \frac{\lambda}{4}$) thus imparting a calculated acceleration to the device, with an amplitude of $r_{max} = \frac{\lambda}{4}\Omega^2$.

In our experimental characterisation of the system, the value of the applied axial acceleration varies from 1.3 m g (at vibration frequency, f = 40 Hz) to 51 mg (at f = 250 Hz), where g is the gravitational acceleration, $g \simeq 9.8ms^{-2}$. Two different approaches were used to overcome the signal fading problem, based upon homodyne signal processing. The first, used to recover very small phase changes, is based on the closed-loop wave-length tracking homodyne technique, discussed in chapter (1), where the interferometer was locked, via the laser diode injection

current, at quadrature (with a low gain bandwidth product servo) maintaining $Sin\phi_o = 1$. For small arguments of the Bessel function $J_1(\Delta\phi) \approx \Delta\phi/2$ and hence the phase change is measured directly by measuring the amplitude of the first harmonic. This method was useful to characterise the accelerometer performance at frequencies lower than 100 Hz, when it was not accurate to measure the amplitude of the higher order harmonics relative to the noise floor of the output signal. At higher frequencies (higher values of the applied acceleration) the second open-loop homodyne approach was used, based on evaluating the ratios of both the odd and the even harmonic amplitudes ($I_\Omega/I_{3\Omega}$ and $I_{2\Omega}/I_{4\Omega}$) and hence two output signals, independent of the interferometric static phase were obtained. Using the usual Fourier expansion of phase modulated signals, as described by equation (5.11), the optical phase change ($\Delta\phi$) arising from the acceleration was determined.

The spectrum of the intensity output of the sensing interferometer was measured using a spectrum analyser, in peak hold mode. This function allows the automatic recording of the peak amplitudes of the harmonics of the output of the accelerometer by holding the maximum signal levels measured. In this mode, the values of the odd and even harmonics can both be measured at maximum accuracy by allowing the system to run unlocked through a long time. This method of signal processing was expedient and accurate to characterise the accelerometer and to measure the mechanical properties of the diaphragm. More appropriate techniques based on the use of modulated semiconductor laser diodes [17] and on white light interferometric techniques [18], demonstrated in chapter (3), will be reviewed in chapter (6).

The signal to noise ratio, at the accelerometer output, was measured when it was vibrated with an amplitude corresponding to one interference fringe observed at the output of the sensing interferometer, I_1, with the interferometer locked at quadrature. This experiment was repeated at different vibration frequencies, hence the accelerometer resolution was estimated, as a function of the vibration frequency.

The mechanical properties of the diaphragm were tested experimentally, by measuring the diaphragm response in the vicinity of its fundamental resonance frequency. Finally, the cross-

sensitivity to accelerations orthogonal to the symmetry axis of sensor was measured by mounting the accelerometer with its axis perpendicular to that of the vibrator and then measuring the ratio of the phase change induced in I_1 relative to that phase change induced when the accelerometer is vibrated along its axis of symmetry.

(5.4.4) Performance :

The diaphragm assembly was an under-damped mechanical oscillator with a quality factor of about 36. The fundamental resonance frequencies of the diaphragm mass assembly were 465 Hz (for M = 0.91 grammes) and 582 Hz (for M = 0.59 grammes) which are in good agreement with theoretical prediction.

Figure (5-3 a) shows the variation of the experimentally determined optical phase change ($\Delta\phi$) induced at the output of I_1 as a function of the frequency, while figure (5-3 b) shows the interferometer phase resolution. At each frequency the value of the induced phase was used together with the corresponding value of the phase resolution to calculate the resolution, R, of the accelerometer, the accelerometer resolution as a function of frequency is shown in figure (5-4). The mean signal to noise ratio was 78.2 dB in a bandwidth of 9.55 Hz, corresponding to a mean phase resolution of $4x10^{-5} rad/\sqrt{Hz}$. The noise arises from (i) intensity and frequency fluctuations of the optical source, and is hence smaller at higher frequencies, (ii) acoustic noise affecting the sensing diaphragm and (iii) electronic noise. It may be seen that the accelerometer static resolution is better than $5\,\mu g$, ($g \approx 9.81 ms^{-2}$) and its static sensitivity is ≈ 9.5 rad/g. Figure (5-4) shows also a nearly constant resolution within the working frequency range ($0 - f_o/3$). It may be seen that as the mass, of the diaphragm assembly decreases the fundamental frequency, and hence the working frequency range, increases while the resolution is reduced. These results are in good agreement with that predicted using the mass-spring model introduced before. The output waveforms of the interferometers I_1 and I_2 are shown in figure (5-5). The cross-sensitivity to orthogonal components of acceleration was measured to be better than -32.1 dB. Considering the maximum deflection of the diaphragm as described by equation (5.9) the dynamic range of the accelerometer is $\approx 6.8 \times 10^6$.

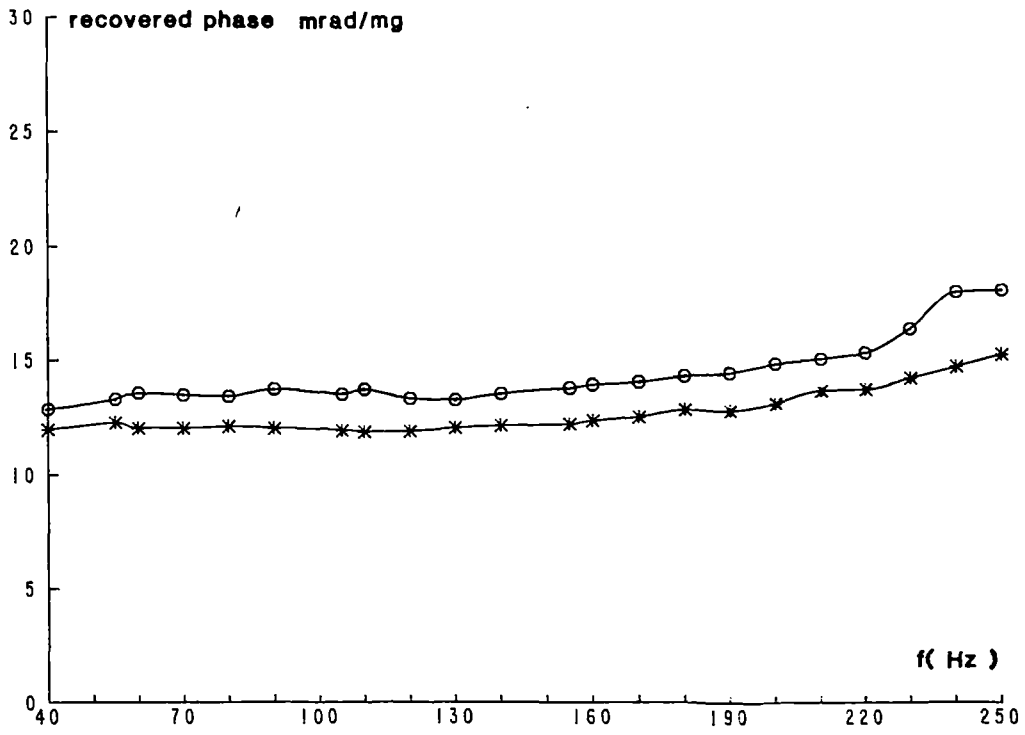

Figure (5-3 a) : The variation of the optical phase change induced in the sensor against frequency, circles : M = 0.91 g and * * * : M = 0.59 g.

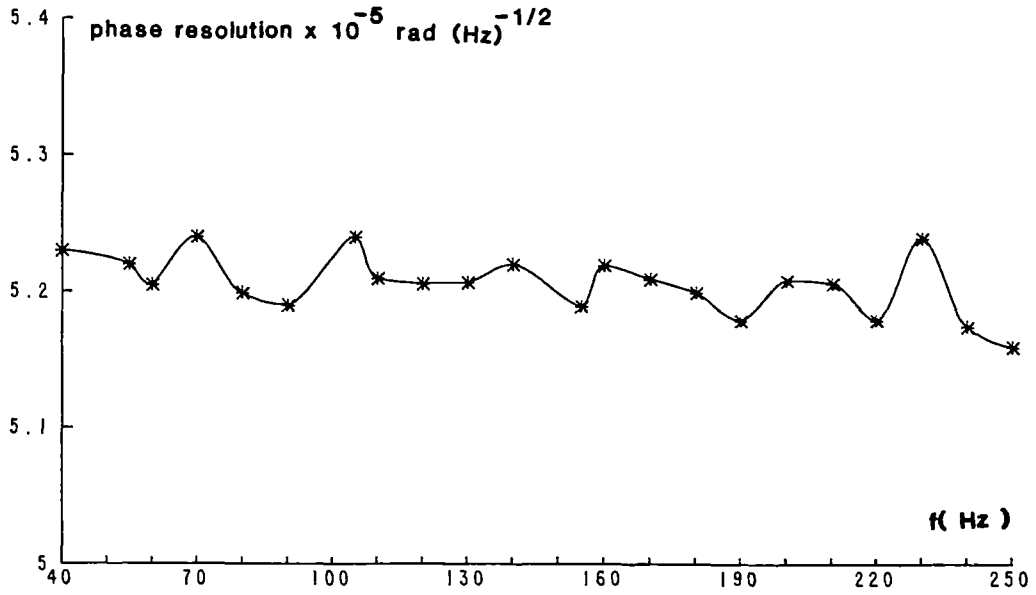

Figure (5-3 b) : The phase resolution of the sensing interferometer against frequency.

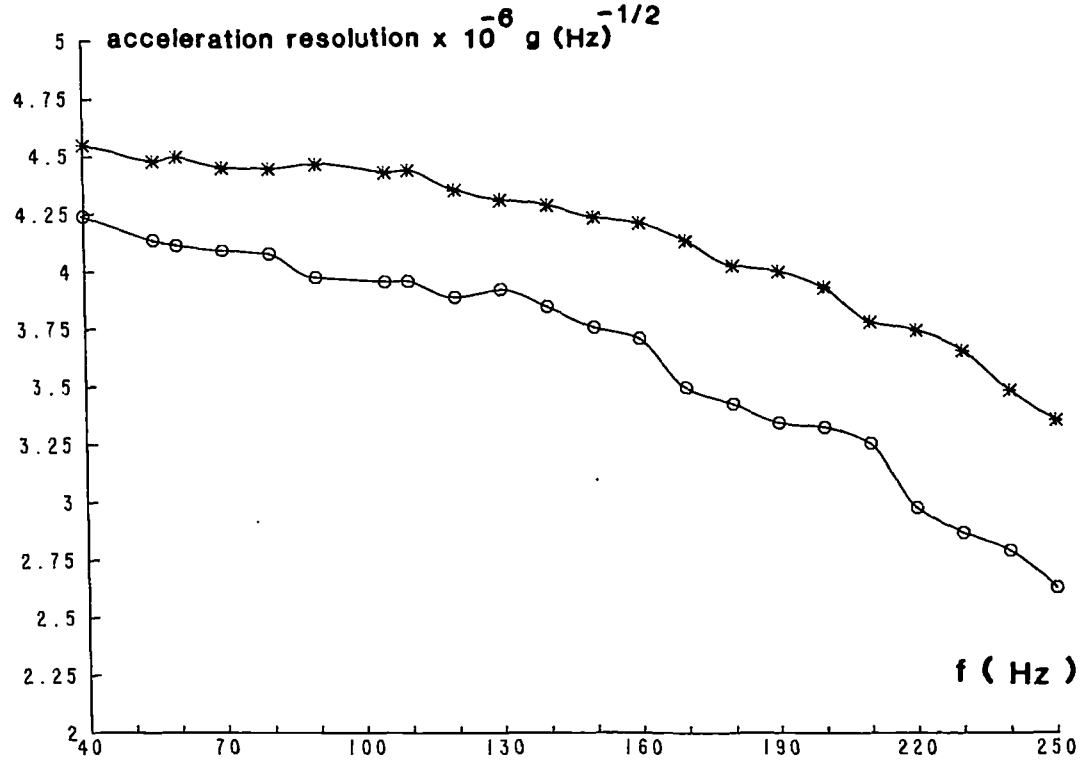

Figure (5-4) : The accelerometer resolution as a function of frequency.

Circles : M = 0.91 g and * * * : M = 0.59 g

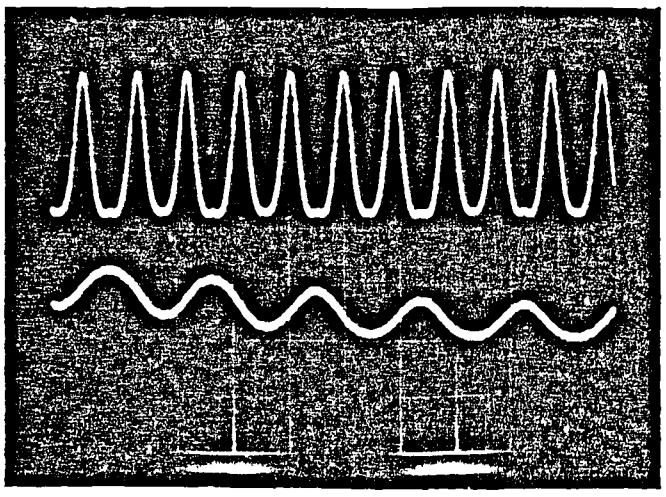

Figure (5-5) : The output waveform of I_2 (upper) and I_1 (lower).

(5.4.5) Temperature effects on the sensing diaphragm :

A change in temperature will change the dimensions of the diaphragm and its modulus of elasticity as well. As a result, the sensitivity of the sensing diaphragm, and hence its fundamental frequency will change with the variations in temperature. Using equations (5.2 - 5.7) the accelerometer sensitivity (S) may be expressed in the form :

$$S = \frac{3M A_s(1-\nu^2)}{\lambda} \times \frac{a^2}{Eh^3} \tag{5.12}$$

The sensitivity due to temperature change of Δt from t_o to t is :

$$S = \frac{3M A_s(1-\nu^2)}{\lambda} \times \frac{[a_o\,(1+\alpha\,\Delta t)\,]^2}{E_o\,(1+c_e\,\Delta t)\,[\,h_o(1+\alpha\,\Delta t)\,]^3} \tag{5.13}$$

where a_o, h_o and E_o are the diaphragm radius, thickness and modulus of elasticity in tension at the temperature t_o respectively, α is the coefficient of thermal expansion of the diaphragm material and c_e is the thermal coefficient of modulus of elasticity in tension per degree change in temperature. Equation (5.11) may be written as the ratio of the diaphragm sensitivities at t_o and at temperature t as :

$$(S)_t/(S)_o = \frac{1}{(1+c_e\,\Delta t)(1+\alpha\,\Delta t)} \tag{5.14}$$

The sensitivity error S% may be defined as :

$$S\,\% = [1- \frac{1}{(1+c_e\,\Delta t)\,(1+\alpha\,\Delta t)}] \times 100 \tag{5.15}$$

From equation (5.7) it can be proved that the ratio of the fundamental frequencies at temperature t and t_o is :

$$(f_o)_t/(f_o)_o = \sqrt{(1+c_e\,\Delta t)\,(1+\alpha\,\Delta t)} \tag{5.16}$$

The value of c_e is usually larger than α, thus it has a more pronounced effect on the sensitivity error [19]. Since the thermal coefficient of elasticity is usually negative and the thermal coefficient of expansion is usually positive, it may be possible to design a diaphragm with nearly

constant sensitivity within the required temperature range.

The temperature effects on the sensing diaphragm were experimentally studied as follow : With the accelerometer fixed horizontally to the vibrator an electric tube-furnace was installed around the sensing head, its temperature was elevated in steps of 10^oC and monitored using a high temperature thermo-couple. The accelerometer performances were studied at different values of temperature. Care was necessary to achieve a steady state condition at each increment of temperature. The accelerometer sensitivity (at a frequency of 180 Hz) was measured over the temperature range $20^o - 400^oC$.

The theoretical and experimental variations of the sensitivity error (S%) as a function of the sensor temperature are shown in figure (5-6). The negative values of the sensitivity error indicates that the original sensitivity (at room temperature) is less than that at elevated temperature ($t>t_o$). Above 120^oC experimental values of the change in S with temperature, ie the slope of the curve in figure (5-6), correspond to that predicted theoretically. However below 120^oC there is evidentially a much stepper slope. This is thought to be due to initial stresses arising during the manufacture of the assembly and their subsequent release at higher temperatures, as a result of the differential thermal expansivity between the membrane and its support.

(5.5) Conclusions :

A practical optical accelerometer has been introduced in which the sensing element is completely passive. The sensing element is a weighted diaphragm. The displacement of the diaphragm produced by acceleration is measured using a miniature hemispherical air-spaced Fabry-Perot interferometer, of which one mirror is mounted on the diaphragm. The interferometer is illuminated by a diode laser and addressed via a monomode optical fibre.

The range and resolution of the accelerometer depends on the properties of the diaphragm, which may be designed appropriately for a given application. The cross-sensitivity observed arises from the non-optimal design of the mass-diaphragm assembly, in which the centre of mass does not lie in the plane of the diaphragm; this could be rectified readily in future implementation

designs. Alleviation of cross-sensitivity effects, which are strong in previously reported fibre-optic accelerometers, would allow construction of a multiplexed system using three orthogonal sensors to measure the full acceleration vector.

Diaphragm technology is mature (for example, for pressure measurement), and a range of materials and designs exist. This facilitates the practical implementation of our technique for a wide range of applications.

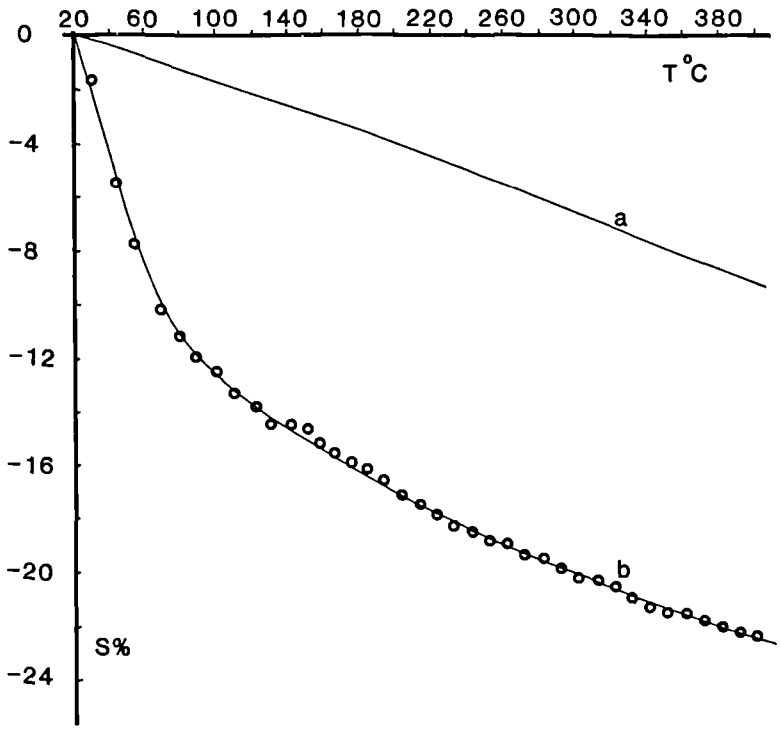

Figure (5-6) : The variation of the sensitivity error as a function of the diaphragm temperature, (a) : theoretical and (b) : experimental.

References

[1] B.E.Noltingk, "Instrumentation reference book", Butterworth and Co. Ltd, 1988, Chapter (6).

[2] Bruel and Kjaer, "Short form catalogue", Bruel & Kjaer, Naerum, Denemark, 1986, P. 10.

[3] Y.Fathi, H.Reimann, " accelerometer and sub-Psi pressure sensor, a new generation of monolithic silicon chips ", Proceedings of Sensors Exposition Detroit, MI, USA, 15-17 September 1987, P. 295.

[4] I.Igarashi, "Semiconductor dynamic sensors", Sens. Actuators (Switzerland), Vol.13, No.1, Jan 1988, P.53.

[5] " Silicon accelerometers " Euro Sensor, London, Technical Note, TN-008, December 1988

[6] A.B.Tveten, A.Dandrige, C.M.Davis and T.G.Giallorenzi " Fibre optic accelerometer " Electronics Letters, Vol.16, No.22,1980, P.855.

[7] A.D.Kersey, D.A.Jackson and M.Corke " High sensitivity fibre optic accelerometer " Electronics Letters, Vol.18, No.13, 1982, P.559.

[8] D.L.Gardner, t.Hofler, S.R.Baker, R.K.Yarber and S.L.Garrett, " A fibre-optic interferometric seismometer ", J. Lightwave Technology, Vol.LT-5, No.7, July 1987, P.953.

[9] F.Bucholtz, A.D.Kersey and A.Dandridge " DC Fibre optic accelerometer with sub micro g sensitivity " Electronics Letters, Vol.22, No.9, 1986,P.451.

[10] R.Jones, " The development and application of a thermally self-compensated fibre optic linked accelerometer " Proceeding of the 4TH sensor and their applications (S+A IV), Canterbury, U.K., September 1989, P.39.

[11] A.S.Gerges, T.P.Newson, F.Farahi, J.D.C.Jones and D.A.Jackson " A Hemispherical Air Cavity Fibre Fabry-Perot Sensor " Optics Communication, Vol.68, No.3, Oct.1988, P.157.

[12] S.Timoshenko " Theory of plates and shells " McGraw-Hill 1940,Chap. (3).

[13] M.DiGiovanni " Flat and corrugated diaphragm design handbook " Marcel Dekker,Inc., 1982, Chap. (12,13).

[14] R.C.Smith and P.Smith, " Mechanics ", John Wiley & Sons LTD, 1971, P. 189, 190.

[15] W.Gough, J.P.G.Richards and R.P.Williams, " Vibrations and waves " Ellis Horwood Limited, 1983, Chapter (3), P. 55.

[16] " Workshop on single mode optical fibre sensor technology ", Course notes, University Of Kent and Sira Ltd., U.K., 1985, P.144.

[17] D.A.Jackson and J.D.C.Jones," Fibre Optic Sensors ",Optica Acta,V ol.33,No.12, 1986,P.1469.

[18] A.S.Gerges, F.Farahi, T.P.Newson, J.D.C.Jones and D.A.Jackson, " Fibre optic interferometric sensor using a low coherence source: dynamic range enhancement", International Journal of Opto-Electronics, Vol.3, No.4, 1988, P.311.

[19] G.W.C.Kay and T.H.Laby, " Tables of physical and chemical constants", Longman, 1986, Chap. (1-4).

CHAPTER (6)

A practical low frequency fibre–optic based accelerometer, with common mode compensation

(6.1) Introduction

In chapter (5) we introduced a novel form of fibre-optic accelerometer, where its performance was tested and analysed when it was operated as a contact vibration sensor for relatively high frequency periodic measurands. In this chapter we study the use of the device as a low frequency accelerometer, and identify aspects of the design which limit the applicability of the accelerometer. These limitations arise from : (i) the erroneous phase changes induced in the sensing interferometer as a result of the laser source frequency drifts, (ii) errors due to temperature perturbations caused by the expansion of the housing forming the body of the accelerometer and (iii) initialisation problems arising as the system is illuminated with a single monochromatic source (see chapter-2).

Considerations of the accelerometers working environment necessitate the use of only electrically passive components to construct the sensing head. This forms another major difficulty when choosing the most appropriate signal processing technique, especially when the sensing interferometer is relatively short. It is often an advantage to use a short sensing interferometer, as this reduces the phase noise induced in the output signal and permits a small sensing head which reduces its susceptibility to environmental influences.

Here we review some of the commonly used interferometric signal processing techniques suitable for use with a relatively short passive sensing interferometers, and discuss in detail the most appropriate technique to characterise the low frequency performance of the accelerometer. Next we introduce a new configuration for this type of accelerometer in which the deleterious effects of both the short and long-term frequency jitter of the optical source as well as environmental effects are strongly reduced. Finally we demonstrate the use of a dual wavelength technique to extend the dynamic range of the accelerometer and hence to solve the initialisation problem within the limits of the accelerometer working range.

(6.2) Interferometric signal processing techniques for relatively short electrically-passive sensors :

In this section various methods of signal processing, suitable for use with relatively short passive sensing interferometers ($\Delta L \approx 1cm$) are reviewed. The signal processing technique is required to be accurate, stable and to have a reasonably large operational range. In this review we will consider how the signal processing affects the operation of the accelerometer, introduced in chapter (5). The same concepts are valid for any interferometric system with a short path-length imbalance. According to the required measuring range and resolution the most appropriate technique is chosen.

(6.2.1) Signal processing techniques using semiconductor laser-diodes :

A major advantage of laser-diodes over gas-lasers is that their frequency is a function of the injection current [1]. Different signal processing techniques, based on closed loop homodyne tracking [2] or frequency modulation [3,4] can be used enabling passive interrogation of the sensor, as discussed below.

(a) Active and passive wavelength tuning homodyne techniques :

The concept of active homodyne signal recovery, in fibre optic interferometric sensors, was

discussed in chapter (1). It was shown that the sensing interferometer can be maintained at maximum sensitivity (i.e quadrature) by an electronic feedback servo, with limited gain bandwidth product, in which the servo output is fed back to the optical source (often a laser diode) to tune its wavelength. It was also shown that if the interferometer has two outputs, such as a Mach-Zehnder interferometer, then at a quadrature point the two outputs are equal. It is straightforward to design an electronic servo which controls the interferometer such that these signals are equal, hence maintaining the interferometer at a quadrature point. If the interferometer has only one output then a reference voltage, equal to the mean output voltage of the photodetector, is required as an alternative for the second input to the servo. The total phase change that can be compensated by the feedback servo is $\frac{2\pi}{C}\,\Delta\nu\,\Delta L$, where $\Delta\nu$ is the maximum frequency excursion of the laser diode and ΔL is the optical path-length imbalance of the interferometer. As $\Delta\nu$ is usually small the tracking range is governed by ΔL such that for an interferometer with a small optical path-length imbalance it becomes difficult to use closed loop homodyne signal processing. Frequency modulation of the laser diode also causes variation in its output power, hence the reference signal for the servo must vary as the emitted power from the laser.

It was shown in chapter (1) that if the measurand frequencies are below the corner frequency of the feedback servo the induced phase, within the interferometer, is recovered at the output of the servo. The maximum tracking range of the feedback servo is limited by the maximum allowable change in the laser-diode injection current ($\pm\Delta i$), where :

$$\Delta i \leq \frac{i_{\max} - i_{th}}{2} \tag{6.1}$$

here $i_{\max}$ and i_{th} are the maximum and threshold values of the laser injection current respectively. Typically $\Delta i \approx \pm 6$ mA; the corresponding change in the laser emission frequency $\Delta\nu \approx \pm 18 GHz$ [5].

For example in the case of the hemispherical Fabry-Perot interferometer used in the accelerometer, the optical path-length imbalance was $\Delta L \approx 8mm$, hence the corresponding maximum allowable tracking range is relatively small, $\approx \pm 3$ optical radians. The static sensitivity of

the accelerometer, discussed in chapter(5) was $\approx 9.5 rad/g$, thus this technique of signal processing permits a restricted low frequency (within the bandwidth of the tracking servo) acceleration measurement range of $\pm 0.3g$.

As also shown in chapter (1), the active homodyne technique can be used to recover signals with frequencies above the corner frequency of the servo, now the phase information is measured directly at the photodetector output . For sufficiently small phase changes $\Delta\Phi \ll 1$ rad, the amplitude of the first harmonic of the output signal is proportional to $J_1(\Delta\Phi)$, which in-turn may be considered proportional to the optical phase change itself ($J_1(\Delta\Phi) \approx \frac{1}{2}\Phi$) [6]. For our example this corresponds to an acceleration amplitude << 0.1 g.

Passive homodyne signal processing techniques are discussed in chapter (1). One of these techniques, based on switching the absolute frequency of the laser source between two optical frequencies to generate two quadrature outputs, could be possibly be used to advantage as $\Delta\nu$ needs only to be equivalent of $\pi/4$ radians. The range of this type of processing in short interferometers may be restricted as any significant variation in the optical path-length imbalance will require that $\Delta\nu$ changes by a corresponding amount [4].

(c) Pseudo-heterodyne techniques :

In chapter (1) we show that the heterodyne type of signal processing offers many advantages over the homodyne unfortunately with a passive interferometric sensor true heterodyne signal processing cannot be used. However a heterodyne-type carrier can be produced by appropriately modulating the phase of the interferometer and subsequent manipulation of the output signal of the interferometer [7]. The carrier may be produced at the output of an unbalanced interferometer by modulating the emission frequency of the laser diode by controlling its injection current about its operating D.C. current [3]. The rate of change in the carrier phase caused by the variation in the emission frequency of the laser for an interferometer of path-length imbalance (ΔL)

is given by :

$$\frac{d\phi}{dt} = \frac{2\pi \Delta L}{C} \frac{d\nu}{dt}$$

$$= \frac{2\pi \Delta L}{C} K_d(\nu) \frac{di}{dt} \qquad (6.2)$$

where $K_d(\nu)$ represents the rate of change of the optical frequency with injection current, which is dependent upon the modulating frequency [4].

If the laser diode injection current, and hence its emitted frequency, is modulated with a serrodyne wave-form of the appropriate amplitude, the interferometer output will be driven over an integral number (q = 1,2,3,...) of complete interference fringes during each period of the modulating ramp signal [8]; the modulation amplitude corresponds to $q\ \pi$ radians. The phase modulated carrier is obtained by band-pass filtering the photodetector output signal at frequency $q\ f'$, where f' is the frequency of the serrodyne modulation.

Another form of pseudo-heterodyne signal processing relies on sinusoidal modulation of the laser diode injection current, this technique has significant advantageous over serrodyne modulation in that; (i) it enables the production of a higher frequency carrier, (ii) the required modulation amplitude is $\simeq$ 10 % less and (iii) the modulation signal is harmonic, hence the laser diode current is not subject to the rapid current transients which occur with serrodyne modulation - these transients can produce several electronic problems, especially if the modulation frequency is high [9].

When the laser diode is modulated sinusoidally, the output spectrum of an unbalanced interferometer consists of a series of harmonics of the modulation frequency with amplitudes determined by the arguments of the related Bessel function components. To produce the carrier the output signal may be produced in several ways. For example gating the output using synchronous square pulses, driven from the modulating source with a fixed duty cycle. If a 50:50 duty cycle is used the interferometer is driven with an amplitude of (2.82) optical radians and the carrier is produced by band-pass filtering the gated output at a frequency of $2f'$,(f' is the modulating frequency) [10, 11]. An advantage of this gating technique is that it is possible to produce two anti-

phase electronic carriers which contain the interferometric phase in equal magnitude, hence the relative phase shift between the two carriers becomes double the interferometric phase, thus improving the resolution of the demodulated signal by a factor of $\sqrt{2}$.

Using this signal processing technique, both the acceleration and the frequency working ranges are extended. The frequency working range extends from true D.C. to the maximum frequency permitted by the phase demodulator used to measure the phase changes of the carrier. Various electronic recovery systems, such as phase locked loops and digital phase trackers, have been used [12,13]. The minimum detectable phase shift (acceleration) is set by the noise floor of the generated electronic carrier. In a true heterodyne signal processing system, the maximum detectable phase shift is, in principle, unlimited as there are no frequency components above that of the carrier, however the method of the carrier production described here generates higher harmonics which limit the maximum frequency deviation of the carrier. In our application, of acceleration measurement, the working ranges are then limited by the mechanical properties of the sensing diaphragm, as discussed in chapter (5), the noise floor at the output of the interferometer and the method of carrier generation, although the later effect was not the predominant.

Although both serrodyne and sinusoidal modulation techniques are simple to implement, intensity modulation will also occur when it is applied to short interferometers, for the reasons discussed above. This intensity modulation will give rise to additional noise in the recovered signal, additional electronic processing can be used to effect some reduction in this noise. As sinusoidal modulation require a slightly lower modulation amplitude (2.82 rad) the amplitude of this noise is slightly less, moreover as the carrier is produced by filtering at twice the modulation frequency, the effect of amplitude modulation are also reduced.

(6.2.2) Signal processing based on white light interferometry :

The optical phase change induced in a short-length sensing interferometer can be recovered using 'white light' interferometry, as discussed in chapter (2), where the output signal is recovered at the output of a receiving interferometer which is 'coherence tuned' to the sensing

interferometer [14]. The working frequency and acceleration ranges are then limited by the properties of the tracking element used in the receiving interferometer and the noise floor at the output of the system.

(6.2.3) The most appropriate technique for the accelerometer :

It is well known that active homodyne signal processing offers the highest possible resolution for interferometric sensors [6]. However from the above discussion, we can see that the main disadvantage associated with this technique is its limited tracking range.

White light interferometry offers a solution for two of the major problems discussed in section (6.1), (i) the system is almost independent of the optical source wavelength and (ii) the sensor could be re-initialised. these advantages indicate that white light interferometry may be the most suitable technique for this type of short cavity sensing interferometer. However this technique does not allow one to recognise the phase errors generated, in the sensor, by environmental effects from the desired signal, in addition a second highly stable interferometer is required for signal recovery, as discussed in chapter (2). For these reasons we have modified the optical design of the accelerometer by incorporating a second interferometer on the opposite side of the diaphragm. This second interferometer is constructed in the same form as the original hemispherical interferometer with its mirror attached to the central part of the diaphragm. Hence its performance is identical to that of the first interferometer including its susceptibility to environmental perturbations. As discussed below, by appropriately combining the outputs from the modified system it is possible to double the sensitivity and achieve a high reduction in the error signals produced by environmental effects.

From the discussions above it would appear that, for this sensor, the pseudo-heterodyne technique of signal processing, based upon a sinusoidally modulated laser diode is the most suitable.

(6.3) Testing the sensor as a low frequency accelerometer :

The optical arrangement used to characterise the quasi-static performance of the accelerometer is shown in figure (6-1). To increase the accelerometer sensitivity a sensing diaphragm with a fundamental resonance frequency of 243 Hz was used. The accelerometer was mechanically coupled to a motor/gear box mechanism such that it could be rotated very slowly through an angle θ about a horizontal axis. The corresponding variation on the axial acceleration was $r = gCos(\theta)$, where g is the gravitational acceleration ($g \approx 9.81 ms^{-2}$).

A laser diode, sinusoidally modulated at frequency ($f' \approx 2KHz$), was used to illuminate the system with mean wavelength of 787 nm. The photo-detector output was gated by synchronous 50-50 duty cycle square pulse and filtered at frequency of $2f'$ to generate a phase modulated carrier. The modulation amplitude was adjusted (2.82 rad) to minimise the carrier amplitude modulations. The square pulses were also band-pass filtered at $2f'$ to generate a reference carrier.

The quasi-static performance of the accelerometer was determined by rotating the set-up very slowly. A linear potentiometer, mechanically coupled with the system was used to generate a voltage proportional to θ, this voltage was measured using a calibrated digital voltmeter. A phase detector was used to sequentially measure the relative phase change between the output of the interferometer and the reference carrier. The low frequency sensitivity of the accelerometer was measured by determining the induced phase change at the output of the accelerometer as it was slowly rotated such that its axis changed from the horizontal ($\theta = 90^o$) to the vertical ($\theta = 0^o$) positions and back again. The time for each 90^o rotation was 5.2 minutes.

The variations in the induced phase in the accelerometer as a function of the angle of rotation (θ), is shown in figure (6-2 a,b). A phase change of 66 rad/g was measured. The signal to noise ratio at the output of the interferometer was approximately 77 dB, within a bandwidth of 47.7 Hz, equivalent to an optical limit of the phase resolution of $2.1x10^{-5} rad(Hz)^{-1/2}$, which corresponds to an acceleration resolution of about $3.1x10^{-7} g(Hz)^{-1/2}$ at a frequency of 0.034 Hz. Figure (6-3) shows the form of the photodetector output signal, the 50:50 gated output and the phase modulated carrier.

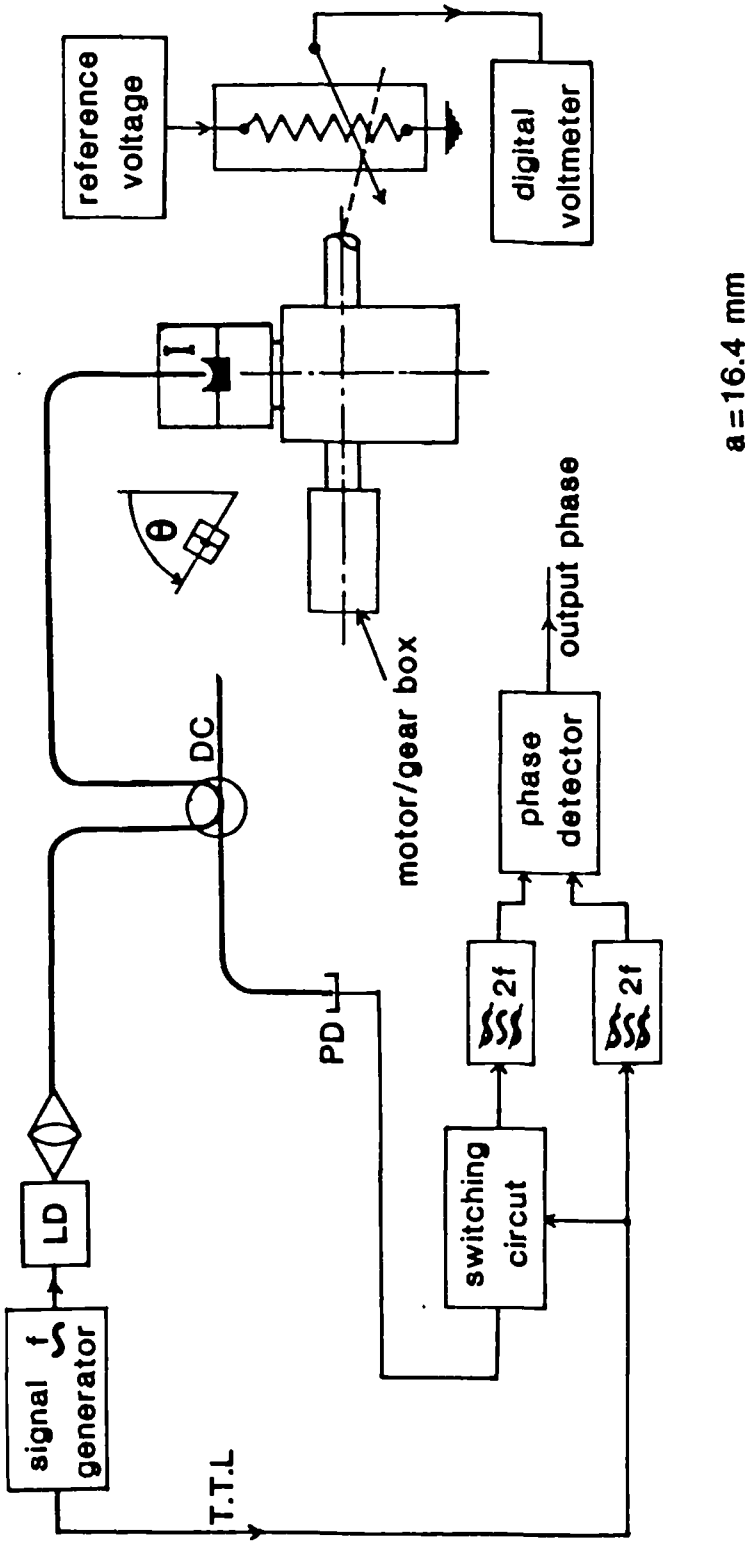

Figure (6-1) : The optical arrangement used to characterise the low quasi-static performance of the (single cavity) accelerometer.

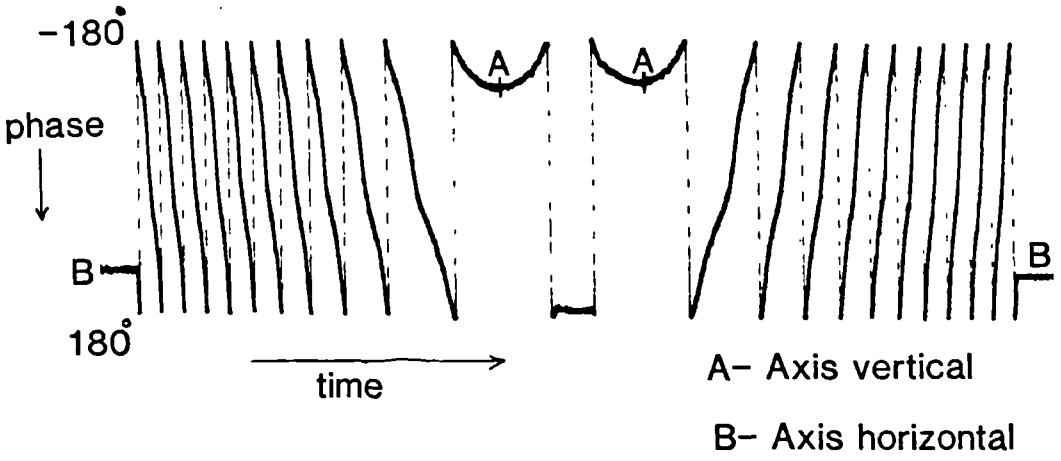

(a)

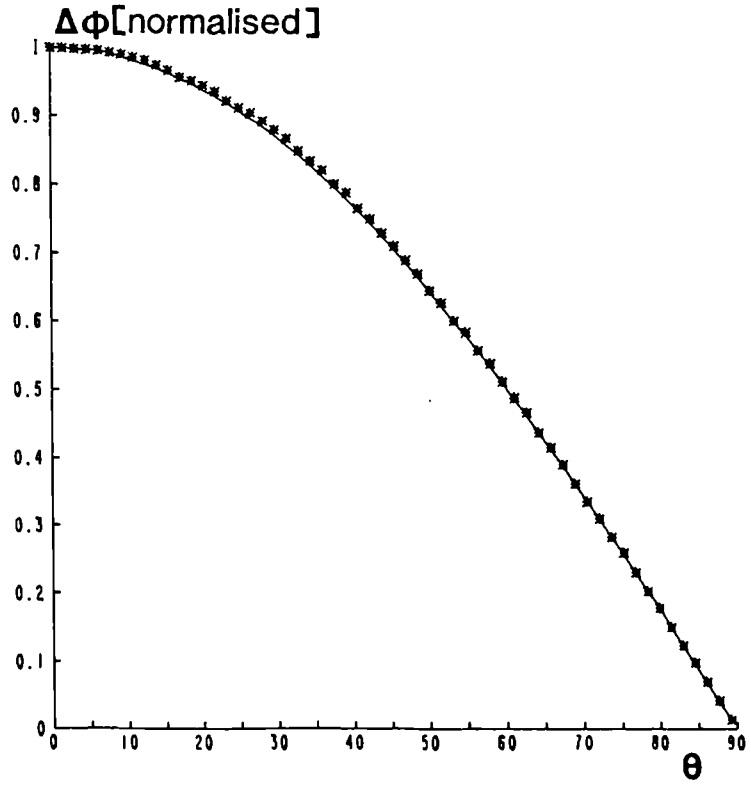

(b)

Figure (6-2) : The variations in the induced phase in the accelerometer verses the angle of rotation (θ).

(a) : using an X-Y plotter and (b) : using the computer.

Solid curve : the function Cos (θ) and * * * ; measured points.

(6.4) The modified 'back-to back' configuration; common mode compensation :

In this section we introduce a new concept for this type of accelerometer. The design is such that the deleterious effects of both short and long-term frequency jitter of the optical source as well as environmental effects are strongly reduced. Moreover, with appropriate signal processing, it can be used simultaneously as a temperature sensor.

(6.4.1) Construction of the accelerometer :

The modified construction of the accelerometer head is as shown in figure (6-4). It basically consists of two identical hemispherical Fabry-Perot interferometers (I_a and I_b), illuminated via separate monomode optical fibres. Two identical spherical metal mirrors, with radius of curvature of about 4 mm, centrally attached to the diaphragm, one on each side, form the outer mirrors of the interferometers, while the ends of the fibre serve as the inner mirrors. The two spherical mirrors act as the mechanical load and form the rigid centre of the sensing diaphragm. To reduce the cross-coupling of the device, the mass and the dimensions of the two mirrors were made equal, such that the centre of mass of the diaphragm/mirrors assembly lay in the plane of the diaphragm. The length of the two cavities (l_a and l_b) were adjusted such that the condition of maximum fringe visibility was obtained in each interferometer. As discussed in chapter (4), this occurs when $l_a = l_b$.

As the axial acceleration changes, the corresponding phase changes, induced in the interferometer I_a will be :

$$\phi_a = \frac{4\pi}{\lambda} (l_a + Y_o) \tag{6.3}$$

where Y_o is displacement of the centre of the diaphragm, as discussed in chapter (5). The optical phases induced in the interferometer I_b are :

$$\phi_b = \frac{4\pi}{\lambda} (l_b - Y_o) \tag{6.4}$$

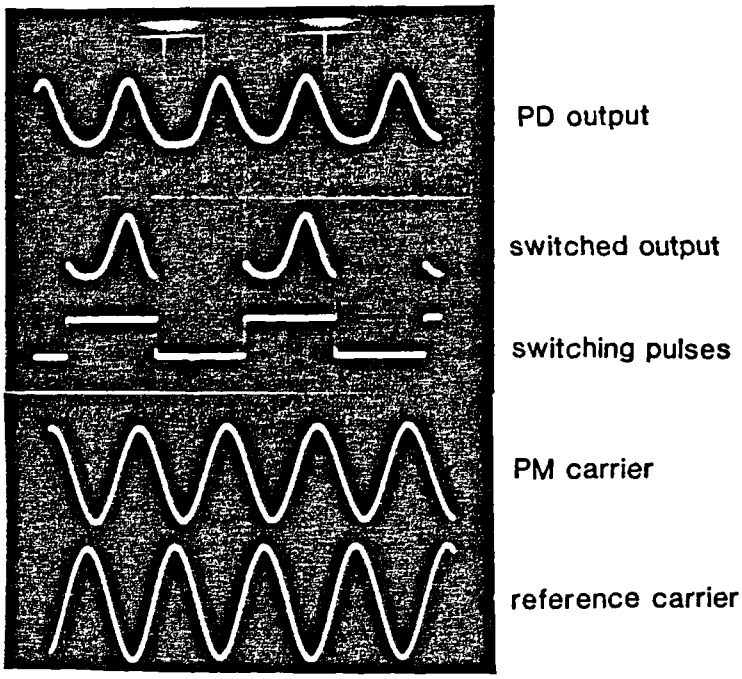

Figure (6-3) : The photodetector output signal, the 50-50 gated output and the phase modulated carrier.

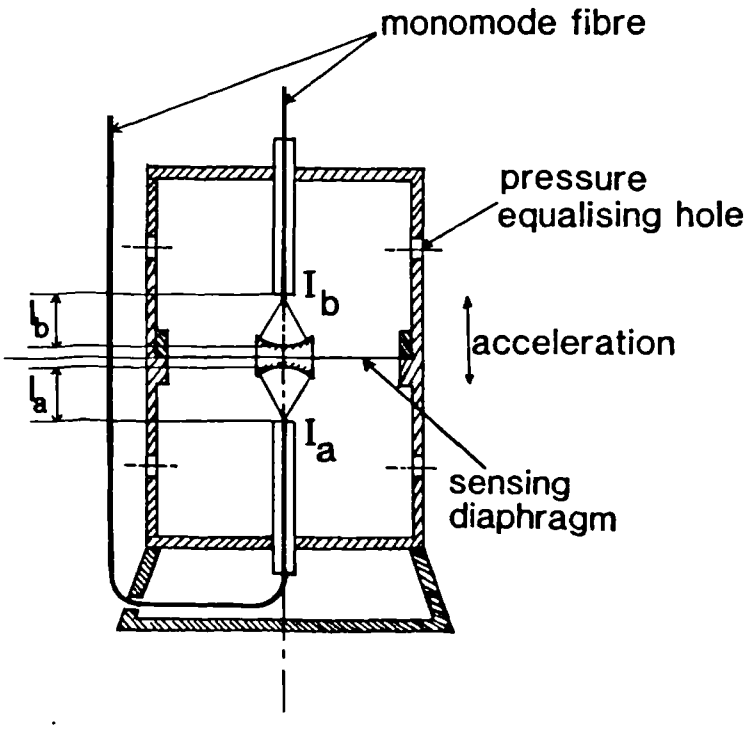

Figure (6-4) : Construction of the 'back-to-back' accelerometer head.

The optical phase change, induced in each interferometer are equal in magnitude but opposite in sign, such that by measuring the relative phases between the two interferometers (ϕ_{ab}) the sensitivity of the accelerometer is effectively doubled, where :

$$\phi_{ab} = \frac{8\pi}{\lambda} Y_o \tag{6.5}$$

Self compensation of common-mode errors is the main another advantage of this configuration apart from doubling the acceleration sensitivity. If the light wavelength drifts by ΔF, the relative phase change between the two interferometers will be $\frac{4\pi\Delta F}{C}(l_a - l_b)$, which vanishes as $l_a = l_b$ (ignoring second order effects due to the movement of the diaphragm $Y_o \ll l_a$ or l_b). It is clear that the system perturbation due to wavelength (frequency) drifts will be reduced by the ratio $(l_a - l_b)/l_a$. It is also clear that any errors caused by temperature changes are greatly reduced, as both interferometers suffer a common mode perturbation, caused by the expansion of the housing forming the body of the accelerometer, indeed this thermally induced error in the differential phase change vanishes if the dimensions of the interferometers are precisely equal. Moreover if the phase changes induced in the two interferometers are added, the same sensor can be used as a temperature sensor with an output free from acceleration perturbations.

The resolution of the system is determined by the accuracy of measuring the phase change of the output carrier of one interferometer relative to that of the other. The minimum detectable phase change between two carriers is limited by the signal to noise ratio of each. The phase resolution (ϕ_{min}) is given by :

$$\phi_{min} = \sqrt{(n/s)_1^2 + (n/s)_2^2} \tag{6.6}$$

where $(s/n)_1$ and $(s/n)_2$ are the signal to noise ratios of the first and second carrier respectively.

(6.4.2) Testing the device :

The optical arrangement, used to characterise the device, is shown in figure (6-5). The same technique of signal processing, used in section (6.3), was used to generate two phase modulated

carriers, each corresponds to one interferometer.

In order to test the performance of the accelerometer, it was fixed on the top of a mechanical vibrator with its axis parallel to the direction of vibration. The vibrator was mechanically coupled to the motor/gear box mechanism such that the whole system could be rotated very slowly through an angle θ about a horizontal axis. This experimental set-up enabled us to characterise the accelerometer over a wide frequency range starting from very low frequencies. A linear potentiometer, mechanically attached to the rotor of the system, was used to generate a voltage proportional to θ, this voltage was measured with a digital voltmeter and then transferred to a computer. A digital phase tracker was used to sequentially measure the relative phase changes between the outputs of each interferometer with respect to the reference carrier ϕ_{ar} and ϕ_{br} and then the differential phase changes between the two interferometers ϕ_{ab}. The sensitivity of the accelerometer was measured, as discussed before, by determining the induced phase ϕ_{ar} etc. as it was slowly rotated such that its axis changed from the horizontal to the vertical positions and back again, the time for each 90^o rotation was 5.2 minutes.

The common mode rejection properties of the accelerometer for temperature and source fluctuations were measured by setting it horizontally and;

a) heating it over a 20^oC range (20–40^oC), hence the ratio of $(\phi_{ba}/\phi_{br})_T$ was calculated.

b) varying the injection current of the laser diode such as to vary its output frequency by about $\pm 12GHz$ around its operating value, allowing the ratio $(\phi_{ba}/\phi_{br})_f$ to be obtained. Finally the cross-coupling sensitivity of the accelerometer was measured as described in chapter (5) by determining the amplitude of the induced phase changes produced by shaking the accelerometer, with the same vibration frequency and amplitude, along and perpendicular to its axis of symmetry.

(6.4.3) Performance :

The variations in the induced phases in the accelerometer as a function of the normalised axial acceleration (r/g) is shown in figure (6-6 a,b). A phase change of 66 rad/g was measured in each interferometer relative to the reference carrier, while the differential phase change, of one

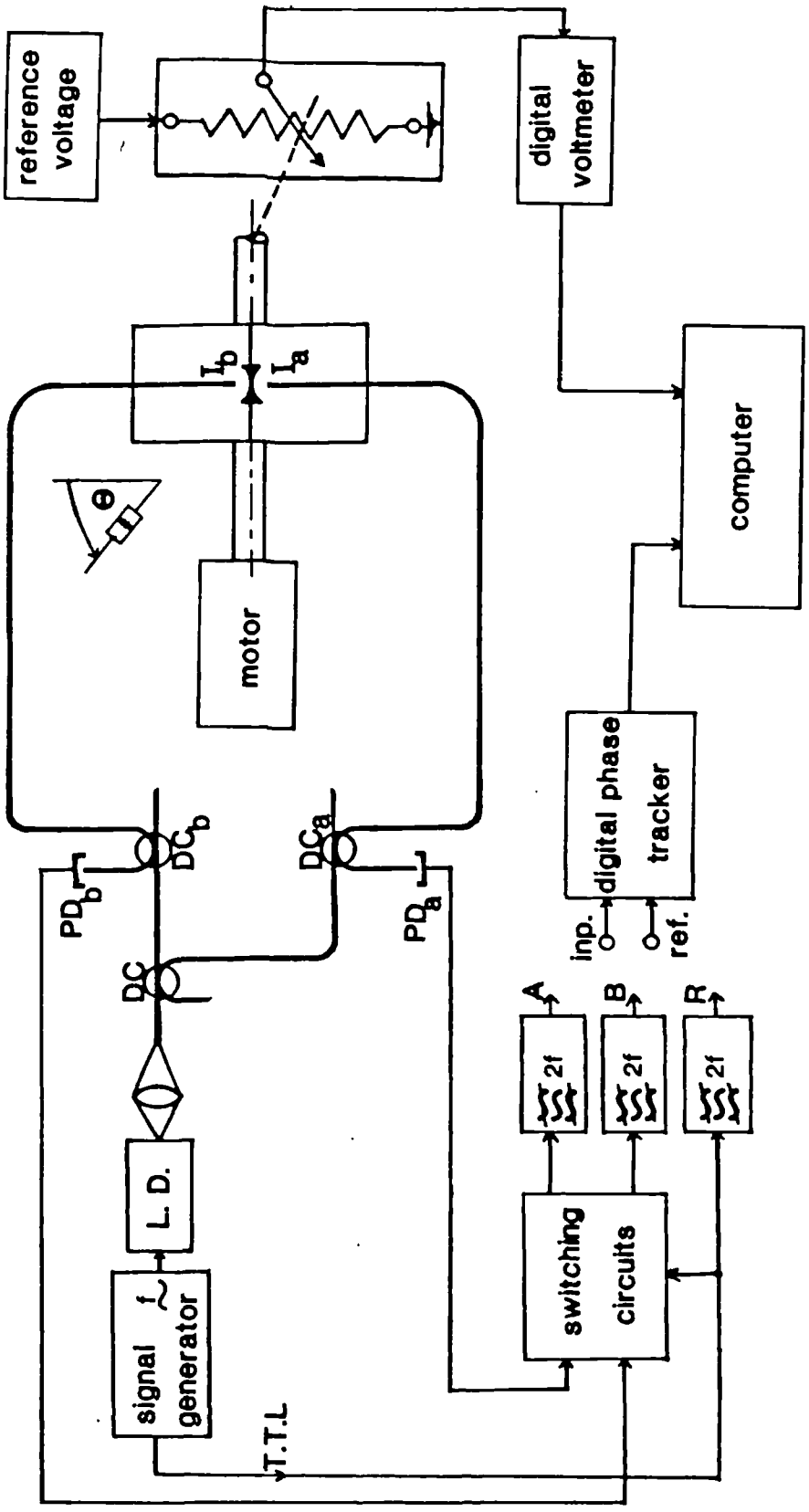

Figure (6-5) : The optical configuration used to test the 'back-to-back' accelerometer.

relative to the other, was doubled. In both interferometers the signal to noise ratio at the output of the filter was approximately 77 dB, within a bandwidth of 47.7 Hz, equivalent to an optical limit of the phase resolution of $2.1\times10^{-5} rad(Hz)^{-1/2}$, (output of one interferometer relative to the reference carrier). According to equation (6.6) the differential phase resolution is $2.9\times10^{-5} rad(Hz)^{-1/2}$, which corresponds to an acceleration resolution of about $2.2x10^{-7} g(Hz)^{-1/2}$ at a frequency of 0.067 Hz (about 21 interference fringes per 5.2 minutes). The common mode rejection of the temperature and wavelength drifts were -27.3 dB and -45.8 dB respectively. The system cross-coupling, as measured, was better than -36.9 dB.

(6.5) Extending the unambiguous range using dual wavelength technique :

In this section we demonstrate how the use of dual wavelength techniques can be used to extend the unambiguous dynamic range of the accelerometer, solving the third problem discussed in section (6.1) within a reasonable working range.

(6.5.1) Interferometry using dual wavelength :

Dual wavelength interrogation of interferometers is a well known technique to increase their unambiguous dynamic range, as discussed in chapter (1). The use of this technique in fibre-optic sensors has been described by several authors [15,16]. An effective wavelength $\lambda_{eff} = \lambda_1 \lambda_2 / (\lambda_2 - \lambda_1)$ is generated, which is longer than either of the wavelengths of the individual sources λ_1 and λ_2. As $\lambda_2 - \lambda_1$ decreases, the effective wavelength, and hence the unambiguous range of the system increases.

However there are practical considerations which restrict the minimum value of $\lambda_2 - \lambda_1$ which can be used. This is because the error induced in λ_{eff} by wavelength drift, of either source, becomes significant in interferometers with a finite path-imbalance. We greatly reduce the problems associated with wavelength drift by the geometrical design of the accelerometer which incorporates dual interferometers of nearly equal optical path difference, where the wavelength dependence, of the whole device, is reduced as a common mode.

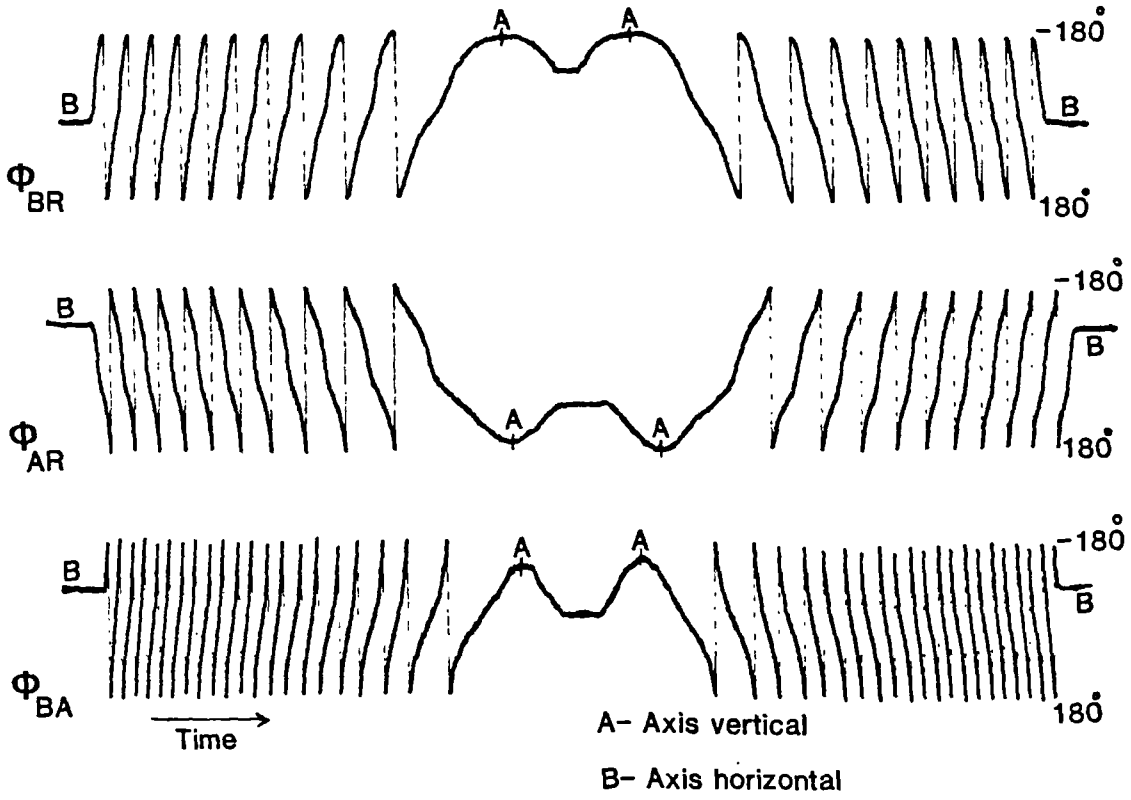

(a)

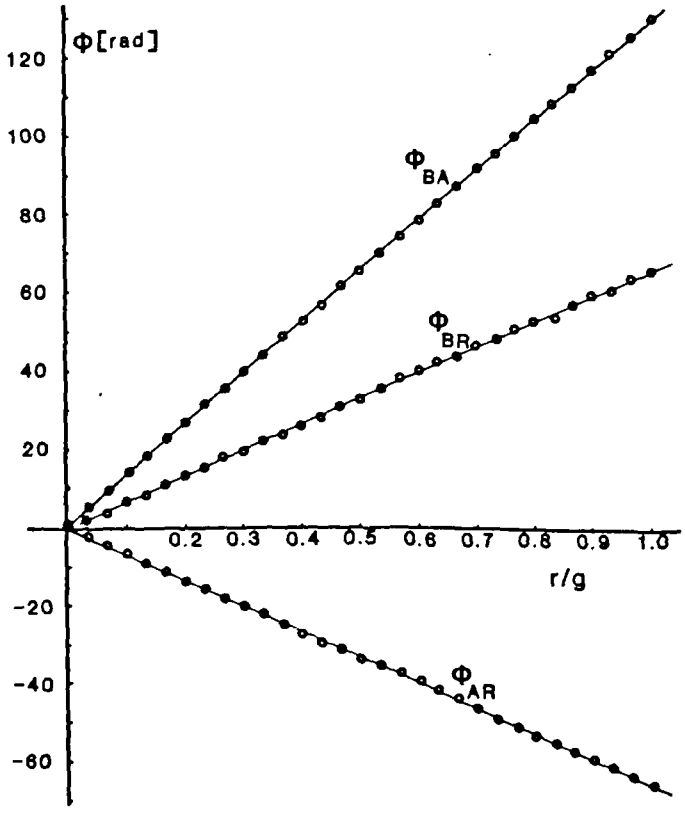

(b)

Figure (6-6) : The induced phase changes in the accelerometer cavities.

(a) : using an X-Y plotter and (b) : using the computer, verses the normalised axial acceleration (r/g).

As the axial acceleration of the sensor changes, the corresponding relative phases between the two interferometers are :

$$\phi_{ab\,1} = \frac{8\pi}{\lambda_1} Y_o \tag{6.7}$$

$$\phi_{ab\,2} = \frac{8\pi}{\lambda_2} Y_o \tag{6.8}$$

Hence the difference between these relative phases ($\Delta\phi$) will be :

$$\Delta\phi = \phi_{ab\,1} - \phi_{ab\,2} = \frac{8\pi}{\lambda_{eff}} Y_o \tag{6.9}$$

(6.5.2) Experimental verification :

The optical arrangement used is shown in figure (6-7). The outputs from two laser diodes were fed into separate ports of a monomode-fibre directional coupler, where the two wavelengths were mixed and transferred from the two output ports of the coupler to illuminate the two hemispherical Fabry-Perot interferometers. The laser diodes used were a Hitachi HL7801E, emitting at a wavelength of 790.7 nm and a Hitachi HLP-1400, emitting at a wavelength of 855.4 nm. The two laser diodes were thermally isolated, such that a long-term frequency stability of about 1 GHz is obtainable for each. A sinusoidal modulation current, at frequency $f \approx 2KHz$, was applied to each laser simultaneously, where the modulation amplitude was adjusted for each laser to minimise the carrier amplitude modulations. The optical outputs of the two interferometers were collimated and separated using a ruled echellete diffraction grating, with 1200 lines/mm and a blaze angle of 75^o. Four outputs, two corresponding to each interferometer, were detected and gated by synchronous 50-50 duty cycle square pulses and filtered at 4 KHz to generate four phase modulated carriers. The reference carrier was produced by band-pass filtering the synchronous switching pulses as shown in figure (6-7). This technique of wavelength separation potentially has better performances than the switching technique, described by Kersey et el [15], as the shot noise in each photo detector is reduced by a factor of $\sqrt{2}$ and laser switching noise is completely avoided.

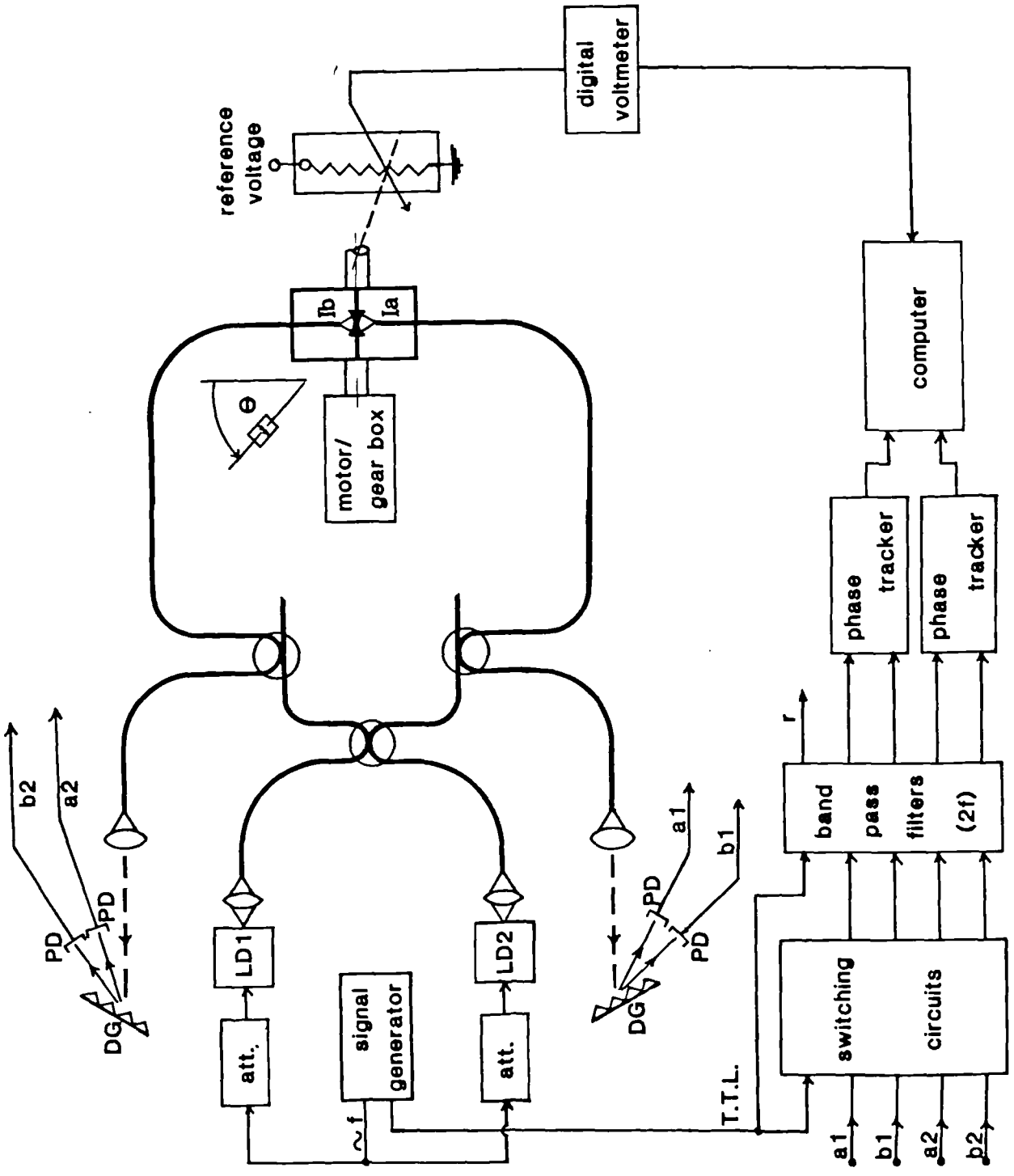

Figure (6-7) : The optical arrangement used to demonstrate the dual wavelength technique.

The relative phase changes between the output of one interferometer with respect to the other (ϕ_{ab1} and ϕ_{ab2}) together with the angle θ were measured and then transferred to a computer, where the differential phase ($\Delta\phi$) was calculated. The sensitivity of the accelerometer was measured by determining the induced phase ϕ_{ar} etc. as it was slowly rotated such that its axis changed from the horizontal ($\theta = 90^o$) to the vertical ($\theta = 0^o$) positions and back again. This process was repeated many times in order that the system's repeatability could be studied.

(6.5.3) Performance and analysis :

Figure (6-8) illustrates the outputs of the four photo-detectors. The variations in the induced phases in the accelerometer as a function of the normalised axial acceleration (r/g) is shown in figure (6-9). The relative phase changes, of the output of one interferometer relative to the other (ϕ_{ab1} and ϕ_{ab2}) were 131.3 rad/g and 121.4 rad/g respectively, with repeatability better than $\pm 8.7x10^{-4}$ rad/g. The differential phase change $\Delta\phi$, corresponding to λ_{eff}, was 9.9 rad/g. The mean signal to noise ratio, at the output of the filters, was approximately 75 dB, within a bandwidth of 59.7 Hz, equivalent to an optical limit of the differential phase resolution of $3.3x10^{-5} rad(Hz)^{-1/2}$, which corresponds to an acceleration resolution of about $2.5x10^{-7} g(Hz)^{-1/2}$ at a frequency of 0.067 Hz (neglecting laser long-term instability). The long-term stability of the system was 34.2 m rad (during a period of 4 hours), which corresponds to $2.6x10^{-4} g$.

From the results it can be seen that the unambiguous range of the single wavelength output is approximately 0.05 g, whereas that of the phase difference output is about 0.64 g. This represents an extension in the unambiguous range of 12.8 times, which could be increased further using two sources with smaller difference in their emitting wavelengths, for example with $\Delta\lambda = 16$ nm a dynamic range of 2.5 g could be obtained whilst the resolution would remain unchanged.

The long-term stability of the system is governed by the stability of the two sources. A technique has been reported that demonstrates a mode hopping-free stable single mode semiconductor

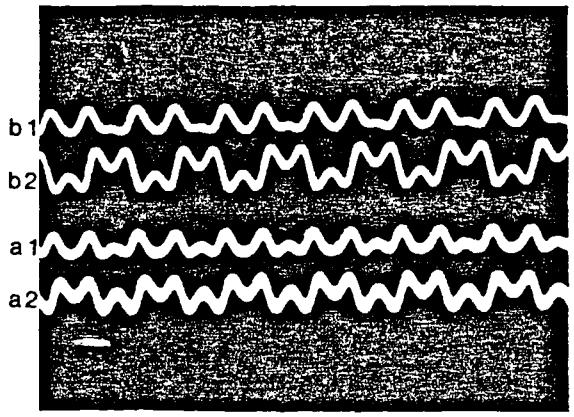

Figure (6-8) : The four photodetector output signals.

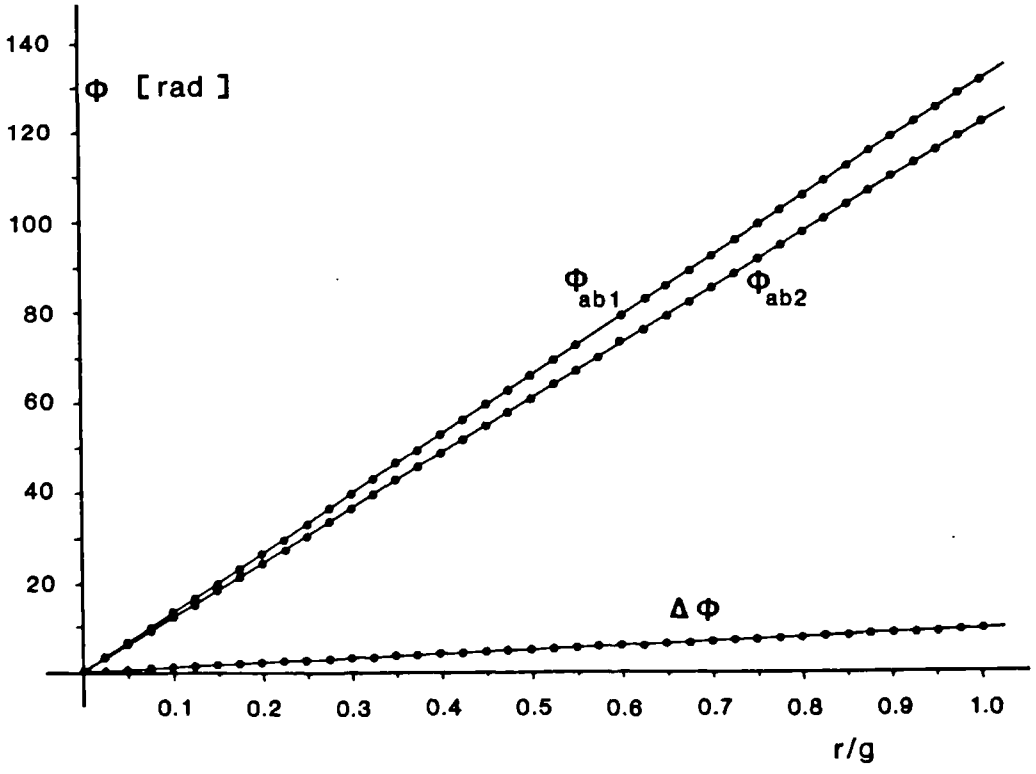

Figure (6-9) : The induced relative phase changes in the accelerometer cavities as a function of the normalised axial acceleration (for each wavelengths and then for the effective wavelength).

laser, with a frequency stability of 28 MHz/24 hours [17]. According to this figure for long-term frequency stability, the corresponding phase stability of one interferometer, in this system, will be about 18.8 m rad/24 hours (path-length imbalance of about 1.6 cm). This value will be reduced to be $9.6x10^{-5}$ rad/24 hours when measuring the relative phase between the two interferometers. This gives the accelerometer a long-term measuring stability of $7.3x10^{-7}$ g/24 hours. In this system the differential phase measurement (corresponding to λ_{eff}) needs to be accurate to $2\pi/12.8$. These figures could be achieved by stabilising one of the laser sources, as described in reference (17), and leaving the other one un-stabilised, other than to provide some thermal isolation from sharp environmental changes.

(6.6) Conclusions :

In this chapter the low frequency performance of the fibre optic based accelerometer, introduced in chapter (5), was studied. An improved design of the accelerometer was introduced where the displacement, produced by acceleration, is measured using two miniature hemispherical air-spaced Fabry-Perot interferometers, constructed either side of the sensing diaphragm. The interferometer outputs are processed differentially such that the effects of the environmental drifts are strongly minimised. The optical configuration of the accelerometer showed a minimised dependency on the wavelength drifts of the light source. This enabled us to extend the accelerometer unambiguous measurement range using two un-stabilised optical sources with different wavelengths.

Using this modified configuration of the accelerometer with a dual wavelength technique gives a highly stable practical sensor. This design could also form the basic measurement unit for a range of measurands such as differential pressure and refractive index. A unique feature of this system is that the diaphragm/mirrors assembly is all metal, which enables the accelerometer to operate over a wide temperature range.

References :

[1] S.Kebayashi, Y.Yamamoto, M.Tto and T.Kimura, " Direct frequency modulation in AlGaAs semiconductor lasers", J. Of Quantum Electronics, Vol. QE-18, No.4, 1982, P.582.

[2] A.Dandridge and A.B.Teveten, " Phase compensation in interferometric fibre optic sensors ", Optics Letters, Vol. 7, 1982, P.279.

[3] A.D.Kersey, M.Corke, J.D.C.Jones and D.A.Jackson,"Signal recovery techniques for unbalanced fibre interferometric sensor illuminated by laser diodes ", IEE Conference On Optical fibre sensors, London, 1983, P.43.

[4] A.D.Kersey, D.A.Jackson and M.Corke, "Demodulation scheme for fibre interferometric sensors employing laser frequency switching ", Electronics Letters, Vol.19, February 1983, P.102.

[5] A.Dandridge and L.Goldberg, " Current induced frequency modulation in diode lasers ", Electronics Letters, Vol.18, 1982, P.302.

[6] D.A.Jackson, R.Priest, A.Dandridge and A.B.Teveten, " Elimination of drift in a single mode optical fibre ", Applied Optics, Vol.19, 1980, P.2926.

[7] D.A.Jackson, A.D.Kersey, M.Corke and J.D.C.Jones, " Pseudo-heterodyne detection scheme for optical interferometers ", Electronics Letters, Vol.18, 1982, P.1081.

[8] " Workshop on single mode optical fibre sensor technology ", Course notes, University Of Kent and Sira Ltd., U.K., 1985, P. 161.

[9] E.Voges, O.Ostwald, B.Schiek and A.Neyer, " Optical phase and amplitude measurements by single side-band homodyne detection ", IEEE J. Quantum Electronics, Vol. QE-18, 1982, P.124.

[10] B.Y.Kim and H.J.Shaw, " Phase-reading, all-fibre-optic gyroscope ", Optics Letters, Vol.9,

No.8, August 1984, P.378.

[11] A.C.Lewin, A.D.Kersey and D.A.Jackson," Non-contact surface vibration analysis using a monomode fibre optic interferometer incorporating an open air path ", J.Physics E. Scientific Instruments, Vol.18, 1985, P.604.

[12] M.A.Nokes, B.C.Hill and A.E.Barelli, " Fibre optic heterodyne interferometer for vibration measurements in biological systems ", Rev. Scientific Instruments, Vol. 49, June 1978, P.722.

[13] D.A.Jackson, " A prototype digital phase tracker for the fibre interferometers " J. Physics E: Scientific Instruments, Vol.14, 1981, P. 1274.

[14] A.S.Gerges, F.Farahi, T.P.Newson, J.D.C.Jones and D.A.Jackson ," Fibre optic interferometric sensor using a low coherence source: dynamic range enhancement ", International Journal of Opto-Electronics, Vol.3, No.4, 1988, P.311.

[15] A.D.Kersey and A.Dandridge, " Dual-wavelength approach to interferometric sensing ", SPIE, Vol. 798 Fibre Optic Sensors-2, 1987, P.176.

[16] D.J.Webb, J.D.C.Jones and D.A.Jackson, " Extended range interferometry using a coherence tuned synthesised dual wavelength technique with multimode fibres ", Electronics Letters, Vol.24, No.18, September 1988, P.1173.

[17] Z.Bingkun, Z.Hanyi, W.Yuanxiang, Z.Jianying, L.Jian and P.Zhenwu, " 24 h frequency stabilisation of an slm external-cavity semiconductor laser " Electronics Letters, Vol 23, No. 5, February 1987, P.194.

CHAPTER (7)

Conclusions

(7.1) Introduction :

In this thesis several fibre-optic-based interferometric sensors designed to sense quasi-static measurands such as displacement, temperature and acceleration , have been introduced. The systems have been designed to be capable of re-initialisation when switched on, insensitive to environmental perturbations, with an extended measurement range and long term stability. The main topics covered in the thesis are:

(i) Novel techniques of signal processing, exploiting 'white light' interferometry. These techniques avoid the ambiguities which arise from the use of a coherent source in interferometers, where the transfer function is periodic.

(ii) A novel form of remote sensor, in which the sensing element is a miniature hemispherical cavity Fabry-Perot interferometer.

(iii) The measurement of temperature and acceleration using the hemispherical cavity based sensor exploiting both coherent and low coherence techniques for signal processing.

(7.2) Summary :

The general bases of fibre-optic interferometric sensors was discussed in the early part of

the thesis, which identifies the difficulties of routinely measuring slowly varying measurands. After detailed consideration of these difficulties and possible means of eliminating, or greatly reducing, their effects it has been possible to design several fibre optic interferometric sensors. A summary of the systems and their performance is given below.

(a) Interferometry using partially coherent light :

The theoretical bases of white light interferometry, using a single interferometer and a system consisting of a remote interferometer coherently tuned with a receiving interferometer, have been studied. It is shown that, in these systems, their transfer functions have unique features which can be exploited to determine the optical path difference of the interferometer when it is switched on.

The properties of the partially coherent optical sources, previously used in fibre-optic sensing applications have also been reviewed. The main disadvantage of such sources is the low launching efficiency in coupling the output power into a monomode fibre and hence the resolution, in measuring the optical path difference, is poor, by comparison to that obtained when the device is illuminated by a monochromatic source (laser). We have studied also the transfer function of the system when illuminated by a multi-mode laser diode, which demonstrated the possibility of using a multi-mode laser as an alternative to the low power, low-coherence length sources, normally used in 'white light' fibre-optic interferometric sensors. The main advantage being that as more power may be coupled into the system, the overall resolution may be improved.

Two signal processing techniques have been developed for fibre interferometric sensors illuminated by low coherence-length sources. In each technique an automatic feedback servo system has been constructed to maintain the path-length imbalance, of the sensing interferometer, close to zero. In the first technique the sensing interferometer was locked to the maximum of the visibility function, which corresponds to a zero path-length imbalance in the interferometer. Thus providing a unique operating point for the system, this concept was exploited to measure quasi-

static measurands such as strain and displacement. In the second technique, the interferometer was locked to the quadrature point nearest to the position of maximum visibility; that is, a path-length difference of $\lambda/4$. Such a sensor therefore has the same resolution as that of a conventional interferometer, with the major advantage of an unambiguous operating point. We have demonstrated this technique for measuring both slowly varying and high frequency measurands. Advantages of both techniques are the ability, of the system, to self-initialise, an increase in the unambiguous range and as the path-length imbalance of the interferometer is adjusted to be near zero, the errors produced by frequency instabilities of the light source (on the sensor resolution and long-term stability) are greatly reduced. The resolution of the sensor was limited only by the photo-diode shot noise and uncertainty in the tracking system. The measurement range was limited by the tracking range of the balancing transducer.

Finally the use of multi-mode laser diodes in a practical fibre-optic interferometric displacement sensor has been demonstrated. An experimental set-up of two interferometers in tandem was used to study the coherence properties of the multi-mode laser diode Mitsubishi ML-4406 and then to demonstrate the possibility of using it in coherence tuned multiplexing systems. The results of this experiment show that a multi-mode laser, with specific properties can be used as an alternative source in coherent tuned interferometric systems, the main advantage being that the overall resolution is improved by several orders of magnitude as a result of the greatly increased coupled power.

(b) The hemispherical Fabry-Perot cavity :

The next stage of the work was centred around a novel form of fibre optic based sensor, in which the sensing element was a miniature hemispherical cavity Fabry-Perot interferometer. The optical properties of the hemispherical cavity were analysed theoretically. Simple techniques were used to form the sensing element, and then the properties of the cavity, as an optical interferometer were investigated experimentally, which showed good agreement with theoretical prediction. This sensor does not require any conventional optical components to be installed inside the cav-

ity, is easy to construct and to operate as a practical sensor even in difficult environments. The nature of the interferometer's transfer function is such that the interference visibility can be easily set at a specified value, in addition as the spherical mirrors can be inexpensively reproduced with high repeatability it is possible to manufacture large numbers of identical systems. The properties of this sensor are independent of the properties of the monomode fibre used in its construction, thus it has greatly reduced environmental sensitivity when compared with all fibre sensors.

(c) Fibre-optic based temperature probes :

Two different designs of remote temperature probes, designed on the bases of the hemispherical cavity, were introduced. In the first design the probe was tested at temperatures below $100^{o}C$ while the second probe was designed to measure very high temperatures. These temperature probes showed high-stability, low sensitivity to environmental effects and repeatable performance within a dynamic ranges over 10^{5}. In both experiments a 'white light' signal processing technique was used, where both a laser diode operated below threshold and a multi-mode laser diode were used for the source.

(d) High sensitivity fibre-optic based accelerometers :

A highly simplified fibre optic-based accelerometer having a displacement resolution comparable to that of a typical interferometric optical sensor and the stability and re-producibility of a conventional reference grade accelerometric device, was demonstrated. The design of this new type of accelerometer permits low sensitivity to orthogonal components of acceleration. Other features of this device are its small size, low weight and its fabrication from materials which will enable it to operate at very high temperatures. The sensing element of the accelerometer is a weighted circular diaphragm, where the displacement of the centre of the diaphragm produced by acceleration was measured by a hemispherical air-spaced interferometer, as discussed before. The properties of the accelerometer was studied with the device used as a contact vibration sensor. The measurement range and sensitivity of the device depends critically on the properties of the

diaphragm, hence it may be designed for a given application.

The very low frequency performance of the accelerometer was also studied, to establish if its performance would be suitable for applications such as inertial guidance. To achieve very high performance it was found necessary to modify the optical design to reduce some of the low frequency detrimental effects on the sensor. This was achieved by measuring the displacement of the centre of the diaphragm using two miniature hemispherical air-spaced interferometers constructed either side of the sensing diaphragm. The optical path-length imbalances of the two interferometers were the same (within experimental limits), hence the induced phase change in one interferometer relative to the other showed a minimal dependence on variations of the mean wavelength of the source and temperature fluctuations in the sensing head. The unambiguous measurement range of the accelerometer was also extended by using two un-stabilised optical sources with different wavelengths. A dynamic range in excess of 10^6 was obtained with resolution of $2.5\times10^{-7}\ g/\sqrt{Hz}$.

(7.3) Limitations and future work :

As with all prototypes, there are also some limitations in the design and implementation of the sensing systems introduced in this thesis. Possible methods to overcome these limitations are discussed below.

(a) The accuracy of the techniques, described in chapter (3), are fundamentally limited by, (i) the properties of the path length compensating transducer and (ii) the optical path-length stability of the reference arm of the interferometer (when using a single active sensing interferometer) or of the receiving interferometer (when using a passive sensing interferometer coherently tuned by a receiving interferometer).

Transducers having a much better positional accuracy can be designed based on measuring the displacement compensated by the transducer either electronically (capacitance measurement) or interferometrically using a highly-stabilised laser. Commercial capacitance transducers are available with accuracy better than 1 nm, unfortunately as with a highly stabilised laser the price

would exclude it from general purpose applications. Further research to realise a miniature receiving interferometer, to give a higher-stability and a wider tracking range at low cost, is clearly necessary.

(b) In chapter (4) sensing elements based on a hemispherical Fabry-Perot cavity were studied, where the sensing element was interrogated using monomode optical fibre. The reflectivities of the un-coated fibre end and the low quality curved mirror were low, hence the interferometer was regarded as a two beam interferometer. It would be logical to try to study the hemispherical Fabry-Perot cavity as a high finesse interferometer by coating the fibre end and using a high-quality spherical mirrors.

It would also be interesting to study the properties of the hemispherical Fabry-Perot interferometer when illuminated with a low coherence-length source via multi-mode fibre. The increase in the optical power, coupled to the cavity, may serve to increase the signal to noise ratio at the sensor output and hence its resolution. This not an easy theoretical problem because of the effects of the power distribution among the different fibre modes. Moreover the large-area source presented at the output of the multi-mode fibre must be considered.

(c) A novel design for a high temperature probe was introduced, where the sensing element was an optical hemisphere. In our demonstration a fused-silica hemisphere was used, making it possible to test the sensor up to $1000^{o}C$ (The maximum working temperature of fused silica is about $1100^{o}C$). It should be possible to increase this temperature to about $1800^{o}C$ if a sapphire sensing element is used together with suitable refractory materials to support the probe.

(d) In chapters (5,6) the properties of a new type of fibre optic-based accelerometer were studied over a range of frequencies. The possibilities of modifying this device to sense pressure (absolute and relative) or acoustic signals have been discussed, however no experimental work has yet been carried out on these systems. The properties of the sensing diaphragm would require careful consideration in order to predict the performance of such devices.

The cross-sensitivity of the prototype accelerometer was low, hence it should be possible to develop the concept into a three-axis accelerometer to determine the full acceleration vector. Coherence tuning probably being the optimum method of multiplexing outputs of the individual units. The device's sensitivity to rotation about its axis of symmetry has yet to be studied, but if were proved to be low then it could be integrated with a fibre-optic gyroscope to form the basic block of a fibre-optic navigational system.

Appendix (A)

The circuit diagram of the 'maximum visibility tracking' feedback servo

Figure (A-1) shows a simplified circuit diagram of the 'maximum visibility tracking ' digital feedback servo, discussed in section (3.2). The servo consists of three main stages, the first stage is used to measure the envelope of the input amplitude while the other two stages are used to locate the position where the interference amplitude is maximum.

The input signal, proportional to the interference fringe amplitude, is AC coupled through a buffer amplifier (OP-1), which has a very high input impedance and a very low noise. An OP-071 operational amplifier was chosen for this purpose, its output is amplified and rectified through a precision rectifier stage and then low-pass filtered. The cut off frequency of the filter was chosen such that the envelope of the input signal is only detected and not the signal itself. This output is fed through another buffer amplifier (OP-3) as an input (O_1) to the second stage of the servo, which we call 'the low accuracy stage'. The same output is limited and amplified again to increase the accuracy of determining the position of the peak of the envelope of the input signal. This amplified output (O_2) is used as an input to the third stage of the servo, which may be called 'the high accuracy stage'.

The second stage starts with the storage and decision circuit. Here OP-7 is used as a comparator, comparing the level of O_1 with the level of the signal stored in the low-leakage capacitor C_{s1} , $C_{s1} = 1\mu F$, leakage resistance = $10^{12}\Omega$. If O_1 is higher, the output of OP-7 is high and the

level of O_1 is stored in the capacitor C_{cs} , via the gated FET analogue switch AS-1. The corresponding output of the circuit is the a logical 1 level. If the level of O_1 is less than the level of the signal stored in C_{s1} the output of the circuit is low switching off the analogue switch. The level stored in C_{s1} remains unchanged due to its very high leakage resistance. For the same reason the output of capacitor C_{s1} is buffered by a high input impedance FET operational amplifier (OP 355), the off resistance of the FET analogue switch is also very high (in the order of $10^{12}\Omega$). It is clear that the output of this decision circuit is logic 1 if the new level of O_1 is higher than the old level of the same signal, stored in the capacitor, and then the new level is stored in the capacitor instead of the old. This happens as the path-length imbalance of the interferometer approaching the zero position. If the path-length imbalance is increased away from the zero, the new level of the signal O_1 will be less than the old level and the output of the circuit will be logic 0. A similar decision making circuit controls the operation of the high accuracy stage of the servo. This circuit works as follows : After the manual adjustment of the path-length imbalance, as discussed before, the servo is triggered (pulse T).This pulse clears the counters, discharges the storage capacitors and presets the flip flop F-1. The output of F-1, Q-1 = 1, enables a series of clock pulses to be counted on the up counter C-1. The counter output is converted to an analogue voltage to control PZT-1. As the path-length imbalance approaches zero, this stage continues in operation, as described, increasing the feed back voltage to drive the interferometer towards the zero path-length imbalance position. At the same time the inverse output $\overline{Q-1}=0$, hence no clock pulses are counted in the up/down counter C-2, which controls the high accuracy stage.

When the path-length imbalance passes through the zero, with one step corresponding to the low accuracy stage ($\simeq \lambda/4$), the input signal of the servo decreases changing the state of the decision making circuit in the second stage to logical 0. This 0 clears F-1, hence Q-1 changes to logical 0 state stopping the counting of the up counter, C-1, and triggering monostable multivibrator, MV-1, which generates a pulse to preset F-2 and to discharge the storage capacitor of the third stage, C_{s2}, and hence initialising the third stage sequence. In the third phase $\overline{Q-1}=1$ and $Q-2=1$, the counter C-2 starts to count up. The corresponding analogue voltage increases in

much smaller steps than that of the previous stage. The total feedback voltage, $V_{fb} = V_1 - V_2$, decreases as V_2 increases and hence the path-length imbalance approaches the zero from the opposite directions in steps of about $\lambda/240$. This process continues until the path-length imbalance passes the zero again with one step corresponding to the high accuracy stage, at this point the decision of the stage changes from 1 to 0 and this excites the multivibrator MV-2 to produce a single pulse. This pulse is used to change the states of F-2 (connected as a T flip flop) and to discharge C_{s2} again to change the decision to 1. As Q-2 = 0 and $\overline{Q-2} = 1$ the counter starts to count down increasing the total feedback voltage and approaching the zero position again. This process continues locking the system about the position of zero path-length imbalance with an accuracy of $\pm$ one step of the high accuracy stage.

As shown in the circuit diagram, the system resolution may be determined by the minimum step size which is limited by the level of the digital noise, at the output of the counters. Practically the minimum step size was about $\lambda/1024$, (a 10-bit counter was used) which is much smaller than the limited resolution, as defined using equation (3.4).

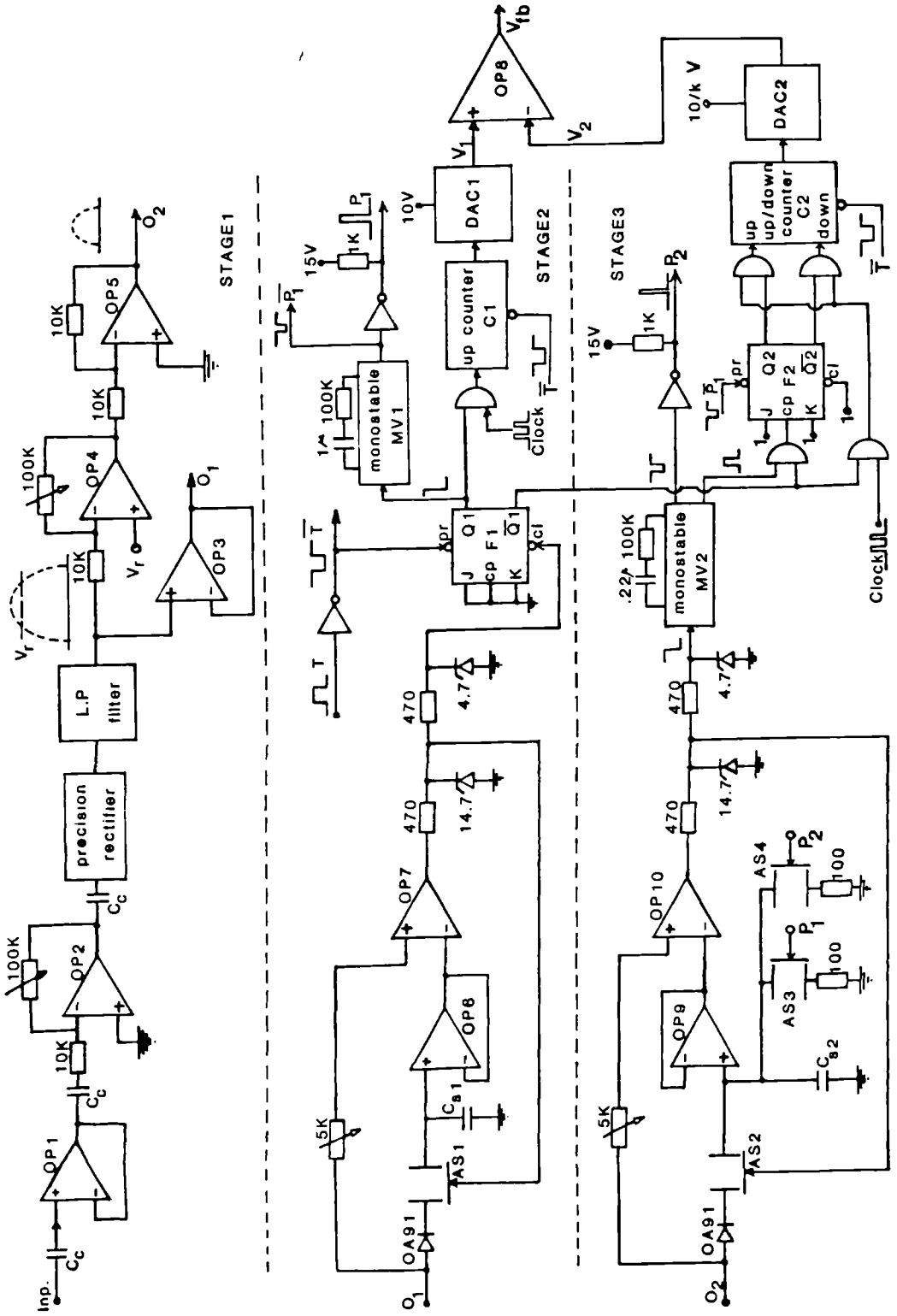

Figure (A-1) : A simplified circuit diagram of the 'maximum visibility' tracking servo.

Appendix (B)

The circuit diagram of the 'first quadrature tracking' feedback servo

The circuit diagram of the 'first quadrature-point tracking' electronic feedback servo, discussed in section (3.3), is shown in figure (B-1). The output voltage of the two photodiodes, shown in figure (3-1), are differentially amplified using a low noise-high input impedance operational amplifier. The differential output is fed to the second digital stage, the analogue stage and to an envelope detector, such as the first stage of the previous servo. A similar decision circuit is used to locate the position of the zero path-length imbalance.

Triggering the servo, manually (pulse T), the counter of the first stage, C-1, starts to count a 10 KHz clock pulses. This decreases the path-length imbalance with steps less than $\lambda/4$ and producing a set of interference fringes with frequency of about 2.5 KHz, the envelope of these fringes is measured as discussed before. Just beyond the matched position (point 1 in figure 3-3-b) the first stage is switched off when the decision changes from logical 1 to 0 and hence the output Q-1 of the flip flop F-1. This change excites the multivibrator MV-1 to produce a pulse for presetting the flip flop F-2 and hence to allow a very low frequency clock pulses (100 Hz) to be counted in the counter C-2. Each count increases the path-length imbalance, far from the zero position, with steps of about $\lambda/240$. when the path-length imbalance is exactly $\lambda/4$ the differential output of the photodiodes is zero and hence the zero level detector produces a negative pulse required to clear F-2 and hence stop counting the 100 Hz clock pulses. The analogue switches AS-3 and AS-4

short circuit the integrator capacitor C and connecting the stage output to the ground both to ensure that the analogue voltage is zero during the duty time of the two digital stages. The importance of the second stage is to ensure a continuous smooth start-up of the analogue stage with its input signal equals zero. This condition is necessary to avoid any jump from one quadrature to another during the initial phase when the analogue circuit takes control. Simply the function of the two digital stages is to locate the first quadrature point and then the analogue stage is used for tracking. The analogue stage consists of an integrator, with a 3 dB cut off frequency of about 120 Hz [10] and an amplifier. after the first stages the two analogue switches AS-3, AS-4 are switched off permitting the integrator output signal to be included in the system feedback voltage. This error signal is required to keep the phase difference between the interferometer arms at $\pi/2$ radians, it also contains information about environmental drift noise and low frequency input signals. The output of the analogue stage is rectified by a precision rectifier and then low-pass filtered and compared to a resetting voltage level, V_{rest}, which is chosen to give the tracking range permitted for the analogue stage. A short output pulse from the level detector triggers two monostable multivibrators, MV-2, one multivibrator is used to discharge the storage capacitor of the decision circuit C_s , the other generates a pulse (R), which is narrower, and is used to reset the whole system and initiate the procedure to locate the first quadrature point again.

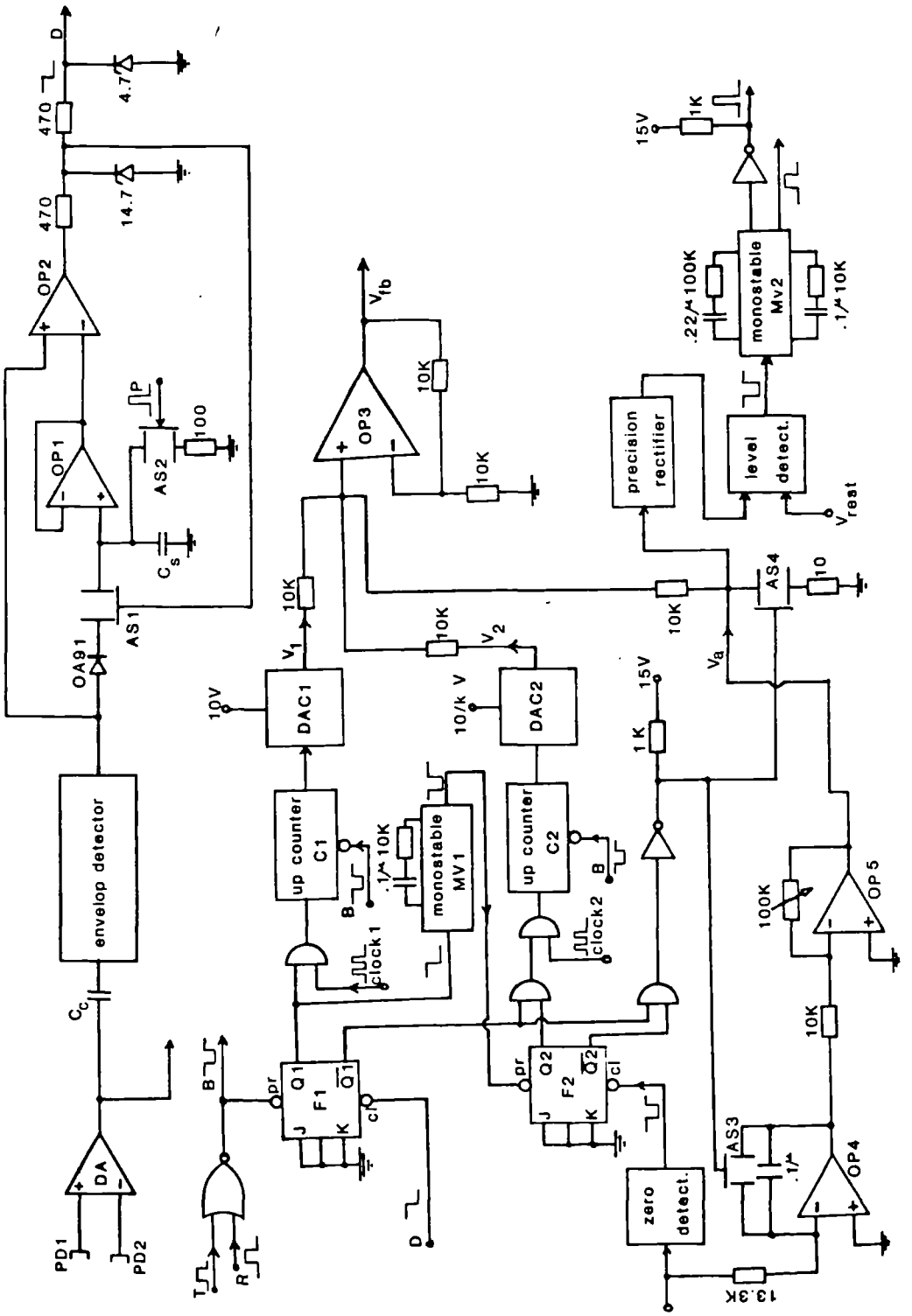

Figure (b-1) : A simplified circuit diagram of the 'first quadrature point' tracking servo.

Supplementary

Time–division multiplexing of fibre optic interferometric sensors using frequency modulated laser diode

Electronics Letters, Vol. 24, No. 1, 1988, Page 54.

Time-division multiplexing of fibre optic interferometric sensors using a frequency modulated laser diode

F. Farahi, A.S. Gerges, J.D.C. Jones and D.A. Jackson

Physics Laboratory, University of Kent, Canterbury, Kent, CT2 7NR, U.K.

Abstract

A multiplexed sensing system based on a frequency modulated laser diode is demonstrated, where a time addressing technique is used to identify signals from different interferometers. It is shown that sensor interferometers with the same path differences can be deployed in the system and cross-talk between different interferometers is avoidable.

Recently three methods for multiplexing sensor arrays have been discussed. Coherence multiplexing of the fibre interferometric sensors has been realised using a short coherence length source with an array of interferometers in the receiver [1]. The receiving interferometers are paired with sensing interferometers, therefore interference occurs for each matched pairs. A frequency division technique has been used for a system made up of unbalanced interferometers where the path imbalances are different and are restricted by certain constrains [2,3]. Consequently a heterodyne carrier is created for each interferometer. Time division multiplexing of fibre sensors has also been discussed for both multi-mode fibre sensing systems [4], and single-mode hydrophone arrays [5].

In this letter we present a time-domain addressing scheme by modulating a laser diode with a gated saw-tooth current. Delay lines between the fibre interferometers can be deployed to generate time delays (at least) corresponding to the time duration of the ramp applied to the laser. Figure 1 shows schematically a multiplexed system based on this time-division technique using a frequency modulated laser diode. Each symbol ⟨ ⟩ represents the interference fringes corresponding to a specific interferometer which depends on the path imbalance in that interferometer and also the change in frequency of the laser when the injected current is linearly modulated. The photodiode output can be gated such that all the independent interferometric outputs are separated. For a change $\Delta\nu$ in the frequency of the laser the phase of an

interferometer changes as

$$\Delta\phi = K\ \ell\ \Delta V$$

where $K = 2n\pi/\lambda$ or $4n\pi/\lambda$ in reflective configuration, ℓ is the path imbalance of the interferometer and n is the effective refractive index of the fibre.

A phase modulation $\Delta\phi$ of $2m\pi$ is required to have a carrier output without amplitude modulation [6], where m is an integer number. For the proposed sensor arrays this imposes the condition of

$$\frac{\ell_k}{\ell_{min}} = k$$

where ℓ_k is the path imbalance of the kth interferometer and ℓ_{min} is the minimum path imbalance in the system. Because de-multiplexing is achieved in the time domain, it is clear that no mutual constraint between the interferometers is required i.e. sensors with exactly the same path imbalances can be deployed in a system. This is an advantage over previously presented coherence multiplexed localised sensors with approximately equal lengths [7] and also frequency division based multiplexed system [8]. One further condition requires to be satisfied as

$$T_l \leq \Delta T \leq T$$

where T is the time between two successive ramps, ΔT is the maximum time delay between any two interferometers and T_l is the period of applied ramp. This condition limits the maximum number of sensors to

$$N = T/T_l$$

In our experiment two Mach-Zehnder interferometers with path imbalances of approximately 15 and 30 cm with a delay line of 1 km were used [Figure 2]. The effective optical delay is 2nL which corresponds to the time delay of 5 μs, where L is the length of the delay fibre. This requires a maximum modulating time of 5 μs. We gated the saw-tooth wave form with an "on time" of 5 μs and adjusted the amplitude of modulation to drive the interferometers over one and two periods of their transfer functions. The multiplexed output with two successive interferometer outputs corresponding to a single applied ramp is shown in figure 3-b. The output was gated twice such that the outputs of the individual interferometers were separated

(Fig.3c,d). It is clear that by band pass filtering each output a pseudo-heterodyne carrier is created, so that the phase information of each interferometer can be recovered. Alternatively the laser injection current can be modulated by a gated sinusoidal wave form, then the method described by Lewin et al [9] is required to generate the pseudo-heterodyne carriers.

A new technique in multiplexing all fibre interferometric sensors was described. Two interferometers were used in a system where the laser injection current was modulated by a gated saw-tooth and consequently the output was demultiplexed in time domain. The resultant demultiplexed outputs were thus two independent pseudo-heterodyne carriers.

References

[1] J.L. Brooks, R.H. Wentworth, R.C. Youngquist, M. Tur, B.Y. Kim and H.J. Shaw,"Coherence multiplexing of fibre optic interferometric sensors" Journal of Lightwave Technology, LT3, No.5, pp.1062, 1985.

[2] I. Sakai, G. Parry and R.C. Youngquist,"Multiplexing fibre optic sensor by frequency modulation: cross term consideration" Optics Letters, No.11, pp.183, 1986.

[3] I. Sakai,"Frequency division multiplexing of fibre sensors using a frequency modulated source" Optical and Quantum Electronics, Vol.18, pp.279, 1986.

[4] A.R. Nelson, D.H. Mc Mahon and R.L. Gravel,"Passive multiplexing system for fibre optic sensors" Applied Optics, Vol.19, No.17, pp.2917, 1980.

[5] M. Henning, C. Lamb and R, Mc Eleny,"Improvements in reflectometric fibre optic hydrophones" SPIE, Vol.586, Fibre Optic Sensors, 1985.

[6] D.A. Jackson, A.D. Kersey, M. Corke and J.D.C. Jones,"Pseudo heterodyne detection scheme for optical interferometers" Electronics Letters, Vol.18, No.25, pp.1081, 1982.

[7] F. Farahi, T.P. Newson, J.D.C. Jones and D.A. Jackson,"Coherence multiplexing of remote

fibre optic Fabry-Perot sensing system" Optics Communication, Submitted, 1987.

[8] F. Farahi, T.P. Newson, P. Akhavan Leilabady, J.D.C. Jones and D.A. Jackson,"A multiplexed remote fibre optic Fabry-Perot sensing system" Journal of Modern Optics, Submitted, 1987.

[9] A.C. Lewin, A.D. Kersey and D.A. Jackson,"Non-contact surface vibration analysis using a monomode fibre optic interferometer incorporating an open air path" Journal of Physics E: Scientific Instruments, Vol.18, pp.604, 1985.

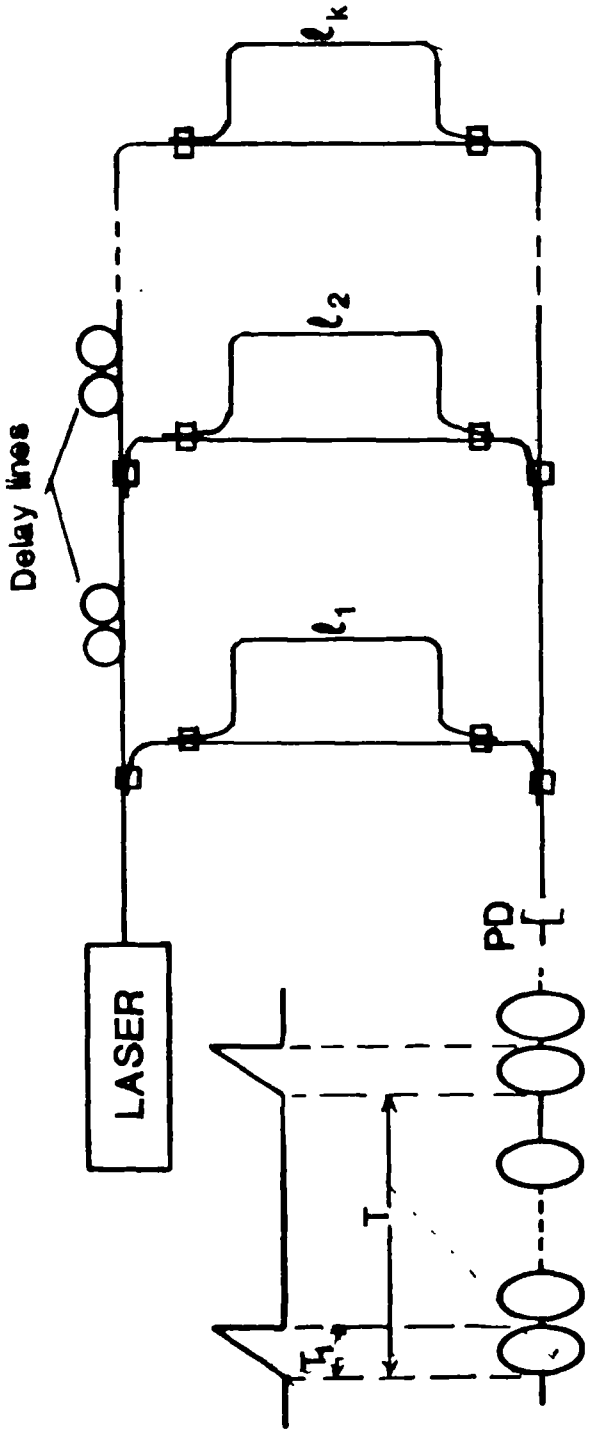

Figure (1) : Schematic of a parallel configuration for a time division multiplexed sensing system when the laser diode injection current is modulated with a gated ramp.

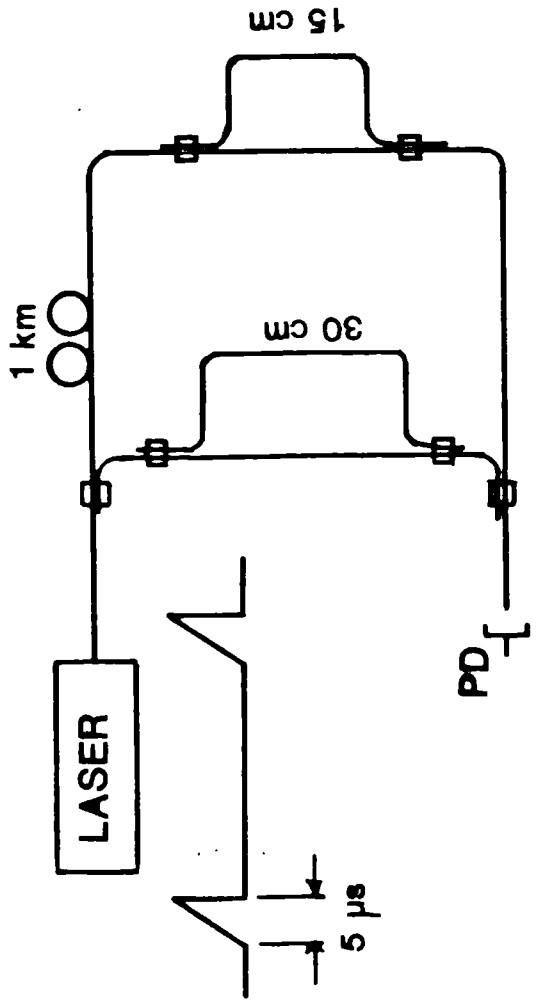

Figure (2) : Experimental arrangement for two all-fibre Mach-Zehnder interferometers.

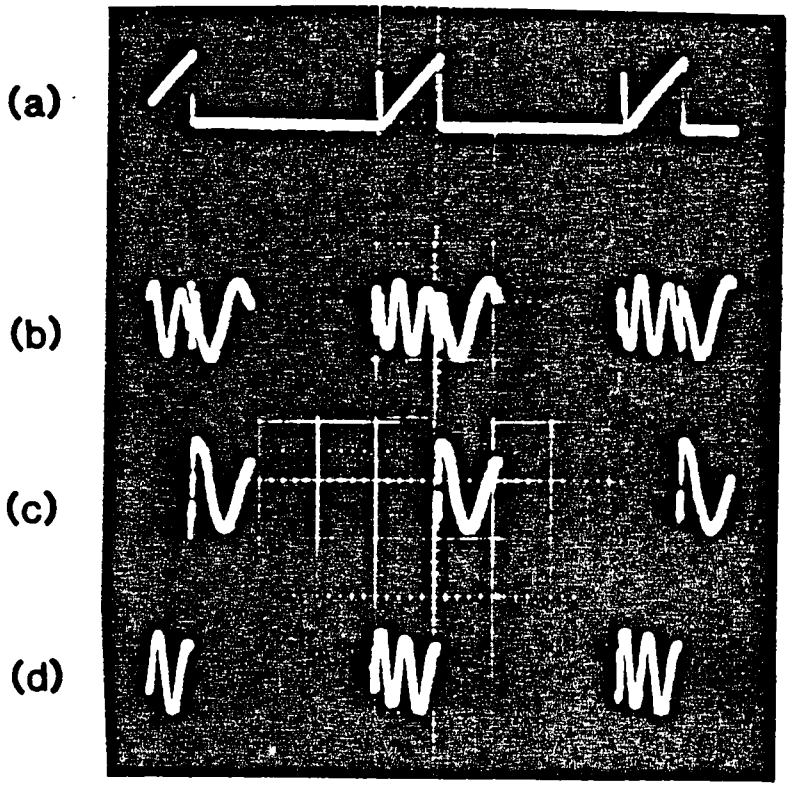

Figure (3) : The signals in the time domain ; (a) : laser injection, (b) : photodiode output,

(c) : gated photodiode output corresponding to the first interferometer and

(d) : gated output corresponding to the second interferometer. X-axis; 5 μS */division.*